Syracuse University

SURFACE

Mechanical and Aerospace Engineering - Dissertations

College of Engineering and Computer Science

8-2012

Development of a Novel Statistical Method and Procedure for Material Characterization and a Probabilistic Approach to Assessing the Hygrothermal Performance of Building Enclosure Assemblies

Jianhua Zhao
Syracuse University

Follow this and additional works at: https://surface.syr.edu/mae_etd

Part of the Mechanical Engineering Commons

Abstract

In this research, a systematic approach was introduced to establish a high quality and comprehensive material database. The method was applied to a great number of materials in different material categories. The database provides a solid base for hygrothermal simulation and further research.

A method was developed to derive the generic material from the material cluster comprising specific materials with similar characteristics. A novel approach was developed by using the generic material to extrapolate less incomplete material data set to full data set that is suitable for the hygrothermal simulation. The approach extends the material database, and hence enhances the usability of existing hygrothermal simulation tools.

Moisture storage characteristics (i.e., the moisture retention function) are one of the most difficult aspects to measure in developing a high quality database. In this study, a method was developed to simplify the procedure for moisture storage measurement with the aid of statistical analyses. For the building brick and plaster/mortar categories, results show that properly selected three measurements in the overhygroscopic range and one measurement in the hygroscopic range were sufficient to get the knowledge of moisture storage characteristics.

A probabilistic approach based on the Monte Carlo method was developed and incorporated into a current hygrothermal simulation tool, to assess hygrothermal

performance of building enclosure assembly against different performance criteria. The uncertainties from different sources, including material properties, boundary coefficients, indoor conditions, dimensions of the material layers, and orientation of the construction, were accounted for. The rank correlations of basic material parameters in different material categories were obtained and incorporated in the Latin hypercube sampling.

The probabilistic approach was then applied to assess the durability, thermal efficiency, and mold growth risk of a retrofitted wall assembly. The most influential input variables against the specific performance criterion were identified by sensitivity analysis.

DEVELOPMENT OF A NOVEL STATISTICAL METHOD AND
PROCEDURE FOR MATERIAL CHARACTERIZATION AND A
PROBABILISTIC APPROACH TO ASSESSING THE HYGROTHERMAL
PERFORMANCE OF BUILDING ENCLOSURE ASSEMBLIES

By

Jianhua Zhao

B.S. Dalian University of Technology, 2001

M.S. Dalian University of Technology, 2004

DISSERTATION

Submitted in partial fulfillment of the requirement for the

Degree of Doctor of Philosophy in Mechanical and Aerospace Engineering

in the Graduate School of Syracuse University

August 2012

Copyright © 2012 Jianhua Zhao

Acknowledgements

Foremost I would like to thank Professor Jianshun Zhang, whose wisdom, kindness, and guidance help me to complete my PhD.

I would like to express sincere appreciation to Professor John Grunewald. He provides me the opportunity to study and work in Dresden University of Technology (DUT) to success my dissertation. From him I gained the state-of-the-art knowledge in building science.

I would like to thank Dr. Rudolf Plagge who gives me invaluable suggestion in terms of the theoretical background and experimental techniques in building physics.

Thanks to my colleagues in Syracuse, with whom I have a pleasure time.

I am grateful for my colleagues in DUT who assist my research in different aspects. Andreas Nicolai and Heiko Fechner advise and help me on the programming. Ulrich Ruisinger gives me the suggestion on the evaluation of the building performance. Gabriele Gärtner and Philips Heinz have the fruitful discussion with me on the research work. Frank Meißner supports me on the experimental data.

My parents deserve my deepest gratitude for their patience and support all the time.

Last but not least I would offer my regards and blessings to all of those who supported me in any respect during the completion of this dissertation.

Content

List of Figures

List of Tables

Chapter 1 Introduction

1.1 Background

Application of heat, air, and moisture (HAM) simulation to predict and assess the

hygrothermal performance of the building enclosure / assembly is widely used

nowadays. Such simulation helps the designer to understand how the construction

responds to the surrounding environments. Based on the hygrothermal analysis, the

designer can identify the possible performance problems, estimate the energy flow

through the enclosure, and optimize the design. A good knowledge of the HAM

modeling and the accurate input data are crucial to obtain reliable results. The models

describing heat, air, and moisture transport phenomena in the enclosure/ assembly

have been well developed in previous studies. However, there is a severe lack of

high-quality material data for the simulation use. Only a limited amount of material

data are available in current simulation tools. Therefore, a material database that

includes a great number of representative building materials on the market, and a

systematic approach to organize and characterize new materials for the purpose of

hygrothermal performance simulation are needed by both the developers and users of

the simulation tools.

A full material characterization requires detailed material properties, i.e., moisture

transport and storage data. Many international standards have been well established to

measure these properties, but full measurements are quite time-consuming and

laborious. Some tests, e.g., sorption isotherm, take several weeks. The long test period increases the experimental expense and prolongs the analysis process. Thus, a method is needed to simplify the measurement procedure while still maintaining acceptable data quality.

In the literature, there is much data that is not sufficiently complete or is of a low quality, e.g., including only basic parameters or incomplete material functions. Such data is not adequate for the purpose of simulation, but still can be considered a valuable resource. Therefore, an approach is required to qualify the incomplete material data to be used for the simulation.

In the simulation, the input variable normally comes from a design value, so called "best fit" data and the corresponding simulation is called a deterministic model. However, input variable is subject to uncertainty. For instance, the indoor humidity is influenced by many factors, e.g., ventilation rate and user behavior, and it is impossible to exactly describe it by a fixed function.

Uncertainty is the deviation from the design value, which is not accounted for by a deterministic model. In the field of building physics, the uncertainties arise from different aspects: material properties, workmanship, the climatic condition, etc.

The influence of the uncertainty in the input variable on the output variable can be assessed by altering one variable in each simulation, the so called differential method. With this method, the individual influence of an input variable can be identified. The

differential method is suitable in the case that the number of the input variable is small or the designate input variable is exactly known. But the interaction effects of all the input variables are not detected.

Alternatively, another method is to vary all or part of the variables simultaneously, the so called Monte Carlo simulation, where the overall influence of input variables is observed and evaluated. Uncertainties in the inputs are propagated to the output by the simulation model. The variation range and the distribution of the input variable will influence the possible span of the associated output variable. Therefore, the reliability of the input variable should be checked before other steps. e.g., is the correlation between the thermal conductivity and density reproduced in the samples?

The performance of a building construction may be assessed in many aspects, e.g., the durability, the thermal efficiency and mold growth risk. Moisture plays a crucial role in the damage of the construction and reduction of effective thermal insulation. The drastic variation of the moisture on the building façade could produce excessive stress and lead to surface crack and spalling. Moreover, mold often observed in the high moisture condition is harmful to residents. The uncertainties in the analysis inputs will have more or less impact on the performance evaluation.

A deterministic method lacks the ability to provide a reliable performance assessment in case the uncertainties in the inputs are accounted for. Thus, a probabilistic approach is preferred. In addition, the contributions of the input variables on the variation of the

output are not the same. It is necessary to identify the influential variables in the design stage, so the uncertainties in the influential input variables can be controlled in a limit range to improve the accuracy of the output of the simulation.

To fill the knowledge gaps, the present study was designed to answer the following specific research questions:

1) is there a modeling approach suitable to characterize a great number of materials for establishment of a comprehensive material database?

2) is it possible to quality the incomplete material data in the literature to be used for the simulation tools?

3) is there an approach able to simplify the procedure for the complex moisture storage measurements but still guarantee data quality and reliability?

4) how can a probabilistic approach can be developed and incorporated in existing hygrothermal tools to assess the hygrothermal performance of the building enclosure assemblies against different evaluation criteria?

1.2 Objectives and Scope of Research

The objectives and scope of this research are:

1. Establish a comprehensive material database with a great number of high-quality material data for use by hygrothermal simulation tools.

A systematic method was introduced to classify and characterize the materials. By applying this method, a great number of building materials were evaluated and characterized in different categories, including the anisotropic materials. The correlation matrixes of material parameters in different material categories were obtained based on the measurements of a number of the material data.

2. Develop an approach to simply the procedure for moisture storage measurements.

By the application of cluster analysis, the measured moisture storage data of 20 bricks and 47 plaster/mortars were aggregated into different clusters, respectively. Regression analysis was conducted to derive the relationships between moisture contents in the same cluster. By only measuring one moisture content, the others in the same cluster were predictable by the regression models. The relationships between moisture content and basic material parameters were explored.

3. Develop a novel approach to make use of the incomplete material data reported elsewhere so as to extend the material database.

A method to identify the material clusters, in which individual materials have similar characteristics, was developed. The criterion variables in the material clustering were defined. An approach to derive the generic material from the identified material cluster was developed. The generic material represents a type of the specific materials that have similar characteristics. A method to qualify the incomplete material data was developed by applying the generic material and regression analysis.

4. Develop a probabilistic approach to be incorporated into a current hygrothermal simulation tool to assess the hygrothermal performance of the building enclosure assemblies.

Different sources of uncertainties in the hygrothermal simulation were addressed. The uncertainties in the model parameters were quantified. The probability density functions of material parameters were explored. The relations between material parameters and between material parameters and material functions were discussed. Those relations were incorporated in the Latin hypercube sampling. A probabilistic approach was developed to assess the hygrothermal performance of the building enclosure assemblies against different evaluation criteria. Sensitivity analysis was performed to identify the influential variables against the output of interest.

1.3 Dissertation Organization

Chapter 2 reviews the fundamental knowledge in the heat, air, and moisture simulation. Existing models in terms of moisture storage and the moisture transport are introduced and compared. Current hygrothermal simulation tools are summarized in brief. Finally, the need to build a comprehensive material database for the simulation use is discussed.

Chapter 3 describes a systematic method to organize, classify, and characterize the materials. The experimental methods to measure the material properties and the modeling approach to derive material functions are introduced. A material database is

established to provide significantly more new material data in different material categories. The rank correlation matrixes of material parameters in different material categories are derived.

Chapter 4 presents the application of statistical methodologies in the hygrothermal material characterization. First, a method is developed to simplify the procedure for the moisture storage measurements of the building brick and plaster/mortar. Then, an approach to identify the material cluster from a set of material data is developed. Further, the method to derive generic material from the identified material cluster is introduced, for the purpose of qualifying the incomplete material data.

Chapter 5 describes the different sources of the uncertainty in the hygrothermal simulation. The uncertainties in the associated variables are quantified. Then, the probability density functions of material parameters are explored. Two sampling techniques are introduced. Finally, sensitivity analysis techniques suitably applied for this study are discussed and compared.

Chapter 6 presents a probabilistic approach that implements the propagation of uncertainty in the analysis inputs through the simulation model to the analysis output. The relationships between material parameters and between material parameters and material functions are discussed. Those relationships are incorporated in the Latin hypercube sampling. Different criteria for evaluating hygrothermal performance of the building enclosure assemblies are discussed.

Chapter 7 exemplifies the developed probabilistic approach to assess the hygrothermal performance of a retrofitted wall assembly in terms of durability, thermal efficiency and mold growth risk. The most influential variables against the specific performance evaluation criterion are addressed by applying sensitivity analysis.

Chapter 8 summaries the major conclusions in this research work and provides recommendations for the future work.

Chapter 2 Literature Review

In this chapter, basic knowledge of heat, air, and moisture transport in porous material is first reviewed. Then, moisture storage and transport phenomena are described and the modeling approaches are introduced. In the end, the available hygrothermal simulation tools are compared in brief and the necessity to build a comprehensive material database is discussed.

2.1 Heat, Air, and Moisture Transport in Porous material

2.1.1 Representative Elementary Volume

The structure of the pore system in a porous medium is complex and difficult to describe at the microscopic level. Alternatively, the spatial averaged quantities at the macroscopic level ignoring the actual geometry of the microscopic pore structure can be considered in modeling the physical phenomena. The continuum model describes the heat and mass transfer at the macroscopic level based on the Representative Elementary Volume (REV) approach, which replaces the microscopic geometrical and physical properties of the real porous medium by the macroscopic properties depending on the time and spatial coordinate (Descamps1997). The average of a quantity E in the phase of α over the REV is expressed as:

$$E_{REV}^{\alpha} = \frac{1}{V_{REV}} \int_{V_{REV}} \gamma(x) \cdot E^{\alpha} dV \qquad (2.1)$$

The integration over the entire spatial domain of the REV may include the portion where no phase α exists. So an indicator γ (x) is introduced, with the value of 1 if the position is within the phase of α and the value of 0 if not.

For a homogenous material, the selected size of the volume determines the variation of the properties. The smaller the selected volume, the larger variation in the properties. The size of the REV is typically related to the pore size distribution. The REV can be defined as the smallest volume at which the macroscopic value of a property is independent of the size, shape and the orientation of the volume (Bear 1975). By analogy with the REV, the representative elementary area (REA) is the minimum area needed so that measurements are independent of the sample size and account for spatial variations. Figure 2-1 shows a REV in solid, liquid and gas phases in a porous medium.

If the studied phase has a moving velocity relative to a stationary coordinate system, the density of a quantity E will be a function of both position and time, $\rho^{E(x,\,t)}$. The temporal change of the conserved quantity is:

$$\frac{d\rho^E}{dt} = \frac{\partial \rho^E}{\partial x}\frac{dx}{dt} + \frac{\partial \rho^E}{\partial t} \qquad (2.2)$$

If the REV is defined in a stationary reference system with a sufficiently small mean velocity of the selected phase, the velocity term dx/dt is set equal to zero and the REV becomes a "local system". The mathematical equations, introduced in the following sections, are based on the "local" REV.
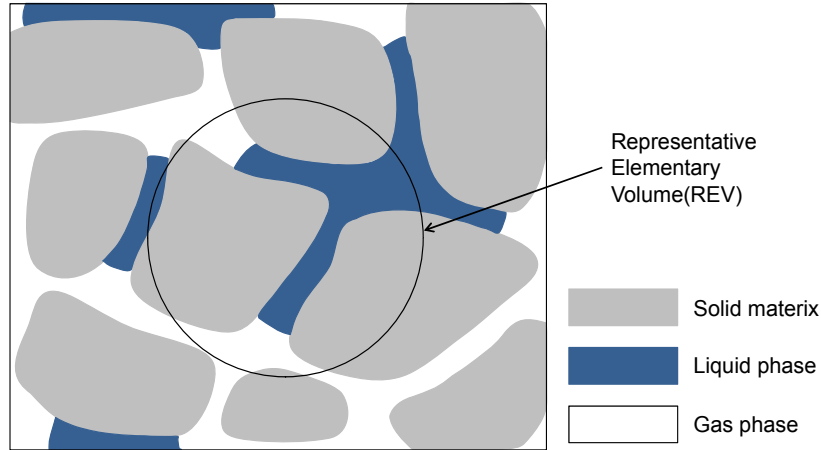
Figure 2-1 Representative Elementary Volume (REV) in a porous medium (consisting of impermeable solid matrix, liquid phase with water and soluble chemicals, and gas phase including dry air and water vapor)

2.1.2 Balance Equations

Balance equation is based on the fact that the rate of change in time of a conserved quantity within the REV must be equal to the sum of all the incoming and outgoing fluxes together with the source/sink production rates. Equation 2.3 gives the general form of the balance equation:

$$\frac{\partial \rho_{REV}^{E}}{\partial t} = -\frac{\partial}{\partial x_k}\left[\sum_i j_{k,i}^{E}\right] + \sigma_{REV}^{E},$$

(2.3)

where j is the quantity flux, E is the general quantity, k is the spatial coordinate index, i is the flux index (e.g., mass and energy), and σ_{REV}^{E} is the source/sink term of the quantity.

Some assumptions in the formulation of the heat, air, and mass balance equations should be noted.

- Distortions of the solid material matrix are neglected.

- The gas phase is incompressible and only the laminar gas flux is considered. The volume fraction of the gas phase is constant.

- The driving forces derived from the thermodynamics of gas mixtures are also valid in the REV.

- The conversion of kinetic energy of the gas phase to internal energy by compression and friction is neglected.

Moisture mass balance

Without ice formation, moisture exists in the phase of liquid water and water vapor. Therefore, the moisture mass balance equation is a merged two- phase equation. The moisture mass balance relates the rate of change of moisture mass density over time in REV to advective liquid water flux, advective water vapor flux, diffusive water vapor flux, as well as moisture generation source/sink.

$$\frac{\partial \rho_{REV}^{m_{l+v}}}{\partial t} = -\frac{\partial}{\partial x_k}\left[j_{k,adv}^{m_l} + j_{k,adv}^{m_v} + j_{k,diff}^{m_v} \right] + \sigma_{REV}^{m_{l+v}} , \tag{2.4}$$

where $\rho_{REV}^{m_{l+v}}$ is moisture density in REV (kg/m_{REV}^3), $j_{k,adv}^{m_l}$ is advective liquid water flux ($kg/m_{REA}^2 s$), $j_{k,adv}^{m_v}$ is advective water vapor flux ($kg/m_{REA}^2 s$), $j_{k,diff}^{m_v}$ is diffusive water vapor flux ($kg/m_{REA}^2 s$), and $\sigma_{REV}^{m_{l+v}}$ is moisture source/sink in REV ($kg/m_{REV}^3 s$).

Air mass balance

The air mass balance relates the rate of change of air mass density to the sum of net rate of advective and diffusive dry air flux, as well as source/sink of the dry air. In a

barycentric reference system, diffusive dry air flux and diffusive water vapor flux

have the same magnitude, but opposite direction. This balance equation is usually set

equal to zero since the air needs very short time to become constant in the porous

medium, compared to other quantities (e.g., temperature or moisture).

$$\frac{\partial \rho_{REV}^{m_a}}{\partial t} = -\frac{\partial}{\partial x_k}\left[j_{k,adv}^{m_a} - j_{k,diff}^{m_v} \right] + \sigma_{REV}^{m_a} , \qquad (2.5)$$

where $\rho_{REV}^{m_a}$ is mass density of dry air in REV (kg/m_{REV}^3), $j_{k,adv}^{m_a}$ is advective dry air

flux ($kg/m_{REA}^2 s$), $j_{k,diff}^{m_v}$ is diffusive water vapor flux ($kg/m_{REA}^2 s$), and $\sigma_{REV}^{m_a}$ is dry air

mass source/sink in REV ($kg/m_{REV}^3 s$).

Energy balance

Assuming temperature in the REV is at equilibrium in all phases, the energy balance

is associated to the heat flux conducted through the material matrix, the energy carried

by advective liquid water flux and advective gas flux (including dry air and water

vapor), as well as vapor diffusion flux. In addition, an external energy source/sink is

also included.

$$\frac{\partial \rho_{REV}^{u}}{\partial t} = -\frac{\partial}{\partial x_k}\left[j_{k,diff}^{Q} + h_l j_{k,adv}^{m_l} + h_g j_{k,adv}^{m_g} + (h_v - h_a) j_{k,diff}^{m_v} \right] + \sigma_{REV}^{u} , \qquad (2.6)$$

where ρ_{REV}^{u} is internal energy density in REV (J/m_{REV}^3), $j_{k,diff}^{Q}$ is conduction

(diffusive) energy flux ($J/m_{REA}^2 s$), h_l is specific internal energy of liquid water

(J/kg), h_g is specific internal energy of gas phase (J/kg), h_a is specific enthalpy

of dry air (*J/kg*), h_v is specific enthalpy of water vapor (*J/kg*), σ_{REV}^u is Energy

source/sink in REV ($J/m_{REV}^3 s$).

2.1.3 Constitutive Equations

Balance equations introduce several fluxes, which describe the transport of heat, air

mass, liquid water and water vapor in the porous material. These fluxes can be

defined by constitutive equations, expressed by the product of the driving force and

the associated transfer coefficient.

Heat transport

According to Fourier's law, heat flux by conduction is proportional to the temperature

gradient, given in equation 2.7.

$$j_{k,diff}^Q = -\lambda \cdot \frac{\partial T}{\partial x_k} , \qquad\qquad (2.7)$$

where λ (*W/m·k*) is the thermal conductivity of the material. Depending on the

moisture content level, λ is determined by the thermal conductivity of dry material

and thermal conductivity of liquid water. In addition, temperature condition of the

material may also have an influence on λ.

Air mass transport

The advective flux of the gas phase is related to the gas pressure gradient and the gas

permeability, K_g. In addition, the buoyancy or gravitational effect of the gas phase is

accounted for by the term $\rho_g g_k$..

14

$$j_{k,adv}^{m_g} = -K_g \cdot \left[\frac{\partial p_g}{\partial x} + \rho_g g_k \right] \qquad (2.8)$$

The advective air mass flux is specified by the product of dry air mass concentration in the gas phase and the advective flux of the gas phase.

$$j_{k,adv}^{m_a} = \rho_g^{m_a} j_{k,adv}^{m_g}, \qquad (2.9)$$

where $\rho_g^{m_a} = \dfrac{p_a}{p_a + p_v} \cdot \dfrac{R_v}{R_a}$ is dry air mass concentration in the gas phase (kg/kg), $j_{k,adv}^{m_g}$ is advective flux of the gas phase ($kg/m_{REA}^2 s$), p_v is partial pressure of water vapor in gas phase (Pa), p_a is partial pressure of dry air in gas phase (Pa), R_a is gas constant of dry air ($J/kg\cdot K$), R_v is gas constant of water vapor ($J/kg\cdot K$).

The diffusive air mass flux has the same magnitude as diffusive water vapor flux, but opposite direction.

Moisture mass transport

The total moisture flux in the porous material is comprised of advective liquid water flux, advective water vapor flux and diffusive water vapor flux.

Advective liquid water flux

As shown in Figure 2-2, when a narrow capillary is inserted into an open liquid container, the liquid level in the capillary is usually different from that in the container due to capillary force, which is the pressure difference between the gas phase and the liquid phase.

$$\alpha < 90 \qquad\qquad\qquad \alpha > 90$$
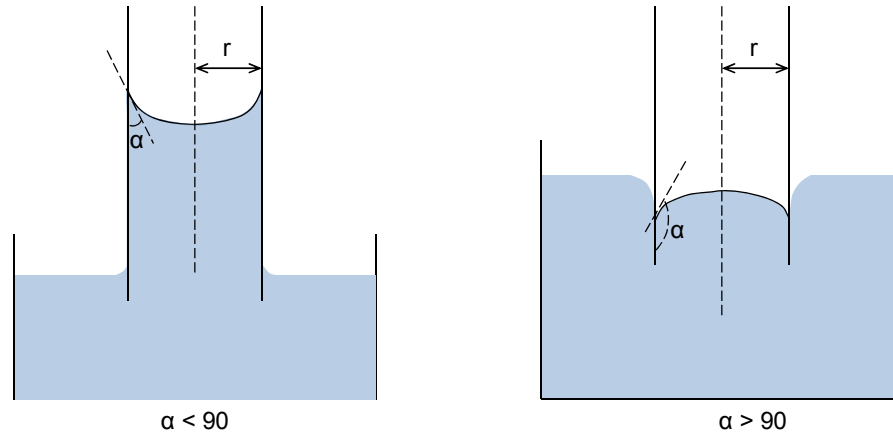
Figure 2-2 Schematic drawing of capillary phenomena in cylindrical capillaries

Young-Laplace equation defines the capillary pressure in a cylindrical capillary as a function of water surface tension σ_l, contact angle α and capillary radius r, given in equation 2.10 (The derivation of Young-Laplace equation is in Appendix A). Depending on the contact angle, the meniscus is either downwardly concave ($\alpha<90°$), e.g., water as the liquid in tube made of hydrophilic materials, or upwardly convex ($\alpha>90°$), e.g., mercury as the liquid or water as the liquid in a tube made of hydrophobic materials (e.g., most synthetics and water-repellent surfaces).

$$p_g - p_l = -p_c = \frac{2\sigma_l \cos(\alpha)}{r} \tag{2.10}$$

Above equation indicates that absolute value of capillary pressure increases inversely with the radius of the capillary. The larger the radius of capillary, the smaller capillary suction force. When the capillaries with different radii are connected to each other, the smaller capillaries with higher suction force will draw off the water out of the larger capillaries until their meniscus have the same radius of curvature or the larger capillaries are empty (Krus 1996).

Assuming isobaric condition in gas phase and no positive water pressure, the advective liquid water flux can be determined by the product of the liquid water conductivity and the gradient of capillary pressure.

$$j_{k,adv}^{m_l} = K_l(\theta_l) \cdot \left[\frac{\partial p_c}{\partial x_k} + \rho_l g_k \right], \tag{2.11}$$

where $K_l(\theta_l)$ is the liquid water conductivity (s), which is strongly dependent on the pore structure and moisture content level, as well as the temperature condition.

By employing the moisture content as the motive potential, the advective liquid water flux can be expressed by:

$$j_{k,adv}^{m_l} = -\rho_l \cdot D_l(\theta_l) \cdot \frac{\partial \theta_l}{\partial x_k}, \tag{2.12}$$

where $D_l(\theta_l)$ is liquid water diffusivity (m^2/s), which depends on moisture content level and character of the pore medium, ρ_l is liquid water density (kg/m^3).

Advective water vapor flux

The advective water vapor flux is determined by the concentration of the water vapor mass in the gas phase and the advective flux of the gas phase.

$$j_{k,adv}^{m_v} = \rho_g^{m_v} j_{k,adv}^{m_g}, \tag{2.13}$$

where $\rho_g^{m_v} = \frac{p_v}{p_a + p_v} \cdot \frac{R_a}{R_v}$ is water vapor mass concentration in the gas phase (kg/kg).

Diffusive water vapor flux

Under isobaric condition, according to Fick's law, water vapor diffusion can be described as a transport process proportional to the vapor pressure gradient. In case diffusion occurs in the free air, this process can be expressed by equation 2.14.

$$j_{k,diff}^{m_v} = -\frac{D_{v,air}}{R_v \cdot T} \cdot \frac{\partial p_v}{\partial x_k},$$
(2.14)

where $D_{v,air}$ is vapor diffusivity in still air (m^2/s).

Schirmer (1938) gives an empirical equation to account for vapor diffusivity in still air as a function of temperature and air pressure.

$$D_{v,air} = 2.306 \times 10^{-5} \cdot \frac{p_0}{p} \cdot (\frac{T}{273.15})^{1.81},$$
(2.15)

where p_0 is standard air pressure 101,325 (pa) and p is the ambient air pressure.

In the porous material, water vapor diffuses less than it does in the still air because of the resistance due to the tortuosity and porosity of the material. This phenomenon can be described by a factor called vapor diffusion resistance factor μ, which indicates how many times less vapor can diffuse through the material than through the still air. The vapor diffusion coefficient of a porous material is defined by:

$$D_{v,mat} = \frac{D_{v,air}}{\mu}$$
(2.16)

Substituting equation 2.16 into 2.14 yields the water vapor diffusion flux within a porous material.

$$j_{k,diff}^{m_v} = -\frac{D_{v,air}}{\mu \cdot R_v \cdot T} \cdot \frac{\partial p_v}{\partial x_k},$$
(2.17)

where $K_v = \dfrac{D_{v,air}}{\mu \cdot R_v \cdot T}$ is the water vapor conductivity/permeability (s).

2.2 Moisture Storage and Transport Characteristics

Moisture influences the stability and durability of the building constructions and it is considered one of the major factors leading to the building damages, e.g., the corrosion and condensation. In addition, mold growth, which is the harmful to the human health, is highly dependent on the moisture level. Moisture in building materials is mainly in the form of water vapor, liquid water or both of them. The study of moisture characteristics in porous material involves two aspects: moisture storage and moisture transport.

2.2.1 Moisture Storage Characteristics

Moisture storage characteristics demonstrate the ability of a building material to preserve the moisture that is in equilibrium with the surrounding environments.

Moisture storage in the pores can be characterized either by a potential of relative humidity $\theta(\varphi)$ or by a potential of capillary pressure $\theta(p_c)$, shown in Figure 2-3. Both potentials are connected by Kevin equation (2.18), which describes the change of the

free enthalpy of water vapor and liquid water due to the curved liquid/vapor interface. The derivation of this equation is in Appendix B.

$$p_c(\varphi) = -\rho_l \cdot R_v \cdot T \cdot \ln \varphi,$$ (2.18)

In addition, Young-Laplace equation (2.10) gives the relation between capillary pressure and pore radius, thus allows the connection between the moisture storage characteristics and pore volume distribution.
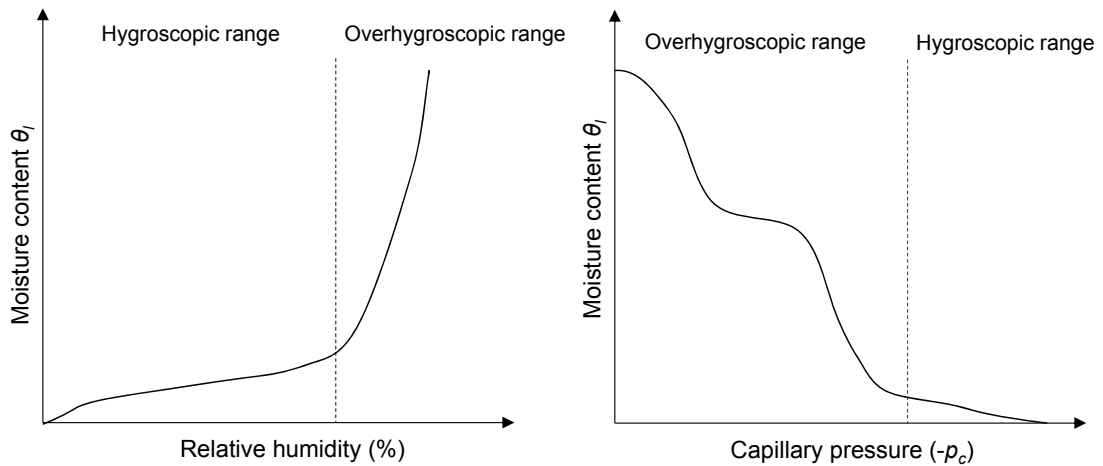
Figure 2-3 Moisture content as a function of relative humidity (left) and capillary pressure (right)

2.2.1.1 Moisture content range

Moisture content range is composed of two regions: the hygroscopic range and the overhygroscopic range.

- The hygroscopic range characterizes the moisture range up to a relative humidity of 95 to 98%. Determination of the equilibrium moisture content in this range is usually obtained by a sorption isotherm test.

- The overhygroscopic range follows the hygroscopic range and reaches up to the effective saturation moisture content. The moisture content sharply increases in this region and moisture in the porous material is mainly in the form of the liquid phase. The measurement of equilibrium moisture content can be achieved by a pressure plate test.

The moisture adsorption in a capillary-active porous medium can be described by a process in which this medium continuously reacts to the moist air, At roughly 15% relative humidity, a monomolecular coating is formed on the inner surface. As relative humidity increases, more molecules attach on the pore wall to form the multi-molecular layer. Up to 50% relative humidity, the multi-molecular coating linearly increases (Krus 1996). Further increases in the moisture level will lead to capillary condensation in small pores.

2.2.1.2 Hysteresis effect

Typically, moisture storage characteristics are different in the adsorption and desorption process. The moisture difference between two processes is caused by the hysteresis effect due to many factors. Besides other factors, three major effects are pore space geometry, air entrapment and contact-angle. Pore space geometry can produce the so called ink-bottle effect, which is due to structural differences in the pore diameter and shape, resulting in a moisture content difference in the adsoprtion and desorption process. Entrapped air in the pore reduces the ability of a porous

medium to contain moisture. And finally, the contact angle determines a material's

ability to produce an advancing and a receding water front at the solid-liquid

interface. In addition, sorption history is also important to determine the present

moisture content in the material.

2.2.1.3 Moisture retention function

Moisture storage characteristics can be described by a moisture retention function,

which is able to connect and smooth the scattered measured data to form a continuous

and complete curve. The closed-form retention function is widely used. The number

of function or modality is determined from pore volume distribution. The functional

parameters are adjusted to fit the measured data.

The moisture retention function was originally developed in soil science. Van

Genuchten (1980) introduced a uni-modal function to characterize the moisture

retentions of the soils. Based on Van Genuchten model, Durner (1994) proposed a

multi-modal function. Those functions are applicable in building physics. In addition,

several functional approaches are well developed to describe the moisture storage

characteristics of building materials (Künzel 1995; Carmeliet 2002; Häupl 2003;

Grunewald 2003).

The moisture potential in the model can be either relative humidity, or capillary

pressure, or both of them. Carmeliet et al. (2002) compared different functions to the

measured data and found that the multi-modal function can achieve better accuracy

than the uni-modal function. With more modals in the function, the required

functional parameters also correspondingly increase. So the appropriate number of

modals needs to be decided with the consideration of the accuracy of fitness and the

number of parameters.

Different moisture retention functions are summarized in Table 2-1. The same

notation is used to represent the moisture content although different authors use their

respective symbols in the model. The multi-modal model from Durner (1994) requires

the iterative adjustment of parameters to minimize the difference between the fitted

values and measured data. The weighted sum of Gauss distribution functions from

Grunewald et al. (2003) can well fit the measured data in the whole moisture content

range, and the parameters in the functions can be easily determined according to the

measured moisture storage data.

Table 2-1 Moisture retention functions and their descriptions

Authors	Function	Description
Van Genuchten (1980)	$\theta(p_c) = \theta_r + \dfrac{\theta_s - \theta_r}{\left[1 + (\alpha P_c)^n\right]^m}$ with $m = 1 - 1/n$	Uni-modal model used for the approximation of the moisture retention curve. Not flexible for the multi-pore material
Durner (1994)	$\theta(p_c) = \dfrac{\theta - \theta_r}{\theta_s - \theta_r} = \sum\limits_{i=1}^{k} w_i \left[1 + \left|\alpha_i p_c\right|^{n_i}\right]^{-m_i}$ With $\sum w_i = 1$, $m_i + 1/n_i = 1$	The related n and m cannot provide a unique value. Not well fit in the hygroscopic range
Künzel(1995)	$\theta = \theta_{cap} \cdot \dfrac{(b-1)\varphi}{b - \varphi}$	Uni-modal model used for the approximation of the moisture retention curve. Not flexible or accurate

Carmeliet (2002)	$\theta = \theta_{\lim} \varphi^n + (\theta_{cap} - \theta_{\lim}) \cdot$ $\left[1 + \left(\alpha \cdot p_c\right)^m\right]^{-(1-1/m)}$	Two driving forces in different moisture ranges, the parameter θ_{lim} is difficult to define
Grunewald et al. (2003)	$\theta_l(pC) = \sum_{i=1}^{N} \left[\frac{\Delta\theta_i}{2} \left(1 + erf\left(\frac{pC_i - pC}{\sqrt{2}S_i} \right) \right) \right]$	Every parameter has a physical meaning and can be directly estimated from measurements. Well fit in the whole moisture content range
Häupl and Fechner (2003)	$\theta(p_c) = \sum_{j=1}^{m} \left(1 + \left(\pi \frac{r_{oj}}{4\sigma} \cdot p_c \right)^4 \right)^{-1/2} w_{sj}$ or $\theta(p_c) = \sum_{j=1}^{m} \left(1 - \left(1 + \left(\frac{2\sigma}{p_c R_j} \right)^2 \right)^{1-nj} \right) w_{nj}$	Accurately describes the moisture storage in the whole range, but requires knowledge of the pore radius

2.2.2 Moisture Transport Characteristics

Moisture transport in porous material involves different mechanisms from the dry region into the saturation region. In the hygroscopic range with a low relative humidity, water vapor diffusion is the only form of moisture transport. As relative humidity increases, capillary condensations in the small pores form the liquid short-cuts, which enhance water vapor diffusion. Thus, water vapor transport still dominates moisture transport. As moisture content further increases, previously isolated liquid short-cuts are connected to form a continuous liquid water phase. As a consequence, the available space in pore structure for water vapor diffusion is dramatically reduced. Liquid water transport starts to dominate moisture transport. When moisture content reaches the effective saturation, the connected pores are entirely filled with liquid water and there is no path for water vapor diffusion.

The methods to measure and model water vapor and liquid water transports in porous material are summarized as follows.

2.2.2.1 Water vapor transport

Water vapor transport consists of advective and diffusive water vapor transports. The advective water vapor transport has a minor contribution to the whole moisture transport due to the low air permeability of most building materials. It is usually neglected unless highly permeable materials are used (i.e., fiberglass insulation batt). Thus, water vapor transport in the porous material is mainly by diffusion. The diffusive water vapor flux in the porous material is given in equation 2.17.

The water vapor transmission test is used to measure the water vapor diffusion rate under different humidity conditions under specific temperature.

2.2.2.2 Liquid water transport

The liquid water transport can be described as a diffusivity method with moisture content as the driving potential, or as a conductivity method with capillary pressure as the driving potential.

Liquid water diffusivity

With moisture content as the governing variable, one-dimensional liquid transport in porous medium under isothermal conditions can be expressed by a nonlinear diffusion equation.

$$\frac{\partial \theta_l}{\partial t} = \frac{\partial}{\partial x}(D_l(\theta_l)\frac{\partial \theta_l}{\partial x}),$$ (2.19)

where $D_l(\theta_l)$ is the liquid water diffusivity as a function of moisture content (m^2/s).

The determination of liquid water diffusivity requires the moisture content profile, which can be obtained from either water absorption or drying test. Currently, many non-destructive techniques are available to obtain the transient moisture content profile, e.g., gamma-ray attenuation method or nuclear magnetic resonance.

Once the moisture content profile is known, with the application of the Boltzmann transformation $\lambda = x/\sqrt{t}$, equation 2.19 can be reduced to an ordinary differential equation:

$$2\frac{d}{d\lambda}(D_l(\theta_l)\frac{d\theta_l}{d\lambda}) + \lambda\frac{d\theta_l}{d\lambda} = 0$$ (2.20)

With initial and boundary conditions: $\theta_l = \theta_0$ for $\lambda \to \infty$; $\theta_l = \theta_{cap}$ at $\lambda = 0$.

Equation 2.20 has only one solution: the characteristic curve. All moisture profiles collapse to form only a single curve in the $\theta(\lambda)$ scale. The moisture profiles in a calcium silicate plate during water absorption test and the corresponding Boltzmann transformed data are shown in Figure 2-4 (Carmeliet 2004).

The moisture diffusivity from water absorption test can be determined by integrating equation 2.20 with respect to λ:

$$D_l(\theta_l) = -\frac{1}{2}\frac{d\lambda}{d\theta_l}\int_{\theta_0}^{\theta_l}\lambda d\theta_l'$$ (2.21)
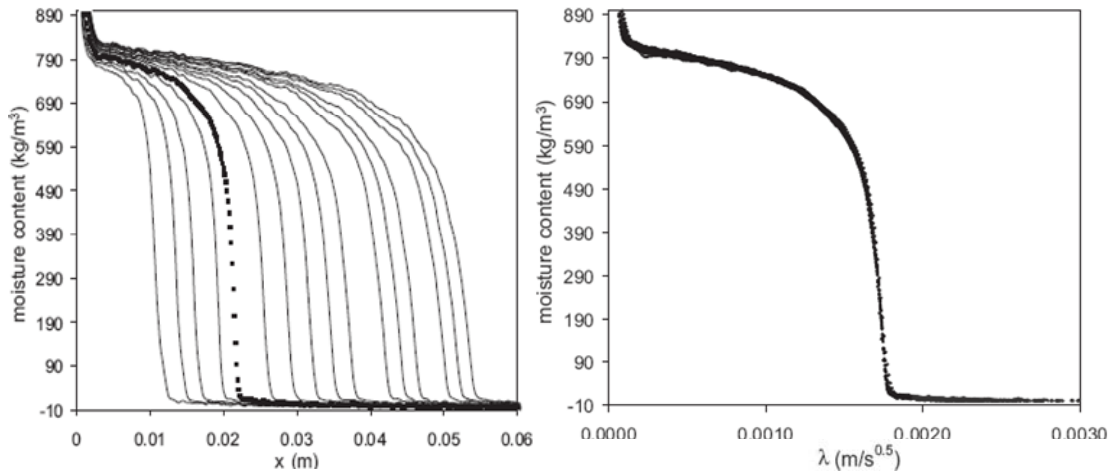
Figure 2-4 Moisture content profiles in the calcium silicate plate subjected to water absorption test (left) and the corresponding Boltzmann transformed data (right) (Carmeliet 2004)

Roels et al. (2004) compared six different non-destructive techniques (the NMR-technique, the MRI technique, the γ-ray attenuation technique, the capacitance method, the X-ray projection method, and the TDR-technique) to analyze moisture flux in the calcium silicate plate and ceramic brick by scanning their moisture content profiles during water absorption tests. Carmeliet et al. (2004) analyzed the uncertainty in determination of the liquid water diffusivity using the Boltzmann transformation method and proposed a methodology to improve the accuracy of the liquid water diffusivity from moisture content profiles measured in a water absorption test.

The measurement on moisture content profile is quite sophisticated and time-consuming. Many researchers pursued simple approaches to approximate the liquid water diffusivity.
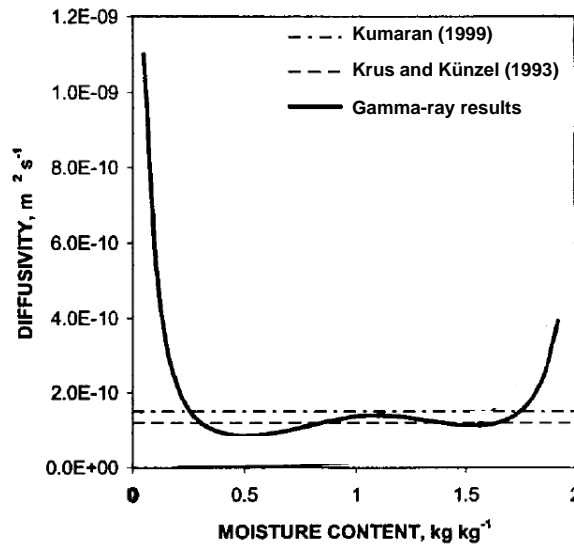
Figure 2-5 Approximation of average liquid water diffusivity by basic parameters from water absorption test (modified graph from Kumaran 1999)

As presented in Figure 2-5, Kumaran (1999) compared the liquid water diffusivity calculated from simple water absorption measurements with the values determined by sophisticated methods (e.g., the gamma-ray method), and drew the same conclusion as krus and Künzel (1993): the liquid water diffusivity calculated from water absorption coefficient together with capillary saturation moisture content can give a good approximation of the magnitude of the average liquid water diffusivity. The drawback of this approximation is that the calculated diffusivity is a constant value, independent on the moisture content.

The liquid water diffusivity can be parametrically described by exponential functions. Several functions have been proposed during the last few decades (Künzel 1995; Pel 1995; Krus and Holm 1999; Häupl and Fechner 2003; Carmeliet 2004). Most functions used capillary saturation moisture content and water absorption coefficient to derive the moisture dependent liquid water diffusivity. Scheffler et al. (2007)

compared different liquid diffusivity functions by using simulations to reproduce the water absorption and drying tests. He found that for a material with a separate pore system most functions could catch the process of the first stage of water absorption but deviate from the second stage of water absorption and the drying process (Figure 2-6). There are no universal parameters suitable for all the functions.
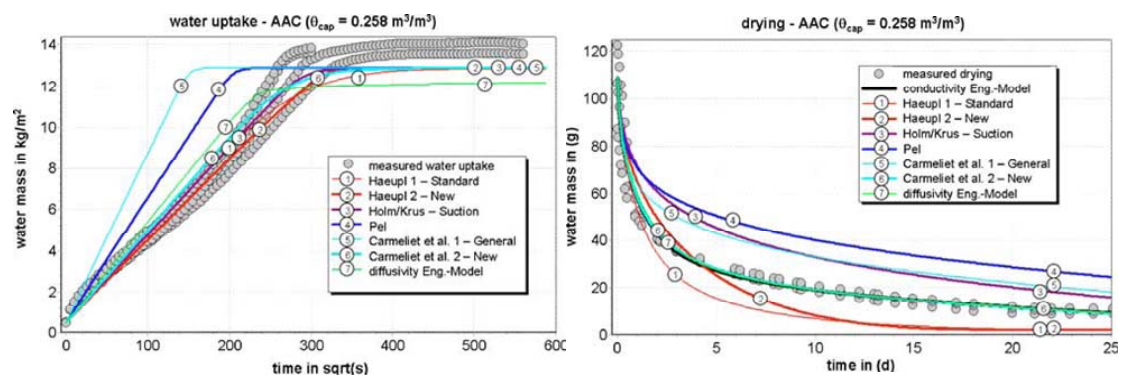
Figure 2-6 Comparison of measured and calculated water absorption (left) and drying (right) behaviors by different diffusivity functions for aerated concrete (Scheffler et al. 2007)

The moisture diffusivity is the sum of liquid water diffusivity and water vapor diffusivity. The moisture diffusivity exhibits a non-linear decrease in a lower moisture content range and reaches the lowest value at the transition point, where moisture transport dominated by water vapor becomes moisture transport dominated by liquid water. Further increase of moisture content leads to a quasi-exponential increase of moisture diffusivity (Carmeliet 2004). Some authors found that a single exponential function cannot accurately describe the moisture diffusivity in the whole moisture range, so two or more exponential functions are suggested in the different moisture content ranges (Descamps 1997; Brocken 1998; Carmeliet 2004).

Liquid water conductivity

Unlike the diffusivity method, the determination of liquid water transport by the conductivity method requires the knowledge of moisture storage characteristics. The conductivity method is widely applied in soil science (Van Genuchten 1980; Durner 1994): A relative liquid conductivity is first derived from the moisture retention curve. By adjusting this relative liquid conductivity to match measured data at reference saturation moisture content, the absolute conductivity function in the whole moisture content range is obtained. This approach usually overestimates the liquid water conductivity in the lower moisture content range.

Carmeliet et al. (1999) proposed a multi-scale network approach to derive liquid water conductivity of porous building materials covering the hygroscopic and overhygroscopic ranges under isothermal conditions. This method applied standard experiments to model the combined liquid water and water vapor transfer over a wide saturation range. The network approach used the water vapor permeability of dry material as the matching value to scale the relative conductivity function to an absolute value. The maximal conductivity is adjusted to match the liquid water inflow rate determined from the water absorption test. This method can model the hysteresis effect due to the air entrapment. However, the calculation process performed by employing network approach is quite complicated and requires much effort. So it is not appropriate for characterizing a large amount of materials to establish a material database.

Grunewald et al. (2003) introduced an engineering model in which the pore domains in the medium were separated into a serial-structured pore domain and a parallel-structured pore domain. The water vapor and liquid water had different transport characteristics in these two structured pore domains. For a medium with the volume larger than the REV, the water vapor diffusivity was dependent on the moisture content, the ratio of the serial-structured pore volume to the parallel-structured pore volume, as well as the water vapor diffusion resistance factor. The relative liquid water conductivity function governed by capillary pressure gradient was first derived through the bundle of tubes model. The absolute conductivity function is then obtained by matching the relative curve to the conductivity at effective saturation moisture content.

Scheffler (2007) extended Grunewald's work and developed a mechanistic model which allowed the flexible adjustment of liquid water conductivity and water vapor diffusivity in the whole moisture content range by some standard experiments, e.g., water absorption and drying tests.

Links between liquid water conductivity and diffusivity

Liquid water diffusivity can be transformed from liquid water conductivity with the application of reversed moisture retention curve.

$$D_l(\theta_l) = \rho_l^{-1} \cdot K_l(\theta_l) \cdot \left| \frac{dp_c(\theta_l)}{d\theta_l} \right|, \qquad\qquad (2.22)$$

where $\left|\dfrac{dp_c(\theta_l)}{d\theta_l}\right|$ is determined by the derivative of the reverse moisture retention

curve.

It needs to be noted that the quality of the derivative of the reverse moisture retention

curve is dependent on the methods of spline interpolation between the measured

moisture contents (e.g., linear spline and exponential spline). In addition, the spline

interpolation may lead to some numerical problems. For instance, the nearly vertical

interpolation performed between the measured moisture contents in Figure 2-7 would

yield extreme values in equation 2.22.
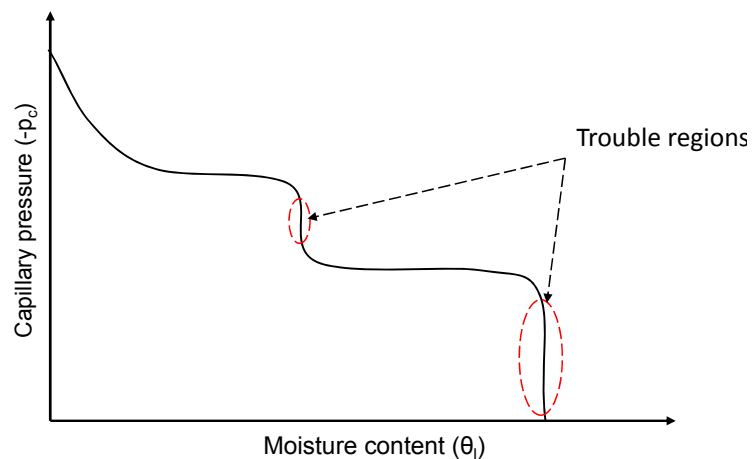
Figure 2-7 Spline interpolation between the measured moisture contents yielding numerical problem

2.3 HAM Modeling Tools and the Need to Build a Comprehensive Material Database

Currently, there are many HAM modeling tools available for the users to predict

hygrothermal performance of building enclosure assemblies. Some of them can only

deal with one-dimensional simulation, while others have the ability to run two- and

three-dimensional simulations. Those models are different on the driving potentials (vapor pressure, relative humidity, moisture content or capillary suction stress), numerical techniques (finite control volume or finite elements), flow type (steady-state, quasi-static or dynamic), discretization strategies, time integration, etc. Woloszyn and Rode (2008) and Ramos et al. (2010) reviewed current hygrothermal modeling tools available for the public, i.e., IDA-ICE, HAM-Tools, HAMLab, MOIST, MATCH, hygIRC-1D, WUFI-plus, DELPHIN, and summarized their capabilities and limitations.

Material modeling plays an important role in the analysis of the hygrothermal performance of the building enclosure assemblies. The requirement on the quality of material data is dependent on the models and assumptions adapted in the simulation tools. For the model with the application of Glaser method, capillary moisture transport and moisture dependent material properties are ignored. The more complex the material modeling approach, the higher requirement on the material data quality. To acquire a high quality material data requires a large amount of measurements, and the corresponding cost will increase. Thus, currently, only a limited number of material data are available in the simulation tools. Often, it is hard to find an appropriate material for the simulation. On the other hand, indiscreetly choosing a material from the built-in material database of the simulation tools will reduce the reliability of the simulation result.

Different tools may employ distinct modeling approaches, i.e., for liquid water transport, some tools use diffusivity method assuming liquid transport is driven by moisture content gradient, while others use the conductivity method assuming liquid transport is driven by capillary pressure gradient. This increases the encumbrance to share material data between different laboratories or simulation tools. Moreover, material functions in the simulation tools are only given as a curve in the graph, and the detailed values usually cannot be assessed by the user.

So far, only a few project (Annex24 1996; MASEA 2007) and researchers are committed to the development of a material database (Grunewald et al. 2002; Ramos et al. 2012). However, the number of the studied materials is still inadequate. A comprehensive material database containing most of the widely used building materials on the market is urgently required.

2.4 Summary

The fundamental knowledge of heat, air, and moisture transport in the porous material was reviewed. A good understanding of those phenomena enables a better explanation on the hygrothermal response of the building constructions.

Different material models in terms of the moisture storage and moisture transport were reviewed and compared. Most models need either too many parameters or the parameters that are hard to define. To be able to evaluate a large number of materials for establishing a comprehensive material data, a material modeling approach should

be easily implemented and its parameters should be easily defined according to simple measurements.

The material database project, up until this point, lacked a systematic method to classify and identify the materials, and there are no consistent standards to evaluate and characterize the materials.

Various simulation tools have been developed in the last three decades. Many new features have been implemented to deal with more complex problems. However, the upgrade on material database seems to be lagging behind, which limits the usability and capability of the simulation tools. An advanced HAM modeling tool should include enough material data for use.

The above mentioned issues will be addressed in Chapter 3. A systematic approach is introduced to organize, classify and characterize the materials.

Chapter 3 Establishment of a High Quality and Comprehensive Material Database

3.1 Introduction

A coupled heat, air, and moisture simulation relies on the proper input data. Besides climatic conditions, boundary conditions and contact conditions between different construction layers, high quality material data are crucial to obtain the reliable result. Material data are composed of two aspects: basic data and functionalized data. Basic data include some single parameters, e.g., density and thermal conductivity. Functionalized data presents an amount of values derived from material models, e.g., the moisture retention curve.

This chapter starts from the introduction of material data organization, followed by the description of experimental methods to obtain material properties. Subsequently, a modeling approach to derive material functions in the full moisture range and corresponding calibration process are illustrated. By the application of the above procedure, a material database with a great number of high quality material data is established for the simulation use.

3.2 Material Data Organization

3.2.1 Material Category

In addition to material properties, the material identification information, e.g., its category and the producing method, gives insight into a material's natural characteristics. Such information should be included in the material data file. One example is presented in Figure 3-1.

Identification	English	German	French
Category 1	03		
Category 2			
Category 3			
Producer	Wienerberger		
Material Name	Brick Wienerberger	Ziegel Wienerberger	Brique Wienerberger
ProdID			
ProdMethod	extruded		
Charge/Batch			
ProdDate	2000		
Investigator	IBK TU Dresden		
SampleID	TW-NMZ		
Sampling	randomly selected		
SamplingDate	10. Jul. 2002		

Figure 3-1 Material identification information

Good data organization is convenient to quickly search and investigate materials. For easy organization, each material is classified into certain material categories. Table 3-1 lists total thirteen material categories.

Comparing to the Masterformat (CSI 2011), which assorts the materials according to their roles in the construction, this category list more straightforwardly classifies the building materials by their natural characteristics, as well as their usages. Each material will be assigned to at least one but no more than three categories. For instance, in Figure 3-1, category number 03 in Category1 indicates brick Wienerberger is allocated to the building brick category. Calcium silicate board

belongs to both the insulation material category and building board category, thus

category number 06 and 07 will be written in Category1 and Category2, respectively.

Table 3-1 Material category for data organization

Category	Material description
01	Coating
02	Plaster/ mortar
03	Building brick
04	Natural stone
05	Cement containing building material
06	Insulation material
07	Building board
08	Wood
09	Natural material
10	Soil
11	Cladding panel and ceramic tile
12	Foil and waterproofing product
13	Miscellaneous

3.2.2 Material Data Level

Three material data levels are defined according to the different data processing

stages.

- Raw data: measured laboratory numbers from each single specimen. No data

  processing involved.

- Summary data: statistical data with mean, standard deviation, maximum and

  minimum values calculated from the raw data. Summarized in one data sheet.

- Functionalized data: processed summary data by application of material

  characterization models. Used for simulation.
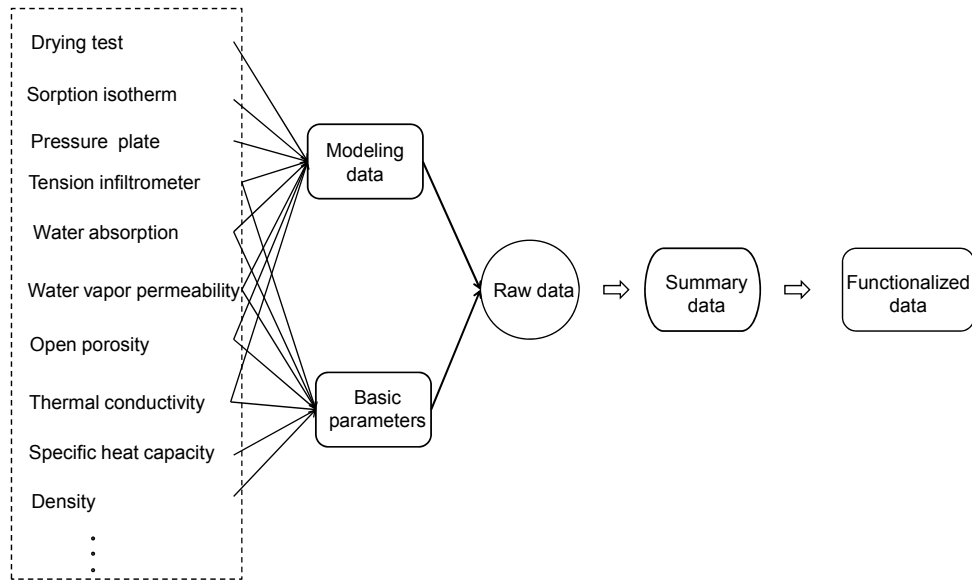
Figure 3-2 Flow chart of material data processing

The flowchart of material data processing is shown in Figure 3-2. To acquire

complete material data for characterization requires a set of measurements. Some

measurements aim to obtain basic parameters, e.g., thermal conductivity and specific

heat capacity, while others are designed for further material modeling, e.g., water

absorption and drying test. First, the raw data from each measurement is written into

an individual excel sheet, which includes the detailed experimental information, e.g.,

dimension of the specimen, measured temperature and relative humidity, the weight

loss or gain over time. The necessary data processing to obtain the statistical summary

data for the material characterization are implemented in those individual sheets.

Then, the summary data (mean, maximum, minimum and standard deviation) from

the individual sheet is extracted and collected in one summary sheet. The data

summary sheet of brick Wienerberger is exemplified in Figure 3-3.

Hygrothermal basic parameters							
Parameter	Symbol	Unit	Mean	StdDev	Min	Max	Remarks
Bulk density	ρ	[kg/m³]	1786.2	9.3	1770.7	1805.2	
Specific heat capacity	c	[J/kgK]	889	10.8	872	901	
Thermal conductivity	λ_{dry}	[W/mK]	0.548	0.042	0.492	0.612	
Open Porosity	θ_{por}	[m³/m³]	0.354	0.003	0.347	0.359	
Capillary saturation	θ_{cap}	[m³/m³]	0.262	0.004	0.259	0.267	
Dry cup value	μ_{dry}	[---]	18.01	0.32	17.78	18.24	
Water absorption coefficient	A_w	[kg/m²s$^{0.5}$]	0.199	0.015	0.181	0.209	

Water Retention (Desorption)

Arguments		Mean	StdDev	Min	Max	Remarks
pc [hPa]	T [°C]	θ_l [m³/m³]				
0	20.0	0.319	0.005	0.308	0.323	
50	20.0	0.301	0.005	0.295	0.310	
100	22.3	0.299	0.005	0.294	0.308	
300	18.5	0.291	0.006	0.285	0.303	
600	14.0	0.275	0.007	0.269	0.287	
1000	21.8	0.265	0.007	0.258	0.278	
2000	23.5	0.209	0.013	0.187	0.228	
3000	22.0	0.172	0.013	0.148	0.196	
4000	22.7	0.143	0.011	0.123	0.160	
10000	22.9	0.103	0.009	0.086	0.113	
14000	20.5	0.075	0.009	0.060	0.088	

Sorption Isotherm (Desorption)

Arguments		Mean	StdDev	Min	Max	Remarks
φ [%]	T [°C]	θ_l [m³/m³]				
96.9	21.4	0.033	0.007	0.024	0.045	
96.0	22.4	0.026	0.006	0.018	0.035	
90.0	20.2	0.019	0.004	0.014	0.023	
84.3	22.9	0.016	0.003	0.013	0.019	
75.2	21.4	0.010	0.001	0.008	0.012	
57.6	22.4	0.006	0.000	0.005	0.007	
43.2	20.2	0.004	0.000	0.004	0.004	
32.8	22.2	0.002	0.001	0.000	0.003	

Water vapor permeability

Arguments		Mean	StdDev	Min	Max	Remarks
φ_{inside} [%]	$\varphi_{outside}$ [%]	μ [-]				
5.0	37.0	18.01	0.32	17.78	18.24	DryCup
84.0	53.0	12.04	2.18	10.50	13.58	Wetcup

Liquid water conductivity

Arguments		Mean	StdDev	Min	Max	Remarks
θ_l [m³/m³]	mean pc [Pa]	K_l [s]				
0.304	8560	2.0E-09	3.1E-10	1.5E-09	2.3E-09	

Sorption Isotherm (Adsorption)

Arguments		Mean	StdDev	Min	Max	Remarks
φ [%]	T [°C]	θ_l [m³/m³]				
32.8	20.40	0.00050	0.00019	0.00021	0.00071	
43.2	24.20	0.00123	0.00019	0.00091	0.00144	
57.6	20.60	0.00180	0.00034	0.00121	0.00213	
75.2	20.40	0.00267	0.00043	0.00195	0.00308	
84.3	24.20	0.00488	0.00055	0.00372	0.00547	
90.0	20.60	0.00630	0.00048	0.00554	0.00708	
96.0	20.60	0.00901	0.00086	0.00808	0.01029	

Figure 3-3 Data summary sheet of brick Wienerberger

Thereafter, the summarized data is imported into material models for generating functionalized data. In this step, the discrete measured data is interpolated to continuous functions, e.g., the measured data from the pressure plate and sorption isotherm tests are used to generate a continuous moisture retention curve (MRC). Furthermore, an iterative calibration process is conducted to derive moisture transport functions. The detailed description of this process is introduced in Section 3.4.3.

3.3 Experimental Methods

A set of international standards have been developed to measure the building materials properties, including:

• Bulk density, matrix density and porosity: DIN ISO 11272 (2001)

• Thermal conductivity: ASTM C177 (2010), ASTM C518 (2010) and DIN EN 12664 (2001)

• Hygric sorption isotherm: ASTM C1498 (2004) and DIN EN ISO 12571 (2000)

• Water retention by pressure plate: ASTM C1699 (2009)

• Water vapor tranmission: ASTM E96 /E96M (2010) and DIN EN ISO 12572 (2001)

• Water absorption coefficient: DIN EN ISO 15148 (2003)

In addition to these well described standards, the HAM modeling tools may require extra tests to acquire high quality data input. Some complementary tests, together with the standard procedures mentioned above, are introduced in the following sections.

3.3.1 Moisture Storage Measurement

Moisture storage capacity of porous building materials is used to describe the amount of moisture accumulated in the material pores at the consecutive environmental conditions. In general, it can be achieved by two tests: sorption isotherm measurement in the hygroscopic range and pressure plate measurement in the overhygroscopic range.

3.3.1.1 Sorption isotherm measurement

Measurement of moisture content in the hygroscopic range is implemented by

standardized isothermal adsorption and desorption methods (ASTM C1498 2004;

DIN EN ISO 12571 2000). Sorption isotherm measurement provides insight into the

relationship between relative humidity (RH) and the equilibrium moisture content of

material at a specified temperature. The apparatus overview is given in Figure 3-4.

For an adsorption measurement, an initially oven dried specimen is conditioned in the

desiccator chamber with a defined relative humidity level under constant temperature

until the static sorption equilibrium is attained between relative humidity in the

desiccator chamber and moisture content of the specimen. The specimen is placed

consecutively in a series of desiccator chambers from a low humidity level to a high

humidity level. For a desorption process, a similar procedure is applied except that the

highly moistened specimen is placed consecutively in a series of desiccator chambers

with humidity levels that range from high to low. Relative humidity in the desiccator

chamber is achieved by saturated salt-in-water solutions (ASTM E104-02 2007). The

saturated salt-in-water solutions and corresponding relative humidity levels are listed

in Table 3-2.

Equilibrium between moisture content and relative humidity is attained when three

successive weightings, at intervals of 24 hours, show a difference in mass less than

0.1 %. The equilibrium moisture content by volume is determined by equation 3.1.

$$\theta = \frac{(m - m_0)}{m_0} \cdot \frac{\rho}{\rho_l},$$ (3.1)

where m is the mean mass of the specimen at equilibrium (kg), m_0 is the weight of dry specimen (kg), ρ_l is the density of liquid water (kg/m^3), and ρ is the density of the specimen (kg/m^3).

Ventilation fan
Humidity sensor

Figure 3-4 Desiccator chambers with the saturated salt-in-water solution

Table 3-2 Saturated salt-in-water solutions and corresponding relative humidity levels

Saturated salt-in-water solution	Relative humidity (%)
Potassium sulphate (K_2SO_4)	97.4
Potassium dihydrogen phosphate (KH_2PO_4)	96.0
Barium chloride ($BaCl_2$)	90.0
Potassium chloride (KCl)	84.7
Sodium chloride (NaCl)	75.4
Sodium bromide (NaBr)	58.2
Potassium carbonate (K_2CO_3)	43.2
Magnesium chloride ($MgCl_2$)	32.9

3.3.1.2 Pressure plate measurement

The pressure plate extractor measures the equilibrium moisture content at high relative humidity levels that cannot be achieved by sorption isotherm (ASTM C1699 2009). The pressure plate extractor and porous ceramic plate are shown in Figure 3-5.

Figure 3-5 Pressure plate extractor (left) and porous ceramic plate with specimens (right)

Pressure plate extractor carries out a desorption measurement. The measurement gives the relationship between equilibrium moisture content and corresponding capillary potential. Relative humidity and capillary pressure can be converted to each other by using Kelvin equation (2.18). The specimen is first effectively saturated by leaving it in contact with water for a long time, e.g., two weeks, until the entrapped air in the pores is dissolved in water. A fine kaolin paste is applied on the surface of the water-saturated ceramic plate to improve hydraulic contact between the specimen and plate. One layer of acetate cloth is placed on the top of kaolin to prevent the kaolin from sticking to the specimens. After pressing the specimen on the ceramic plate and closing the chamber, an overpressure is applied to extract the water out of the specimen until the equilibrium between moisture content of the specimen and the overpressure is achieved. The equilibrium moisture content of the test specimen is determined gravimetrically and calculated by equation 3.1. With the application of different overpressures in the extractor, the successive equilibrium moisture contents can be attained.

In Figure 3-6, the desorption data measured by pressure plate and sorption isotherm tests can form a continuous curve. The adsorption data is only measurable through a sorption isotherm test in the hygroscopic range.
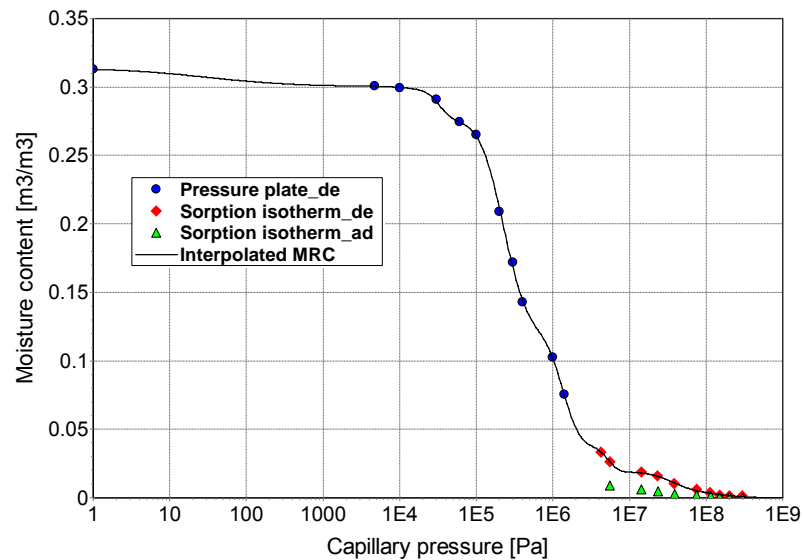
Figure 3-6 Measured moisture contents from pressure plate and sorption isotherm tests

3.3.2 Moisture Transport Measurement

In this section, experimental measurements that give insights into the moisture transport mechanisms in different moisture content ranges are introduced, including water vapor transmission test, water absorption, drying test, the unsaturated liquid water conductivity measurement and saturated liquid water conductivity measurement.

3.3.2.1 Water vapor transmission test

Water vapor transmission test is used to measure the steady water vapor flow through a unit area of the material at a unit of time under specific temperature and humidity conditions.

The specimen is placed at different humidity conditions to get the knowledge of vapor diffusion rate within the material. The desiccant method, also called dry-cup test, uses the desiccant in the cup as the vapor sink. The water method, also called wet-cup test, uses distilled water (ASTM E96/E96M 2010) or salt-in-water solution (DIN EN ISO 12572 2001) in the cup as the vapor source. The experiment apparatus is showed in Figure 3-7.
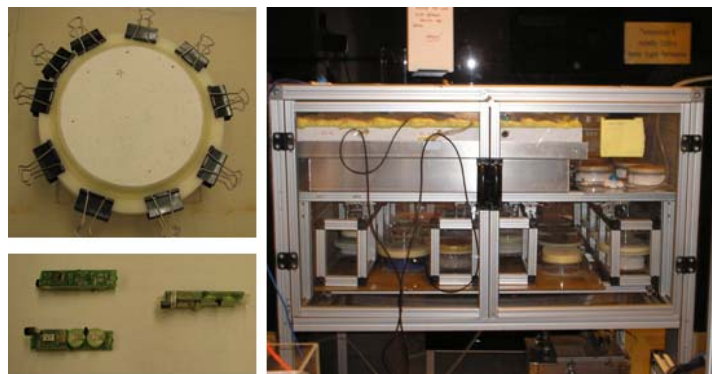
Figure 3-7 Sealed specimen on the cup (left top), wireless relative humidity sensor (left bottom) and humidity controlled chamber (right)

It is preferred to precondition the specimen before the test. The standards recommend storing the specimen in a 50% relative humidity environment, while author suggests conditioning the specimen at the mean relative humidity of the exposed environment, to shorten the time to achieve the steady flow.

First, the specimen is sealed at the open mouth of the test cup, which allows the water vapor flows only through the test specimen. Then, the whole cup with the specimen is placed into the environmental chamber with defined relative humidity. Thus, a water vapor flow is driven by the vapor pressure difference between both surfaces of the specimen. When vapor flow becomes steady, the vapor transmission rate can be

obtained by weighing the mass loss or gain of the system at defined time interval,

given in equation 3.2. By varying the different relative humidity levels on both

surfaces of the test specimen, water vapor permeability as a function of the mean

relative humidity of the exposed environments can be achieved.

$$WVT = G / (t \cdot A) = (G / t) / A , \tag{3.2}$$

where WVT is water vapor transmission rate (kg/m^2h), G is the weight change of the

whole cup (kg), t is the time during G occurred (s), and A is the cup-mouth area (m^2).

Water vapor permeance presents the water vapor transmission rate induced by the unit

vapor pressure difference between two sides of the specimen at specific temperature.

$$permeance = WVT / \Delta p_v , \tag{3.3}$$

where Δp_v is the water vapor pressure difference (pa).

The water vapor permeability is the arithmetic product of water vapor permeance and

the thickness of the specimen.

The additional corrections due to the still air in the test cup, the edge masking, etc,

can be included in the calculation (ASTM E96/E96M 2010; DIN EN ISO 12572

2001).

The ability of water vapor diffusion of a porous material can be also described by the

water vapor diffusion resistance factor defined in equation 2.16.

$$\mu = \frac{1}{d}(\delta_a \cdot \frac{\Delta p_v}{G / t \cdot A} - d_{air}) = \frac{1}{d}(\delta_a \cdot \frac{\Delta p_v}{WVT} - d_{air}) = \frac{1}{d}(\delta_a \cdot \frac{1}{permeance} - d_{air}), \tag{3.4}$$

where d is the thickness of the specimen (m), d_{air} is the thickness of the still air layer

in the cup (m). The water vapor permeability in free air δ_a ($kg/m{\cdot}s{\cdot}Pa$) is calculated

by:

$$\delta_a = \frac{D_{v,air}}{R_v \cdot T},$$
(3.5)

where $D_{v,air}$ is the water vapor diffusivity in free air given in equation 2.15, and R_v is

the ideal gas constant for water vapor (461.5 $J/kg{\cdot}K$).

Table 3-3 Water vapor diffusion resistance factors of various building materials

	μ value	
	Dry cup (5-36)	Wet cup (96-84)
Brick Wienerberger	18.1	12.1
Sandstone Hildesheim	13.8	10.3
Calcium silicate	5.4	2.3
Lime plaster	12.1	9.4
Mortar	11.8	11.2
Aerated Concrete	5.7	2.7
Cellulose	2.4	1.5
Spruce longitudinal	4.5	1.4
Spruce radial	236.2	11.6
Gypsum board	6.9	6.3

Table 3-3 lists water vapor diffusion resistance factors of some building materials. It

is obvious that each material owns a smaller wet-cup value than dry-cup value. The

reason is that in the low relative humidity range, water vapor transport dominates the

moisture transport, so dry-cup value gives the information of water vapor diffusion in

the material. As relative humidity increases, the liquid water transport starts to

contribute to the moisture transport. The wet-cup value provides the knowledge of

both water vapor and liquid water transport in the porous material. For anisotropic

materials, e.g., spruce, their vapor diffusion resistance factors may have a significant difference in the spatial directions.

3.3.2.2 Water absorption test

The one-dimensional water absorption test is well known as a simple measurement performed with the aim to determine water absorption coefficient and capillary saturation moisture content. Water absorption coefficient A_w ($kg/m^2s^{0.5}$) is defined as the slope of the cumulative, one-directional water inflow versus the square root of time. It represents the capillary transport ability of a porous material. An automated water absorption apparatus is shown in Figure 3-8. The device consists of a water container, the container lifter, a rigid suspension frame connected to a digital balance and a data logger for instantaneously recording the mass change of the specimen. Before the measurement, the specimen is fixed on a sample holder and placed on the suspension frame. Then, the container lifter is adjusted to allow the water level in the container to lie above the specimen surface by1-2 mm.

Figure 3-8 Automated water absorption apparatus (A); specimen fixed in specimen holder hanging above the water by suspension frame (B); different types of specimen holders (C)

To provide one dimensional vertical water movement, the specimen is protected and sealed at the lateral sides. The bottom surface of the initially oven-dried specimen is in contact with the free water surface to allow water absorption. The increasing weight of the specimen is measured at the defined intervals. For homogeneous and isotropic material, the test consists of two stages as shown in Figure 3-9: the first stage is characterized by a linear mass increase versus the square root of time. The water absorption measurement in this stage is mainly governed by the capillary force and viscous force (Roels et al. 2004). The transition from the first to the second stage proceeds when the moisture front reaches the top side of the specimen. A further mass increase is due to the water redistribution involving the dissolution of entrapped air in water. Capillary saturation moisture content is taken as the mean moisture content which is the intersection between the first and second stage.
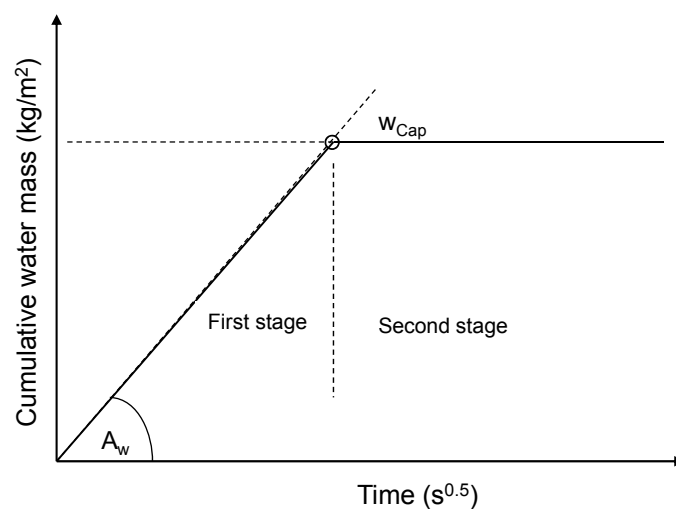
Figure 3-9 Schematic view of one-dimensional water absorption process

The water absorption courses of various building materials are shown in Figure 3-10. The water absorption rate is mainly determined by the liquid conductivity in the high

moisture content range. The calcium silicate has the higher liquid water conductivity,

so it has a faster liquid transport in comparison to others. The liquid water

conductivity of the plaster is relatively low, so it takes more time for the water front to

reach the top surface of the specimen.
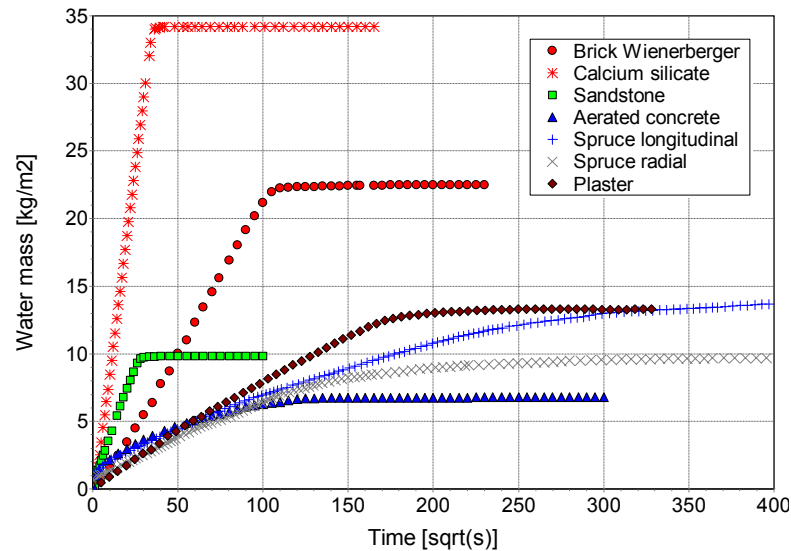
Figure 3-10 Measured water absorption courses of various building materials

3.3.2.3 Drying test

Drying process of a porous material gives insight into the moisture transport

characteristics in the low moisture content range. A drying apparatus is presented in

Figure 3-11. Prior to the test, the effectively saturated specimen is sealed on the lateral

and bottom sides, allowing only the top side exposing to the specific environment.

During the test, the specimen is periodically weighed to get the information of water

mass loss and the corresponding time. The drying process is strongly influenced by

the climatic conditions and boundary conditions, as well as the material properties of

specimen itself (Scheffler 2008). Therefore, the detailed information regarding to

those conditions should be recorded.
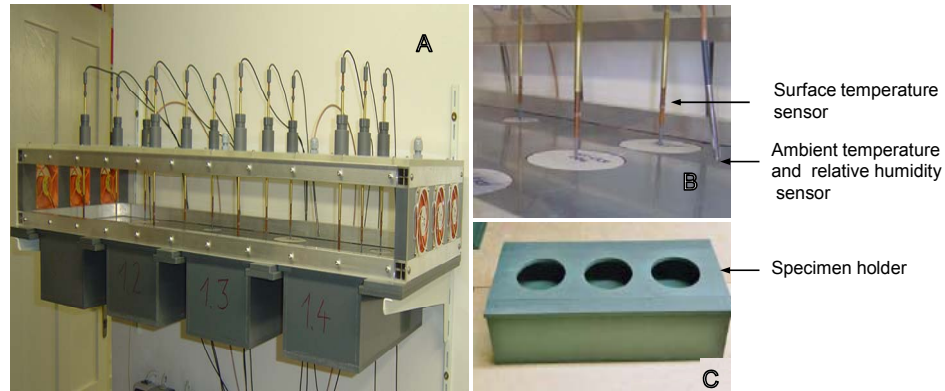
Figure 3-11 Automated drying apparatus (A); Temperature and relative humidity sensors (B); Specimen holder (C) (Plagge et al. 2007)
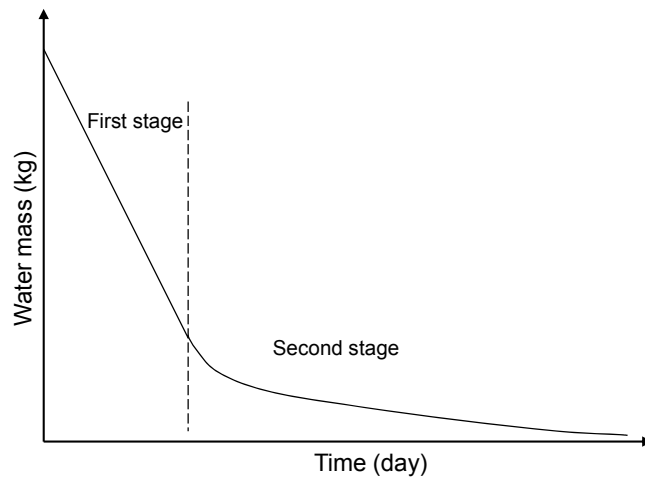
Figure 3-12 Schematic drawing of the drying process

Drying process is comprised of two stages, as shown in Figure 3-12. The first stage, beginning at high moisture content, is characterized by a linear water mass loss over time and mainly impacted by the boundary conditions, i.e., air flow rate above the evaporation surface. In this stage, the specimen is able to deliver stored liquid water to the evaporation surface. The surface temperature will decrease due to the water evaporation. In the second stage, the drying rate becomes slow and moisture transport is dominated by the water vapor flow within the material. This process is mainly governed by the material properties of the specimen itself. Therefore, the dry process

presents a transition of moisture transport from liquid water to water vapor transport.

This transition can be detected when surface temperature of the specimen increases or linear mass decrease over time is no longer maintained.

The measured drying curves of various building materials are shown in Figure 3-13. The values are normalized to remove the difference in the initial moisture content and the geometry of the specimen for easy comparison. The environmental conditions and boundary conditions mainly determine the length of the first drying stage, whereas the liquid water conductivity in the low moisture content range primarily affects the second drying stage. The plaster has a low liquid conductivity in this range, so it owns a long second drying stage. Calcium silicate has relatively higher liquid conductivity, so it undergoes a fast second drying stage. For spruce, the liquid water transport in longitudinal direction is much faster than that in radial direction.
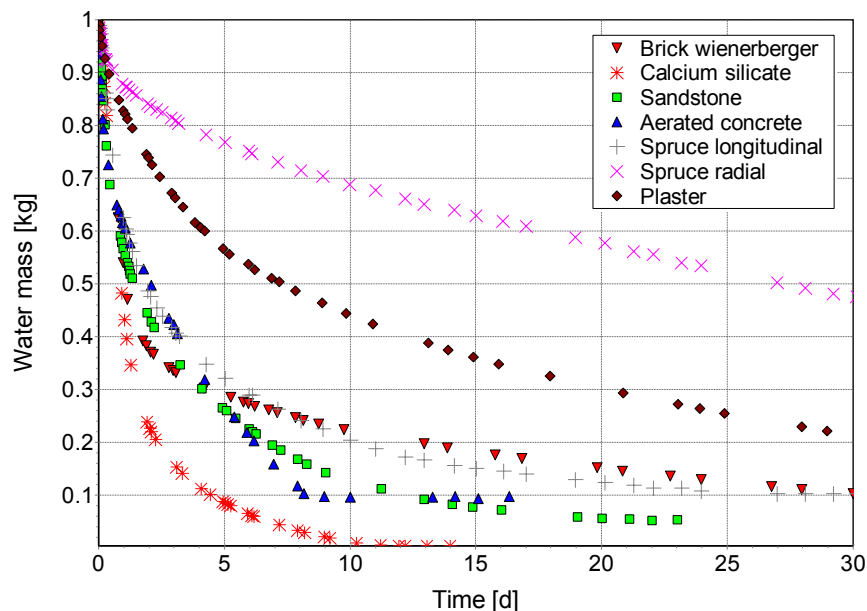
Figure 3-13 Drying behaviors of various building materials

3.3.2.4 Unsaturated liquid conductivity, K_l

The unsaturated liquid conductivity measures the ability of the liquid water transport through a porous material near the saturation moisture content region. The unsaturated liquid conductivity can be obtained by using a tension infiltrometer, which is composed of a water-filled tube and a porous ceramic plate connected by a vacuum pump as shown in Figure 3-14.
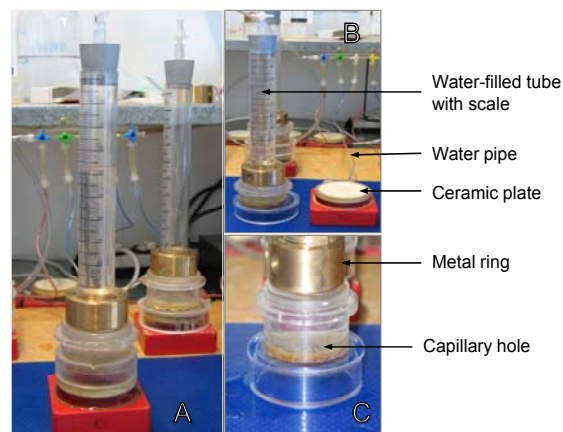
Figure 3-14 Tension infiltrometer apparatus (A); water filled tube and ceramic plate (B); Capillary hole on the lateral –bottom side of the tube (C) (Plagge et al. 2007)

The water-filled tube with a small-diameter capillary at the lateral-bottom side provides a threshold pressure on the top of the specimen. The constant suction pressure is kept up by inducing the air bubble through the capillary into the water-filled tube if the pressure falls below the desired threshold pressure. Before measurement, the moistened specimen is attached on the ceramic plate by the kaolin paste to enhance their contact. The heavy metal ring is used to tighten the contact between the specimen and water-fill tube by its gravity. If the applied suction pressure on the bottom side of the ceramic plate exceeds the threshold pressure, then the

pressure gradient will force the liquid water flowing through the specimen to form a steady state flux rate. The different degrees of moisture saturation are achieved by adjusting the suction pressures.

The liquid water conductivity at certain degree of moisture saturation is calculated by:

$$K_l = \frac{\Delta V}{t} \cdot \frac{d}{A \cdot \Delta p \cdot g},$$
(3.6)

where ΔV is the volume of liquid water flowing through the material (m^3), t is the time during the measurement (s), d is the thickness of the specimen (m), A is the cross-sectional area of the specimen (m^2), Δp is the pressure difference between two sides of the specimen (pa), and g is the gravity acceleration (m/s^2).

The unsaturated liquid water conductivities of various building materials at certain degree of saturation are listed in Table 3-4.

Table 3-4 Unsaturated liquid water conductivities of various building materials at certain degree of saturation

Material	Moisture content (m^3/m^3)	Mean suction pressure (Pa)	Liquid conductivity (s)
Brick Wienerberger	0.304	8650	2.0e-09
Sandstone Hildesheim	0.21	395	1.8e-07
Calcium silicate	0.87	1441	8.5e-09
Lime plaster	0.22	710	6.8 e-09
Mortar	0.39	4466	1.1 e-09
Aerated concrete	0.18	2205	9.3 e-12
Spruce longitudinal	0.69	1473	2.7e-09
Spruce radial	0.32	1453	2.7 e-09
Gypsum board	0.42	870	2.7e-10

3.3.2.5 Saturated liquid conductivity, K_{eff}

The saturated liquid conductivity can be measured by a head permeameter apparatus as shown in Figure 3-15.
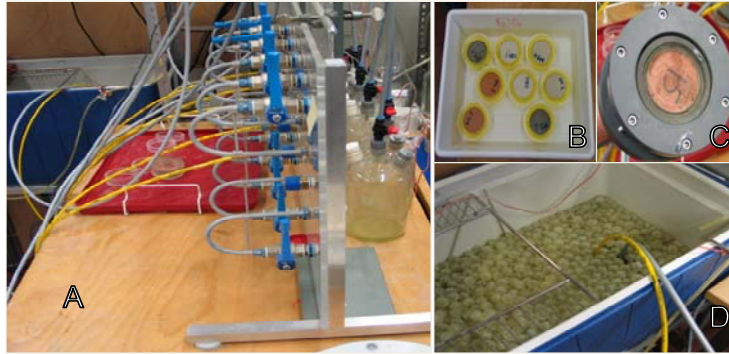
Figure 3-15 Head permeameter apparatus (A); laterally sealed specimens (B): head permeameter with specimen (C); water container (D) (Plagge et al. 2007)

It is composed of a head permeameter connected to a vacuum pump and a water container. The lateral sealed specimen is initially saturated and installed in the head permeameter, allowing one dimensional liquid water flow. The head permeameter with the specimen is then put into the water container with controlled temperature. With the application of suction pressure via the vacuum pump from one side of specimen, the liquid water will flush the specimen and flow into a glass flask through a capillary tube. The steady liquid flow rate can be calculated by measuring the increasing weight in the glass flask in the defined time intervals. By converting mass flow rate to volumetric flow rate, the saturated liquid conductivity can be determined by the equation 3.6.

3.4 Material Modeling

Material modeling includes two aspects: moisture storage modeling and moisture transport modeling. With the comparison of different material modeling methods described in Section 2.2, the selected modeling approaches that can be easily implemented and applicable for a large number of materials are detailedly introduced in the following sections.

3.4.1 Moisture Storage Modeling

A multi-modal model developed by Grunewald et al. (2003) applies the weighted sum of Gauss distribution functions to present N-modal pore volume distribution function, given in equation 3.7.

$$\frac{\partial \theta_l}{\partial pC}(pC) = -\sum_{i=1}^{N}\left[\frac{\Delta\theta_i}{\sqrt{2\pi}S_i}\exp\left(-\frac{(pC-pC_i)^2}{2S_i^2}\right)\right],\qquad(3.7)$$

where pC denotes logarithm of capillary suction p_c, $pC=\log(-p_c)$.

Moisture retention function can be obtained by integrating equation 3.7 over pC.

$$\theta_l(pC) = \sum_{i=1}^{N}\left[\frac{\Delta\theta_i}{2}\left(1+erf\left(\frac{pC_i-pC}{\sqrt{2}S_i}\right)\right)\right]\qquad(3.8)$$

Pore structure analysis can be used to determine the number of modality N (number of local maxima in the pore size distribution). The characteristic logarithmic capillary pressures pC_i give the position of the pore maxima, i.e., peaks of pore size distribution. S_i affects the steepness of the curve, which is the standard deviation of

the pore volume distribution function. Partial volume fractions $\Delta\theta_i$ provide the level of different modalities' plateau: $\theta_1 = \theta_{eff}$; $\Delta\theta_i = \theta_i - \theta_{i+1}$ for $i < N$; $\Delta\theta_N = \theta_N$. The sum of $\Delta\theta_i$ should be equal to θ_{eff}.

The advantage of this model in comparison to other multi-modal models is more flexible, thus, it is easy to fit the measured data from sorption isotherm and pressure plate tests. Every parameter in the model can be directly estimated from the measurements with a clear meaning.

Moisture retention function and pore volume distribution of brick Joens according to the measured moisture storage data is exemplified in Figure 3-16.
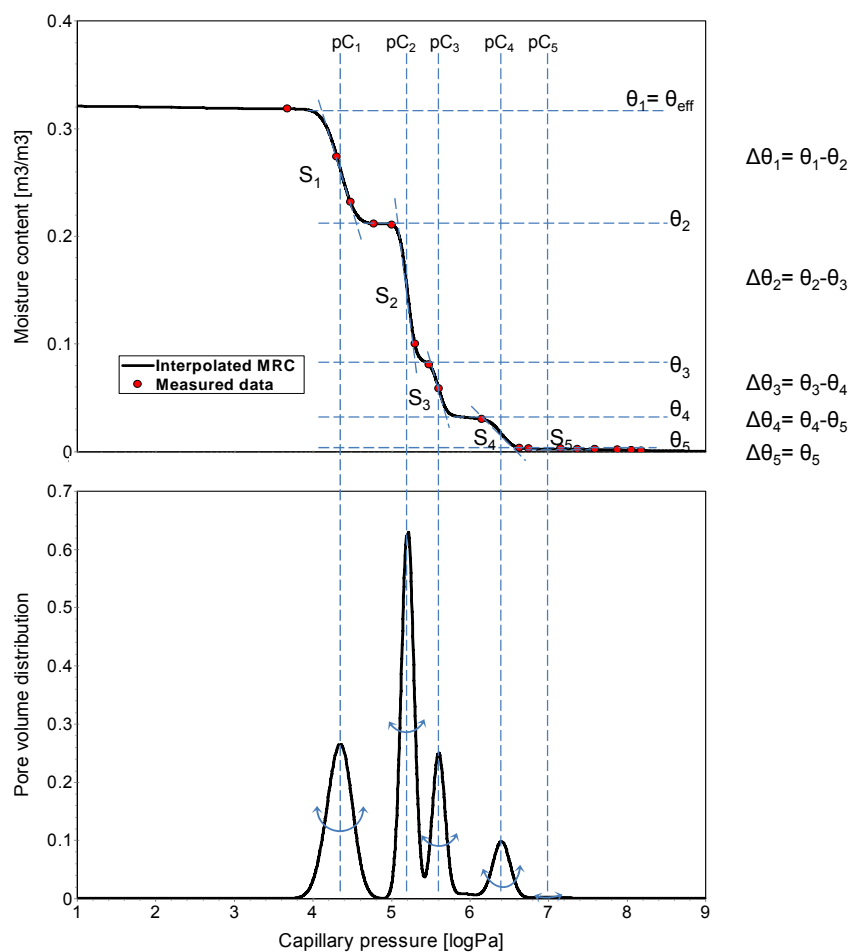
Figure 3-16 Moisture retention function and pore volume distribution of brick Joens

3.4.2 Moisture Transport Modeling

3.4.2.1 Bundle of tubes model

In the bundle of tubes model, the pore structure in porous material is represented by a bundle of parallel capillary tubes, which vary in different radii and are interconnected without any resistance. The incompressible laminar liquid water flow in a single tube with length Δx can be expressed by Hagen-Poiseuille equation, which describes the volume flow rate V as the function of tube radius r, the liquid dynamic viscosity η_l and the gradient of capillary pressure.

$$V(r) = \frac{\pi r^4}{8\eta_l} \cdot \left(\frac{\partial p_c}{\partial x_k} + \rho_l \cdot g_k \right)$$ (3.9)

Multiplying $V(r)$ with the density of the liquid phase ρ_l yields the mass flow rate $j_{k,adv}^{m_l}(r)$

$$j_{k,adv}^{m_l}(r) = -\rho_l \frac{\pi r^4}{8\eta_l} \cdot \left(\frac{\partial p_c}{\partial x_k} + \rho_l \cdot g_k \right)$$ (3.10)

Integrating equation 3.10 over the pore radii distribution density dn/dr (the density function describes the number of pores per radius interval $r...r+dr$) extends the volumetric flux within a single tube to a bundle of tubes with different radii.

$$j_{k,adv}^{m_l}(r) = \int_0^R -\rho_l \frac{\pi r^4}{8\eta_l} \cdot \frac{\partial p_c}{\partial x_k} \left(\frac{\partial p_c}{\partial x_k} + \rho_l \cdot g_k \right) \cdot \frac{dn}{dr} dr$$ (3.11)

The pore radii distribution density dn/dr can be derived by counting pore volume distribution density $d\theta/dr$ within the cross section πr^2, given in equation 3.12.

$$\frac{dn}{dr} = \frac{1}{\pi r^2} \frac{d\theta}{dr}$$ (3.12)

Taking equation 3.12 to equation 3.11 yields the mass flow rate as a function of the capillary radius $r(\theta)$.

$$j_{k,adv}^{m_l}(\theta_l) = -\left[\frac{\rho_l}{8\eta_l}\int_0^{\theta_l} r(\theta)^2 d\theta\right] \cdot \left(\frac{\partial p_c}{\partial x_k} + \rho_l \cdot g_k\right)$$ (3.13)

In comparison to equation 2.11, the first part in the right hand side of equation 3.13 is the liquid water conductivity expressed as a function of moisture content.

$$K_l(\theta_l) = -\frac{\rho_l}{8\eta_l}\int_0^{\theta_l} r(\theta)^2 d\theta$$ (3.14)

Substituting $r(\theta) = -\frac{2\sigma \cos(\alpha)}{P_c(\theta)}$ in equation 3.14, the liquid conductivity can be expressed as:

$$K_l(\theta_l) = -\frac{\rho_l \cdot \sigma^2 \cos(\alpha)^2}{2\eta_l}\int_0^{\theta_l} \frac{1}{P_c(\theta)^2} d\theta$$ (3.15)

In equation 3.15, the term before the integral is independent of liquid content. Thus, normalized or relative liquid water conductivity can be written as:

$$K_{rel}(\theta_l) = \int_0^{\theta_l} \frac{1}{P_c(\theta)^2} d\theta \bigg/ \int_0^{\theta_{eff}} \frac{1}{P_c(\theta)^2} d\theta$$ (3.16)

The absolute liquid conductivity function can be obtained by matching K_{rel} with the measured liquid conductivity at saturation moisture content K_{eff}.

$$K_l(\theta_l) = K_{eff} \cdot K_{rel}(\theta_l)$$ (3.17)

This means that the liquid water conductivity in the entire moisture content range can be determined by the reversed moisture retention function plus the single measured parameter, K_{eff}.

3.4.2.2 Mechanistical model

The bundle of tubes model assumes all the pores are interconnected to form a continuous capillary flow. This simplification is suitable in the high moisture content range, but overestimates the liquid transport in the low moisture content range and the hygroscopic range in which the liquid phase is isolated and vapor transport dominates the moisture transport. Therefore, the serial-parallel pore theory introduced in the engineering model by Grunewald et al. (2003) and further developed by Scheffler (2008) is applied to couple with the bundle of tubes model.

In the model, the volume of a material is divided into two parts: the serial-structured pore domain and the parallel-structured pore domain. As shown in Figure 3-17, in a serial-structured pore, vapor diffuses through the air filled pore space on both sides of a liquid island in the direction from higher to lower vapor pressure. Condensation occurs at the capillary meniscus faced to the side with the higher vapor pressure. At the same time, water molecules evaporate at the opposite side. In between (in the liquid short-cut), water is transported in the liquid phase (liquid water flux) (Philip 1957). The local vapor pressure gradient (in the air-filled space) increases due to the liquid short-cut assuming immediate pressure equalization between the menisci. Serial

transport mainly happens in the hygroscopic and lower overhygroscopic moisture

range.
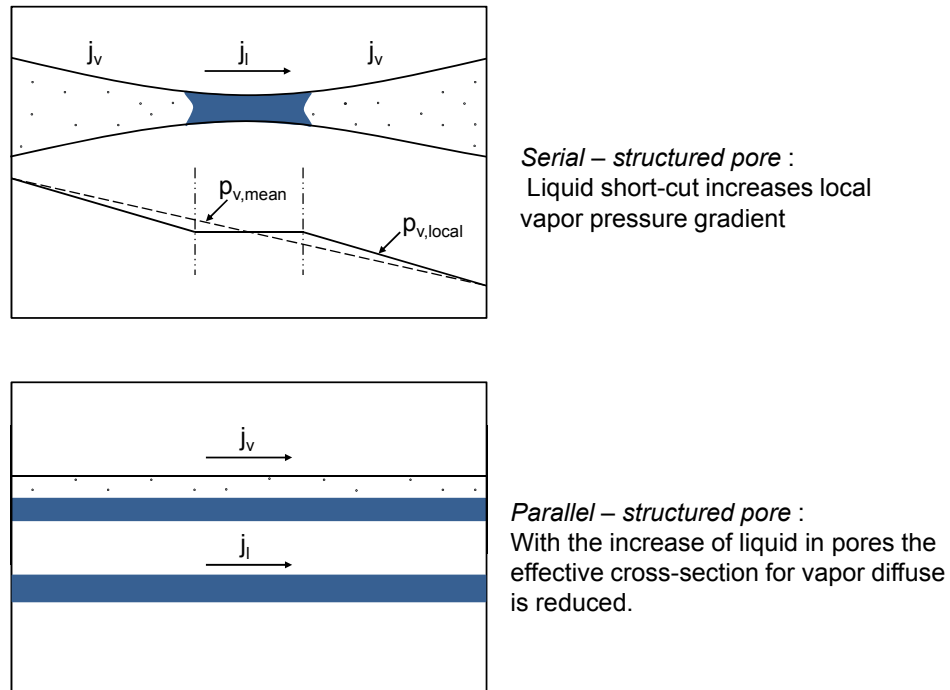
Figure 3-17 Serial and parallel structured pores (Grunewald et al. 2003)

In a parallel-structured pore, the vapor diffusion flux declines with the reduced

diffusion cross section. Thus, it can be assumed to be inversely proportional to the

water content. In comparison to serial transport, parallel transport is more powerful in

the liquid phase, so it usually happens in the upper moisture content range until

saturation.

To account for the proportion of serial transport and parallel transport in dependence

on the moisture content in the pore structure, two scaling functions are introduced:

$f_v(\theta_l)$ given in equation 3.18 represents scaling function for vapor transport and $f_l(\theta_l)$

given in equation 3.19 denotes scaling function for liquid transport.

$$f_v(\theta_l) = \dfrac{1 - \dfrac{\theta_l}{\theta_{por}}}{\left(\dfrac{\theta_l}{\theta_{por}}\right)^{\eta_{sp}} + \left(1 - \dfrac{\theta_l}{\theta_{por}}\right)^2 \cdot \left(1 - \left(\dfrac{\theta_l}{\theta_{por}}\right)^{\eta_{sp}}\right)} \quad , \tag{3.18}$$

$$f_l(\theta_l) = \dfrac{\left(\dfrac{\theta_l}{\theta_{por}}\right)^{\eta_{sp}}}{\left(\dfrac{\theta_l}{\theta_{por}}\right)^{\eta} + \left(1 - \dfrac{\theta_l}{\theta_{por}}\right)^2 \cdot \left(1 - \left(\dfrac{\theta_l}{\theta_{por}}\right)^{\eta_{sp}}\right)} \quad , \tag{3.19}$$

where η_{sp} is the scaling factor to describe the volumetric fraction of the parallel-structured pore domain as a function of relative water content θ_l/θ_{por}. This factor influences water vapor permeability and liquid water conductivity in the low moisture content range. η_{sp} is adjusted according to the simulation of drying test.

Thus, the vapor diffusion function can be expressed by multiplying equation 2.16 with the scaling function for vapor transport $f_v(\theta_l)$.

$$D_{v,mat}(\theta_l, T) = \dfrac{D_{v,air}(T)}{\mu_{dry}} \cdot f_v(\theta_l) \tag{3.20}$$

For liquid water conductivity function, in addition to the scaling function $f_l(\theta_l)$, another scaling parameter η_{cap} is introduced to adjust liquid water conductivity in the high moisture content range. η_{cap} is adjusted by the simulation of water absorption test.

$$K_l(\theta_l) = \eta_{cap} \cdot K_{eff} \cdot K_{l,rel}(\theta_l) \cdot f_l(\theta_l) \tag{3.21}$$

The derived vapor diffusion function and liquid water conductivity function provide an initial estimation of the moisture transport in the porous material. The additional

adjustments by numerical simulations to reproduce the physical transport phenomena in the experiments will be introduced in Section 3.4.3.

3.4.2.3 Liquid water transport in the hygroscopic range

Under an isothermal condition, a vapor pressure gradient can be converted to a capillary pressure gradient with the application of Kelvin equation (2.18). This allows the summation of liquid and vapor fluxes, and relating the moisture transport to only one driving potential, either vapor pressure or capillary pressure.

$$\frac{\partial p_v}{\partial x} = \frac{\partial p_v}{\partial p_c} \cdot \frac{\partial p_c}{\partial x} = \frac{\rho_v}{\rho_l} \frac{\partial p_c}{\partial x},$$ (3.22)

where ρ_v and ρ_l are water vapor and liquid water densities, respectively.

One-dimensional moisture flux driven by capillary pressure gradient is given in equation 3.23.

$$j_k^{m_{l+v}} = j_{k,conv}^{m_l} + j_{k,diff}^{m_v} = -K_l \cdot \frac{\partial p_c}{\partial x_k} - K_{v,p_c} \cdot \frac{\partial p_c}{\partial x_k} = -(K_l + \frac{\rho_v}{\rho_l} K_v) \cdot \frac{\partial p_c}{\partial x_k} == -K_{l+v} \cdot \frac{\partial p_c}{\partial x_k},$$ (3.23)

where K_{l+v} is moisture conductivity (s).

Moisture transport at the low relative humidity range, i.e., below mean relative humidity of the dry-cup measurement, is assumed to be only water vapor diffusion. Cup measurement at the higher relative humidity range, called the wet-cup measurement, gives the information for both the liquid water and the water vapor

transport. Therefore, moisture conductivity in equation 3.23 can be determined by the vapor diffusion resistance factor from wet-cup measurement.

$$K_{l+v}(\mu_{wet}) = \frac{D_{v,air}}{\mu_{wet} \cdot R_v \cdot T} \frac{\rho_v(\varphi_{cup})}{\rho_l} ,$$

(3.24)

where φ_{cup} is the mean relative humidity of the exposed environment in wet-cup measurement.

The liquid transport in this range is slight and cannot be directly measured. Alternatively, it can be determined from the difference of the moisture conductivity and water vapor conductivity, given in equation 3.25.

$$K_l(\mu_{wet}) = K_{l+v}(\mu_{wet}) - K_v(\mu_{dry})$$

(3.25)

It should be noted that the cup test can only provide the information of moisture transport in the hygroscopic range. The determination of moisture transport in the entire moisture content range requires additional experiments and different calculation processes.

3.4.3 Implementation of Material Characterization

To implement material characterization, the summarized material data in the excel sheet is imported into the "Material Generator", which is an in-house developed software that integrates the material models introduced above and allows to flexibly adjust material functions to reproduce the measured experimental courses.

First, the multi-modal moisture storage function (equation 3.8) is parametrically

adjusted to match the measured moisture retention and sorption data. The number of

modal is dependent on the pore size distribution. Then, the linear spline interpolation

is performed to generate a continuous moisture retention curve (MRC) and a reverse

moisture retention curve (RMRC). The special check is implemented to guarantee the

monotonicity of data points and the accuracy of these two functions. The water vapor

diffusivity derived from equation 3.20 and the liquid water conductivity derived from

equation 3.21 are initially estimated according to the methods described in Section

3.4.2.2.

Subsequently, a set of experiments are used to adjust and calibrate the initially

estimated transport functions. In the hygroscopic range, the liquid water conductivity

is linearly interpolated among the calculated values that are the difference of moisture

conductivity derived from the wet-cup measurement and the water vapor conductivity

derived from the dry-cup measurement (Section 3.4.2.3). The liquid water

conductivity above capillary saturation moisture content until saturation is

interpolated between the $K_{l,cap}(\theta_l)$ and the measured values from the tension

infiltrometer or head permeameter test. The $K_{l,cap}(\theta_l)$ is determined with the aid of the

adjustment of η_{cap} at capillary saturation moisture content. The simulation of water

absorption test is used to adjust the function in the capillary moisture content range,

and the simulation of the drying test is applied to adjust the function in the lower

moisture content range. The liquid water conductivity derived from these experiments in the entire moisture content range is presented in Figure 3-18.
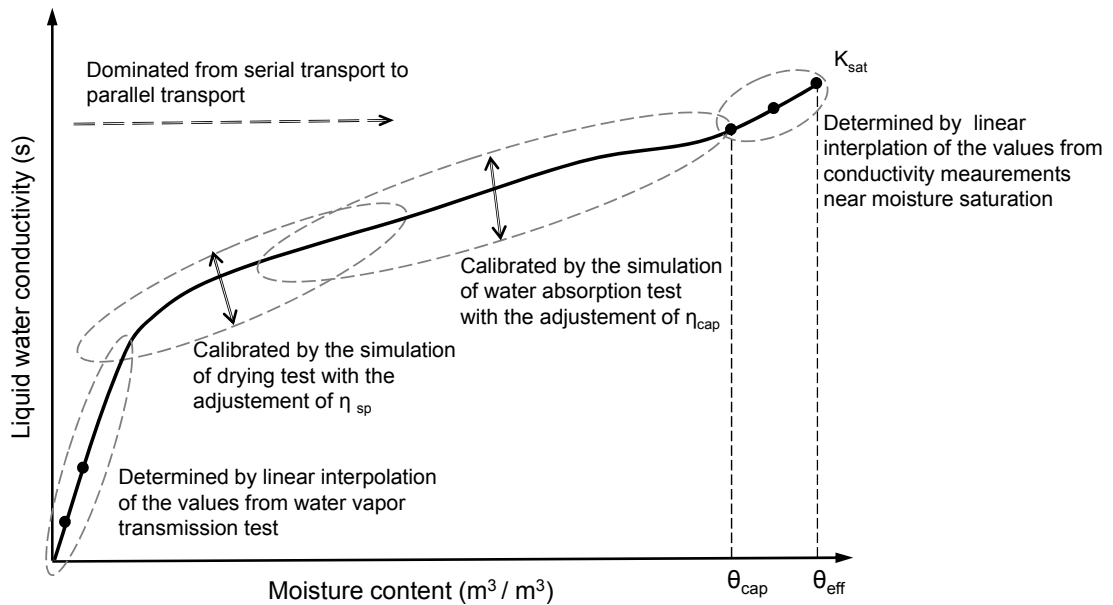
Figure 3-18 Liquid water conductivity function derived from different experiments according to Scheffler (2008)

The water vapor permeability is adjusted by the scaling factor η_{sp} according to the simulation of the drying test.

The calibration procedure is an iterated process. The simulations by the application of the calibrated functions should reproduce the process of both water absorption and drying test. The flowchart of this process is presented in Figure 3-19. The simulation of water absorption process precedes that of drying process since the adjustment of the liquid water conductivity function in the higher moisture range can have a large influence on the function in the lower moisture range. On the other hand, the adjustment on the lower part has no or limited effect on the higher part.
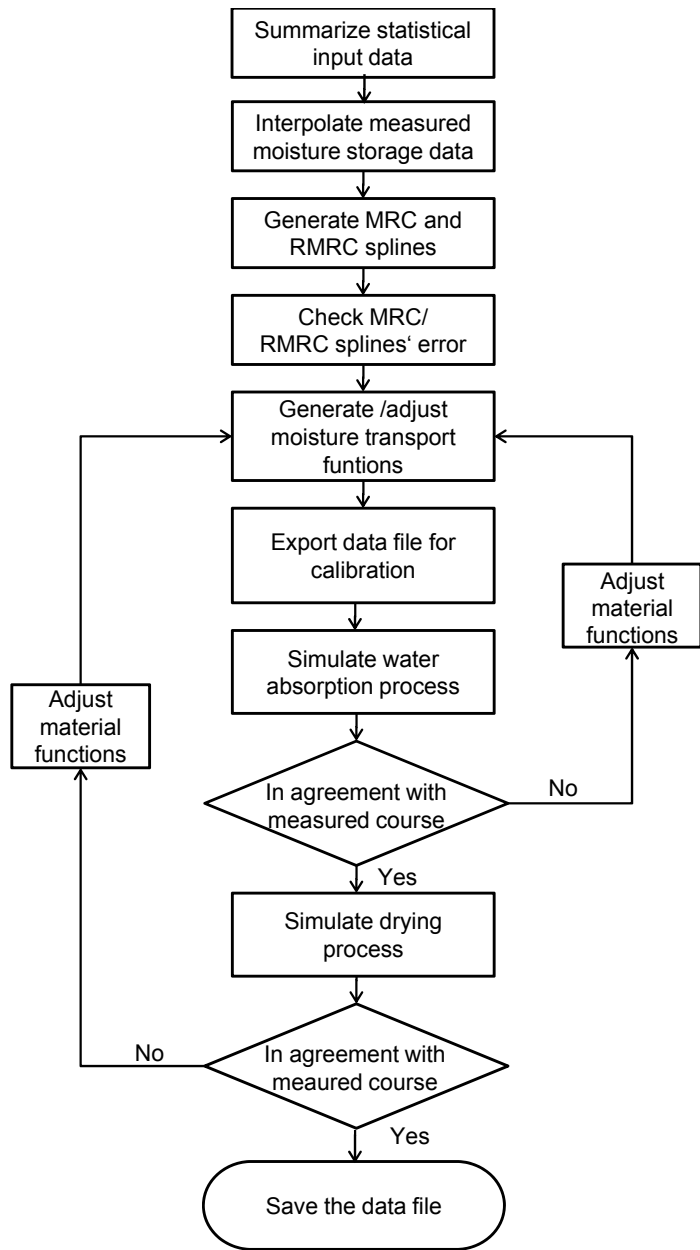
Figure 3-19 Implementation of material characterization

The adjustment of liquid water conductivity function in the high moisture content range to match the measured water absorption course and in the low moisture content range to match the measured drying course is exemplified in Figure 3-20.
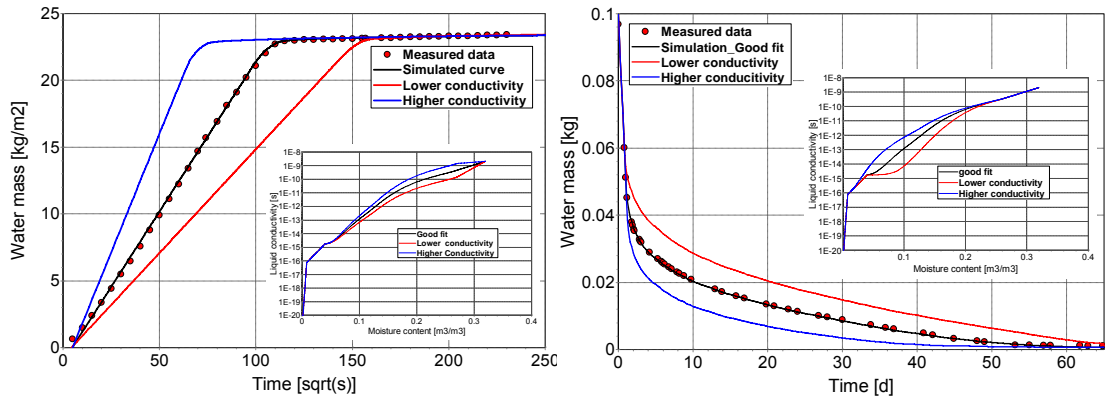
Figure 3-20 Adjustment of liquid water conductivity to match the measured water absorption and drying courses

Since there is no suitable hysteresis model that can be easily implemented in material characterization, the adsorption data in the overhygroscopic range is only from estimation. Therefore, at the current stage, moisture transport functions are derived by applying the desorption data. In the calibration process, the simulated course can reproduce the first stage of water absorption test by the adjustment of the liquid conductivity function, so the water absorption rate (represented by water absorption coefficient, A_w in kg/m^{2}s$^{0.5}$) can be kept. However, the equilibrium moisture content at the second stage of simulation course may differ from capillary saturation moisture content. This may produce a different moisture distribution from the case if the adsorption data is applied. So use of the desorption data is an expedient before the well established hysteresis model is included.

Material functions of brick Wienerberger derived according to the above approach are exemplified. The sorption isotherm, moisture retention curve, pore volume distribution, water vapor permeability, liquid water conductivity, and moisture dependent thermal conductivity are demonstrated in Figure 3-21.
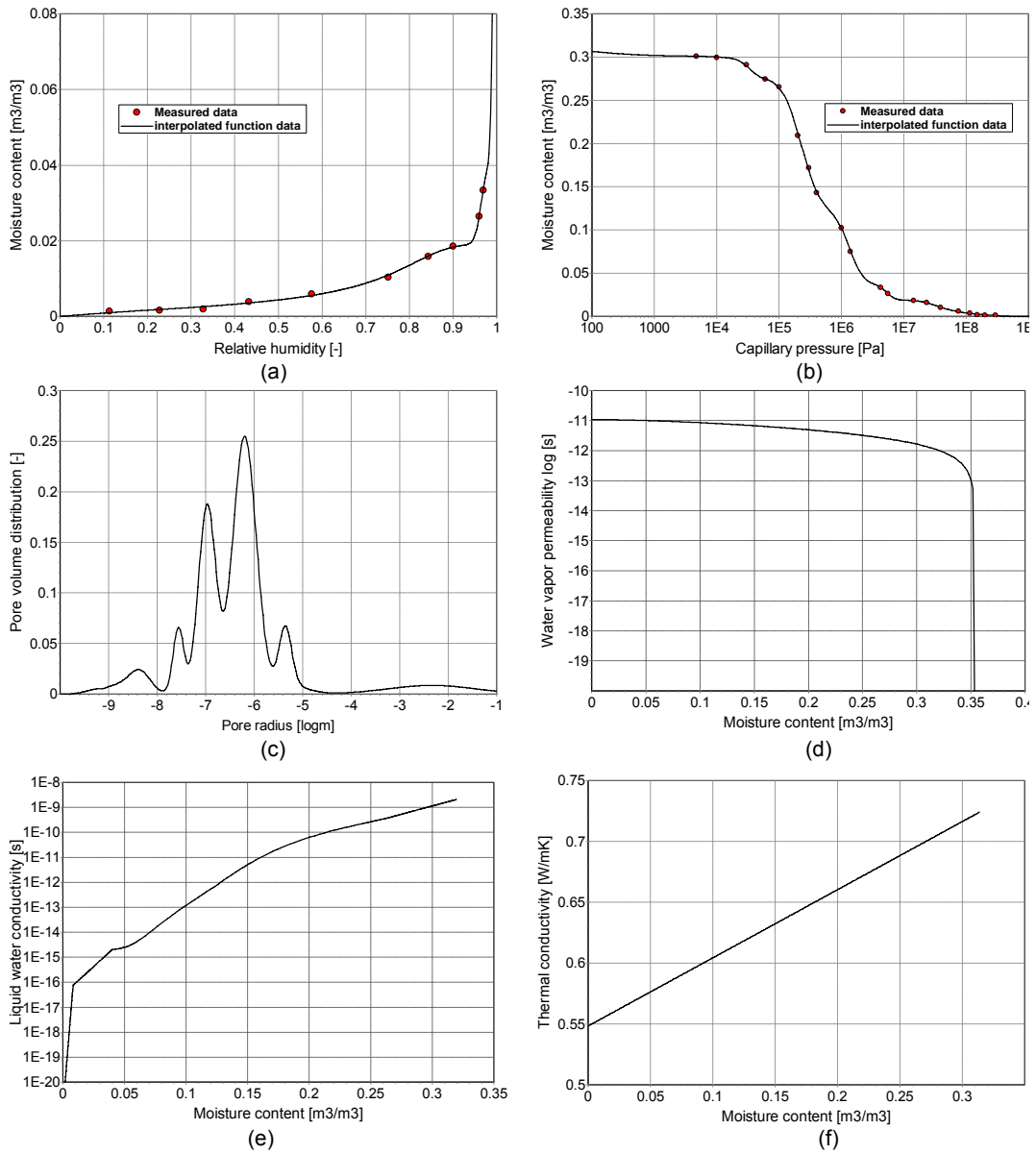
Figure 3-21 Material functions of brick Wienerberger. Sorption isotherm (a); moisture retention curve (b); pore volume distribution (c); water vapor permeability (d); liquid water conductivity (e); and moisture dependent thermal conductivity (f)

The comparisons of the measured water absorption and drying courses with the simulated curves are shown in Figure 3-22. The simulated curve achieves good agreement with the measured data.
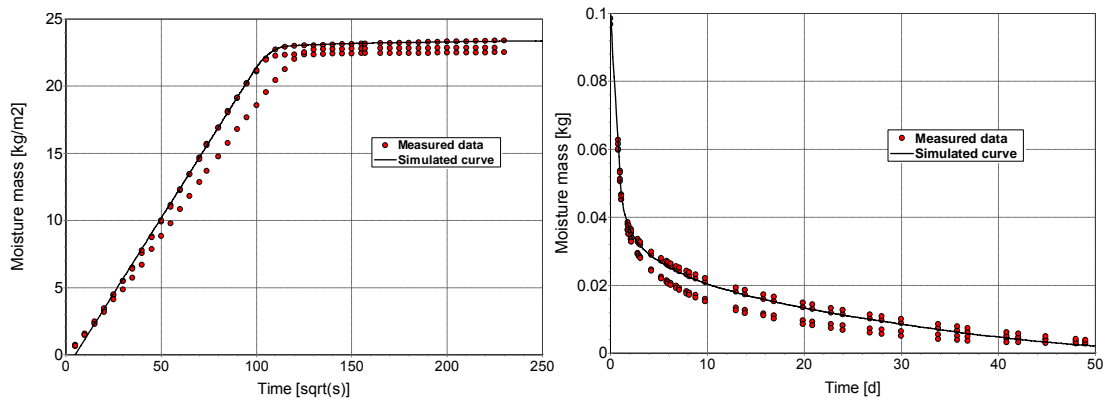
Figure 3-22 Comparisons of the measured water absorption (left) and drying (right) courses with the simulated ones

3.5 Establishment of a Comprehensive Material Database for Hygrothermal Simulation Tools

According to the material category described in Section 3.2.1, several representative materials in each category are selected for characterization and their material functions are derived.

In the plaster / mortar category, the exterior lime cement plaster, interior lime plaster and mortar are covered. In the building brick category, classical clay and loamy bricks, as well as lime sandstone brick are analyzed. The natural stone category includes lime stones, granite and marble from different sites in the world, e.g., India and Japan. Sand stone exhibits distinct moisture transport behaviors on the sedimentary direction and the direction perpendicular to the sedimentary layer. So it is characterized in both directions. The cement containing material is composed of the normal concrete and aerated concrete. The insulation material category contains a wide range of materials, including the capillary active material (e.g., calcium silicate)

71

and non-capillary active material (e.g., foam), hygroscopic material (e.g., cellulose) and non-hygroscopic material (e.g., mineral wool). The building board category contains the material manufactured and applied as board, e.g., orientated strand board (OSB), gypsum board and particle board. The wood category includes the hardwood and softwood, e.g., spruce and oak. Each wood material is evaluated in longitudinal and radial directions due to its heterogeneous characteristics. The building foil and waterproofing product category contains the normal vapor retarders and moisture adapted vapor retarder, which has the property of water vapor diffusion resistance factor decreasing with the increase of relative humidity in the atmosphere surrounding the vapor retarder.

A total of 173 materials have been evaluated for the simulation tools. They represent most common building materials on the market and expand the current material database. The number of the characterized materials in each category is summarized in Table 3-5.

Table 3-5 Summary of the characterized materials in each category

Category	Material description	Number
02	Plaster/ mortar	57
03	Building brick	28
04	Natural stone	21
05	Cement containing building material	3
06	Insulation material	35
07	Building board	5
08	Wood (longitudinal and radial direction)	3
12	Foil and waterproofing product	21

Each material data file includes the basic material properties, identification

information (material category, manufacture, the sampling method, etc.), and the

material functions (MRC, RMRC, water vapor permeability/diffusivity, liquid water

conductivity/diffusivity, and the moisture dependent thermal conductivity).

3.6 Correlations between material parameters

There exist some instinct relationships between material parameters. With the

investigation of 22 building bricks, 45 plaster/mortars, 35 insulations, and 21 natural

stones, the rank correlation matrixes of some basic parameters in different material

categories are derive and presented in Table 3-6, Table 3-7, Table 3-8 and Table 3-9.

Table 3-6 Rank correlation matrix of basic parameters in the building brick category

Ranked Correlation	ρ	c_0	λ	μ_{dry}	θ_{por}
ρ	1				
c_0	-0.84	1			
λ	0.76	-0.56	1		
μ_{dry}	0.49	-0.32	0.51	1	
θ_{por}	-0.94	0.81	-0.68	-0.60	1

Table 3-7 Rank correlation matrix of basic parameters in the plaster/mortar category

Ranked Correlation	ρ	c_0	λ	μ_{dry}	θ_{por}
ρ	1				
c_0	-0.42	1			
λ	0.97	-0.37	1		
μ_{dry}	0.60	0	0.65	1	
θ_{por}	-0.99	0.43	-0.97	-0.59	1

Table 3-8 Rank correlation matrix of basic parameters in the insulation category

Ranked Correlation	ρ	c_0	λ	μ_{dry}	θ_{por}
ρ	1				
c_0	-0.56	1			
λ	0.94	-0.40	1		
μ_{dry}	0.72	-0.41	0.65	1	
θ_{por}	-0.91	0.44	-0.92	-0.62	1

Table 3-9 Rank correlation matrix of basic parameters in the natural stone category

Ranked Correlation	ρ	c_0	λ	μ_{dry}	θ_{por}
ρ	1				
c_0	-0.23	1			
λ	0.55	0.14	1		
μ_{dry}	0.71	-0.32	0.12	1	
θ_{por}	-0.98	0.19	-0.57	-0.7	1

3.7 Summary

In this chapter, a systematic approach was introduced to organize, classify and characterize the materials. The standardized and complementary experiments to get the complete material properties for material characterization were introduced. For the purpose of characterization of a large number of materials, the material model should be easily implemented and its parameters should be controlled within the limited numbers. A multi-modal model was employed to derive the moisture storage function and a mechanistical model was applied to derive the moisture transport functions. These two models allow flexibly adjusting material functions in the entire moisture content range, according to the standard experiments. By applying this approach, a

comprehensive material database, including 173 materials in 8 material categories, was established for the simulation use.

The rank correlations of basic material parameters in different material categories were derived based on the investigation of a number of measured material data.

Chapter 4   Application of Statistical Methods for Hygrothermal Material Characterization

4.1 Introduction

In the early design stage, the exact building information is usually not provided in detail. For instance, only the general type of the brick is given, but the full material properties are unknown. With such limited information, it is hard to accurately predict the hygrothermal performance of the building enclosure assembly. In addition, material data in the literature is usually not complete, i.e., the density and thermal conductivity are known, but other properties are missing. Therefore, one generalized material, which represents a type of materials with similar characteristics, is needed for the analysis, in case the detailed material information is unavailable or a method is pursued to qualify the incomplete material data to be used for the simulation tools.

As introduced in the last chapter, material modeling requires a set of experiments to acquire either basic material parameters, or the data for further functionalization. Some of these experiments may need a long test period (e.g., pressure plate measurement), which prolongs the analysis process and increases the experimental expense. Thus, most simulation tools have only a few material data that cannot satisfy the increasing simulation need. However, evaluating every material, through

conducting full measurements, is also impractical. Therefore, a method is needed to simplify the measurement procedure, while still ensuring the data quality.

By applying the available high-quality material data to detect the natural relationships between data and utilize those relationships for data processing is a promising approach to achieve the above mentioned expectations.

Some statistical methods, which can agglomerate the similar data (cluster analysis) and reveal the relationships between in-group data (regression analysis), are employed in building physics.

4.1.1 Derivation of Generic Materials

Three material classification levels are first differentiated in the analysis of material data:

- Material database: the collection of all the individual materials with the complete properties.

- Physical material group: the collection of the materials which exhibit common physical characteristics. It has a broader definition compared to material category, e.g., all the materials can be differentiated as one porous material group (brick, plaster/ mortar, etc.) and one non-porous material group (steel, foil, etc.).

- Material cluster: the refined group in the physical material group. In each cluster, specific materials have the similar characteristics.

Thereafter, the definitions of specific material and generic material are given.

- A specific material is an individual material. It has its particular name to differentiate from others. Its material properties are unique.

- A generic material is a "derived" or "artificial" material from one material cluster. It represents a type of specific materials which have the similar characteristics.

The definitions of these two terms can be exemplified as follows: historical brick ZM and brick ZE are specific materials. These two bricks have similar material properties and can be grouped into a cluster "historical brick fabricated by the classic loam and clay", represented by one generic material "historical building brick".

The procedure to derive a generic material is shown in Figure 4-1.The material database is first classified into several physical material groups according to material's physical characteristics. Then, cluster analysis is employed to aggregate the specific materials in each physical group to different material clusters, in which specific materials have the similar characteristics. Thereafter, one generic material is derived in each material cluster, by the application of generic synthesis, to represent the common material characteristics of this cluster.
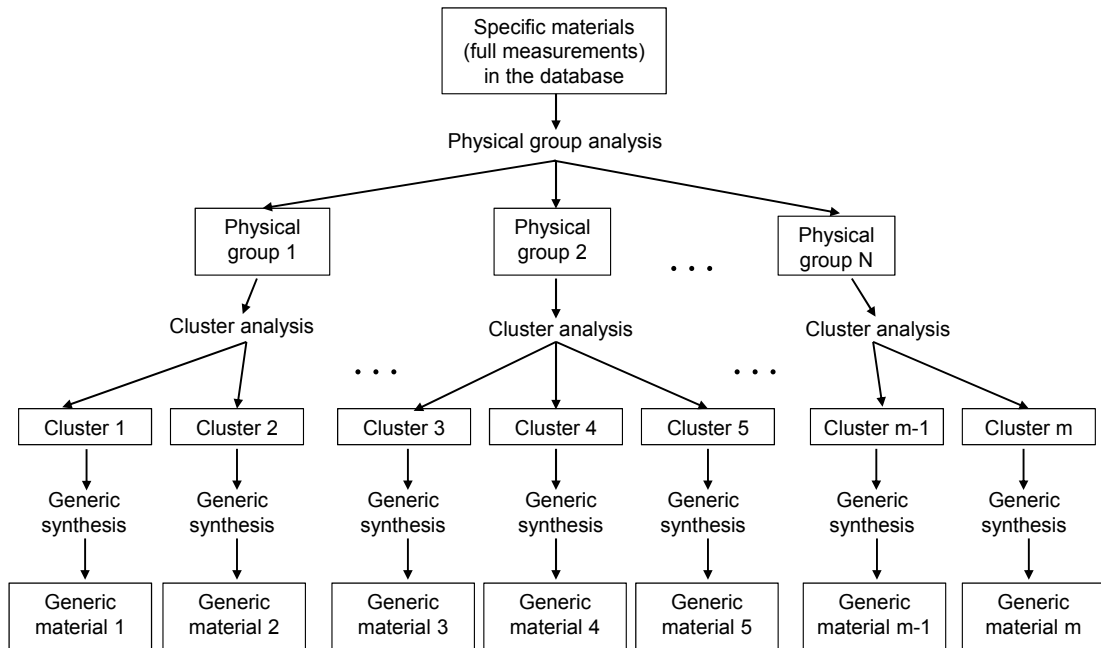
Figure 4-1 Schematic drawing of a systematic procedure to derive generic materials

The application of generic materials has the practical benefits. The generic material can be used in the early design stage to increase the reliability of the simulation results. No detailed material information is required any more, only the knowledge of the type of the material is sufficient. In addition, the incomplete material data can be qualified by extrapolating the missing properties from the most similar generic material. The detailed description of this method is introduced in Section 4.4.4.

4.1.2 Necessity to Simplify the Moisture Storage Measurement

The moisture storage characteristics of porous materials are important for material characterization. Moisture storage measurement is comprised of pressure plate test in the overhygroscopic range and sorption isotherm test in the hygroscopic range. The experimental approach on how to obtain moisture content at the specified capillary

pressure or relative humidity has been introduced in Section 3.3.1. The successive

measurements are very time-consuming and tedious. It may take a few weeks, even

several months, and requires many efforts during the measurement. Therefore, an

approach to simplify the measurement step is explored by the application of statistical

methods.

This chapter starts with the introduction of two statistical methods: cluster analysis

and regression analysis. Thereafter, the application of these analyses for material

characterization is described and exemplified.

4.2 Cluster Analysis

Cluster analysis is a multivariate procedure for exploring natural groups in data so

that the objects or individuals in one group are similar to each other and different

from the individuals in the other groups (Everitt et al. 2011). It is widely used in

biology, psychology, and market research, etc., to classify and summarize the data for

the purpose of data organization and processing.

Cluster analysis measures the similarity or dissimilarity between individuals in order

to identify the clusters.

The dissimilarity between two individuals is determined by their distance. There are

different ways to measure it. The most commonly used one is the Euclidean distance,

given in equation 4.1.

$$d_{jk} = \left[\sum_{i=1}^{n} (x_{ji} - x_{ki})^2 \right]^{1/2},$$ (4.1)

where x_{ji} and x_{ki} are, respectively, the ith variable of n-dimensional observations for individuals j and k.

The distance d_{jk} can be interpreted as physical distances between two n-dimensional points $\tilde{x}_j = (x_{j1}, \ldots x_{jn})$ and $\tilde{x}_k = (x_{k1}, \ldots x_{kn})$ in the Euclidean space.

The individuals are similar if the distance between them is small. The most similar individuals are then jointed into one cluster.

The distance between groups of individual or clusters can be measured by different methods, including:

- Single linkage. This method is also called the nearest neighbour approach. It defines the distance of two clusters from the shortest distance between pairs of individuals, with one individual from each cluster.

- Complete linkage. It is the opposite of single linkage. The method is also called the furthest neighbour approach. It defines the distance of two clusters from the furthest distance between pairs of individuals, with one individual from each cluster.

- Average linkage. The method defines the distance of two clusters from the average of the distance between all pairs of individuals, with one individual from each cluster.

81

- Centroid method. The method uses the mean value of all individuals in a

  cluster as the reference vector to define the distance to the other cluster.

- Ward's method. It is also called the minimum variance method. The method

  tries to find the objects or clusters whose fusion increases the sum of the

  squared distances between objects or cluster centroid as little as possible.

The inter-cluster distance measures of single linkage, complete linkage and average

linkage methods are illustrated in Figure 4-2 (Everitt et al. 2011).
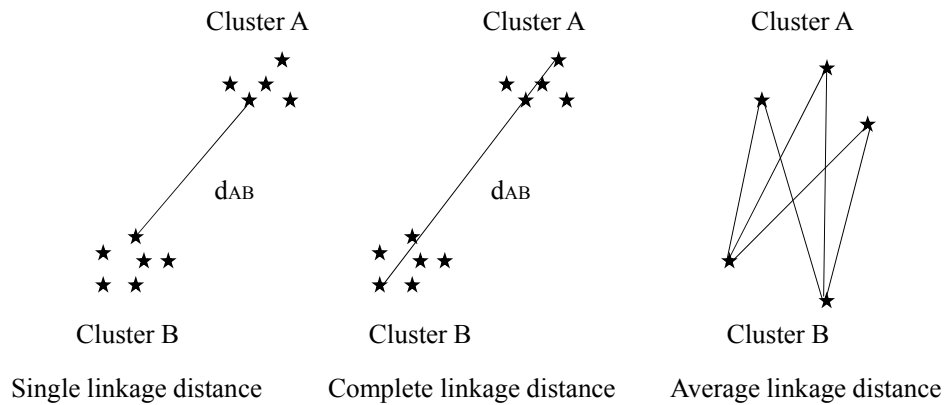
Figure 4-2 Illustration of single, complete and average linkage distance measures (Everitt et al. 2001)

Hierarchical clustering technique is one of the most used cluster analysis techniques.

It is comprised of the agglomerative method and divisive method. The former

successively fuses individuals into groups until a single group containing all the

individuals. The latter successively splits the whole data set into the finer groups until

individuals. These two methods proceed in the opposite direction, as illustrated in

Figure 4-3. The agglomerative process and divisive process can be represented

graphically by a tree-like diagram, known as dendrogram, which can demonstrate both

the cluster-subcluster relationship and the order of fusion or division at each successive

stage (Everitt et al. 2011).

Agglomerative process

```
a
      a, b
b
              a,b,c, d
c
      c, d                      a,b,c,
d                                d,e,f
e
              e, f
f
```
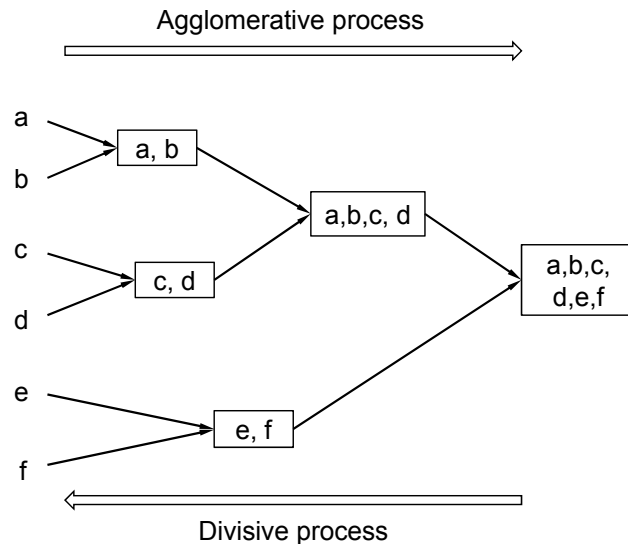
Divisive process

Figure 4-3 Schematic drawing of the agglomerative process and divisive process

Euclidean distance can be significantly affected by the scale of the objective. In

addition, it is not sensible to treat the variables measured in the different units

equivalent. So prior to the analysis, each variable should be standardized.

In building physics, Plagge et al. (2004) applied cluster analysis to group the different

specific bricks by employing their moisture storage data as the criterion variables. The

results showed that cluster analysis can well classify the bricks into their respective

clusters.

4.3 Statistical Regression Analysis

Regression analysis is widely used for the purpose of data description, control and

prediction. The regression model is generally applied to obtain the relationship

between variables.

4.3.1 Linear Least-squares Regression

Linear regression analysis relies on the method of least squares to estimate the parameters in the model. The least-squares method minimizes the sum of the squared residuals, which are the difference between the observed value and their fitted value.

When the regression coefficients are linear, it is called a linear regression. A regression model that involves more than one predictor variable is called a multiple regression model.

The general form of a multiple linear regression is given in equation 4.2.

$$y = \beta_0 + \beta_1 x_1 + \beta_2 x_2 \cdots \beta_k x_k + \varepsilon, \tag{4.2}$$

where y is the response variable, x is the predictor variable, β_k is the regression coefficient, and ε is random error that accounts for the failure of the model to fit the data exactly.

The regression model in equation 4.2 can be also written as:

$$\begin{aligned} y_i &= \beta_0 + \beta_1 x_{i1} + \beta_2 x_{i2} + \ldots \beta_k x_{ik} + \varepsilon_i \\ &= \beta_0 + \sum_{j=1}^{k} \beta_j x_{ij} + \varepsilon_i \end{aligned} \tag{4.3}$$

where $i=1,2\ldots n$, n is the number of observations.

In most cases, it is more convenient to use the matrix form of equation 4.3 to determine the regression coefficients.

$$y = X\beta + \varepsilon, \tag{4.4}$$

where

$$y = \begin{bmatrix} y_1 \\ y_2 \\ \vdots \\ y_n \end{bmatrix}, \quad X = \begin{bmatrix} 1 & x_{11} & x_{12} & \cdots & x_{1k} \\ 1 & x_{21} & x_{22} & \cdots & x_{2k} \\ \vdots & \vdots & \vdots & & \vdots \\ 1 & x_{n1} & x_{n2} & \cdots & x_{nk} \end{bmatrix}, \quad \beta = \begin{bmatrix} \beta_0 \\ \beta_1 \\ \vdots \\ \beta_k \end{bmatrix}, \quad \varepsilon = \begin{bmatrix} \varepsilon_1 \\ \varepsilon_2 \\ \vdots \\ \varepsilon_n \end{bmatrix}$$

y is $n \times 1$ vector, X is $n \times (k+1)$ matrix of the levels of the predictor variables, β is

$(k+1) \times 1$ vector of the regression coefficients, and ε is $n \times 1$ vector of random errors.

The regression coefficient β by the least-squares estimation can be expressed by:

$$\hat{\beta} = (X'X)^{-1}X'y \tag{4.5}$$

If the predictor variables are not taken into account, the total sum of squares will be

written as:

$$\sum_{i=1}^{n}(y_i - \bar{y})^2 = \sum_{i=1}^{n}(\hat{y}_i - \bar{y})^2 + \sum_{i=1}^{n}(y_i - \hat{y}_i)^2 , \tag{4.6}$$

where $\hat{y}_i$ denotes the fitted value of observation y_i from the regression model and

$\bar{y}$ is the mean of all the observations.

The equation 4.6 can be also written as:

$$SS_T = SS_R + SS_{Res} , \tag{4.7}$$

where $SS_T = \sum_{i=1}^{n}(y_i - \bar{y})^2$, $SS_R = \sum_{i=1}^{n}(\hat{y}_i - \bar{y})^2$, $SS_{Res} = \sum_{i=1}^{n}(y_i - \hat{y}_i)^2$.

The total sum of squares of the regression model is represented by SS_T. It is composed

by the sum of squares due to the regression SS_R, and the residual sum of squares or

error sum of squares SS_{Res}. SS_T measures the total variability in the observations. The

greater variability of the observation, the larger the total sum of squares will be. If all the observations are the same, then $SS_T=0$. SS_R measures the amount of variability in the observation y_i associated with the regression line. SS_{Res} accounts for the residual variation which cannot be explained by the regression line.

Residual mean square

The residual mean square MS_{Res} defined in equation 4.8 measures the quality of the model. The smaller the value is, the better the model will fit the observed data. MS_{Res} is also the unbiased estimator of variance σ^2.

$$MS_{Res} = \frac{SS_{Res}}{n-k-1} = \sigma^2 \tag{4.8}$$

Regression mean square

A sum of squares due to regression divided by its associated degrees of freedom is called regression mean square, given in equation 4.9.

$$MS_R = \frac{SS_R}{k} \tag{4.9}$$

4.3.1.1 Statistical significance testing

Statistical significance testing is a procedure to measure the likelihood that an event occurs, assuming that the null hypothesis is true. The significance level or critical *p*-value is the possibility to observe an extreme value by chance. Typical levels of significance are 0.1, 0.05 and 0.01. Statistical significance testing involves comparing a calculated test value to certain critical value for the statistics (e.g., *F*, *t*, chi-square).

If the calculated statistic value is larger than the corresponding critical value, or calculated *p*-value is smaller than the preset significant level, the null hypothesis is rejected, which means the result is statistically significant. In the regression analysis, one can utilize test statistics to examine the significance of regression and significance of the individual regression coefficient.

Test for significance of regression

The test for the significance of regression is performed to verify if there is a linear relation between the response variable and any predictor variable. The null hypothesis will be rejected if at least one predictor variable has a significant contribution to the model. The hypothesis is given by:

$$H_0 : \beta_0 = \beta_1 = \cdots = \beta_k = 0$$
$$H_1 : \text{not all } \beta_j = 0$$

(4.10)

The significance of regression measured by F statistic is expressed by:

$$F = \frac{SS_R / k}{SS_{Res} / (n-k-1)} = \frac{MS_R}{MS_{Res}}$$

(4.11)

Where, *n* is the number of observations; *k* is the number of regression coefficients excluding the constant.

The null hypothesis H_0 is rejected if $F > F_{\alpha,k,n-k-1}$

$F_{\alpha,k,n-k-1}$ is determined from the significant level α, the number of degree of freedom of SS_R and the number of degree of freedom of SS_{Res}. The analysis of the variance for the significance of regression is summarized in Table 4-1.

Table 4-1 Analysis of variance for general linear regression model

Source of variation	Sum of squares SS	Degree of Freedom df	Mean square MS	F
Regression	SS_R	k	$MS_R = SS_R/k$	MS_R/MS_{Res}
Residual	SS_{Res}	n-k-1	$MS_{Res} = SS_{Res}/(n-k-1)$	
Total	SS_T	n-1		

Test for significance of individual regression coefficient

The test for the significance of a regression coefficient is performed to examine if the regression variable is really useful to explain the regression model. The hypothesis is given in equation 4.12:

$$H_0 : \beta_j = 0; H_1 : \beta_j \neq 0 \tag{4.12}$$

The significance of the coefficient can be measured by the *t* statistic:

$$t_0 = \frac{\hat{\beta}_j}{\sqrt{\hat{\sigma}^2 C_{jj}}} \tag{4.13}$$

Where, $\hat{\sigma}^2 = \dfrac{SS_{Res}}{n-k-1} = MS_{Res}$; C_{jj} is the *j*th diagonal element of $(X'X)^{-1}$ corresponding to $\hat{\beta}_j$.

The null hypothesis H_0 is rejected if $|t_0| > t_{\alpha/2, n-k-1}$.

A t test could be used for a one-sided hypothesis e.g., either $H_0:\beta_1 < 0$ or $H_0:\beta_1 > 0$, while the F test considers the two-sided hypothesis.

The regression sum of squares in equation 4.7 can be decomposed into two parts: one part is the regression sum of squares due to the regression model containing *p*

variables, and another part is the extra sum of squares due to regression model containing the remaining *k-p* variables.

$$SS_R(x_1,\cdots,x_k) = SS_R(x_{p+1},\cdots,x_k) + SS_R(x_1,\cdots,x_p \,|\, x_{p+1},\cdots,x_k) \tag{4.14}$$

To test whether some of the coefficients are equal to zero, the following hypothesis is tested.

$$\begin{aligned} &H_0 : \beta_1 = \beta_2 \cdots \beta_p = 0 \\ &H_1 : not\ all\ \beta_j\ in\ H_0\ equal\ to\ zero \end{aligned} \tag{4.15}$$

The associated F statistic is:

$$F = \frac{MS_R(x_1,\cdots,x_p \,|\, x_{p+1},\cdots,x_k)}{MS_{Res}} \tag{4.16}$$

The null hypothesis H_0 is rejected, if $F > F_{\alpha,p,n-k-1}$

If $p=1$, the statistic is to test whether a single regression coefficient β_j is equal to zero.

$$F = \frac{MS_R(x_j \,|\, x_1,\cdots,x_{j-1},x_{j+1},\cdots,x_k)}{MS_{Res}} \tag{4.17}$$

4.3.1.2 Model adequacy check

Coefficient of determination

The goodness of fit of the regression model to the data can be measured by the coefficient of determination R^2, which represents the amount of variance in the dependent variable explained by the regression model. A higher value of R^2 implies that most of the variability in y is explained by the regression model.

$$R^2 = \frac{SS_R}{SS_T} = 1 - \frac{SS_{Res}}{SS_T} \qquad\qquad 0 \le R^2 \le 1 \qquad\qquad\qquad (4.18)$$

The high coefficient of determination is one but not the only standard to evaluate the suitability of the regression mode. Other criterion should be used together to determine the adequacy of the model.

Adjusted coefficient of determination

The coefficient of determination R^2 never decreases when additional predictor variable x is included into the model, since SS_{Res} will not increase with additional predictor variable x and SS_T always remains the same with the fixed numbers of the responses. So it is important to address if the added predictor variable really contributes to the decrease of the total variability of the regression model. The adjusted coefficient of determination, given in equation 4.19, will only increase when the added variable reduces the residual mean square (Montgomery 2006). R^2_{Adj} is equal to or less than R^2.

$$R^2_{Adj} = 1 - \left(\frac{n-1}{n-k-1}\right)\frac{SS_{Res}}{SS_T} \qquad\qquad\qquad (4.19)$$

The assumptions to build linear regression model include:

- The error terms ε_i has a mean value of 0 and a constant variance.
- The error terms ε_i is normally distributed and uncorrelated to each other.

A small deviation of these assumptions will not lead to serious model issues. But a large violation of the assumption will lead to a wide range of standard error of the

regression coefficient, even the wrong regression model. The normal method to check the model adequacy is to study the model residual, which can be regarded as the observed error to reflect the properties assumed for the ε_i (Kutner et al. 2004). Two forms of the residual are introduced as follows:

Residual of regression

The residual e_i is the difference between the observed value y_i and the corresponding fitted value $\hat{y}_i$.

$$e_i = y_i - \hat{y}_i \tag{4.20}$$

Standardized residual

The standardized residual is a kind of scaling residual for residual analysis.

$$d_i = \frac{e_i}{\sqrt{MS_{Res}}} \qquad i = 1, 2...n, \tag{4.21}$$

where MS_{Res} is the residual mean square. A larger standardized residual (if >3) may indicate an outlier.

The diagnostic plot of the residual is an effective way to examine the departure of the model assumption and the aptness of the regression model. The residual plot clearly shows the deviation departure from the fitted regression line. The usual plots include the normal probability plot of residuals, the plot of residuals against predictor variable and the plot of residuals against fitted value. They are introduced as follows.

Normal probability plot of residuals

A normal probability plot of residuals is useful to check the assumption if the error term is normally distributed. It plots each ordered residual against its z-score value under normality assumption. The z-score value measures the divergence of a individual data from the mean of the data set. If the normality assumption is fulfilled, the points in the graph will follow a straight line. A small deviation from the normality assumption will not lead to a serious problem. A large violation needs to be concerned, and correction methods should be applied, such as variable transformation.

Plot of residuals against fitted value

A plot of residuals against the corresponding fitted values can assess the appropriateness of the regression and examine whether the variance of the error terms is constant. Moreover, it can also help to identify the outlier and the nonlinearity of the function. If the assumption is met, the plotted point will lay between horizontal bands.

Plot of residuals against predictor variable

A plot of residuals against each predictor variable has the same usefulness as the plot of residuals against the fitted value. It helps to check if there is an outlier in the predictor variable and examine whether the variance of the error terms is constant.

Transformation of response and predictor variable

If the assumption of the regression model is not satisfied, e.g., the variance of error term is not constant, the validation and correctness of the model is questionable and suspect. Some techniques offer useful strategies to transform the data to remedy the departure of the assumptions, e.g., the scaled response variable and predictor variable in the appropriate form.

The new regression model, with the transformed form of response and predictor variable, still needs to be examined to determine whether it is appropriate and meets the assumptions.

4.3.1.3 Regression model selection

A regression model can include one or part of the candidate predictor variables. For the n predictor variables, there are 2^n alternative models to fit the observed data. In the model-building process, not all the predictors have the same contribution. The appropriate selection of predictors in the model is important: if the key predictors are ignored, the model cannot adequately explain the relation between the response and predictor variables and produce the bias estimation on the regression coefficients. If unnecessary predictors are included, the variance of the estimated parameters will become larger and the corresponding cost on acquiring those unnecessary predictors will rise (Kutner et al. 2004). The regression model selection is a procedure that uses specified criterion to identify the most suitable model.

The stepwise regression selection procedure is one of the most used model selection methods. In the selection process, the model is evaluated in each step with adding or deleting a predictor variable by certain criterion, e.g., t statistic, F statistic, p-value. The stepwise select ends with a single "most suitable" candidate model.

There are two methods in the stepwise selection. The first method is the forward stepwise selection, which begins without any predictor variable in the model assuming only the intercept is included. At each step, one predictor is added into the model and the corresponding p-value is calculated to compare with the predefined "threshold" value, which is the α-to-enter for adding a variable and α-to-remove for deleting a variable. If the calculated p-value is smaller than the α-to-enter, then this predictor is added into the model. This method not only calculates the p-value of newly added predictor, but also that of the predictors already in the model. If the p-value of the predictor already existed in the model is larger than α-to-remove after the new predictor enters, this existed predictor will be dropped. The stepwise selection stops when no more calculated p-value is smaller than the α-to-enter, or the last predictor variable is reached.

In contrast to the forward stepwise regression method, the backward stepwise regression is the opposite procedure, which begins with all the predictors in the model. At each step, the predictor variable with the calculated p-value larger than α-to-remove is dropped from the model until the "most suitable" model is obtained,

or no more predictor variables can be dropped. The advantage of this method is that it accounts for the effect of the important predictors.

The stepwise regression method may require the judgment of the experienced experts in the associated research field to determine if the selected predictor variables in the "final" model are reasonable to the response variable.

4.3.1.4 Indicator for qualitative variable

In addition to the quantitative variable, the qualitative variable can also be used in the regression model. In building physics, the qualitative variables could be the orientation (East, West, etc.), the weather condition (cloudy, sunny, etc.), and the type of buildings different in height (high-rise or low-rise).

Normally, if there are n levels in the qualitative variable, assuming the nth level are selected to be dropped, the qualitative variable can be represented by the other n-1 indicator variables, each taking on the values of 0 and 1 (Kutner et al. 2004). If all the n-1 indictor variables take the value of 0, it indicates that the nth level is chosen. The advantage of this method is to avoid computational difficulties, such as the singularity in the matrix of coefficients (Frey et al. 2003). It is important to explain the meaning of the regression coefficient of the qualitative variable. Since the indicator variable is only represented by 0 and 1, the coefficients of the indicator variable do not represent the magnitude of the importance. Therefore, the estimated regression coefficient of the indicator variable is not comparable with that of the quantitative input with respect

to evaluating the sensitivity of output variable to input variable (Frey et al. 2003). If there is no interaction between qualitative and quantitative variables, the estimated coefficient of indicator variable adjusts the intercept of the regression model, i.e., lead to the intercept shifting up or down. When the indicator variable is employed for the qualitative variable, the quantitative variable in the model do not make any change.

Here, one example in building physics is used to explain the concept described above. Supposing the solar radiation incident on the external wall assembly is only related to the solar radiation intensity and the orientation of the wall assembly, without consideration of other factors. The first predictor variable, the solar radiation intensity, is a quantitative variable. The second predictor variable, orientation of the wall assembly, is a qualitative variable and composed of four classes: East, South, West, and North. Therefore, there are three indicator variables (x_2, x_3, and x_4), and each can be expressed by the values of 0 and 1. The data input of indicator variable is listed in Table 4-2.

Table 4-2 Data input of indicator variable

Orientation classes	x_2	x_3	x_4
East	0	0	0
South	1	0	0
West	0	1	0
North	0	0	1

A first-order regression model to present the introduced relation is expressed as:

$$y = \beta_0 + \beta_1 x_1 + \beta_2 x_2 + \beta_3 x_3 + \beta_4 x_4 + \varepsilon, \tag{4.22}$$

where x_1 is the solar radiation intensity, x_2 is the South orientation, x_3 is the West orientation, x_4 is the North orientation.

$$x_2 = \begin{cases} 1 \text{ if South orientation} \\ 0 \text{ otherwise} \end{cases} \quad x_3 = \begin{cases} 1 \text{ if West orientation} \\ 0 \text{ otherwise} \end{cases} \quad x_4 = \begin{cases} 1 \text{ if North orientation} \\ 0 \text{ otherwise} \end{cases}$$

In case that the East orientation is adopted, $x_2=0$, $x_3=0$, and $x_4=0$. Equation 4.22 will become:

$$\begin{aligned} E(y \mid x_{2,3,4} = 0) &= \beta_0 + \beta_1 x_1 + \beta_2(0) + \beta_3(0) + \beta_4(0) \\ &= \beta_0 + \beta_1 x_1 \end{aligned}$$

(4.22 a)

Similar, for South, West, and North orientations, equation 4.22 will be written as:

$$\begin{aligned} E(y \mid x_2 = 1) &= \beta_0 + \beta_1 x_1 + \beta_2(1) + \beta_3(0) + \beta_4(0) \\ &= (\beta_0 + \beta_2) + \beta_1 x_1 \end{aligned}$$

(4.22 b)

$$\begin{aligned} E(y \mid x_3 = 1) &= \beta_0 + \beta_1 x_1 + \beta_2(0) + \beta_3(1) + \beta_4(0) \\ &= (\beta_0 + \beta_3) + \beta_1 x_1 \end{aligned}$$

(4.22 c)

$$\begin{aligned} E(y \mid x_4 = 1) &= \beta_0 + \beta_1 x_1 + \beta_2(0) + \beta_3(0) + \beta_4(1) \\ &= (\beta_0 + \beta_4) + \beta_1 x_1 \end{aligned}$$

(4.22 d)

The plot of the relations denoted by equation 4.22a to 4.22d is presented in Figure 4-4.
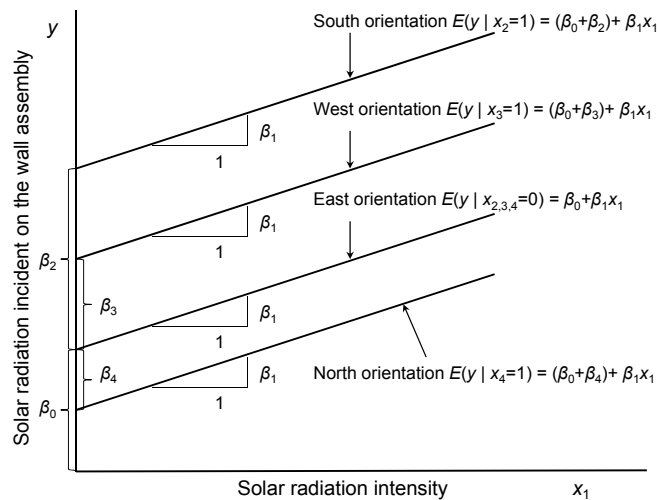
Figure 4-4 Illustration of regression model with the variation of orientation

The four regression models have the same slope of β_1. The coefficients β_2, β_3 and β_4 indicates respectively how much higher or lower the West, South, and North oriented walls gain the solar radiation than the East oriented walls does with respective to the same solar radiation intensity. Thus, β_2, β_3, and β_4 measure the effect of different orientations on the solar radiation incident on the wall assembly, compared to the East orientation. Of course, this influence can be compared between orientations, i.e., the difference of incident solar radiation between South and West orientation can be obtained by $\beta_2 - \beta_3$.

The application of the indicator variable in the regression model for sensitivity analysis is exemplified in Section 7.4.4.

4.3.2 Robust Regression

Validity of the ordinary least-square regression requires several fundamental assumptions, as described in Section 4.3.1.2. If those assumptions cannot be satisfied by the nature of the data, the prediction and estimation of the model may be biased, e.g., the outlier can seriously affect the least-squares estimation since it pulls the regression line in the direction that deviates from the majority of the data.

Once the residual plot or standardized residual identifies the outlier, the next step is to check the source of the outlier. If it is due to an erroneous measurement or other errors, it could be discarded to increase the accuracy of the model. However, in most of the cases, there is no compelling reason to explain the outlier; and in those cases,

the outlier should be included in the model. Robust regression analysis is developed as an alternative to the least-squares estimation when the assumptions cannot adequately be fulfilled. It keeps the outlier in the dataset but tries to dampen its influence on the estimation of the regression coefficients. So the regression model will not be sensitive to these unusual outliers.

Different algorithms are implemented for robust regression, e.g., least absolute deviations (LAD) regression and least median of squares (LMS) regression. Iteratively reweighted least square (IRIS) is one of the widely used robust methods. The method employs the weighted lease-squares to reduce the influence of the outliers by adjusting the weights that vary inversely to the size of the residual (Kutner et al. 2004). The case with a large residual is assigned with relatively small weight. In each iteration, the weights are revised until the convergence criteria are reached or the maximum iteration number is attained.

4.4 Application of Cluster Analysis and Regression Analysis

Cluster analysis and regression analysis are applied in this section to simplify the procedure for the moisture storage measurement, identify the material cluster, derive the generic material and qualify the incomplete material data.

4.4.1 Statistical Analysis on Moisture Storage Data in the Building Brick Category

As mentioned in Section 4.1.2, conducting pressure plate and sorption isotherm tests to get the knowledge of moisture storage characteristics of building material is very time-consuming. A statistical approach to detect the natural relations among moisture contents and apply these relations to reduce the measurement steps is introduced in this section.

4.4.1.1 Clustering of moisture storage data in the building brick category

Moisture storage data of 20 specific bricks are collected for cluster analysis in order to find the natural groups among moisture contents. For each brick, moisture contents come from 11 measurements in the overhygroscopic range and 8 measurements in the hygroscopic range. For convenience, logarithmic capillary pressures is represented by *pC* (*pC=log$_{10}$(-P$_c$))*. The symbol *w3.48* denotes moisture content at *pC3.48*. *w6.56 (97.4%)* denotes moisture content at 97.4% relative humidity, corresponding to *pC6.56*.

Prior to cluster analysis, moisture contents at the specific capillary pressures are first standardized. Then, the normalized Euclidean distance between each pair of moisture contents are calculated and compared. Moisture contents that have the smallest distance are joined into one cluster. Then, the Ward's clustering method is applied to measure the distance between the clusters or groups of moisture contents, due to its

high efficiency and good performance (Hands and Everitt 1987; Everitt et al. 2011). The clusters with the closest distance are fused together. The agglomerative process continues until all the moisture contents are joined into a single cluster.
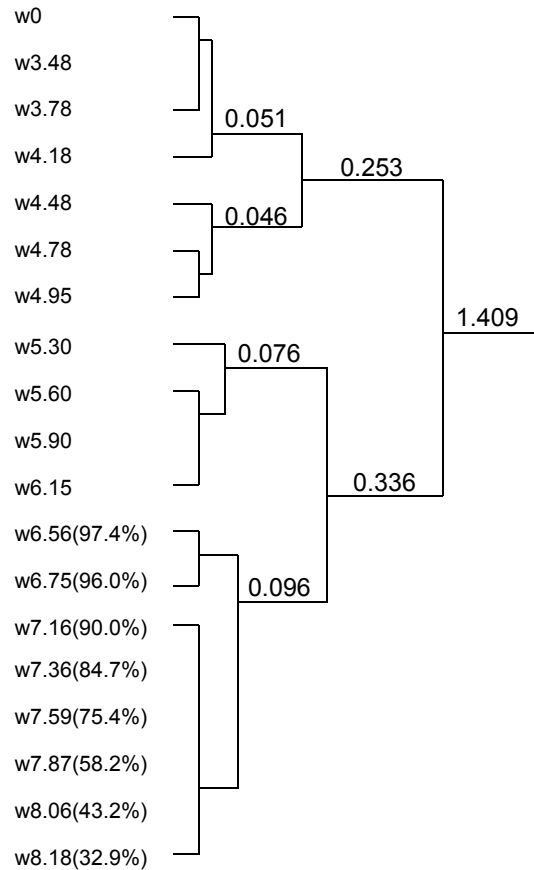
Figure 4-5 Tree diagram of clustering of moisture storage data in the building brick category by using Ward's method

Tree diagram of clustering of 19 moisture contents is presented in Figure 4-5. In this tree diagram, the leaves on the left side of the structure are the specific moisture contents. The numbers above the stem is distance at which two clusters or individuals are joined. The nodes of the diagram represent the clusters. The root of the tree on the right side of the diagram has the largest joining distance or dissimilarity.

Four sub-clusters are identified in the dendrogram. In the overhygroscopic range, moisture contents from $w0$ to $w4.18$ can be grouped into one cluster with a joining distance of 0.051. Moisture contents $w4.48$, $w4.78$, and $w4.95$ are merged into another cluster with a joining distance of 0.046. Moisture contents from $w5.30$ to $w6.15$ are in one cluster with a joining distance of 0.076. In the hygroscopic range, moisture contents at the different relative humidity levels (from 97.4% to 32.9%) are similar and are grouped in one cluster with a joining distance of 0.096. Subsequently, in the next agglomeration, moisture contents from $w0$ to $w4.95$ are merged to a second-stage cluster with a joining distance of 0.253. Moisture contents from $w5.30$ to $w6.15$ in the overhygroscopic range and moisture contents from $w6.56$ to $w8.18$ in the hygroscopic range are grouped into a second-stage cluster with a joining distance of 0.336. Finally, these two second-stage clusters are agglomerated into one cluster with the largest distance 1.409.

The clustered moisture contents from Figure 4-5 can also be illustrated in the moisture retention curve as shown in Figure 4-6. Moisture contents in the moisture retention curve are divided into four groups: three groups in the overhygroscopic range and one group in the hygroscopic range.
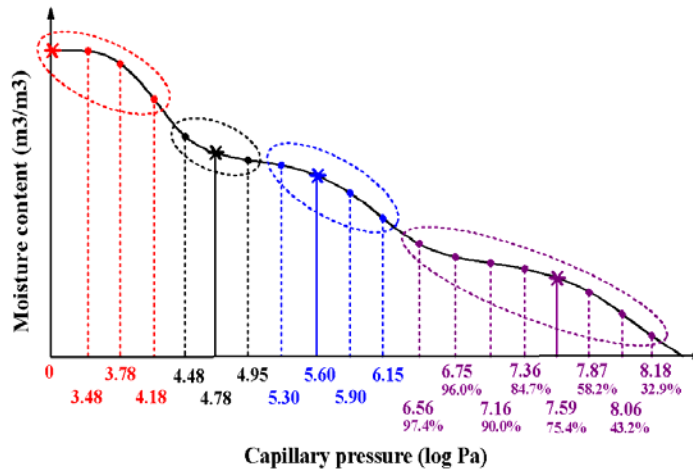
Figure 4-6 Clustered moisture storage data on the moisture retention curve

4.4.1.2 Scatterplot matrixes of the clustered moisture contents

Based on cluster analysis, the scatterplot matrixes of moisture contents at different

logarithmic capillary pressures (or relative humidly levels) in each identified cluster

are presented in Figures 4-7, 4-8, 4-9, and 4-10, respectively. In the graph, each circle

represents one specific brick. From the plot matrix, it is easy to find that the moisture

contents in the same cluster form a good linear relationship to each other. For

instance, in Figure 4-7, moisture content *w0* has a good linear relationship with

moisture contents *w3.48, w3.78,* and *w4.18,* respectively.
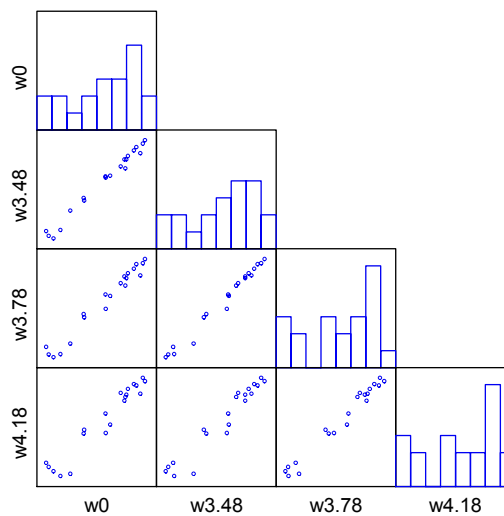
Figure 4-7 Scatterplot matrix of moisture contents w0, w3.48, w3.78 and w4.18 in the building
brick category
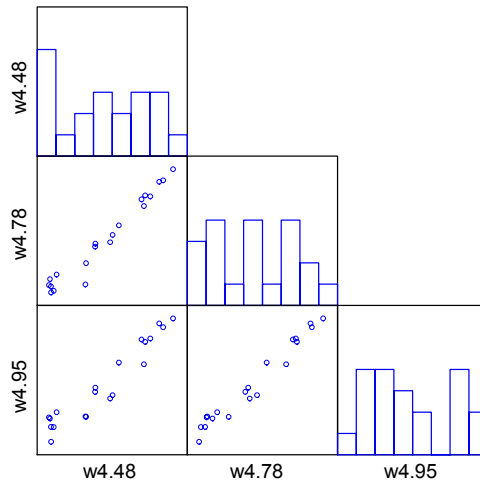
Figure 4-8 Scatterplot matrix of moisture contents w4.48, w4.78 and w4.95 in the building brick category

The transformation of variables in a certain form could help to build a better linear relationship between them. Figure 4-9 presents the scatterplot matrix of moisture contents *w5.30*, *w5.60*, and *w5.90*, without transformation and with logarithmic transformation. After logarithmic transformation, these three moisture contents gain a better linear relationship with each other.
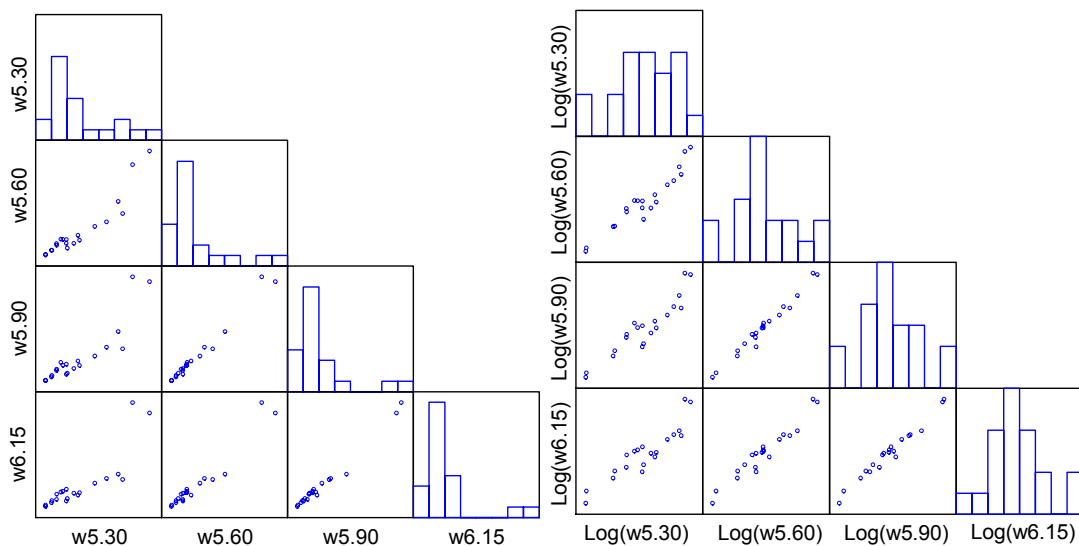
Figure 4-9 Scatterplot matrixes of moisture contents w5.30, w5.60, and w5.90 without transformation (left) and with logarithmic transformation (right) in the building brick category

104
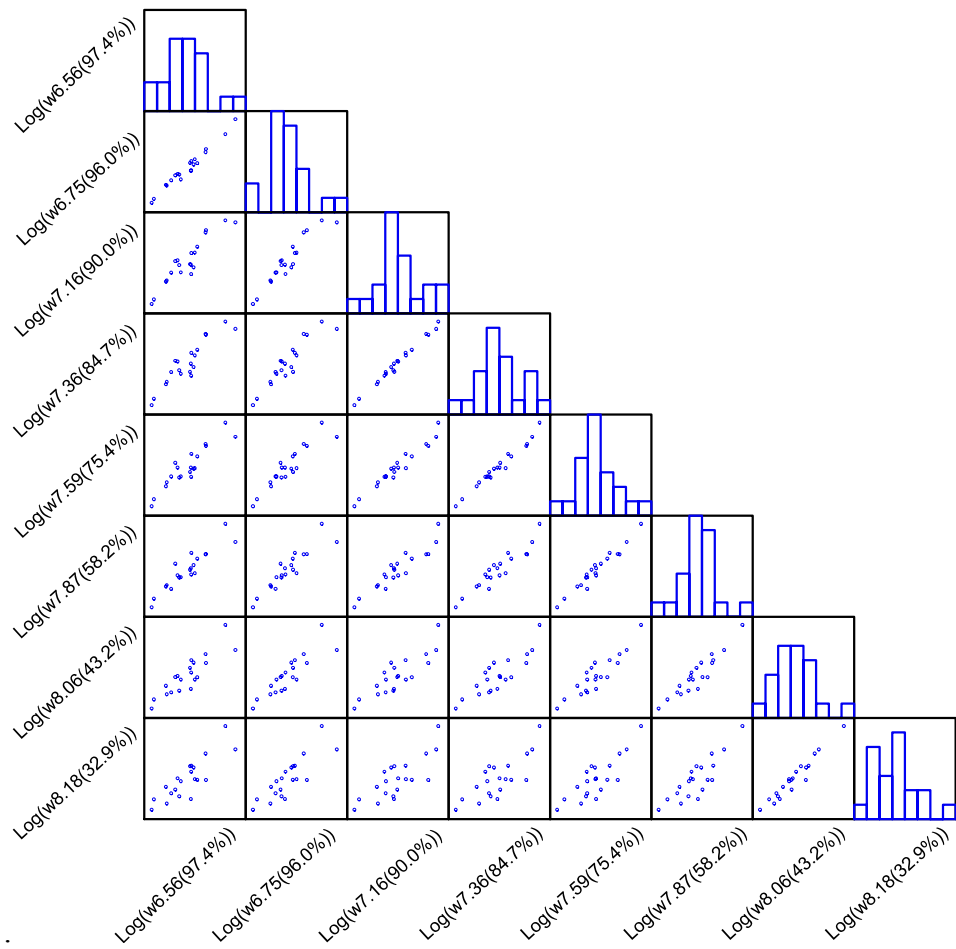
Figure 4-10 Scatterplot matrix of logarithmic-transformed moisture contents in the hygroscopic range in the building brick category

The scatterplot matrix of the logarithmic-transformed moisture contents in the hygroscopic range is shown in Figure 4-10. From the graph, one can easily find that moisture content *w7.59* (*75.4%*) form has a good linear relationship with other moisture contents.

4.4.1.3 Regression analysis on the clustered moisture contents based on the reference moisture content

Once cluster analysis and scatterplot matrix detect that there exist some relationships between moisture contents in each group, the next step is to use the regression

analysis to examine and derive these relationships. One advantage for creating the relationship between moisture contents is that it can help to reduce the measurement steps, therefore, save experimental resource in terms of the time and expense. By only measuring one moisture content as the reference value, other moisture contents in the same group can be predicted by employing the regression models. The strategy to choose the reference moisture content follows two criteria: 1, it should have a good linear relationship with the others. In one cluster, the regression analyses among all moisture contents are conducted, and the one which forms the best relationships with all the others is selected as the reference one; and 2. the value should not be difficult to measure.

The relationship between the reference and predicted moisture contents can be represented by a simple linear regression model:

$$w_{predicted} = constant + coefficient \cdot w_{reference} \tag{4.23}$$

The output of regression model on moisture contents $w0$ and $w3.48$, calculated from statistical software SYSTAT11 (2002), is shown in Figure 4-11a. The p-value of the regression coefficient and p-value of the analysis of variance are less than 0.01, indicating the significance of the regression model and the regression coefficient. The coefficient of determination has the value of 0.985, which implies the adequacy of the model. The fitted value and residual of each case are listed in Figure 4-11b.

Dep Var: w3.48   N: 20   Multiple R: 0.992   Squared multiple R: 0.985
Adjusted squared multiple R: 0.984   Standard error of estimate: 0.009

Variable	Coefficient	Std Error	Std Coeff.	Tolerance	t	P(2 Tail)
Constant	-0.025	0.009	0.000	.	-2.813	0.012
w0	1.053	0.031	0.992	1.000	33.834	0.000

Variable	Coefficient	Lower 95%	Upper 95%
Constant	-0.025	-0.044	-0.006
w0	1.053	0.987	1.118

Analysis of Variance

Source	Sum-of-Squares	df	Mean-Square	F-ratio	P
Regression	0.094	1	0.094	1144.767	0.000
Residual	0.001	18	0.000		

Case	w3.48	Fitted value	Residual
ZA	0.2774	0.2726	0.0048
ZC	0.2063	0.1984	0.0079
ZD	0.3580	0.3549	0.0031
ZE	0.3507	0.3505	0.0002
ZF	0.1519	0.1531	-0.0012
ZG	0.2972	0.3138	-0.0166
ZH	0.2800	0.2722	0.0078
ZI	0.3166	0.3118	0.0048
ZJ	0.2815	0.2821	-0.0006
ZK	0.3166	0.3159	0.0007
ZL	0.3430	0.3368	0.0063
ZM	0.3358	0.3316	0.0042
ZN	0.3240	0.3192	0.0047
ZO	0.1646	0.1779	-0.0132
ZP	0.1622	0.1478	0.0144
ZQ	0.1465	0.1633	-0.0168
ZHS	0.2334	0.2264	0.0070
ZBD	0.2280	0.2276	0.0004
ZJN	0.3300	0.3451	-0.0151
ZWB	0.3015	0.3041	-0.0026

a) Basic SYSTAT output   b) Basic regression data

Figure 4-11 Output of least-square regression analysis on moisture contents *w3.48* and *w0* a) and the basic regression data b)

According to the output presented in Figure 4-11, the regression model to build the relationship between moisture contents *w3.48* and *w0* is expressed as:

$$w3.48 = -0.025 + 1.053 \cdot w0 \tag{4.24}$$

The scatter plot of these two moisture contents and corresponding residual diagnostic plots are presented in Figure 4-12. The plot of residuals against the fitted value (Figure 4-12b) and the plot of residuals against the predictor variable (Figure 4-12c) indicate the assumption of constant error variance is fulfilled. In the normal probability plot of residual (Figure 4-12d), the data partly deviates from the straight line in the lower left quarter. This deviation is probably due to the small sample size. The coefficient of determination and residual diagnostic plots verify the rationality and validity of the regression model.

a) Scatter plot of two variables

b) Residual against fitted value Ŷ

c) Residual against predictor

d) Normal probability plot
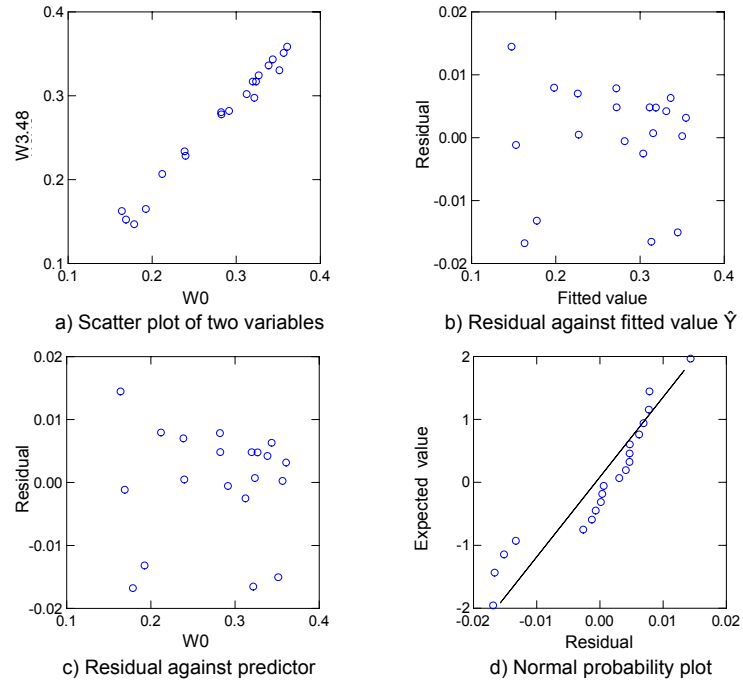
Figure 4-12 Scatter plot of moisture contents w0 and w3.48 and corresponding residual diagnostic plots

In some cases, the transformation of moisture contents in a certain form is needed to obtain the better relationship, as shown in Figure 4-9. The regression model for logarithmic-transformed moisture contents *w5.30* and *w5.60* is expressed as:

$$Log(w5.30) = 0.161 + 0.987 \cdot Log(w5.60) \tag{4.25}$$

After transformation, equation 4.25 becomes:

$$w5.30 = 10^{0.161} \cdot w5.60^{0.987} \tag{4.26}$$

If the outlier exists in the data and there is no indication that the outlier is unreasonable and should be eliminated, the robust regression is used to reduce the influence of the outlier.

The ordinary linear least-square regression model for moisture contents *w4.48* and *w4.78* is given by:

$$w4.48 = 0.045 + 0.875 \cdot w4.78 \qquad \text{with} \qquad R^2 = 0.961 \qquad\qquad (4.27)$$

The residual plots in Figure 4-13 indicate that there is one outlier in the dataset. With

a careful check on the measured data, there is no obvious evidence to prove that this

outlier comes from a measurement error. In this case, robust regression is adopted to

weaken the influence of the outlier, while still keeping it in the analysis. The output of

robust regression by iteratively reweighted least square method and basic regression

data with fitted value and residual of each case is shown in Figure 4-14.

a) Residual against fitted value Ŷ   b) Residual against predictor
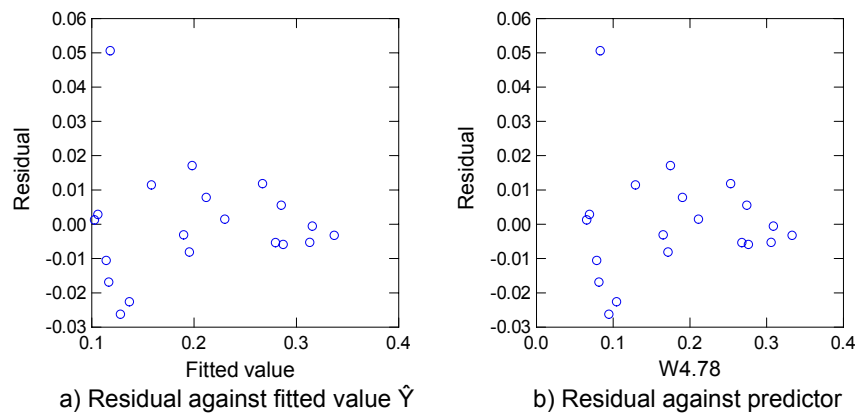
Figure 4-13 identification of the outlier by the residual diagnostic plots

The robust regression model for moisture contents *w4.48* and *w4.78* is given by

equation 4.28.

$$w4.48 = 0.041 + 0.888 \cdot w4.78 \qquad\qquad \text{with} \quad R^2 = 0.961 \qquad\qquad (4.28)$$

The difference between the ordinary least-square regression model (equation 4.27)

and the robust regression model (equation 4.28) is not substantial, so the influence of

the outlier is not significant for this case.

Iteration No.	Loss	Constant	Coefficient
0	0.245355D+00	0.101000D+00	0.102000D+00
1	0.500089D-02	0.452025D-01	0.875319D+00
2	0.221838D-02	0.452025D-01	0.875319D+00
3	0.220149D-02	0.425839D-01	0.884973D+00
4	0.214722D-02	0.417388D-01	0.887838D+00
5	0.209295D-02	0.414859D-01	0.888468D+00
6	0.206254D-02	0.414406D-01	0.888385D+00
7	0.204509D-02	0.414447D-01	0.888234D+00
8	0.203682D-02	0.414577D-01	0.888111D+00
9	0.203283D-02	0.414671D-01	0.888042D+00
10	0.203110D-02	0.414727D-01	0.888005D+00
11	0.203035D-02	0.414755D-01	0.887987D+00
12	0.203004D-02	0.414769D-01	0.887979D+00
13	0.202991D-02	0.414775D-01	0.887975D+00
14	0.202987D-02	0.414778D-01	0.887974D+00
15	0.202985D-02	0.414779D-01	0.887973D+00
16	0.202984D-02	0.414780D-01	0.887973D+00
17	0.202984D-02	0.414780D-01	0.887973D+00
18	0.202984D-02	0.414780D-01	0.887973D+00

Case	w4.48	Fitted value	Residual
1	0.232	0.229	0.002
2	0.291	0.285	0.006
3	0.187	0.189	-0.002
4	0.104	0.100	0.004
5	0.220	0.211	0.009
6	0.334	0.338	-0.004
7	0.114	0.135	-0.020
8	0.279	0.267	0.012
9	0.216	0.197	0.019
10	0.275	0.280	-0.005
11	0.187	0.194	-0.007
12	0.281	0.287	-0.006
13	0.170	0.157	0.013
14	0.315	0.316	-0.001
15	0.308	0.314	-0.006
16	0.102	0.126	-0.024
17	0.100	0.114	-0.014
18	0.104	0.112	-0.008
19	0.109	0.103	0.006
20	0.169	0.116	0.053

b) Basic regression data

HUBER robust regression: 20 cases have positive psi-weights
The average psi-weight is 0.85616

Dependent variable is w4.48

Source	Sum-of-Squares	df	Mean-Square
Regression	0.961	2	0.481
Residual	0.005	18	0.000
Total	0.966	20	
Mean corrected	0.127	19	

Raw R-square (1-Residual/Total) = 0.995
Mean corrected R-square (1-Residual/Corrected) = 0.960
R(observed vs predicted) square = 0.961

Parameter	Estimate	A.S.E.	Param/ASE	Wald Confidence Interval Lower < 95%> Upper	
CONSTANT	0.041	0.009	4.642	0.023	0.060
COEFFICIENT	0.888	0.042	21.224	0.800	0.976

a) Basic SYSTAT output

Figure 4-14 Output of robust regression on moisture contents w4.48 and w4.78 a) and basic regression data b)

In the following analyses, if the outlier is identified and it is verified not from a measurement error, robust regression is applied to substitute linear least-squares regression.

In the overhygroscopic range, moisture contents $w0$, $w4.78$, and $w5.60$ are selected as the reference moisture contents to derive others in the same cluster, as presented in Figure 4-6. The coefficients of regression models are summarized in Table 4-3.

Table 4-3 Coefficients of regression models based on w0, w4.78, and w5.60 in the building brick category

	constant	w0	R^2
w3.48	-0.025	1.053	0.985
w3.78	-0.046	1.100	0.966
w4.18	-0.093	1.178	0.926
	constant	w4.78	R^2
w4.48	0.041	0.888	0.961(Ro)
w4.95	-0.028	1.033	0.964
	constant	Log(w5.60)	R^2
Log(w5.30)	0.161	0.987	0.908
Log(w5.90)	-0.103	0.970	0.979 (Ro)
Log(w6.15)	-0.162	0.986	0.940

Note: Ro denotes that the regression coefficients and R^2 are derived from robust regression

In the hygroscopic range, 75.4% relative humidity is easily achieved by the *NaCl* solution, so moisture content at 75.4% RH is selected as the reference value. The logarithmic-transformed moisture contents are used for analysis. The coefficients of regression models based on *w7.59 (75.4%)* are summarized in Table 4-4.

Table 4-4 Coefficients of regression models based on w7.59 (75.4%) in the building brick category

	constant	Log(w7.59(75.4%))	R^2
Log(w6.56(97.4%))	1.102	1.288	0.846(Ro)
Log(w6.75(96.0%))	0.747	1.199	0.861(Ro)
Log(w7.16(90.0%))	0.196	1.029	0.956
Log(w7.36(84.7%))	0.249	1.075	0.974(Ro)
Log(w7.87(58.2%))	-0.464	0.848	0.953(Ro)
Log(w8.06(43.2%))	-0.824	0.748	0.831
Log(w8.18(32.9%))	-0.915	0.749	0.693

Note: Ro denotes that the regression coefficients and R^2 are derived from robust regression

The results from Table 4-3 and Table 4-4 indicate that the predicted moisture content could be well estimated by the reference one in the same cluster ($R^2 > 0.8$ in most

cases). With this method, the moisture storage characteristics could be determined by three measurements (*w0*, *w4.78*, and *w5.60*) in the overhygroscopic range and one measurement (*w7.59* (*75.4%*)) in the hygroscopic range. The total measurement steps are reduced to four.

4.4.1.4 Regression analysis on the clustered moisture contents based on basic material parameters

In case there is no moisture storage measurement, moisture contents of building bricks in the overhygroscopic range are still predictable by some basic material parameters.

Material parameters related to thermal properties are excluded in the analysis. The considered parameters, including their transformed data (e.g., logarithmic or exponential transformed data) are:

- ρ: density of dry material
- θ_{por}: open porosity
- θ_{eff}: effective saturation moisture content
- θ_{cap}: capillary saturation moisture content
- A_w: water absorption coefficient
- μ_{dry}: water vapor diffusion resistance factor (dry-cup value)
- μ_{wet}: water vapor diffusion resistance factor (wet-cup value)

The variables in the model are selected by using a backward stepwise regression in which unimportant variables are sequentially eliminated from the model. The α-to-enter and α-to-remove use the values of 0.05 and 0.10, respectively, as the

threshold to add or delete a variable. All candidate variables are included in the model at the beginning. In each step, the variable that has the calculated *p*-value larger than α-to-remove is deleted from the model. The removed variable has the opportunity to be added into the model again if its calculated *p* -value is smaller than α-to-enter in the new model. The process continues until no more variable in the model has the calculated *p*-value larger than α-to-remove.

Table 4-5 presents the coefficients of regression models based on basic material parameters. Those models, for example, can be expressed as:

$$w3.48 = 0.0365 + 1.163 \cdot \theta_{cap} \tag{4.29}$$

$$w4.48 = -0.056 + 1.472 \cdot \theta_{cap} - 0.267 \cdot A_w \tag{4.30}$$

$$Logw5.60 = -5.930 + 9.945 \cdot \theta_{por}^{0.5} - 2.752 \cdot A_w^{0.5} \tag{4.31}$$

After transformation, the equation 4.31 becomes:

$$w5.60 = 10^{-5.930 + 9.945 \cdot \theta_{por}^{0.5} - 2.752 \cdot A_w^{0.5}} \tag{4.32}$$

As shown in the Table 4-5, moisture contents in the low capillary pressure range can be determined by capillary saturation moisture content. From *w4.48* to *w5.30*, they are related to two parameters: capillary saturation moisture content and water absorption coefficient. In the high capillary pressure range, the logarithmic-transformed moisture contents can be derived by the square root of open porosity and the square root of water absorption coefficient.

Table 4-5 Coefficients of regression models based on basic material parameters in the building brick category

	constant	θ_{cap}	A_w	R^2
w0	0.056	1.108	-	0.936
w3.48	0.0365	1.163	-	0.919
w3.78	0.017	1.210	-	0.894
w4.18	-0.029	1.312	-	0.880
w4.48	-0.056	1.472	-0.267	0.883(Ro)
w4.78	-0.100	1.655	-0.369	0.864(Ro)
w4.95	-0.134	1.805	-0.516	0.864(Ro)
w5.30	-0.090	1.439	-0.640	0.877
	constant	$\theta_{por}^{0.5}$	$A_w^{0.5}$	R^2
Log(w5.60)	-5.930	9.945	-2.752	0.803(Ro)
Log(w5.90)	-5.782	9.580	-2.760	0.858(Ro)
Log(w6.15)	-5.788	9.542	-2.845	0.870

Note: Ro denotes that the regression coefficients and R^2 are derived from robust regression

4.4.2 Statistical Analysis on Moisture Storage Data in the Plaster/ mortar Category

The measured moisture storage data of 47 plaster / mortars are collected for cluster analysis and regression analysis. Both the exterior and interior plaster/mortars are included. For each material, moisture contents come from 10 measurements in the overhygroscopic range and 8 measurements in the hygroscopic range. The effective saturation moisture content $w0$ is excluded due to its high uncertainty.

4.4.2.1 Clustering of moisture storage data in the plaster/mortar category

The clustering process is the same as the one applied for the moisture storage data in the building brick category. Tree diagram of clustering of 18 moisture contents is demonstrated in Figure 4-15.

As opposed to the tree diagram of the building bricks, the moisture contents in the

plaster/mortar category can be clearly classified as one cluster in the overhygroscopic

range with a joining distance of 0.377, and one cluster in the hygroscopic range with a

joining distance of 0.151. In the overhygroscopic range, there are three sub-clusters:

moisture contents $w3.48$, $w3.78$, and $w4.18$ are in one cluster with a joining distance of

0.030; moisture contents $w4.48$, $w4.78$, and $w4.95$ are in another cluster with a joining

distance of 0.036; and moisture contents from $w5.30$ to $w6.15$ are the third cluster with

a joining distance of 0.049. In the hygroscopic range, moisture contents from $w6.56$

(97.4%) to $w7.59$ (75.4%) are in one cluster with a joining distance of 0.070, and

moisture contents from $w7.87$ (58.2%) to $w8.18$ (32.9%) are in another cluster with a

joining distance of 0.029.
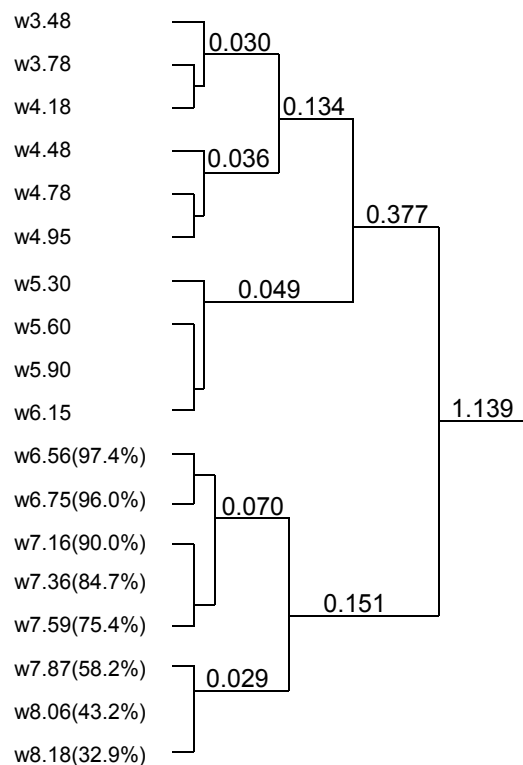
Figure 4-15 Tree diagram of clustering of moisture storage data in the plaster/mortar category
by using Ward's method

4.4.2.2 Scatterplot matrixes of the clustered moisture contents

The scatterplot matrixes of the clustered moisture contents in the overhygroscopic range and in the hygroscopic range are shown in Figures 4-16, 4-17, 4-18, and 4-19, respectively. Each circle in the graph denotes one specific plaster/mortar. Moisture contents in each cluster basically have a linear relationship with each other.
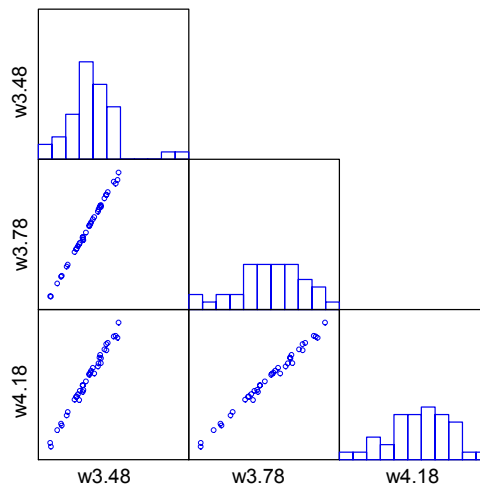
Figure 4-16 Scatterplot matrix of moisture contents w3.48, w3.78 and w4.18 in the plaster/mortar category
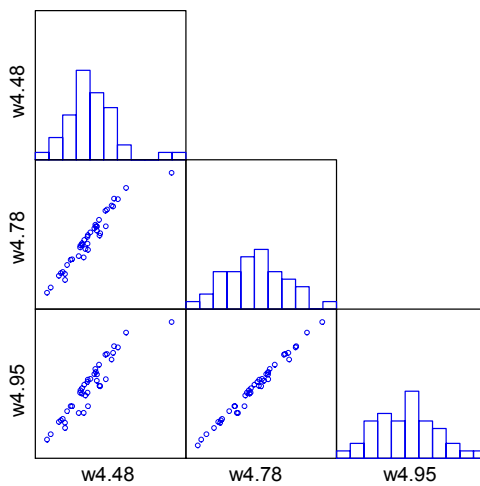
Figure 4-17 Scatterplot matrix of moisture contents w4.48, w4.78 and w4.95 in the plaster/mortar category
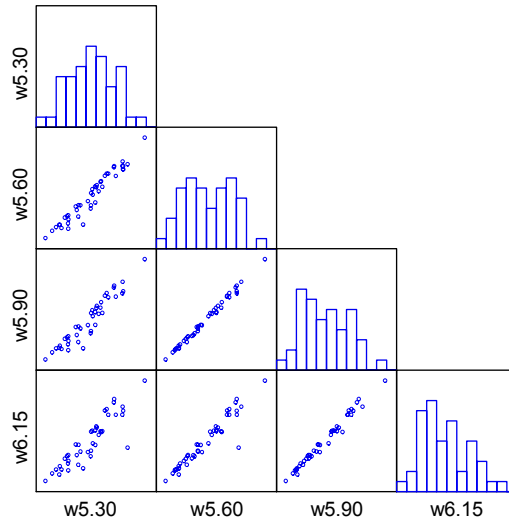
Figure 4-18 Scatter plot matrix of moisture contents w5.30, w5.60, w5.90 and w6.15 in the plaster/mortar category
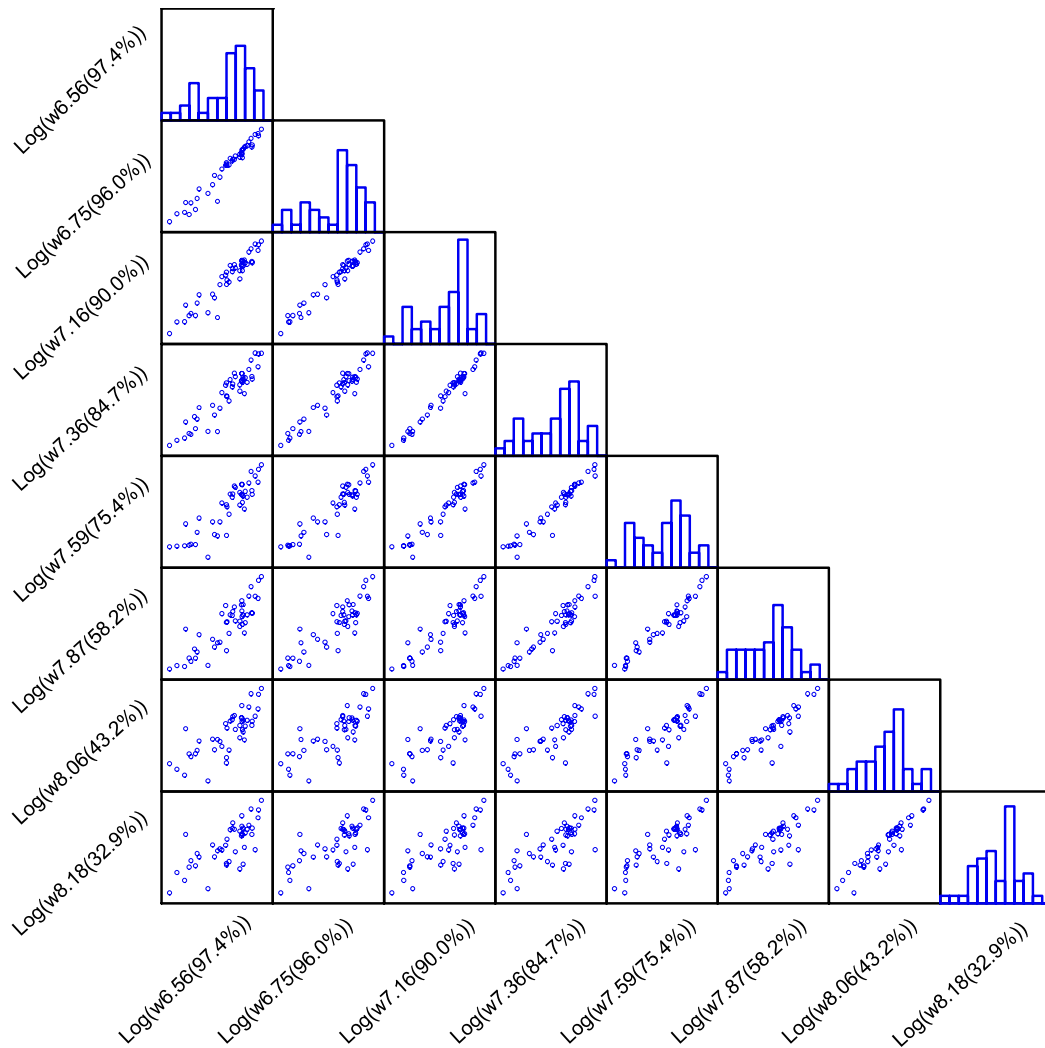
Figure 4-19 Scatterplot matrix of logarithmic-transformed moisture contents in the hygroscopic range in the plaster/mortar category

4.4.2.3 Regression analysis on the clustered moisture contents based on reference moisture content

In each sub-cluster, one moisture content is selected as the reference value, and other moisture contents in the same cluster can be determined by this reference value with the application of either linear least-squared regression or robust regression.

In the overhygroscopic range, the coefficients of regression models based on moisture contents *w3.78*, *w4.78*, and *w5.60* are listed in Table 4-6. In the hygroscopic range, *w7.59 (75.4%)* could have a good relationship with other moisture contents, so the coefficients of regression models based on logarithmic-transformed moisture content *w7.59 (75.4%)* are presented in Table 4-7. All the models have a higher R^2, indicating a good linear relationship between the selected reference moisture content and the predicted one.

Table 4-6 Coefficients of regression models based on moisture contents w3.78, w4.78, and w5.60 in the plaster/mortar category

	constant	*w3.78*	R^2
w3.48	0.001	1.003	0.988(Ro)
w4.18	0.001	0.977	0.988(Ro)
	constant	*w4.78*	R^2
w4.48	0.015	1.004	0.956
w4.95	-0.004	0.972	0.986
	constant	*w5.60*	R^2
w5.30	0.020	0.997	0.935(Ro)
w5.90	-0.004	0.977	0.992
w6.15	-0.003	0.896	0.969

Note: Ro denotes that the regression coefficients and R^2 are derived from robust regression

Table 4-7 Coefficients of regression models based on w7.59 (75.4%) in the plaster/mortar category

	constant	Log(w7.59(75.4%))	R^2
Log(w6.56(97.4%))	0.031	0.766	0.850
Log(w6.75(96.0%))	0.109	0.872	0.895
Log(w7.16(90.0%))	0.065	0.907	0.930(Ro)
Log(w7.36(84.7%))	0.014	0.927	0.964(Ro)
Log(w7.87(58.2%))	-0.276	0.943	0.936
Log(w8.06(43.2%))	-0.460	0.913	0.859
Log(w8.18(32.9%))	-0.463	1.007	0.799

Note: Ro denotes that the regression coefficients and R^2 are derived from robust regression

The results from Table 4-6 and Table 4-7 indicate that in the plaster/mortar category the moisture storage characteristics can be determined by three measurements (*w3.78*, *w4.78* and *w5.60*) in the overhygroscopic range and one measurement (*w7.59 (75.4%)*) in the hygroscopic range. In total, four measurements can gain a good knowledge of the moisture storage characteristics. For the plaster/mortar category, up to now, there are no appropriate regression models detected to derive the relationships between moisture contents and basic material parameters.

4.4.3 Validation of Regression Methods Applied in Moisture Storage Characteristics

The validity of application of the regression method to gain the moisture storage characteristics is examined by comparing the measured data with the predicted data derived from different regression models. Moisture contents at the defined capillary pressures are interpolated to gain the knowledge of moisture storage characteristics. Therefore, the application of the regression method to predict the entire moisture

storage data, instead of individual one, is evaluated. For the regression method based on the reference moisture content, except for the measured reference one, other moisture contents are derived from their respective regression models.

A specific material, brick ZB, is served as one example to demonstrate this approach. The material has the properties of θ_{por}=0.35 m^3/m^3, θ_{cap}=0.25 m^3/m^3, and A_w=0.21 $kg/m^2 s^{0.5}$. The measured moisture contents of brick ZB are compared with two sets of predicted values: the predicted values based on reference moisture contents and predicted values based on basic material parameters. The regression method based on basic material parameters is only feasible in the overhygrosopic range. As shown in Figure 4-20, the predicted moisture contents can basically catch the measured ones although there are some deviations between the measured data and predicted data based on basic material parameters in the overhygrocopic range.
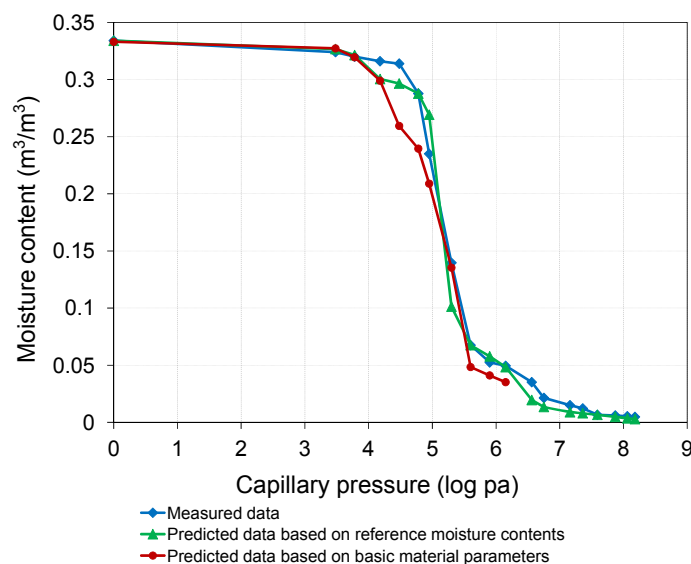
Figure 4-20 Comparison of measured data, predicted data based on reference moisture contents and predicted data based on basic material parameters (brick ZB)

One type of mortar and one type of plaster are also used to examine the validity of this approach. The comparisons of the measured moisture contents and predicted ones are presented in Figure 4-21 and Figure 4-22, respectively. The results show that the predicted curve follows the measured one with the reasonable accuracy.
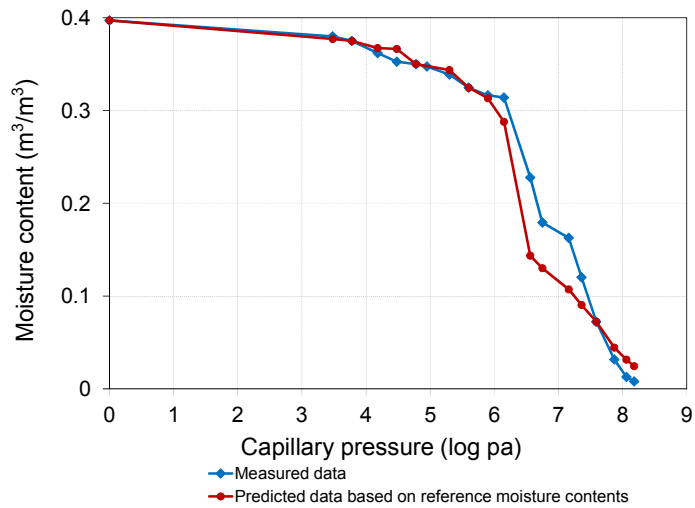
Figure 4-21 Comparison of measured data and predicted data based on reference moisture contents (mortar)
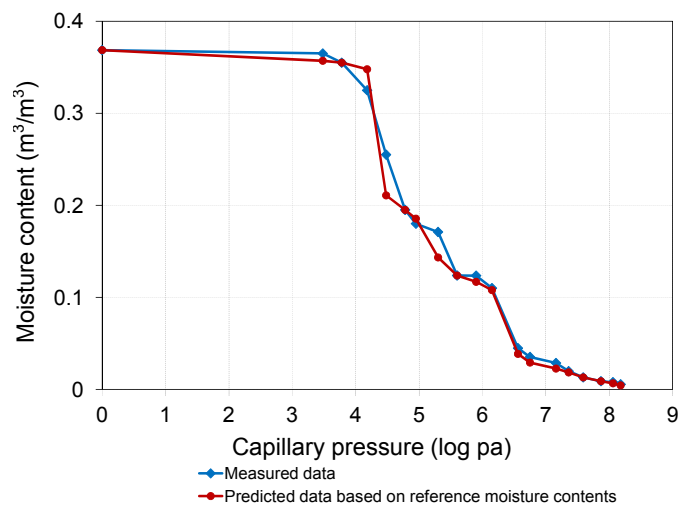
Figure 4-22 Comparison of measured data and predicted data based on reference moisture contents (lime plaster)

In case the difference between two adjacent reference moisture contents is small, e.g., less than 0.02 m^3/m^3, the predicted moisture contents derived from these two adjacent regression models may overlap each other. If this occurs, the unreasonable value can

be removed. For the exemplified mortar, moisture content *w4.95* derived from the reference moisture content *w4.78* is smaller than moisture content *w5.30* derived from the reference moisture content *w5.60*. This is contrary to the fact that moisture content decreases as capillary pressure increases. So *w4.95* is discarded.

4.4.4 Application of Generic Materials for qualifying incomplete material data

First, the procedure to derive a generic brick from one of identified brick clusters is exemplified. Thereafter, the methodology to extrapolate the missing properties of incomplete material data is introduced. This research focuses on the development of a methodology to derive the generic material from an identified cluster of specific materials, so the scope of the analysis is limited on the material category level, but further study should be based on the physical material group level.

Material properties of specific materials in one material category may exhibit significant divergence. For example, scatter plot of measured moisture storage data of 23 specific bricks is demonstrated in Figure 4-23. To avoid the hysteresis effect, only desorption data is presented. It is obvious that moisture contents of those bricks cover a very wide range. The effective saturation moisture contents (moisture content at logarithmic capillary pressure 0) span from 0.165 to 0.361 m^3/m^3. It is hard to generalize material properties from such diverse data. Therefore, the cluster analysis

is employed to aggregate the specific bricks into different material clusters, in which

the specific bricks own the similar characteristics.
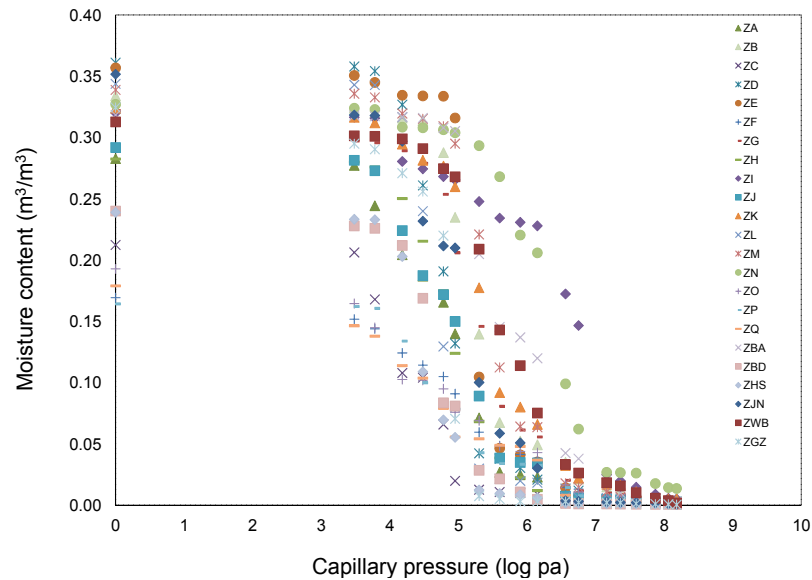
Figure 4-23 Scatter plot of measured moisture storage data of 23 specific bricks

To find the similarity between the specific materials needs to compare their material

properties. In this study, both the basic material properties and several representative

moisture contents in the moisture storage measurement are used as the criterion

variables. Material properties of each brick are presented in Appendix C. As

summarized in the Section 4.4.1.3, the moisture storage characteristics of building

brick can be determined by three values in the overhygroscopic range and one value

in the hygroscopic range. Therefore, those four characteristic moisture contents are

used as the criterion variables. The density and open porosity are highly correlated

(Section 3.6) with each other, so only one of them is selected as the clustering

criterion variable.

Therefore, the selected criterion variables include:

- Open porosity
- Thermal conductivity
- Specific heat capacity
- Effective saturation moisture content
- Capillary saturation moisture content
- Water vapor diffusion resistance factor
- Water absorption coefficient
- Moisture contents at logarithmic capillary pressure 4.78 and 5.60
- Moisture content at 75.4% relative humidity

Prior to the analysis, each selected parameter is scaled to unit variance. The dissimilarity in the selected parameters between each pair of specific bricks is measured by the normalized Euclidean distance. The specific bricks with the smallest distance are first joined into one cluster. Thereafter, the complete linkage and Ward's clustering methods are applied to calculate the distance between different clusters or groups of specific bricks. The most "closest" clusters or groups of individuals are fused together. This clustering process continues until all the specific bricks agglomerate to one set. The tree diagrams of the clustering results are presented in Figure 4-24.

As presented in Figure 4-24, both clustering methods identify four clusters among 23 specific bricks: Cluster 1 includes brick ZN and ZI. Cluster 2 contains brick ZB, ZE, ZG, ZK, ZM, ZBA, ZJN, and ZWB. Cluster 3 is comprised of brick ZA, ZD, ZJ, ZH, ZL, and ZGZ. And cluster 4 includes brick ZC, ZF, ZO, ZP, ZQ, ZBD, and ZHS.
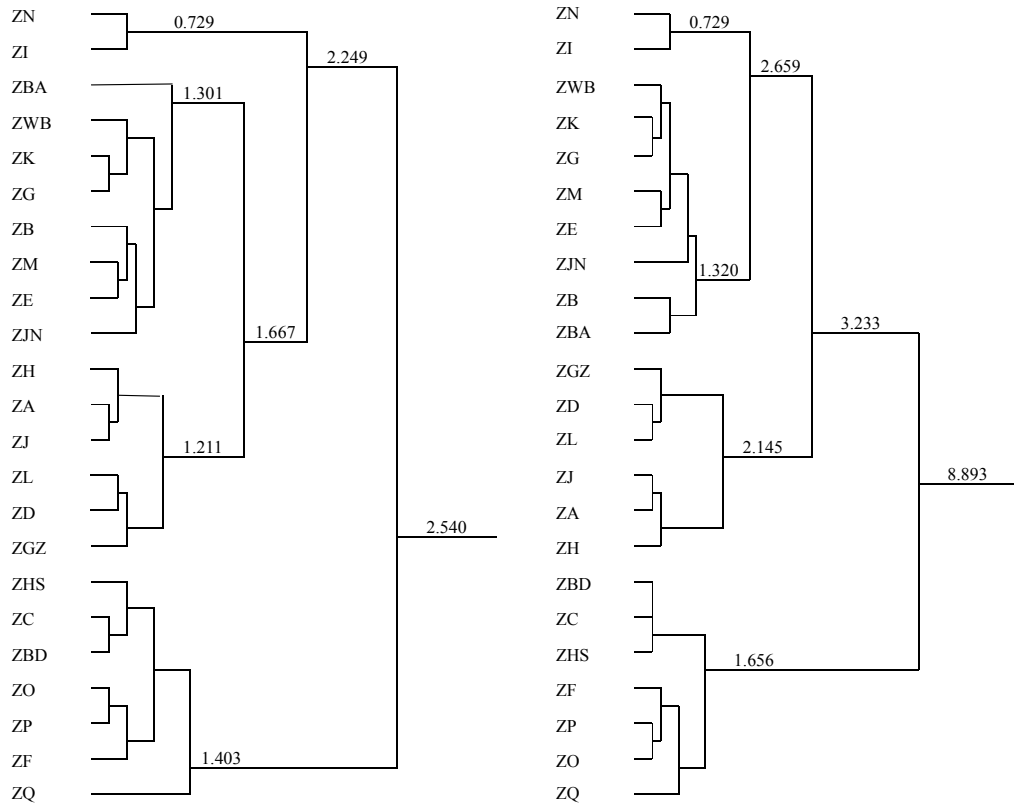
Figure 4-24 Tree diagrams of clustering of specific bricks by using complete linkage method (left) and Ward's method (right)
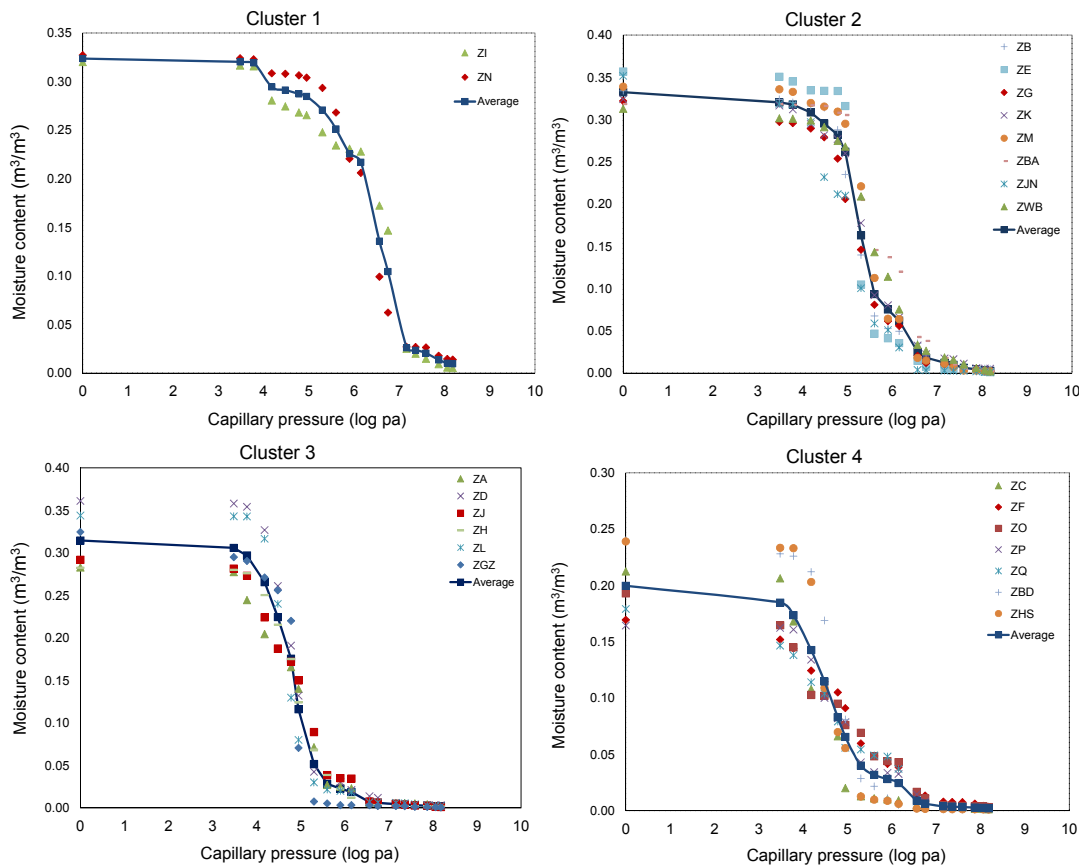
Figure 4-25 Measured moisture storage data and their means in each cluster

The moisture storage data of the specific bricks in each cluster are demonstrated, respectively, in Figure 4-25. It is evident that the moisture storage data in one cluster follows the same shape and tendency. Moreover, the difference among the data in one cluster becomes smaller compared to that in the whole brick set. Within each cluster, the mean moisture contents, by averaging moisture contents of the in-group bricks, are connected by a dark blue curve with the square marker.

The specific bricks in each cluster have some common characteristics. The cluster 1 is composed of modern bricks manufactured with the application of new technology. The cluster 2 mainly includes the historical bricks fabricated by the classic clay and loam. The dimension of the brick is not exactly the same size since its shape is easy to change in the high processing temperature without the bound of sand component. The cluster 3 contains the historical bricks produced by clay, loam and additional sand component. The bricks in the cluster 4 commonly have the higher density and lower liquid water transport ability compared to other clusters, so it is mainly used on the external façade of building construction.

Once the material clusters are identified, the generic synthesis process is conducted thereafter. The properties of the generic brick can be gained by arithmetically averaging material properties of the specific bricks in one cluster. Thus, the generic brick owns the common characteristics of one type of the specific bricks with a relatively small deviation in the material property. The material properties of the generic brick derived from the building brick cluster 2 are presented in Figure 4-26.

Minimum Input Information

Hygrothermal basic parameters

Parameter	Symbol	Unit	Mean	StdDev	Min	Max	Remarks
Bulk density	ρ	[kg/m^3]	1741.0	44.0	1657.2	1787.5	
Specific heat capacity	c	[J/kgK]	939	72.7	868	1092	
Thermal conductivity	λ_{dry}	[W/mK]	0.656	0.117	0.543	0.871	
Open Porosity	θ_{por}	[m^3/m^3]	0.352	0.011	0.336	0.375	
Capillary saturation	θ_{cap}	[m^3/m^3]	0.254	0.011	0.231	0.266	
Dry cup value	μ_{dry}	[---]	18.0	05.8	08.6	24.5	
Water absorption coefficient	A_w	[kg/m^{2}s$^{0.5}$]	0.175	0.047	0.107	0.227	

Water Retention (Desorption)

Arguments	Mean	StdDev	Min	Max	Remarks
pc	θ_l				
[hPa]	[m^3/m^3]				
0	0.332	0.016	0.313	0.357	
30	0.320	0.017	0.297	0.351	
60	0.318	0.016	0.296	0.345	
150	0.308	0.016	0.289	0.335	
300	0.295	0.032	0.232	0.334	
600	0.282	0.038	0.212	0.334	
900	0.262	0.042	0.206	0.316	
2000	0.163	0.047	0.100	0.221	
4000	0.093	0.037	0.047	0.146	
8000	0.075	0.034	0.041	0.137	
14000	0.062	0.028	0.030	0.120	

Sorption Isotherm (Desorption)

Arguments	Mean	StdDev	Min	Max	Remarks
φ	θ_l				
[%]	[m^3/m^3]				
97.4	0.0250	0.0130	0.0037	0.0427	
96.0	0.0182	0.0112	0.0033	0.0380	
90.0	0.0122	0.0060	0.0028	0.0185	
84.7	0.0097	0.0049	0.0025	0.0164	
75.4	0.0062	0.0032	0.0024	0.0111	
58.2	0.0043	0.0016	0.0019	0.0060	
43.2	0.0032	0.0016	0.0013	0.0053	
32.9	0.0026	0.0016	0.0008	0.0051	

Additional Input Information

Water vapour permeability

Arguments		Mean	StdDev	Min	Max	Remarks
φ_{insite}	$\varphi_{outsite}$	μ				
[%]	[%]	[-]				
5.0	30.0	18.0	5.8	8.6	24.5	DryCup
96.0	82.0	13.7	4.6	8.5	20.8	WetCup

Liquid water conductivity

Arguments		Mean	StdDev	Min	Max	Remarks
θ_l	mean pc	K_l				
[m^3/m^3]	[Pa]	[s]				
0.33		3.1E-09	3.4E-09	8.6E-10	1.1E-08	

Figure 4-26 Material properties of the generic brick derived from the building brick cluster 2

For each property, the statistical data, e.g., maximum, minimum and standard deviation, are included to show the variation. It needs to be noted that due to the small number of specific materials in the material cluster, the statistical data for this generic brick is not sufficiently reliable for the further statistic analysis. However, it provides a methodology for deriving the generic material from a identified material cluster.

The variance in the material properties of the generic material can be also used as a

reference for uncertainty analysis.

Regression methods described in the last section is also examined for the generic

material. Comparison of the measured moisture storage data and the predicted

moisture storage data derived from two regression approaches is shown in Figure 4-27.

One may find that the measured values and the predicted values show good agreement.

Thus, this regression method is also applicable for the generic material.
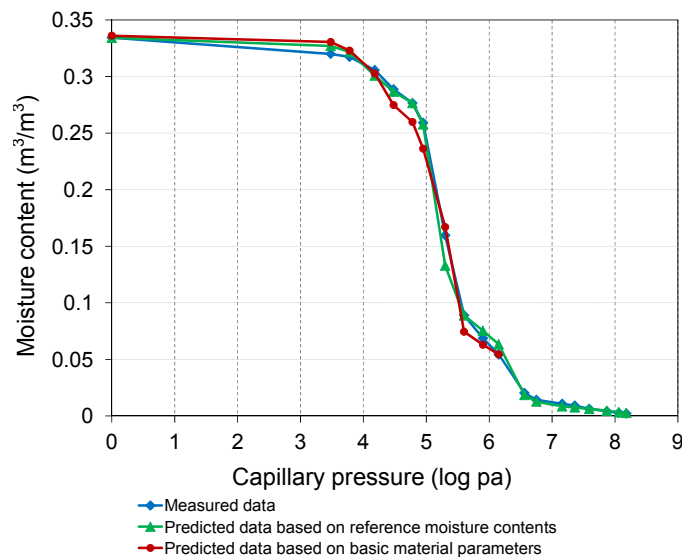
Figure 4-27 Comparison of measured data, predicted data based on reference moisture contents and predicted data based on basic material parameters (generic brick derived from the building brick cluster 2)

As shown in Figure 4-28, the missing properties of incomplete material data can be

completed by two ways: 1. by comparing the available properties of the incomplete

material data with those of generic materials in the same physical material group, a

most similar generic material is selected. The missing properties of the incomplete

material data can be supplemented by the material properties of the most similar

generic material. 2. the relationships among material properties, deduced from the

measured high-quality data by regression analysis, can be applied to complete the missing properties. Regression analysis can be based on the physical material group level, which means more materials are included for the analysis but may lead to a wide range of uncertainty, or based on the material cluster level, which results in a narrow range of uncertainty since fewer materials are involved but may have the problem with statistics basis. The decision on which level to choose is dependent on the number of the materials in the physical material group and in the material cluster, and the quality of the regression model, e.g., the coefficient of determination R^2.
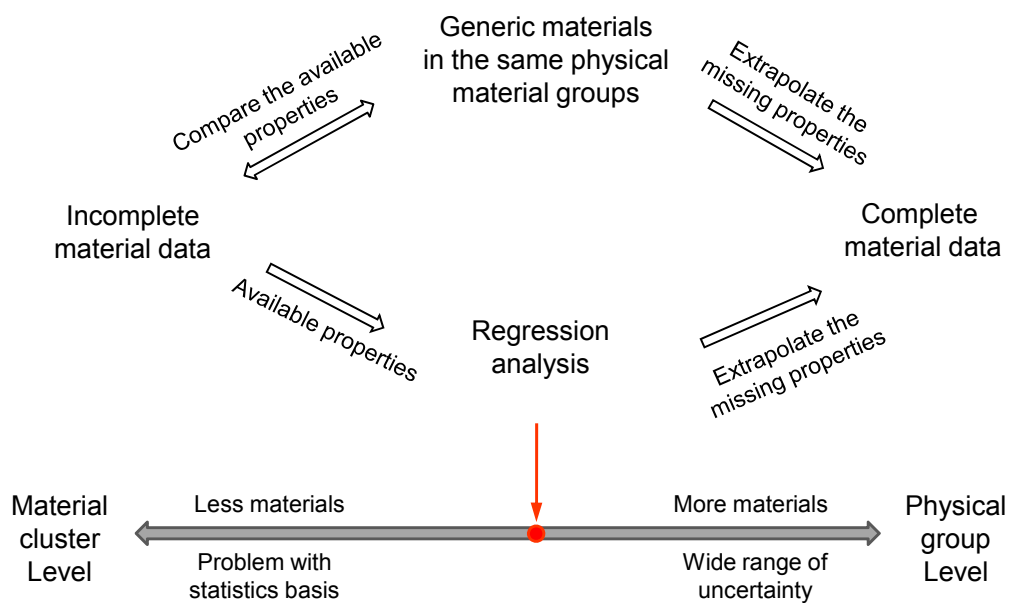
Figure 4-28 Extrapolation of the missing properties of incomplete material data by generic material and regression analysis

4.5 Summary

This chapter focused on the application of the statistical methods for hygrothermal material characterization.

1. Moisture storage data of 20 bricks and 47 plaster/mortars were collected for the investigation. Cluster analysis was applied to detect the natural groups among moisture contents at specific capillary pressures or relative humidity levels. The most similar moisture contents were aggregated into one cluster. Regression analysis was conducted to derive the relationships between moisture contents in the identified cluster. Thus, by only measuring one moisture content, the others in the same cluster are predictable by applying the regression models. Three characteristic moisture contents $w0$ (for building bricks)/$w3.78$ (for plaster/mortars), $w4.78$, and $w5.60$ in the overhygroscopic range and one moisture content $w7.59$ (75.4%) in the hygroscopic range were identified and verified to be sufficient to gain a good knowledge of moisture storage characteristics. The measurement was reduced to four steps.

2. Regression analysis was conducted to investigate the relation between moisture content and basic material parameters. It was found that moisture contents of building bricks in the overhygroscopic range are related to three parameters: capillary saturation moisture content, water absorption coefficient, and open porosity. The relationships between them provide a possibility to quickly estimate the moisture storage data without any moisture measurement.

3. A method to identify the material clusters from a group of specific materials was developed by the application of cluster analysis. The similarity between specific materials was obtained by comparing their parameters. The criterion

variables applied in the material clustering were defined in consideration of the correlation between material parameters and the characteristic moisture contents addressed in the simplification of the moisture storage measurement. The method was applied to cluster 20 specific bricks. Four brick clusters were identified. The specific bricks in each brick cluster exhibit similar characteristics.

4. A method to derive generic material from identified material cluster was developed. The generic material represents a type of specific materials with similar characteristics. A generic brick was exemplarily derived from one building brick cluster.

5. Incomplete material data can be qualified by the application of the generic material and regression analysis.

Future research is needed to

1. investigate the relationship between moisture content and basic parameters in the whole moisture range and in other physical material groups/categories.

2. derive the generic materials in other physical material groups/categories.

3. investigate the relationship between material parameters by regression analysis in different material groups/categories to build a statistical base in order to quality the incomplete material data.

Chapter 5 Uncertainty and Sensitivity Analysis in Building HAM Simulations

5.1 Introduction

An uncertainty analysis quantifies the uncertainty in model's output that responds to the uncertainty in model's inputs, helps researchers to understand the behavior of the simulation model, and explores how the variations of inputs influence output. It could also help to provide a more useful range of results than a deterministic result (Saltelli et. al 2009).

Uncertainty in the application may arise from different sources and generally can be classified into stochastic or aleatory uncertainty and subjective or epistemic uncertainty (Helton 1993; Helton 1997; Macdonald 2002). Stochastic uncertainty is a system inherent behavior and this kind of random error is irreducible. Subjective uncertainty results from the lack of knowledge about an appropriate value for a quantity, and it is reducible by improving the model or getting additional data. Those two types of uncertainty generally cannot be entirely separated in the applications (Helton 1993).

Uncertainty exists in every stage of the building life. In the early design stage, quite a lot of parameters are unknown due to the lack of the knowledge in detail. As more information is completed, many parameters can be progressively fixed. This kind of uncertainty belongs to the subjective uncertainty. However, there still exist some

stochastic uncertainties that cannot be avoided. For instance, the moisture storage data is measured in the laboratory under specific conditions for a long period to reach a steady state. But in the realistic condition, this steady state can never be reached. The experimental results from the standard test procedures, described in Section 3.3, also face the challenge of preciseness and confidence due to uncertainties (Bomberg et al. 2005; Kumaran et al. 2006). Material properties collected from different laboratories may have large variances (Roels et al. 2004). Even the same procedure repeated by different operators in the same laboratory may get distinct results. This may be due to the material's inherent inhomogeneous nature, the production process, and measurement method.

The relative importance of the input variables is not the same. A small perturbation in some input variables may lead to a large variation of the output variable. These influential input variables should be addressed in the early design stage and carefully characterized to reduce their uncertainty. A sensitivity analysis is committed to determine the contribution of the individual input variable to the uncertainty in the output variable (Helton 1993). It is usually performed together with uncertainty analysis to carry out the risk assessment, model verification and validation, and to give insight into robustness of the model results (Hamby 1994; Cullen and Frey 1999; Frey and Patil 2002; Saltelli et al. 2009).

This aim of the study in this chapter is 1) to identify and quantify the uncertainties in the hygrothermal simulation from different sources. 2) to find the suitable sensitivity

analysis technique to address the most influential input variables against performance evaluation criteria.

5.2 Uncertainty in Building HAM Simulations

The designers or engineers commonly assess the risk of failure based on the results from the deterministic simulation, in which mathematical models use the design values or "best fit" values as the input parameters. To consider the occurrence of the unexpected conditions, normally, a safety factor is introduced. For example, in DIN EN ISO 13788, a safety factor of 1.1 is suggested in calculation of the temperature factor to assess the mold growth risk. The limitation of using a safety factor is that it overestimates the result in terms of its maximum range, but the probability of the failure and the mechanisms, which lead to the failure, are not entirely addressed.

The analysis based on a deterministic simulation cannot provide the complete and correct information, if a large amount of uncertainties exist in the model's inputs. The uncertainties in the building simulation come from different sources: orientation of the construction, material properties, indoor moisture loads, etc.

The influence of the uncertainties in the input variables on the predicted hygrothermal performance of the building enclosure assembly has been investigated in the past (Salonvaara et al. 2001; Holm and Kunzel 2002; Cornick et al. 2009; Zhao et al. 2010; Hagentoft 2010). Recently, many researchers carried out uncertainty and sensitivity

analyses to investigate the thermal performance of the building enclosure/ assemblies (Corrado and Mechri 2009; Hopfe 2009; Struck et al. 2009).

5.2.1 Sources of Uncertainty

To perform an uncertainty analysis, the source of the uncertainties needs to be identified first. The previous research in the building simulation (De Wit 2001; Macdonald 2002; Moon 2005) has classified the uncertainties into four categories: (1) enclosure uncertainty, (2) scenario uncertainty, (3) modeling uncertainty, and (4) numerical uncertainty.

- Enclosure uncertainty accounts for the uncertainties of the enclosure /assembly itself, e.g., the uncertainty in the material properties, the orientation of enclosure assembly and the dimension of the material layer.

- Scenario uncertainty relates to all the external uncertainties in the simulation that do not come from the enclosure itself. For instance, the uncertainty comes from the difference between the actual climatic condition and associated boundary coefficients on the enclosure, versus the input values in the program. The uncertainty results from the difference between the actual indoor moisture gain due to human behavior and appliance operation in the real building, versus those assumed by the designer.

- Modeling uncertainty arises from the difference between physical phenomena and the mathematical solution of models by the simplifications and

assumptions. For instance, the hysteresis effect is usually not accounted for in the current HAM models. However, for some insulations, e.g., aerated concrete, the difference between the adsorption and desorption processes is sufficiently large, thus the hysteresis effect is obvious and should be considered. Most simulation models assume the different material layers are perfectly contacted to each other, without any contact resistance. But this idealization will not happen in reality. Those simplifications and assumptions reduce the complex of the simulation, but bring the uncertainties in the performance assessment. Addressing uncertainties in the physical modeling is not the scope of this study, so the different physical models in the simulation are introduced in a deterministic way.

- Numerical uncertainty is the error introduced by the tolerance with respect to the convergence criteria as well as the discretization strategies. For example, the treatment of the nonlinear mechanism, e.g., the liquid transport between the interfaces of two adjacent materials, will determine the accuracy of the outputs. With better design of above concerns, the numerical uncertainty is assumed to be controlled in a sufficiently small range. Thus, the numerical uncertainty is not accounted for in this study.

5.2.2 Quantification of Uncertainty

The uncertainties in the input variables are propagated by the simulation model and induce the uncertainty in the output variable. Therefore, the uncertainties in the input variables determine the possible range and distribution of the corresponding output variable. The uncertainties in the input variables of hygrothermal simulation are introduced as follows.

5.2.2.1 Material property

The uncertainty in material property comes from the material's natural inhomogeneity, the production and measurement, and modeling methodology concerning the functionalization of material data:

- *Nature*: errors come from the natural variability of the physical properties of a specific material. It is an intrinsic property of the material.

- *Measurement*: errors caused by experimental setup, evaluation, and interpretation of experiments (inconsistent standards have different interpretations).

- *Modeling*: errors due to the fact that the material functions (e.g., liquid water conductivity) are generated by using the simplified material models that could not represent the real properties perfectly.

The experimental methods to measure the material properties are described in Section 3.3. The summarized experimental data include the mean, standard deviation, maximum and minimum values of each parameter. These statistical values account for the uncertainties due to the material's natural inhomogeneous variability and measurement error. The uncertainty, resulted from the assumption and simplification in the material models with respect to the functionalization of material data, is not considered here.

5.2.2.2 Boundary conditions

The simulation results are sensitive to the assumed boundary conditions. For instance, the wind-driven rain is one of the major moisture loads on the building constructions. The choice of amount of the rain impinging on the façade will determine if the construction performs properly or not.

In addition, the impact of the surface film coefficients should not be ignored. Beausoleil-Morrison (2002) summarized the previous studies and concluded that the predictions of building energy demand and consumption can be strongly influenced by the choice of the convective surface heat transfer coefficient. Janssen et al. (2007) stated the surface transfer coefficients significantly affect the moisture transfer in permeable building components. Moreover, Steskens (2009) reported the surface heat and moisture transfer coefficients have relatively large impacts on the hygrothermal conditions of the building components and the indoor environment.

Therefore, the uncertainties in the boundary conditions will have a great influence on the performance assessment.

In this section, different models related to the boundary conditions in the hygrothermal simulation are introduced. The empirical value and possible variation range of the associated boundary coefficients are also given.

Short wave radiation

The global radiation is composed of the diffuse and direct radiations incident on a horizontal surface, noted as $q_{H,diff}$ and $q_{H,dir}$ respectively. Diffuse radiation describes the portion of the sunlight, which is scattered by the molecules or particles in the sky, while direct radiation is the portion of the sunlight, which directly comes from the sun. The incident short wave (0.3-3.0 μm wavelength portion of the solar spectrum) radiation flux q_{sw} on the building surface is determined by the daytime, incoming direct and diffuse radiation together with the construction character, e.g., orientation, inclination, and the latitude of the building location.

$$q_{sw} = \alpha_{sw} \cdot (q_{dir} + q_{diff}), \tag{5.1}$$

where

$$q_{dir} = q_{H,dir}\left[\cos\beta + \sin\beta\frac{\cos(\phi_s - \beta_s)}{\tan\theta_s}\right] \quad \text{for} \quad \sin\theta_s > 0 \quad \text{and} \quad -90° < \phi_s - \beta_s < 90°, \tag{5.2}$$

$$q_{diff} = q_{H,diff}\cos^2(\beta/2) + \rho_{s,g}\cdot(q_{H,dir} + q_{H,diff})\sin^2(\beta/2) \tag{5.3}$$

β is the inclination of the construction (0°=flat roof, 90° =vertical wall, 180°=facing downwards, etc.), β_s is the orientation of the construction (0°=North, 90° =East, etc.),

$\rho_{s,g}$ is the ground reflectivity. The solar elevation angle θ_s and the solar azimuth angle ϕ_s can be determined from local latitude Φ and the current sun decline angle δ (Nicolai and Grunewald 2011).

$$\delta(t) = 23.45° \sin(360° \frac{t + 284day}{365day}) \qquad (5.4)$$

$$\sin\theta_s(t) = \sin\Phi\sin\delta - \cos\Phi\cos\delta\cos(360° \cdot t / 1day) \qquad (5.5)$$

$$\tan\phi_s(t) = -\frac{\sin(360° \cdot t / 1day)}{\tan\delta\cos\Phi + \sin\Phi\cos(360° \cdot t / 1day)} \qquad (5.6)$$

Short wave radiation absorptivity α_{sw} accounts for the fraction of total solar radiation absorbed on the building surface. The magnitude of α_{sw} depends on the spectral and directional distribution of the incident radiation, as well as the nature of the absorbing surface (Incropera et al. 2005), e.g., the surface color. The absorptivities of some typical building surfaces are listed in Table 5-2.

In equation 5.3, the incident diffuse radiation on an inclined plane is composed of the sky diffuse radiation (the first part of the right-hand side of the equation) and the ground reflected radiation (the second part of the right-hand side of the equation). The ground reflected radiation is significant in the calculation of the solar energy gained on the building enclosure. Sometimes, this value can reach the order of 100W/m^2 for a vertical plane (Psiloglou et al. 1997). The ground reflectivity $\rho_{s,g}$, also called the ground albedo, is the ratio of the ground reflected radiation to the incoming short wave radiation incident on the ground. Several models have been developed to predict the ground reflectivity (Liu and Jordan 1963; Arnfield 1975; Temps and Coulson

1977; Gueymard 1987; Ineichen et al. 1990). $\rho_{s,g}$ is influenced by the solar elevation, the studied location, the surface condition, etc. The snow cover can strongly influence the ground reflectivity: the value of the snow-covered ground can reach as high as 0.9 (Muneer 2004). In the weather file, the information of snow cover is seldom included. In case the measurements are lacking, the average value of 0.2 is widely accepted and used when the ground was free of snow or covered with less than 25mm thick snow, while 0.7 is used for the snow coverage of 25mm or thicker (Liu and Jordan 1963). The range of $\rho_{s,g}$ for the urban areas is between 0.15–0.25 (Muneer 2004). The typical average ground reflectivity for various surfaces are listed in Table 5-1 (Thevenard and Haddad 2006).

Table 5-1 Estimates of average ground reflectivity for various surfaces (Thevenard and Haddad 2006)

Ground cover	Reflectivity
Water (large incidence angles)	0.07
Coniferous forest (winter)	0.07
Bituminous and gravel roof	0.13
Dry bare ground	0.2
Weathered concrete	0.22
Green grass	0.26
Dry grassland	0.2–0.3
Desert sand	0.4
Light building surfaces	0.6

Long wave radiation

A building surface successively emits the long wave radiation, in the same time it absorbs such radiation from the surrounding objects. The long wave radiation flux on

the surface of enclosure assembly captures the net radiate heat exchange between

enclosure assembly and sky, as well as near the field ground. Long wave radiation

emitted by the sky is called atmospheric counter radiation or sky radiation. Long wave

radiation emitted by the terrestrial surroundings is called terrestrial counter radiation.

Long wave radiation flux between the surface of enclosure and sky, as well as the

surrounding ground can be expressed by:

$$q_{lw} = f_{sky} \cdot (q_{sky} - \sigma \cdot T_s^4) + f_{grd} \cdot (q_{grd} - \sigma \cdot T_s^4), \qquad (5.7)$$

where

$$f_{sky} = \cos(\beta/2)^2 \cdot \varepsilon \qquad\qquad - \qquad \text{Sky radiation factor}$$

$$f_{grad} = \sin(\beta/2)^2 \cdot \cfrac{1}{\cfrac{1}{\varepsilon} + \cfrac{1}{\varepsilon_g} - 1} \qquad - \qquad \text{Terrestrial counter radiation factor}$$

T_s is the surface temperature of building enclosure, $\sigma = 5.67 \times 10^{-8}$ W/m^2K^4 denotes the

Stefan-Boltzmann constant, ε and ε_g are the long wave emissivities of the building

enclosure surface and surrounding ground, respectively, and q_{grd} denotes the

terrestrial counter radiation flux as a function of the ground surface temperature by

the Stefan-Boltzmann law. The atmospheric counter radiation q_{sky} can be taken

directly from the weather file if the measurement is available or calculated from the

sky temperature T_{sky} via the Stefan-Boltzmann law:

$$q_{sky} = \sigma \cdot T_{sky}^4 \qquad W/m^2 \qquad\qquad (5.8)$$

Long wave emissivity indicates the ability of the surface to emit and absorb long

wave radiation. It is independent of the color of the material surface. For most

nonmetallic building material, the surface emissivity is around 0.9 (ASHRAE 2009).

On the contrary, the metallic surface has a very low surface emissivity. The

emissivities of some building material surfaces are listed in Table 5-2 (USAID

ECO-III 2010).

Table 5-2 Absorptivities and emissivities of some building material surfaces (USAID ECO-III et al. 2010)

Material surface	Absorptivity (solar radiation)	Emissivity (thermal radiation $=300K$)
Lime sand stone, gray	0.6	0.96
Concrete, smooth	0.55	0.96
Brick facing, red	0.54	0.93
Aluminum, raw	0.20	0.05
Aluminum, anodized	0.33	0.92
Plaster, white	0.21	0.97
Plaster, gray, blue	0.65	0.97
Glass	0.08	0.88
Paint, white	0.25	0.95

Heat transfer

The temperature difference between the building component surface and surrounding

ambient air leads to their mutual heat transfer. The heat flux is given in equation 5.9.

$$q = \alpha \cdot (T_s - T_{air}) \, , \tag{5.9}$$

where α is the heat transfer coefficient (W/m^2K), T_{air} is the temperature of the ambient

air (K), and T_s is the surface temperature of building enclosure(K).

For simplification, the heat transfer coefficient is usually presented as the sum of the convective and radiation heat transfer coefficients. Convective heat transfer coefficient relies on a few factors: natural convection heat transfer coefficient is a function of the surface's length and temperature difference between the undisturbed air and the wall surface. The forced convection heat transfer coefficient is conditional to the meteorological wind velocity. The radiation heat transfer coefficient depends on the long wave emissivity of the considered surface and temperature ratio for radiation (Hens 2007). It is quite complex to analyze them individually, so in the standards a constant value of the sum of both convective and radiation heat transfer coefficients are given. If long wave radiation components are required to be determinated separately, the radiation heat transfer coefficient should be removed from the heat transfer coefficient.

The exterior heat transfer coefficient is suggested as 23 W/m^2K by Hens (2007) and 25 W/m^2k by DIN EN ISO 6946 (2008). The empirical interior heat transfer coefficients proposed by DIN EN ISO 6946 (2008) are listed in Table 5-3. For the interior surface of construction corner or the interior surface blocked by the furniture, heat transfer coefficient is generally below the empirical value due to the uncirculated air.

Table 5-3 Empirical interior heat transfer coefficient (DIN EN ISO 6946 2008)

Vertical surfaces	7.7 $W/m^2 \cdot K$
Horizontal surfaces	Heat upwards(q↑): 10 $W/m^2 \cdot K$
	Heat downwards(q↓):6 $W/m^2 \cdot K$

In ASHRAE (2009), the exterior heat transfer coefficient is given in a range between $1/0.06$ to $1/0.03$ W/m^2K. The interior heat transfer coefficient is given in a range between $1/0.20$ to $1/0.12$ W/m^2K.

Water vapor diffusion

The water vapor diffusion flux between the building component surface and the surrounding air can be determined by equation 5.10:

$$j_{diff}^{m_v} = \beta \cdot (p_{air} - p_s),$$ (5.10)

The associated enthalpy flux can be expressed as:

$$j_{diff}^{H_v} = h_v(T_v) \cdot j_{diff}^{m_v},$$ (5.11)

where p_{air} is the partial water vapor pressure in the air (pa), p_s is the partial water vapor pressure at the building enclosure surface (pa), $h_v(T_v)$ is specific enthalpy of water vapor (J/kg), and β is called vapor transfer coefficient (s/m). The suffix *i* is used to indicate interior, and the suffix *e* denotes exterior. The reciprocal value of the vapor transfer coefficient is the surface resistance for the diffusion, with the unit of *m/s* and symbol *Z*.

Hens (2007) gives the typical values for the interior and exterior vapor transfer coefficients:

Interior: $\beta_i = 18.5 \cdot 10^{-9}$ *s/m*; Exterior: $\beta_e = 140 \cdot 10^{-9}$ *s/m*

He also suggested certain variations of the vapor transfer coefficient, given in Table

5-4.

Table 5-4 Interior and exterior vapor transfer coefficient (Hens 2007)

Interior vapor transfer coefficient (P_a=1 atm, $0 \le \theta_i \le 20$ °C)		Exterior vapor transfer coefficient (P_a=1 atm, $-20 \le \theta_i \le 30$ °C)	
θ_i-θ_{si} (K)	$\beta_i \cdot 10^{-9}$ s/m	v_a (m/s)	$\beta_e \cdot 10^{-9}$ s/m
2	28.6	< 1	≤110
4	30.0	5	212
6	31.4	5 to 10	280
8	32.8	25	849
10	34.2		
12	36.0		
14	37.4		
16	38.8		
18	40.2		
20	41.6		

where θ_i is the indoor temperature, θ_{si} is the interior surface temperature, y_a is the air velocity.

Wind-driven rain

Wind-driven rain is used to quantify the amount of rain impinging on the building

façade. It is one of the major moisture sources to influence the hygrothermal

performance and durability of the building enclosure (Lacasse and Vanier 1999).

Wind-driven rain is governed by a number of factors, e.g., wind speed, wind

direction, horizontal rain intensity, and building geometry. The standard

meteorological data normally include the information of the wind speed, wind

direction, and horizontal rain intensity. The semi-empirical wind-driven rain model

mainly involves those three factors, as well as the building character itself, guided by

the experimental observation (Blocken and Carmeliet 2004). The wind-driven rain model described by Häupl (2008) is given in equation 5.12.

$$R_{wdr} = \alpha_R \cdot k_{wind} \cdot R_h \,,$$
(5.12)

where R_{wdr} is the wind-driven rain intensity on the façade ($l/m^2 h$), and k_{wind} is wind coefficient as a function of the wind direction, wind velocity, horizontal rain intensity R_h, and the orientation of the enclosure assembly.

The rain exposure coefficient α_R accounts for the possibility of construction exposure to the rain. α_R is in a range between 0 and 1.0. The value of 0 indicates that there is no exposure possibility for the rain impinging on the construction, and 1.0 denotes the maximum rain exposure possibility at normal condition. The choice of the value depends on the topography surrounding the building, i.e., if there are obstacles or trees, and the location where the rain intensity is calculated. The building structure, itself, may also impact the choice of α_R, e.g., the size of the overhang and the type of paint on the surface. Therefore, it is crucial to select an appropriate α_R to evaluate the rain influence on the hygrothermal performance of the building constructions.

If the ambient temperature is below -2 ˚C, the precipitation is snow instead of rain. Consequently, the wind-driven rain flux intensity is set as zero.

The possible variation ranges of the boundary coefficients in the hygrothermal simulation are summarized in Table 5-5.

Table 5-5 Boundary coefficients and their possible ranges

Coefficient	Symbol	Unit	Possible variation range
Heat transfer coefficient_interior	α_i	W/m^2K	5 - 8.33 (ASHRAE 2009) 6 -10 (DIN EN ISO 6946 2008)
Heat transfer coefficient_exterior	α_e	W/m^2K	16.67 - 33.3 (ASHRAE 2009)
Vapor transfer coefficient_interior	β_{pi}	s/m	$2.86\cdot10^{-8}$ - $4.16\cdot10^{-8}$ (Hens 2007)
Vapor transfer coefficient_exterior	β_{pe}	s/m	$1.10\cdot10^{-7}$ - $8.5\cdot10^{-7}$ (Hens 2007)
Short wave radiation absorptivity	α_{sw}	-	0.1 - 0.98 (Incropera et al.2005)
Ground reflectivity	$\rho_{s,g}$	-	0.15 - 0.25 (Muneer 2004)
Long wave emissivity of building surface	ε	-	0.82 - 0.96 (Incropera et al.2005)
Rain exposure coefficient	α_R	-	0 -1.0 (in normal condition)

5.2.2.3 Ambient environmental conditions

In the hygrothermal simulation, the ambient conditions include both the indoor and outdoor environmental conditions to which the construction is exposed.

To assess the transient hygrothermal response of the building enclosure assembly, the instantaneous environmental data is employed. The outdoor condition usually uses the climatic data from the complete meteorological measurement of the previous years or Test Reference Year (TRY). The TRY data assemblies the selected representative portions of the actual measured hourly data to form a one-year weather data. Some extreme periods, e.g., unusually hot summer and extremely cold winter, can also be selected to predict hygrothermal response of the building enclosure assembly in critical condition. The standard weather data usually includes hourly data of temperature, relative humidity, wind direction, wind velocity, sky radiation, diffuse radiation, direct radiation, cloud coverage, and horizontal rain intensity.

Indoor condition is influenced by various factors, e.g., the usage of the appliances, window open frequency, the tightness of enclosure assembly, and HVAC operation schedule. During wintertime in the cold climate, the indoor relative humidity has a great influence on the moisture response of the enclosure assembly. Thus, the indoor relative humidity plays a major role in the assessment of the durability of building enclosure assembly, as well as the health and comfort of the inhabitants.

Based on the measurements of different buildings in Germany, DIN EN 15026 (2007) proposed that indoor design temperature and relative humidity in the heated-only building can be determined according to the daily average outdoor temperature, as shown in Figure 5-1
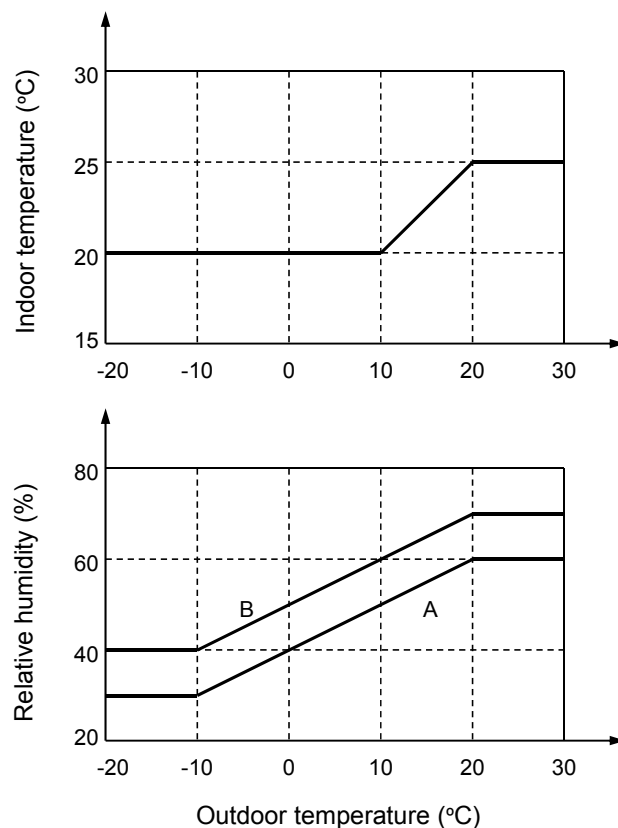
Figure 5-1 Indoor daily average air temperature (top) and relative humidity (bottom, A:low occupancy, B: high occupancy) depending on the daily average outdoor air temperature (DIN EN 15026 2007)

.Two humidity scenarios are defined: relative humidity at normal indoor moisture load in the case of low occupancy and relative humidity at high indoor moisture load in the case of high occupancy. These two scenarios profiles provide a possible variation range of indoor relative humidity. Relative humidity can be also derived from the function profile that varies between these two profiles to account for the case that cannot be described by the defined two scenarios.

5.2.2.4 Workmanship

The quality of workmanship has a great influence on the performance of the building enclosure assembly. The imperfect workmanship could induce the dramatic performance bias from the design requirements. The bad workmanship, e.g., the deficient installation of the insulation in the cavity wall, the perforation of the building board and the vapor retarder, can produce the unexpected vapor flow and the excess moisture. These issues give rise to the degradation of the thermal performance of the building enclosure assembly (Bankvall 1986; Trethowen 1991). The thermal bridges, due to uninsulated wall corner or window lintel, could lead to enormous heat loss and moisture related issues. It is hard to evaluate the workmanship in terms of quantity and quality. In the scope of this study, the dimension of the material layer, which is easily impacted by the craftsmanship, is considered as an uncertain variable.

5.2.2.5 Orientation

In the early design stage, the orientation of the building enclosure assembly may be unknown. Orientation in the simulation is mainly used to calculate the projection angle of the wind, solar radiation and wind-driven rain that fell on the building facade. Thus, it plays an important role to determine both thermal and moisture loads on the enclosure assembly. In the northern hemisphere, a south-oriented wall is exposed to the highest solar radiation intensity in winter and relatively low solar radiation in summer (Givoni 1998), while the north-oriented wall obtains the least solar radiation compared to other oriented walls. A west or south-west oriented wall often has the largest chance to expose to the wind driven-rain, subjecting to the variation due to local micro-climatic conditions. Thus, it is essential to explore the impact of the orientation in the performance assessment.

5.2.3 Probability Density Function of the Input Variable

The uncertainty can be quantified from a probability distribution, which approximates the possible range of the variable. The probability distribution of the inputs will influence the range and distribution of the outputs, thus they should be carefully selected in the Monte Carlo simulation.

The density, thermal conductivity, and specific heat capacity are easily measured material properties, which can be estimated from the normal distribution bounded by a certain value (Lomas and Bowman 1987).

The moisture storage characteristics are important in material characterization. Therefore, the probability distribution of moisture content is crucial and must be addressed. The effective saturation moisture contents of some typical building materials from different material categories are investigated in this research. For each material, the effective saturation moisture contents of 30 to 50 specimens are measured and their probability distributions are examined by using the Kolmogorov-Smirnov test, which can test if the data follows the specified distribution. The null hypothesis is that the data comes from the specified distribution. The null hypothesis is accepted, if the calculated p-value is larger than the predefined significance level α. In addition, the Shapiro-Wilk test is used to examine if the sample is from a normally distributed population. The histogram plots of the measured data are given in Appendix E. The Kolmogorov-Smirnov test, Shapiro-Wilk test, and p-value calculation are conducted for each material. The significance level $\alpha=0.05$ is selected as the threshold. The results show that the effective saturation moisture content can be estimated from a normal distribution.

Lacking the enough information on the possibility density function, other input variables are assumed to follow either the normal distribution or the uniform distribution.

5.2.4 Sampling Technique

The reasonable selection of the representative samples from the population is important for uncertainty analysis. If the selected samples have some bias, the corresponding outputs resulted from the propagation of those samples are also not reliable. Besides the independent sampling, the conditional sampling, i.e., correlated sampling, are also required in many cases. Currently, there exist several sampling techniques, among which the two most common ones are introduced.

Random sampling

Random sampling is a popular sampling technique to produce the variability of the input parameters. It is also known as a pseudo method since the samples are generated by the computer in a deterministic and predictable process. The method provides the unbiased estimates for the means, the variances, and distribution functions (Helton and Davis 2008). The random sampling is easy to implement, but normally requires large samples to achieve a good performance.

Latin hypercube sampling

Latin hypercube sampling is a stratified sampling approach. For the generation of N samples, the domain of each variable is divided into N disjoint intervals with equal probability $1/N$. In each interval, a single sample is randomly selected from the associated probability distribution. Application of this technique can provide a more precise shape of a sampled distribution and better coverage of the variable range than

the random sampling with the same sample size. The method yields the unbiased

estimates of the means and distribution functions, but gives a biased estimation on the

variances (Helton and Davis 2008). If the underlying model is quite computationally

expensive for evaluation, i.e., two-dimensional hygrothermal simulation of a building

enclosure assembly normally requires several hours, even a few days, Latin

hypercube sampling can achieve a quite robust and efficient result even with a small

sample size, i.e., N= 50-200 (Iman and Helton 1991; Helton and Davis 2008).

Correlated variables sampling

A correlation structure should be incorporated in the sampling, if there are two or

more variables that are dependent on each other. Iman and Conover (1982) proposed a

restricted pairing technique to generate a correlation structure collaborated with

random and Latin hypercube samplings. The method is based on the rank correlation

between the variables and can be applied to any type of distribution functions. The

proposed interval in the Latin hypercube sampling and desired correlation between

the variables could be well kept by this method. Helton and Davis (2003) illustrated

this technique in a model for two-phase fluid flow. In their example, the technique can

well reproduce the desired correlations between variables. The detailed description of

this technique is presented in Appendix F.

Sample size

The larger the sample size, the better coverage of the desired distribution of the input. Due to the computational cost, the number of the samples should be controlled in a reasonable limit. Lomas and Eppel (1992) applied the Monte Carlo analysis on building thermal modeling field. They found after 60-80 simulations the accuracy of the confidence interval on the standard deviation of outputs marginally increase, regardless of the number of input parameters. Iman and Helton (1985) recommended that the minimum of the sample size should be larger than $4k/3$, where k is the number of the input variables.

5.3 Sensitivity Analysis

By deliberately and systematically changing the input variables, sensitivity analysis is used to investigate the relationship between the inputs and the outputs and address the most influential inputs versus the outputs of interest. Thus, sensitivity analysis can determine the following questions (Hamby 1994):

- Which input variable is more critical compared to others and need additional investigation? With this answer the precise of the significant variables can be improved to reduce the output uncertainty;

- Which input variable has little contribution to the model? With this answer the insignificant variable can be fixed in the nominal value to simplify the model.

- Is the model performed in a proper way? If the model is sensitive to some

  non-influential variables judged by experienced experts, the chosen range of the

  variable or the model structure need to be further examined.

There are several approaches available to perform sensitivity analysis. Each approach

has its own capability and applicability. To facilitate the decision-maker to select the

most appropriate one, sensitivity analysis approaches are broadly classified into three

categories: mathematical method, statistical (or probabilistic) method, and graphical

method (Frey and Patil 2002).

1. Mathematical method evaluates the impact of the variation range of input variable

on the output variable (Morgan and Henrion 1990; Frey and Patil 2002). Mathematical

method includes nominal range sensitivity, differential sensitivity analysis, etc. The

method typically assesses the sensitivity of the output to a few values of the input

variable and is mostly valid for the linear model (Frey and Patil 2002). When applied

to the non-linear model, the result of the evaluation could be misleading.

Differential sensitivity analysis (DSA) is one type of mathematical methods.   This

approach only varies one input variable in each simulation, while keeping others fixed

in their expected values. Therefore, it is also known as a local sensitivity analysis

method. The sensitivity coefficient can be computed from the first-order partial

derivative of the output variable with respect to the input variable in the Taylor series

approximation of the model (Saltelli et al. 2009). In case nonlinearities are neglected,

the first-order partial derivative can be approximated as the ratio of the corresponding variation in the output to the variation in the input (Downing et al. 1985; Hamby 1994).

2. Statistical method incorporates the influence of both the range and distribution of the input variables by repeatedly implementing the model. This method evaluates the sensitivity of the individual input with varying the other input variables at the same time. Therefore, it considers the interaction effect among the multiple input variables (Frey and Patil 2002). Statistical method includes regression based sensitivity technique, partial correlation, Fourier Amplitude Sensitivity Test (FAST), Sobol's method, etc.

In the statistical sensitivity analysis, one of the important steps which should not be ignored is the definition of the distribution of the input variable. The choice of the distribution of the input variable determines the uncertainty of the output variable, as well as the relative importance of input variable in the model. The inappropriate distribution of the input variable could lead to large influence on the output variable and may even draw the wrong conclusion. The choice of the range and distribution of input variables might base on the measurement, experienced expert opinion, and rational estimation (Saltelli et al. 2004; Helton and Davis 2008).

3. Graphical method detects the relationship between input variable and output variable by the graphs and charts. The graphical method provides a more intuitive

way for the analyst to explore the model behavior. It gives a complement to the

mathematical and statistical methods (Frey and Patil 2002). The commonly used

graphical methods include scatter plots, histograms, and cobweb plots.

The Monte Carlo analysis is performed by executing the models repeatedly with

different sets of input variables, which are simultaneously selected at random from

their respective probability distributions. The application of the Monte Carlo analysis

in the building simulation is the interest of this study. Thus, several statistical

methods, which are suitable for the Monte Carlo analysis, are introduced in detail.

5.3.1 Regression-Based Sensitivity Analysis

Regression-based sensitivity analysis explores the relationship between the output

variable and input variable by a linear model. By standardizing the input variables and

output variable in consideration of the sample size, the influence of the units are

removed. Therefore, all the coefficients are in a comparable level (Iman and Helton

1991). The general linear model, given by equation 4.2, can be restructured as:

$$\frac{y - \bar{y}}{\hat{s}} = \sum_{j=1}^{k} (\frac{\beta_j \hat{s}_j}{\hat{s}})(\frac{x_j - \bar{x}_j}{\hat{s}_j}) , \qquad\qquad (5.13)$$

Where $\bar{y} = \sum_{i=1}^{n} \frac{y_i}{n}$, $\bar{x}_j = \sum_{i=1}^{n} \frac{x_{ij}}{n}$, $\hat{s} = \left[\sum_{i=1}^{n} \frac{(y_i - \bar{y})^2}{n-1} \right]^{1/2}$, $\hat{s}_j = \left[\sum_{i=1}^{n} \frac{(x_{ij} - \bar{x}_j)^2}{n-1} \right]^{1/2}$.

The coefficient $\beta_j \hat{s}_j / \hat{s}$ is called the Standardized Regression Coefficient (SRC).

SRC measures the effect of the input variable on the output variable by varying each

input variable in one unit while keeping other input variables remained at their

expected values. In case the input variables are independent, the absolute value of SRC provides a measure of variable's importance, i.e., the input variable with large SRC has higher importance than the one with small SRC. The sign of the SRC indicates whether the output variable trends to increase (positive coefficient) or decrease (negative coefficient) with the variation of the corresponding input variable (Helton and Davis 2008).

The validity of the regression-based sensitivity technique is conditional to the degree to which the model fits the data (Helton and Davis 2008). Therefore, the coefficient of determination R^2 should be provided to check the assumption of the model' linearity. A R^2 close to 1.0 indicates that the uncertainty in the output variable can be mostly explained by the regression model.

5.3.2 Stepwise Regression Analysis

In contrast to the standard regression analysis, which includes all the input variables in the model, the stepwise regression provides a concise structure containing only the subgroup of the most important variables. A sequence of regression models is constructed in a way that each variable enters the model at each step (Helton and Davis 2008). The first model includes the most influential variable on the uncertainty in the output variable. The second model contains the first selected input variable and one of the remaining variables that has the largest impact on the uncertainty not accounted for by the first selected variable. This procedure continues until there are

no more variables that can satisfy the predefined requirement to allow a variable to

enter the model. The pre-entered variable can be also dropped from the model, if its

contribution on the variation of the output is not significant. At each step, the model

checks if the selected variable in the prior step has an F value below or α-value above

the threshold.

Stepwise regression analysis provides extra hints to rank the importance of input

variables in addition to comparing the absolute value of SRCs in the final model. The

order in which the input variable enters into the model indicates its importance. The

first selected variable is the most important. Likewise, the second selected variable

has the most importance than others, except for the first one, and so on. The

coefficient of determination R^2 at each step provides an indication of how much

uncertainty of the output can be explained by the currently included input parameters

(Iman and Helton 1991).

5.3.3 Partial Correlation

The correlation coefficient $r_{x,y}$ provides a measure of relationship between input

variable x_j and output variable y, given by:

$$r_{x_j y} = \frac{\sum_{i=1}^{n}(x_{ij}-\overline{x}_j)(y_i-\overline{y})}{\left[\sum_{i=1}^{n}(x_{ij}-\overline{x}_j)^2\right]^{1/2}\left[\sum_{i=1}^{n}(y_i-\overline{y})^2\right]^{1/2}}, \tag{5.14}$$

where $\overline{x}_j = \sum_{i=1}^{n}x_{ij}/n$, $\overline{y} = \sum_{i=1}^{n}y_i/n$.

The derivation of partial correlation coefficient (PCC) is based on the concept of correlation and partial correlation (Helton 1993). In the PCC method, two regression models are first built, given in equation 5.15.

$$\hat{x}_j = c_0 + \sum_{\substack{p=1 \\ p \neq j}}^{k} c_p x_p \; ; \;\; \hat{y} = b_0 + \sum_{\substack{p=1 \\ p \neq j}}^{k} b_p x_p \qquad\qquad (5.15)$$

The PCC of the input variable x_j and output variable y is defined as the correlation coefficient between two new variables, $x_j - \hat{x}_j$ and $y - \hat{y}$. So the PCC provides a measure of relationship between the input variable and output variable, excluding the effect due to other input variables (Helton 1993).

The PCC and SRC produce the same ranking when the input variables are uncorrelated to each other. The reliability of the PCC and SRC rely on the linearity of the model. In case the relations are nonlinear but monotonic, the transformation of the actual data to their corresponding ranks can help to improve the linear relationship between input and output (Helton and Davis 2008). Such coefficients in the model are called standardized rank regression coefficients (SRRC) and partial rank correlation coefficients (PRCC). The PRCC and SRRC are in the range between -1.0 and +1.0. A value close to ±1.0 indicates significant monotonic relationship between inputs and output, while a value close to zero indicates a non-significant relationship between the inputs and output (Iman and Helton 1991).

5.3.4 Statistical Test in Regression Analysis

As opposed to the regression coefficient, F test provides a measure of the sensitivity of both the qualitative and quantitative variables. The F statistic calculated from equation 4.16 can be used as a guidance to assess the effect of an input variable on the model prediction (Helton and Davis 2008). A large F value indicates that the standard error for the input variable and the corresponding uncertainty in the estimated coefficient are small. In contrast, a small F value indicates that the standard error for the input variable and the corresponding uncertainty in the estimated coefficient are large. Hence, F value not only considers the magnitude of the coefficient, but also accounts for the amount of error in the coefficient (Frey et al. 2003). For a qualitative variable, the calculated F value equals the square of t value given in equation 4.13.

The importance of the variable can be also measured by p-value, which is usually used together with the F or t statistics. Typical cut-off p-value is 0.01, 0.05, and 0.1. The calculated p-value will be compared with predefined significance level α, which is the probability of rejecting H_0 when it is true. Generally, a small p-value indicates there are more evidences against the null hypothesis H_0, while a large p-value means little or no evidence against the null hypothesis H_0. Thus, p-value provides a criterion to assess the variable importance (Helton and Davis 2008).

5.3.5 Other Sensitivity Analysis Techniques

There are many other sensitivity analysis techniques available, e.g., Morris method, Sobol' method, and FAST method. The detailed introduction for these approaches can be accessed in Saltelli et al. (2009).

5.3.6 Comparison of Sensitivity Analysis Techniques

The regression-based sensitivity analysis, partial correlation technique, stepwise regression analysis, and F test can detect the relationship between the input variables and the output variables, with the consideration of the correlations among the input variables. Stepwise regression analysis gives several aspects of insights into the importance of the input variables. F test provides a measure of the importance of both qualitative and quantitative input variables. However, the validity of those approaches is based on the assumption of the good linear relationship between the input variables and output variables. Morris method is one of the screening methods to identify the most important subset from inputs. It measures the qualitative sensitivity of inputs, but cannot provide the exact magnitude of the importance of the inputs (Saltelli et al. 2009). Sobol' method and FAST method are variance-based sensitivity analysis techniques. They are model-independent, e.g., can cope with nonlinear and non-monotonic model, but they also require substantial calculation cost. The graphical approach provides immediate exploration of the relationship between input variables and output variable. It is useful to observe relationships between a few inputs.

There exist certain correlations between material properties as introduced in Section

3.6, which should be accounted for in random sample generation. Therefore, the

regression-based sensitivity analysis, stepwise regression analysis, partial correlation,

F test, and graphical methods, which are able to rank the importance of the correlated

input variables, are applied in this research. Those techniques will be exemplified in

Chapter 7 to address the influential variables against the performance evaluation

criteria.

5.4 Summary

Uncertainties exists in many aspects of hygrothermal simulation. This may be due to

the lack of information in the design stage, the inherent variation in the material

properties, the assumption and simplification in the mathematical models, etc.

Building enclosure uncertainty and scenario uncertainty were introduced in detail.

The uncertainties from different sources in the hygrothermal simulation, including

material properties, boundary conditions, orientation of the construction, indoor

condition, and workmanship were described and quantified. Probability density

function of effective saturation moisture content was explored based on measurements

of a number of building materials, and it is proposed as a normal distribution. A good

sampling technique can efficiently cover and represent the population. The random

sampling and Latin hypercube sampling techniques were introduced. In addition, the

correlation structure among the variables and the choice of the sample size should be considered in the sampling.

Sensitivity analysis gives insight into the importance of the model's inputs versus model's output. The influential parameter can be treated with more care to reduce its uncertainty and increase the accuracy of the model's outputs. Different sensitivity techniques were introduced, and their advantages and limitations were compared. The suitable techniques for this study, which can take into account the correlation between the input variables, were found.

Chapter 6 Probabilistic Assessment of Hygrothermal Performance of Building Enclosure Assemblies

6.1 Introduction

The previous chapter discussed and addressed the uncertainties from different sources in the building simulation. The uncertainties in the analysis inputs are propagated by the simulation models to the outputs, which will subsequently serve as the input for the performance assessment.

The performance evaluation criteria in building physics mainly concern the thermal efficiency and durability of the construction, as well as the mold growth risk. A good understanding of those evaluation criteria helps designer to reduce the risk of damage and prolong the building's service life. The performance concerning the thermal efficiency can be rated by the amount of heat loss through the enclosure and the thermal resistance of the enclosure. The performance regarding the durability can be assessed by the amount of condensation in the enclosure assembly and the possibility of the damage due to the hygrothermal loads on the surface region of the enclosure assembly. Mold spores contaminate the indoor environment and are harmful to the health of inhabitants, so the knowledge of mold germination mechanisms will help to control the mold issues on a minimum level.

In this chapter, the procedure to integrate uncertainty and sensitivity analysis in the hygrothermal simulation is first introduced. A probabilistic approach is developed to assess the hygrothermal performance of building enclosure assembly. Subsequently, different performance evaluation criteria are given. Finally, a criteria-based statistical evaluation procedure is described.

6.2 Development of a Probabilistic Approach

The previously developed DELPHIN program can run one and two-dimensional, and axial-symmetric three- dimensional transient mass and energy transport simulation by using instantaneous climatic data (Grunewald 1997; Nicolai 2008). In this study, DELPHIN program is used as the platform for the hygrothermal simulation.

A probabilistic performance assessment is composed of multiple steps as presented in Figure 6-1. First, the study case is determined, i.e., is it a wall assembly or roof, and the corresponding scenario is described. Second, the involved input variables and the associated uncertainties are defined, including the variation range and distribution of each input variable. The outputs of interest are decided according to the requirements and expectations from the predefined performance evaluation criteria. Then, the variables are randomly generated from their respective probabilistic density functions by the selected sampling technique, and the uncertainties in the inputs are propagated to the output by iteratively executing the models. In the end, the outputs with uncertainty are collected and used as the inputs in the performance evaluation.

The input variables sampling is first discussed in Section 6.2.1. The process of the uncertainty propagation from inputs to outputs is detailedly introduced in Section 6.2.2.
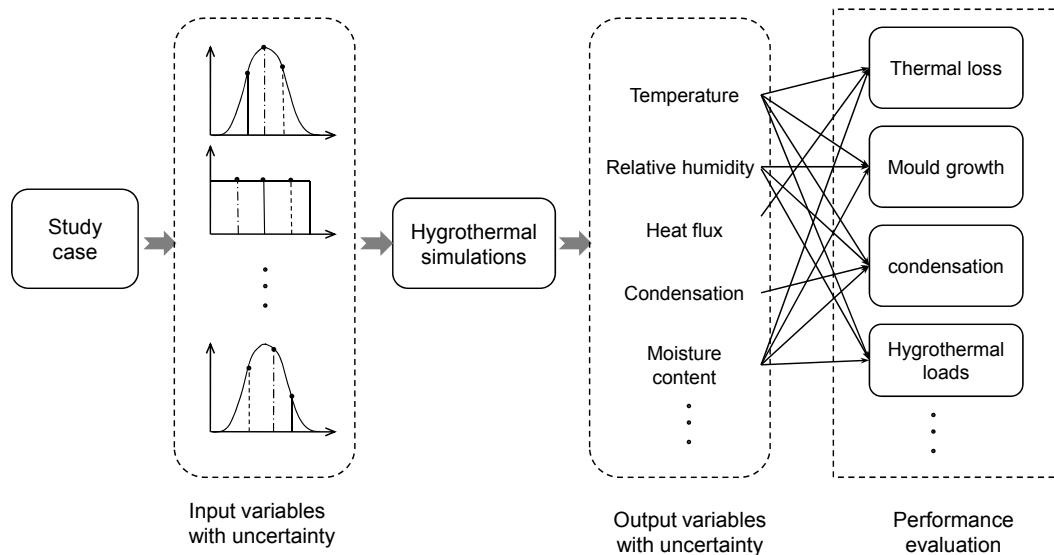
Figure 6-1 Schematic drawing of the probabilistic performance evaluation procedure

6.2.1 Input Variables Sampling

The sampled input variables need to follow the natural phenomena or physical rules. For instance, the upper limit of the short wave absorptivity and long wave emissivity should not be greater than 1.0. In this study, the variable is bounded in a 95% confidence interval to keep its associated variation in the reasonable range. The sample with a value beyond the limited range will be rejected. In addition, the input variables should also obey some intrinsic relationships, described as follows:

Relationship between basic material parameters: There are three parameters in the material model related to the characteristics of moisture storage and pore structure: Open porosity (θ_{por}), effective saturation moisture content (θ_{eff}), and capillary

saturation moisture content (θ_{cap}). They represent the level of the air or water penetration in the materials. θ_{por} is the total pore volume in the material, excluding the closed pores. θ_{eff} is the pore volume that is filled by liquid water and dissolved air without entrapped air. It is a long-term saturation and starting point of the desorption test. θ_{cap} is determined from water absorption test. It is the transition moisture content from the first stage to the second stage during water absorption (Plagge et al. 2004; Roels et al. 2004). The relationship among them is $\theta_{por} \geq \theta_{eff} \geq \theta_{cap}$.

There also exist some correlations among the material parameters. The variation of some parameters indicates the increase or decrease of others. For instance, the increase of the density correlates to an increase of the thermal conductivity due to the reduced pore space in which the air usually has a low thermal conductivity compared to solid matrix. The rank correlation matrixes of some basic parameters in different material categories are presented in Table 3-6, Table 3-7, Table 3-8, and Table 3-9.

Relationship between basic parameter and material function: Several basic parameters are related to material functions, as presented in Table 6-1. For instance, open porosity and water vapor diffusion resistance factor are related to water vapor permeability function; effective saturation moisture content is the upper limit of moisture content in the moisture retention function and liquid water conductivity function. When those basic parameters vary, the related material functions will also be modified by a scale factor, which is the ratio of the new value to the old value of the related parameter. For example, the scaled moisture retention curve will be the old

169

curve multiplied by the scale factor θ_{eff}_new/θ_{eff}_old. So in the sampling, not only are

the basic parameters generated from PDF, but also the related material functions vary

in a certain range. It is important to note that material functions in the sampling are

only modified by the scale factors without considering the physical phenomena as

applied in the deterministic model, i.e., dependence of water vapor diffusion

resistance factor on relative humidity.

Table 6-1 Material functions and their related material parameters

Material function	Unit	Symbol	Parameters that affect the material function
Moisture retention function	m^3/m^3	$\theta(pC)$	θ_{eff}
Water vapor permeability	s	$K_v(\theta)$	θ_{por} and μ_{dry}
Liquid water conductivity	s	$K_l(\theta)$	θ_{eff} and K_{eff}
Thermal conductivity	$W/m \cdot K$	$\lambda(\theta)$	θ_{eff}

When the difference between means of θ_{eff} and θ_{por} is small and standard deviations of

both parameters are relatively large, the randomly generated θ_{eff} may be larger than

θ_{por}. The condition $\theta_{por} \geq \theta_{eff}$ is handled by first generating the samples from their

respective probability density functions with the application of the usual Latin

hypercube sampling technique. The inequality is treated as follows: in each sampling,

the generated θ_{eff} and θ_{por} are examined. If θ_{eff} is larger than θ_{por}, it is replaced by a

new θ_{eff} that is iteratively generated from its probability density function until the new

value fulfills the unequal condition. In this manner, the samples follow the desired

distributions and the inequality is satisfied. The samplings of θ_{eff} and θ_{cap} are treated

in a similar way.

6.2.2 Implementation of Uncertainty Propagation

For a deterministic heat, air, and moisture simulation, the first step is to set up the construction in the program and provide sufficient information, including the description of the building structure, the properties of each material, boundary conditions, climatic conditions, initial conditions, etc. This information can be written into a project file and read by the simulation tool. Then the simulation is carried out, and the corresponding results are collected for the further analysis.

A procedure to implement uncertainty propagation is demonstrated in Figure 6-2. First, a reference project file is created in the same procedure as the above described deterministic simulation. In the next step, an external Python script, which can automatically process multiple simulations, is used to randomly generate samples and modify the reference project file to build the new project file with the generated samples. In each sampling, all the variables are simultaneously selected at random from their respective probability density functions. The program will check if they are in the reasonable range and meet the preconditions, e.g., the correlation between material parameters. If not, they will be discarded and the program will generate a new set of samples until the full conditions are satisfied. Then, this new set of samples is written into the reference project file to substitute the designated variables/ functions. So the new project file is composed of the updated data and unchanged part that is the same as the reference project file. A set number of new project files are

built and simulations are automatically executed. Thus, the uncertainties in the inputs

are propagated by the simulation model to the outputs..
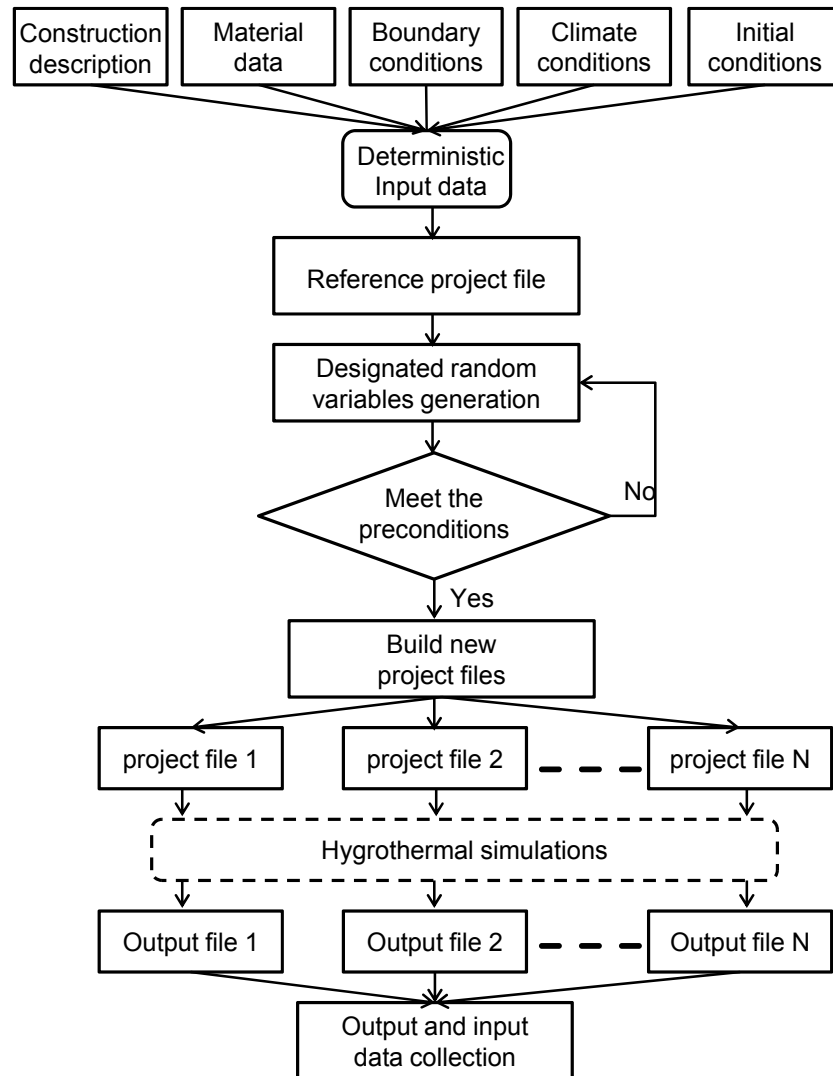
Figure 6-2 Schematic drawing of implementation of uncertainty propagation

The outputs of the simulations can be read in sequence and collected for the

performance evaluation. The randomly generated inputs and the corresponding

outputs are imported into SIMLAB 2.2 (Simlab 2011) for sensitivity analysis

6.3 Performance Evaluation Criteria

A good building design should consider the possible performance problems in advance, and find a solution to minimize the possibility of occurrence of those problems. The performance problems of building enclosure may vary in different aspects. For instance, the excessive moisture in the construction, e.g., interstitial condensation, could diminish the thermal resistance of insulations and reduce energy efficient. The presence of mold is another moisture-induced issue that influences the indoor air quality and the occupant's health. Moreover, the drastic variation of moisture and temperature on the surface of the building component will cause intensified stress and accelerate the material deterioration.

Different criteria against the hygrothermal performance of the building enclosure assembly have been developed to evaluate moisture related deteriorations and problems, as well as the thermal efficiency of the building enclosure assembly.

6.3.1 Condensation

Condensation is one of the major harms for the building enclosure and it can lead to the deterioration of the construction, thus, reduce its durability. The long-term condensation in the enclosure should be avoided.

6.3.1.1 DIN 4108-3 (2001)

Condensation inside the assembly, induced by the increased humidity of the construction and thermal insulation, should not produce the material damage or impair

the safety function. It is considered harmless, if the essential requirements, such as thermal protection, stability of the structure are guaranteed. These conditions are met when the conditions listed below are ensured (DIN 4108-3 2001):

a) The components that contact with the condensed water must not be damaged (e.g., corrosion, fungus).

b) The condensed water that formed in the enclosure during the thaw period must be dried out during the evaporation period.

c) For roof and wall assembly, the amount of condensed water in total should not exceed 1.0 kg/m^2. This does not apply to conditions d) and e).

d) For the condensation that occurs at contact surfaces between non-capillary building materials, the total amount of condensed water should not exceed 0.5 kg/m^2.

e) The moisture content of wood should not increase beyond 5%. For wood based materials, this limit is no more than 3%.

6.3.1.2 DIN EN ISO 13788 (2001)

Interstitial condensation is acceptable, if the sums of the condensation from each interface are expected to evaporate during the evaporation period (summertime). Surface condensation can cause damage to unprotected building materials that are sensitive to moisture. The moisture is allowed temporarily in some place and in small quantity, i.e., windows and tiles in bathrooms, where the surface does not absorb the moisture and precautions are taken to avoid the moisture contact with adjacent

sensitive materials. There is a risk of mold infestation on a surface where relative humidity exceeds 80% for several days.

6.3.2 Mold Growth

Mold fungi are widely observed in the building components where the moisture exists in the high level, such as the floor, interface between interior and exterior wall. The mold may not only lead to the blemish of the surface finishing, the reduction of thermal performance of the construction, but it will also produce the healthy issues for the occupancies, such as respiratory, allergenic, nausea, and other symptoms (Burr et al. 1988; Lewis et al. 1994; Baughman and Arens 1996). In recent years, mold related issues have reached a wide attention.

Mold growth needs moisture, which can be expressed either as water activity (a_w) or as relative humidity in a steady state. Mold can grow in a wide environmental condition. Depending on the species, some xerophilic species can start to germinate when relative humidity is as low as 62% to 65% (Adan 1994), while hydrophilic microorganisms require at least 90% to 95% RH. The favorable temperature range for mold growth is from 0 to 50 °C (Viitanen et al. 2010).

In the past, the criterion to define the germination of mold fungi was relative humidity only. When relative humidity is beyond the limited value, i.e., 80% RH (IEA 1991; ASHRAE 2009), the mold is assumed to germinate. In fact, the germination of mold fungi is not only related to the humidity, but also determined by temperature,

exposure time, and nutrition of the substrates (Hens 1999; Hukka and Viitanen 1999; Sedlbauer 2001). At defined relative humidity, higher temperature and more nutrition on the substrates will shorten the time of spore germination. The mold growth is also dependent on the surface type and dirtiness of the substrate. Under the same conditions, some organic materials, e.g., wood and plywood, require less exposure time than stone based materials. However, when organic dusts accumulate on the surface of stone based material, its surface properties will be become suitable for mold growth (Viitanen 2010). Moreover, light, radiation, oxygen, and air movement may also have influence on the mold growth (Hagentoft 1998; Sedlbauer 2001).

Different mold models are introduced as follows.

6.3.2.1 DIN standards for prevention of mold growth

DIN 4108-3 (2001) adopts a constant value of 80% relative humidity on the interior surface of wall assembly as a threshold to assess the mold growth risk.

The mold easily occurs in the area suffering the thermal bridge effect due to its relatively lower temperature than other regions. In DIN EN ISO 13788 (2001), a temperature factor f_{Rsi} was then introduced to evaluate the thermal bridge and minimize the risk of moisture damage, primarily fungus defacement.#

$$f_{Rsi} = \frac{\theta_{si} - \theta_e}{\theta_i - \theta_e},$$

(6.1)

where θ_{si} is the interior surface temperature, θ_i is the indoor temperature, and θ_e is the outdoor temperature. The knowledge of the interior surface temperature can be obtained from the hygrothermal simulation.

The minimum value of the temperature factor, $f_{Rsi,min}$= 0.70, should be guaranteed to avoid moisture condensation and prevent fungus defacement.

6.3.2.2 Isopleth model

The isopleth model (Sedlbauer 2001) describes the spore germination and mold growth rate in dependence on temperature and relative humidity on different substrates. The model defines several analogous isolines, e.g., Lowest Isopleth for Mold (LIM) line, 8-days line, 2mm/d line, to parameterize either the time that spores start to appear or mycelium growth rate at the specified relative humidity and temperature. The temperature in the model is fixed between 0 and 30 °C in agreement with the range of indoor temperature (Sedlbauer 2001). Under the condition on the LIM line, the spore takes theoretically "infinite" time to germinate. To assess the risk of spore germination, the pairs of temperature and relative humidity from the hygrothermal simulation are compared with the LIM line. If the relative humidity at the specified temperature is under LIM line, then there is no fungi activity.

The type of substrate impacts the surface conditions for the spore germination and mold growth. Four substrate categories were defined to classify different building materials:

- Substrate category 0: Optimal culture medium;

- Substrate category I: Biologically recyclable building materials like wall paper, plaster cardboard, building materials made of biologically degradable raw materials, material for permanent elastic joints;

- Substrate category II: Biologically adverse recyclable building materials such as renderings, mineral building material, certain wood as well as insulation material not covered by I;

- Substrate category III: Building materials that are neither degradable nor contain nutrients, e.g., foils, glass, tiles;

Substrate category 0 is the most favorable medium for spore germination. Therefore, it requires the lowest relative humidity at defined temperature. On the contrary, substrate category III is the worst medium for spore germination. Substrate category I and category II include most of the building materials. Their isopleth systems are shown in Figure 6-3. In this study, the isopleth system of substrate category I is selected as the criteria, since it requires a relatively lower condition for spore germination than category II. Under the same conditions, if there is no spore germination risk on the materials from substrate category I, the same conclusion can be drawn for the materials from substrate category II.
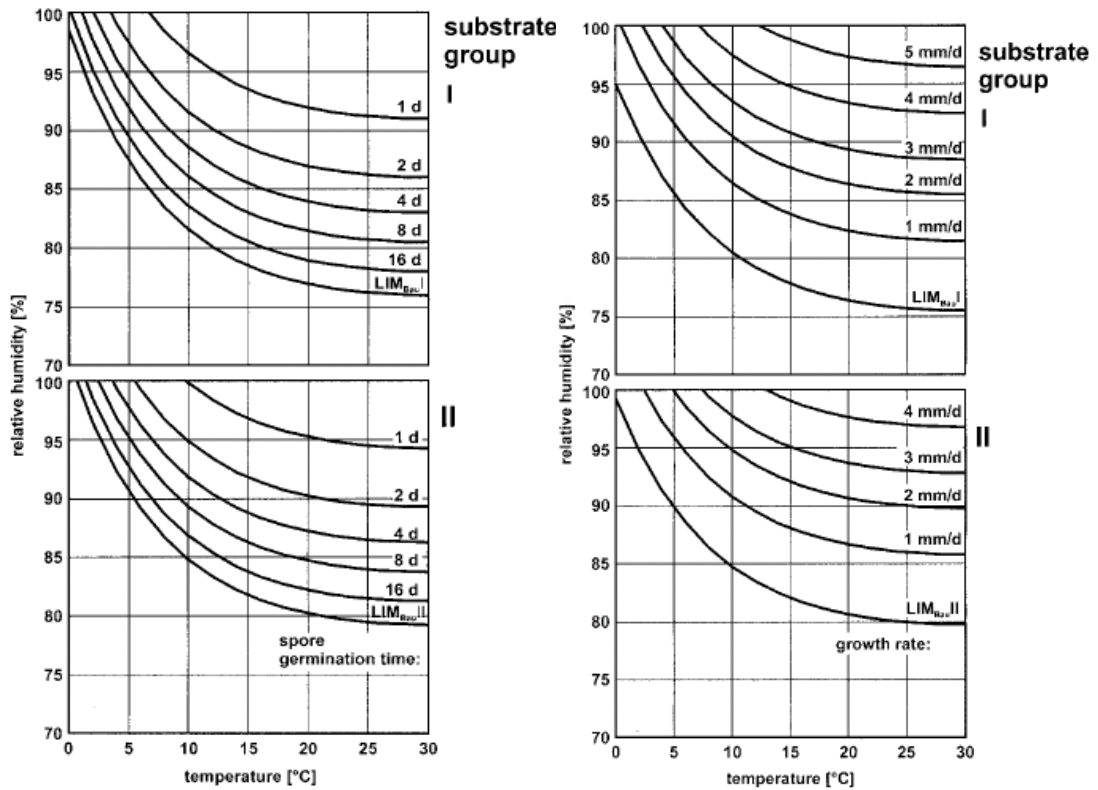
Figure 6-3 Generalized isopleth system for spore germination (left) and mycelia growth (right). Top: isopleth system for substrate category I. Bottom: isopleth system for substrate category II (Sedlbauer 2001)

6.3.2.3 Model index

Hukka and Viitanen (1999) presented a mathematical model to evaluate the mold growth on wooden material based on the laboratory measurements. The experiments covered the temperature range between 5 and 40 °C and relative humidity range between 75 and 100%. They defined a mold index between 0 and 6 based on visual appearance of the substrate surface as listed in Table 6-2. The mold is initiated when the index is beyond 1.

Table 6-2 Mold index for experiments and modeling (Hukka and Viitanen 1999)

Mold index	Description
0	no growth
1	some growth detected only with microscopy
2	moderate growth detected with microscopy (coverage more than 10%)
3	some growth detected visually
4	visually detected coverage more than 10%
5	visually detected coverage more than 50%
6	visually detected coverage 100%

There are some threshold conditions under which mold requires to germinate. The initiation of mold growth is dependent on the temperature, relative humidity, exposure time and surface quality of the substrate. From the experiment result, the critical temperature and relative humidity to initiate mold growth can be described by the equation 6.2 (Hukka and Viitanen 1999):

$$RH_{crit} = \begin{cases} -0.00267T^3 + 0.160T^2 - 3.13T + 100.0 & \text{when } T \leq 20\,^\circ C \\ 80\% & \text{when } T > 20\,^\circ C \end{cases} \tag{6.2}$$

The largest possible mold growth index M_{max} between the mold index 1 in the initiation stage and index 6 in the fully contaminated stage can be expressed by a parabolic equation:

$$M_{max} = 1 + \frac{RH_{crit} - RH}{RH_{crit} - 100} - 2\left(\frac{RH_{crit} - RH}{RH_{crit} - 100}\right)^2 \tag{6.3}$$

A mathematical differential equation to express the mold index linearly increasing over time in days during the initiation stage of mold growth is given in equation 6.4.

$$\frac{dM}{dt} = \frac{1}{7\exp(-0.68\ln T - 13.9\ln RH + 0.14W - 0.33SQ + 66.02)}, \quad M < 1, \tag{6.4}$$

where T is temperature, RH is relative humidity, W is the type of wood as the substrate (0=pine, 1=spruce), and SQ is the quality of the surface (0=re-sawn after drying, 1=original).

The mold growth does not exhibit the same rate: the mycelium growth is much faster in the later stage (M>1) than in the early stage (M>1). This phenomenon can be defined by two correction coefficients, given in equation 6.5 and 6.6 (Hukka and Viitanen 1999).

$$k_1 = \begin{cases} 1 & \text{when M<1} \\ \dfrac{2}{t_v/t_m - 1} & \text{when M} > 1 \end{cases} , \tag{6.5}$$

$$k_2 = 1 - \exp\left[2.3(M - M_{max})\right], \tag{6.6}$$

where t_v is the predicted response time for growth of mold fungi (M=3) in weeks, and t_m is the predicted response time for growth of mold fungi (M=1) in weeks. They can be derived from equation 6.7 and 6.8.

$$t_v = \exp(-0.74 \ln T - 12.72 \ln RH + 0.06W + 61.50) \tag{6.7}$$

$$t_m = \exp(-0.68 \ln T - 13.9 \ln RH + 0.14W - 0.33SQ + 66.02) \tag{6.8}$$

Thus, the mold growth rate with the consideration of the contribution of k_1 and k_2 is given by:

$$\frac{dM}{dt} = \frac{1}{7\exp(-0.68 \ln T - 13.9 \ln RH + 0.14W - 0.33SQ + 66.02)} \cdot k_1 \cdot k_2 \tag{6.9}$$

Mold growth under the fluctuating humidity condition will slow down, and the latent period will become longer than at a constant favorite condition (Adan 1994; Viitanen1997; Hukka and Viitanen 1999). Under the unfavorable condition, the mold activity will reduce. In case temperature is under 0 or relative humidity is below the critical relative humidity, the delay of mold growth can be obviously observed. This delay happens in the period from the start of drying to 6 hours. But there is no drying behavior, if the drying time extends from 6 hours to 24 hours. After 24 hours, this drying delay is prolonged again. The mold index in dependence on the drying period (t-t_1) is written in equation 6.10 (Hukka and Viitanen 1999).

$$\frac{dM}{dt} = \begin{cases} -0.032 & \text{when t-t}_1 \leq 6h \\ 0 & \text{when } 6h \leq \text{t-t}_1 \leq 24h \\ -0.016 & \text{when t-t}_1 > 24h \end{cases} \tag{6.10}$$

The mold index model is best applicable for the wooden based material. Mold growth on other materials has a slower speed than on the wooden materials (Ritschkoof et al. 2000; Viitanen 2007). In the same surface condition and ambient temperature and humidity, concrete and non-organic thermal insulation usually need longer exposure time. So by using the mathematical model based on the wooden material actually overestimates the mold index. But if the result from the worse scenario is on the "safe" side, it will be applicable on other cases.

6.3.2.4 Comparison of the mold models

Previous sections discussed the main features of each mold model. This section will illustrate the strengths and limitations of these models.

In DIN 4108-3 (2001), relative humidity is considered as a sole rule to assess the mold growth risk. The temperature factor (DIN EN ISO 13788 2001) as the threshold is only applicable under stationery conditions. The isopleth model and mold index not only account for the effect of relative humidity, but also consider the impact of the temperature and the substrate under transient condition.

For isopleth model, it covers the worst scenario since the initial inertia phase of the mycelium growth is not considered after the unfavorable condition occurs. Therefore, the result could overestimate the spore germination or mold growth rate. So it is always on the "safe" side to evaluate the risk of mold growth. The disadvantage of the isopleth model is that it cannot assess the interim drying out of the fungi spore when mico-climatic boundary conditions transiently vary.

While the mold index also has some limitations. The model did not consider the situation when temperature is below 0 °C, although some phenomena show that the mold activities in this temperature range decrease or stay constant (Viitanen 2010). The time interval to calculate the mold index also determines the magnitude of the index. In fluctuating conditions, as the shorter time interval adopts, the larger the mold index will be. This is due to the fact that the mold index increases faster than it

decreases (Vinha 2007). The model is established based on the wooden materials, so its expendability to other materials needs to be further validated.

6.3.3 Probability of Damages Induced by the Hygrothermal Loads

Hygrothermal response of the building enclosure dynamically presents the interaction of the enclosure with outdoor and indoor environments. The excessive fluctuation of relative humidity, temperature, and moisture content over time on the material surface may cause the thermal expansion, hygric swelling and shrinkage. The induced possible deterioration phenomena are illustrated in Figure 6-4 a), b), and c).
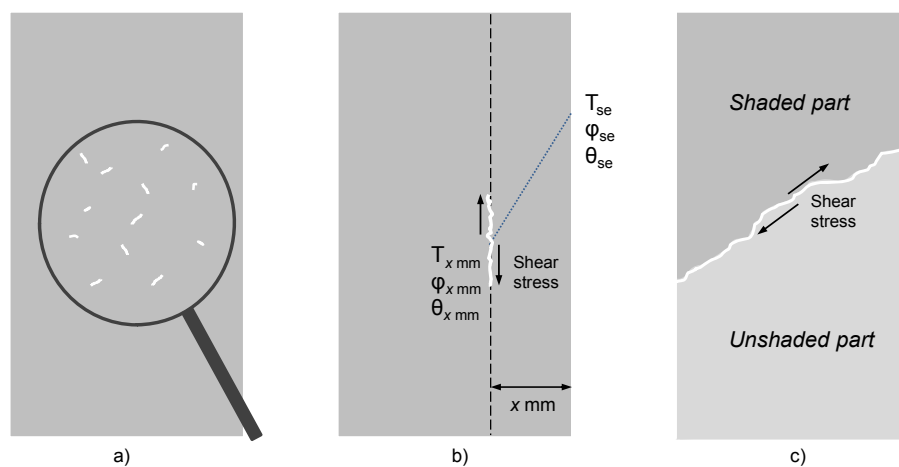
Figure 6-4 Damages induced by hygrothermal loads

Case a presents the micro-cracks on a solid material surface due to the dramatic temperature and hygic variations over time. Those variations build the tension in the pore structure, thus result in the micro-cracks and segregations. Case b presents the crack developed inside the material due to the difference of temperatures, relative humidity levels, and moisture contents between distinct positions of the material over

time. The different responses of the material layers to the temperature and hygric variations will produce a shear stress that could lead to the demolition and crack. Case c presents a surface crack induced by the shear stress due to temperature difference on two adjacent surface regions, resulted from the unevenly incident solar radiation.
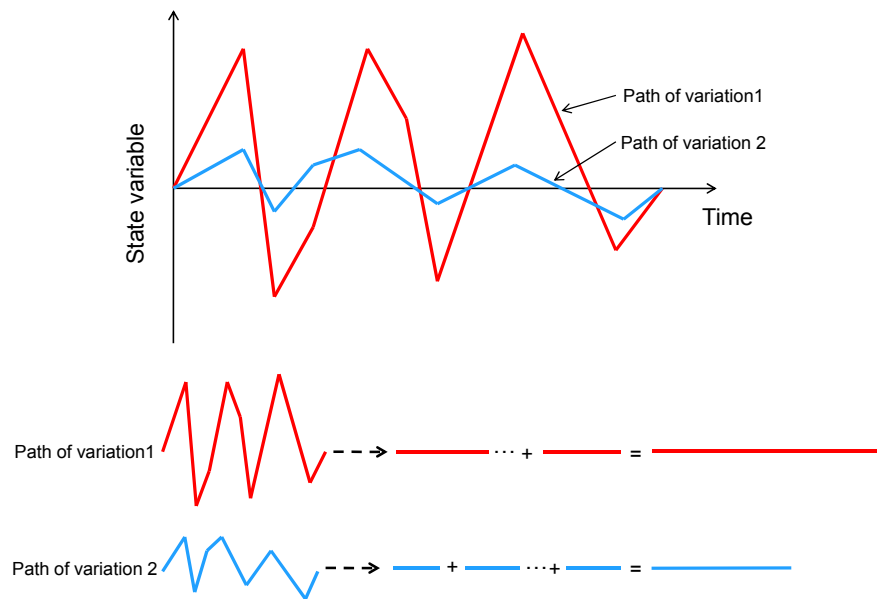
Figure 6-5 Schematic diagram of the mechanism of hygrothermal load impact

Hygrothermal loads provide a measure of the possibility of damages at outer surface region of the construction. To quantify the hygrothermal load, the course length of the hygrothermal parameter, e.g., temperature, relative humidity, and moisture content over time, together with their differences at distinct positions, are summed up in the surface region (Ruisinger and Grunewald 2009).

This means both the amplitude and the frequency of the state variables over time will be measured by their "travel path". For instance, a surface temperature with a large difference between maximum and minimum values or with more frequency variations over time will give rise to a longer course than the relatively uniform temperature

does. Thus, the potential of detriment of this load is correspondingly high. This mechanism is demonstrated in Figure 6-5.

6.3.3.1 Hygrothermal loads on the exterior surface

Hygrothermal loads on the exterior surface of the building enclosure assembly, described by Figure 6-4a, are induced by the variations of the surface temperature, relative humidity, and moisture content over time. The loads are defined *by HLS$_T$, HLS$_\varphi$*, and *HLS$_\theta$* in equation 6.11, which integrate the annual curve lengths of temperature, relative humidity, and moisture content at the outer surface in specific time interval, respectively.

$$HLS_T = \sum_{i=1}^{8760} \sqrt{\Delta T_{s,i}^2 + \Delta t_i^2} \,, \tag{6.11 a}$$

$$HLS_\varphi = \sum_{i=1}^{8760} \sqrt{\Delta \varphi_{s,i}^2 + \Delta t_i^2} \,, \tag{6.11 b}$$

$$HLS_\theta = \sum_{i=1}^{8760} \sqrt{\Delta \theta_{s,i}^2 + \Delta t_i^2} \,, \tag{6.11 c}$$

where $\Delta T_{s,i}$, $\Delta \varphi_{s,i}$, and $\Delta \theta_{s,i}$ are surface temperature difference, relative humidity difference, and moisture content difference in the time interval Δt_i (1 hour), respectively.

The hygrothermal loads on the exterior surface give insight into the frequency and intensity of the swelling and shrinkage, as well as thermal expansion on the outer surface.

6.3.3.2 Hygrothermal loads at the certain depth layer from the exterior surface

Hygrothermal loads at the certain depth layer from the exterior surface, described by

Figure 6-4b, is induced by the difference of temperatures, relative humidities, and

moisture contents between distinct positions of the material over time. The loads are

defined by HLD_T, HLD_φ, and HLD_θ in equation 6.12, which integrate the annual

temperature, relative humidity and moisture content difference between the outer

surface and the material layer at the defined depth in specific time interval,

respectively.

$$HLD_T = \sum_{i=1}^{8760} \sqrt{(\bar{T}_{s,i} - \bar{T}_{xmm,i})^2 + \Delta t_i^2} \quad , \tag{6.12 a}$$

$$HLD_\varphi = \sum_{i=1}^{8760} \sqrt{(\bar{\varphi}_{s,i} - \bar{\varphi}_{xmm,i})^2 + \Delta t_i^2} \quad , \tag{6.12 b}$$

$$HLD_\theta = \sum_{i=1}^{8760} \sqrt{(\bar{\theta}_{s,i} - \bar{\theta}_{xmm,i})^2 + \Delta t_i^2} \quad , \tag{6.12 c}$$

where $\bar{T}_{s,i} - \bar{T}_{xmm,i}$, $\bar{\varphi}_{s,i} - \bar{\varphi}_{xmm,i}$, and $\bar{\theta}_{s,i} - \bar{\theta}_{xmm,i}$ are mean temperature difference,

relative humidity difference, and moisture content difference between the outer

surface and *x mm* depth layer from outer surface in time interval Δt_i (1 hour),

respectively.

The hygrothermal loads at the certain depth layer from exterior surface measure the

stress due to the difference in hygric or thermal response near the outer region of the

construction, i.e., outer surface and 10mm depth layer from the outer surface. A large

difference in temperature or moisture content between these two positions indicates

an increased risk of delamination and spall of the outer layer.

6.3.4 Thermal Resistance

Thermal resistance measures a material's ability to resist the heat flow. The static

method determines the thermal resistance of a material according to its thickness and

thermal conductivity. For a component with multi-layers, the thermal resistance can

be calculated from the equation 6.13.

$$R = \sum_{n=1}^{k} \frac{d_n}{\lambda_n} , \tag{6.13}$$

where d_n and λ_n are the thickness and thermal conductivity of the material layer n,

respectively.

DIN 4108-2 (2003) requires that the thermal resistance of the external wall should not

be less than 1.2 $m^2 \cdot K/W$.

To account for the transient heat loss through the construction, the heat flux density

and the temperature difference between the interior and exterior surface of the

construction are evaluated as time-dependent variables (Ruisinger and Grunewald

2009).

The transient thermal resistance during the heating period (HP) is defined as the ratio

of integral of temperature difference $\Delta\theta_{HP}$ to integral of the heat flux through the

interior surface of the building enclosure q_{HP}.

$$R_{transient} = \frac{\Delta\theta_{HP}}{q_{HP}} = \frac{\int\limits_{HP} (\theta_{si} - \theta_{se}) \cdot dt}{\int\limits_{HP} q(t) \cdot dt},$$ (6.14)

where $q(t)$ is the heat flux through the interior surface of the building enclosure, θ_{si} is the interior surface temperature and θ_{se} is the exterior surface temperature.

Compared to the static method, the transient approach assesses the hygrothermal response of the wall assembly with the consideration of the thermal inertia in the massive wall, moisture-dependent thermal conductivity, and the effect of short wave and long wave radiations (Ruisinger and Grunewald 2009).

6.4 Criteria-based Statistical Evaluation Procedure

The performance assessment relies on two aspects: the input state variables and the selected criterion. As illustrated in Figure 6-1, the state variables (e.g., relative humidity and temperature) obtained from the simulations are used for the probabilistic performance evaluation. Those state variables can be applied either directly or input in the mathematical model to derive a new output, to compare with the target performance criterion. If the value exceeds a certain threshold, one can assume the building enclosure assembly is no longer "safe" in this specific performance. If this is the case, a careful inspection of the design should be fulfilled to reduce the possibility of failure. The performance of the building enclosure assembly can be evaluated in various aspects, including the mold growth risk, inner condensation, thermal efficiency, and the damages induced by the hygrothermal loads.

Different criteria can be applied for one target performance, e.g., the mold growth risk can be assessed by either the isopleth system or mold index. As stated in Section 6.3.2.4, each criterion has its advantages and limitations. Application of multiple criteria to evaluate one performance can provide a diverse estimation on the possibility of failure.
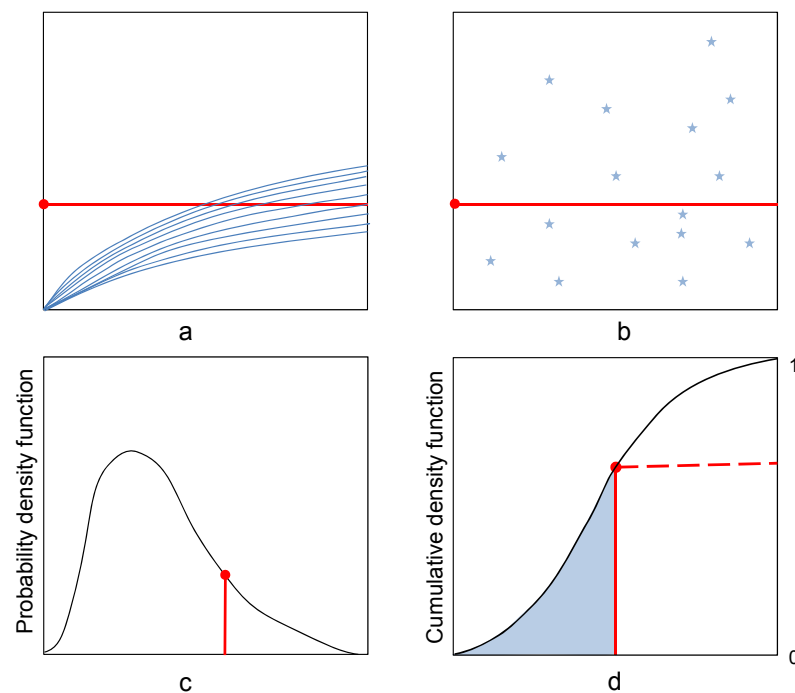
Figure 6-6 Probabilistic performance evaluation

The probabilistic performance evaluation also depends on the selected approach. The possibility of failure can be assessed by either directly comparing the output curves / values with the defined threshold (Figure 6-6 a and b), or calculating the probability from density functions (Figure 6-6 c and d).

6.5 Summary

A probabilistic approach, incorporated into DELPHIN simulation tool, was developed to assess the hygrothermal performance of the building enclosure assemblies.

Compared to the deterministic model with a single output, this approach propagates the uncertainties in the analysis inputs to the analysis outputs by iteratively carrying out the simulations and produces the result in a certain range. Therefore, the risk assessment will not provide just a result of "failure" or "no failure", but will give a possibility of failure.

The relations between the material parameters and between material parameters and material functions were discussed. The variation of basic material parameter will yield the shift of the related material functions. Those relationships were incorporated in the Latin hypercube sampling.

The different criteria to assess the durability, thermal efficiency, and mold growth risk of the building enclosure assembly were discussed and compared. The evaluation of the hygrothermal performance of the building enclosure assembly in the design stage should base on one or more criteria in order to minimize the possibility of damages and maximize the usability.

Chapter 7 Case Study

7.1 Introduction

Before the energy crisis in the 1970s, most external walls in Europe were uninsulated, either constructed as masonry cavity wall with the air layer in-betweens or only as the plastered masonry wall. During the heating season, these buildings consumed considerable amount of energy in order to achieve a comfortable level for the residents. Constructions with low thermal resistance are often accompanied with surface condensation and mold growth issues.

In recent years, to meet energy requirements, many European countries have started to renovate historical buildings by installing interior or exterior insulations. From the aesthetic and artistic point of view, the appearance of the building facade should be maintained. The exterior insulation has the limitations for this aim, so the interior insulation is more suitable. The installation of extra insulation improves the thermal resistance of the building component. On the other hand, it also increases the air tightness of the building and reduces the infiltration/exfiltration, which further raises the risk of the moisture related issues. The appropriate strategy to install the insulation should consider the characteristics of both the surrounding environments and building construction itself, and its reasonability should be examined in the design stage.

In this chapter, the developed probabilistic approach is exemplified. First, the need to renovate a plastered masonry wall is discussed. Then, a retrofitted wall with an

interior insulation installed on the masonry wall is introduced. The uncertainties in the

input variables are described and quantified, and the hygrothermal performance of the

retrofitted wall is assessed by different performance criteria. Finally, sensitivity

analysis is applied to address the most influential variables against the criteria of

interest.

7.2 Wall Assemblies Description

7.2.1 Base Wall

A historic plastered masonry wall is first introduced and it is served as the base wall.

From interior to exterior, it is composed of 15 *mm* historical lime plaster, 380 *mm*

brick, and 20 *mm* lime cement plaster. The basic material properties of each material

are listed in Table 7-1. The static thermal resistance of the wall has the value of 0.532

$m^2 \cdot K/W$, which is far below the value of 1.2 $m^2 \cdot K/W$ required in DIN 4108-2 (2003).

The external wall corner has the thermal bridge effect and usually has a relatively

lower temperature compared to the other parts of the building enclosure. This is

because the low air movement in this region reduces the surface heat exchange with

the indoor environment. Another reason is the difference of the surface area between

the interior side and exterior side of the wall corner. Therefore, the mold growth risk

at this location is assessed by the hygrothermal simulation.

The schematic drawing of the external wall corner and the location of concern are shown in Figure 7-1. The length of the wall on each side is set as 1000 mm in the simulation, to exclude the influence of the thermal bridge.
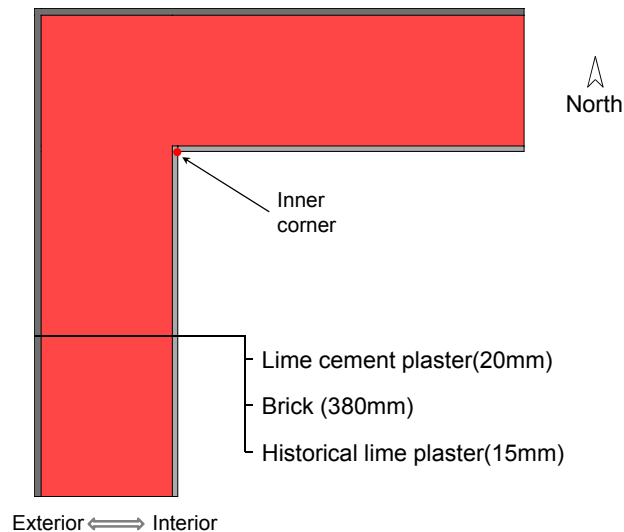
Figure 7-1 Schematic drawing of the base wall corner

The outdoor condition adopted the weather data of test reference year of Potsdam, Germany. The indoor condition was derived according to DIN EN 15026 (2007), in which the indoor temperature and relative humidity are calculated from the daily average outdoor temperature. Indoor humidity has two scenarios: the normal and the high indoor moisture loads (Section 5.2.2.3). The applied boundary coefficients were listed in Table 7-2.

The initial moisture content of each material was set as the equivalent value corresponding to relative humidity of 80% (ASHRAE 160 2009), derived from sorption isotherm. The initial temperature was assumed to be 20°C. The simulation started from July 1 for a period of 2 years. The first year was considered as the

initializing period. Therefore, the second-year outputs of hygrothermal simulation were used for the analysis.

Temperature and relative humidity at the interior surface of the base wall corner from the hygrothermal simulation are shown in Figure 7-2. Relative humidity obtained by using the high indoor moisture load is higher than 80% in most of time.
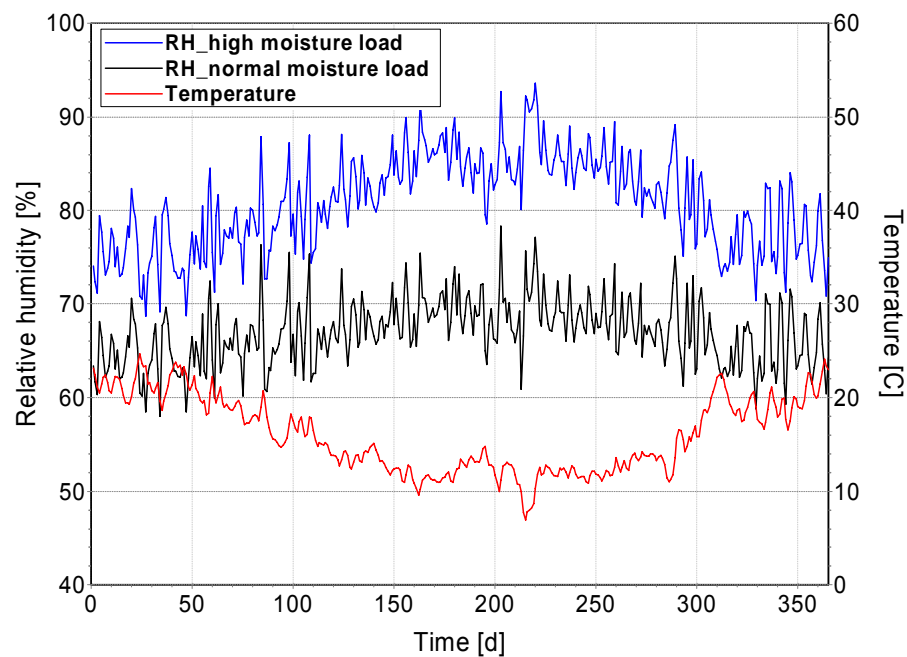
Figure 7-2 Temperature and relative humidity at the interior surface of the base wall corner

Figure 7-3 shows the isopleth system for assessing mold growth risk at the interior surface of the base wall corner. It is clear that, for the result derived by using high indoor moisture load, quite a large amount of values are across the line of spore germination after 8 days, indicating a very high potential of mold growth. For the result derived by using the normal indoor moisture load, only a few points are beyond the line of Lowest Isopleth for Mold, indicating the low potential of mold growth.
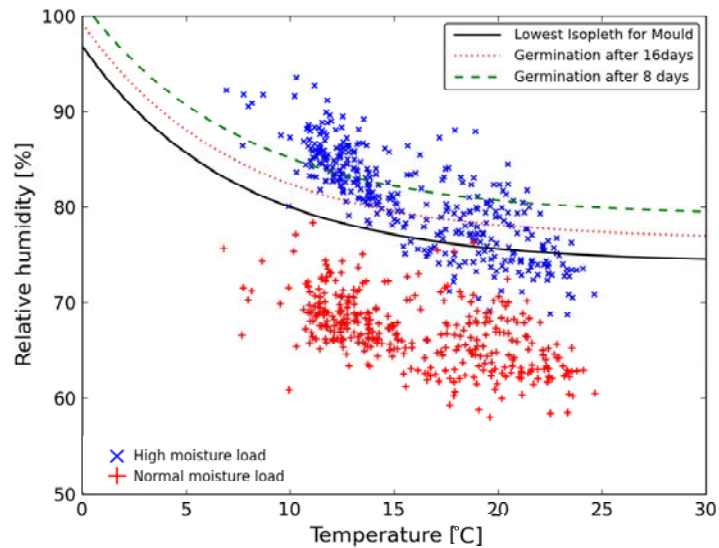
Figure 7-3 Isopleth system for assessing the mold growth risk at the interior surface of the base wall corner

The mold index for assessing the mold growth risk at the interior surface of the base wall corner are presented in Figure 7-4. The mold index above 1 indicates the mold starts to grow. For the scenario with the high indoor moisture load, the result shows that the mold starts to grow during the autumn and reaches the highest value in the spring. If the scenario with the normal indoor moisture load is adopted, there is no mold growth risk.
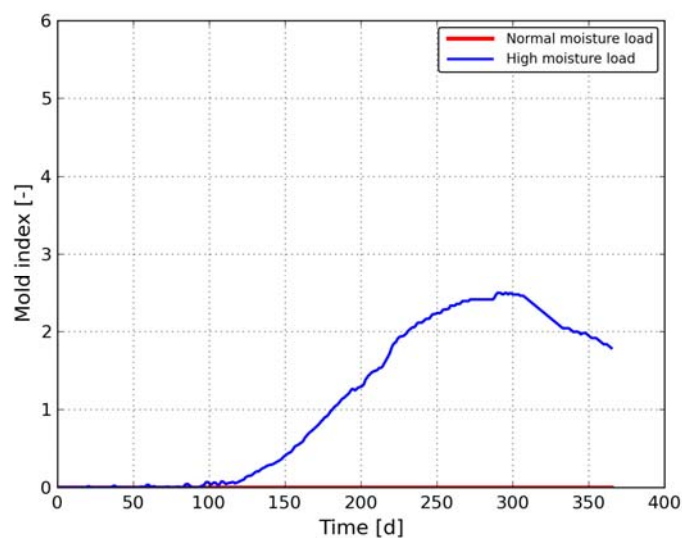
Figure 7-4 Mold index for assessing the mold growth risk at the interior surface of the base wall corner

The analyses from both mold models indicate that there is a possibility of the mold growth at the interior surface of the base wall corner. To improve the thermal performance and reduce the mold growth risk, the renovation of the base wall is needed.

7.2.2 Retrofitted Wall

The calcium silicate is a rigid and capillary-active material. It has a low thermal conductivity and is easy installation. So it is selected for the application.

A 5 *mm* glue mortar is used to attach the calcium silicate board to the inner surface of the base wall, and a 5 *mm* lime plaster is applied on the surface of the calcium silicate. The retrofitted wall with the installation of 30 *mm* calcium silicate, has the static thermal resistance of 1.03 $m^2 \cdot K/W$, which is still less than 1.2 $m^2 \cdot K/W$ required by DIN 4108-2 (2003). So a 50 *mm* calcium silicate, giving rise to the static thermal resistance of 1.34 $m^2 \cdot K/W$, is adopted. The schematic drawing of the renovated wall with dimensions is shown in Figure 7-5.

Lime cement plaster(20mm)
Brick (380mm)
Historical lime plaster(15mm)
Calcium silicate glue mortar (5mm)
Calcium silicate (50mm)
Lime plaster (5mm)

Inner corner

North

Exterior ⟺ Interior
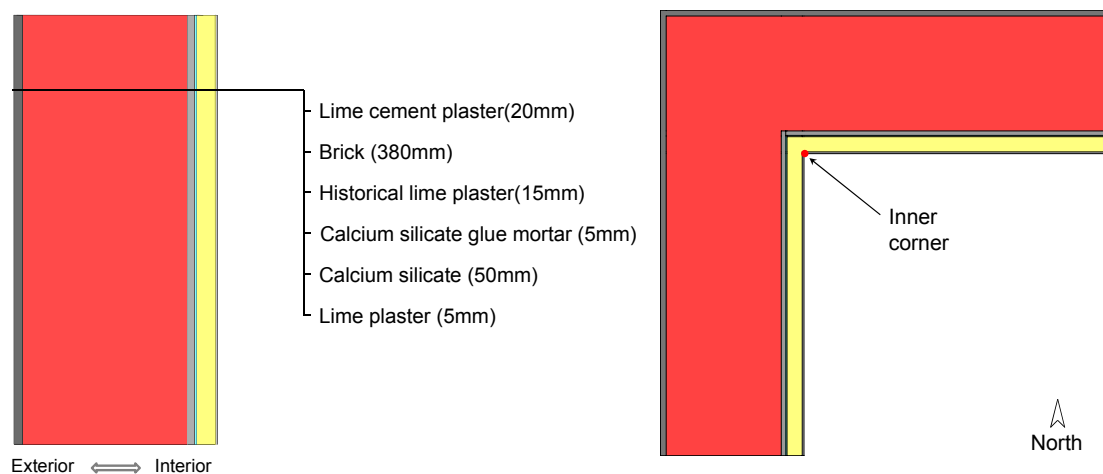
Figure 7-5 Schematic drawing of the retrofitted wall and the corresponding corner

The hygrothermal performance of the retrofitted wall is assessed against different

evaluation criteria described in Section 6.3, in consideration of the uncertainties in the

input variables. The simulation started from July 1 for a period of 2 years. The second

year outputs of the simulations were used for the analysis.

7.3 Uncertainty Analysis on Hygrothermal Performance of the Retrofitted Wall

7.3.1 Uncertainty in the Input Variables

The uncertainties in the hygrothermal simulation may come from different sources. In

this study, the considered uncertain variables include the material properties, the

indoor conditions, boundary coefficients, orientation of the wall assembly, and the

dimension of the material layer. For each variable, the design value for the

deterministic simulation and the deviation/ variation range for the probabilistic

performance evaluation are detailedly introduced as follows.

7.3.1.1 Material properties

As discussed in Section 5.2.3, the material properties were assumed to follow the

normal distributions. The mean value and the standard deviation of each property

used the statistical data obtained from IBK-laboratory measurements. They are listed

in Table 7-1. The perturbation in the basic parameters will lead to the variation of the

related material functions as mentioned in Section 6.2.1. So when the basic parameter

is randomly selected from the normal distribution, the related material functions will also vary in a certain range.

Table 7-1 Material properties and their standard deviations (in the parenthesis)

Basic property	Symbol [Unit]	Lime plaster	Calcium silicate	Calcium silicate glue mortar	Historical lime plaster	Brick	Lime cement plaster
Density	ρ $[kg/m^3]$	1380 (30.0)	235 (10.0)	1480 (40)	1790 (35)	1830 (28)	1800 (30)
Specific heat capacity	c $[J/kg\cdot K]$	650 (20.0)	1250 (25.0)	1020 (45.0)	850 (28)	790 (20)	840 (25)
Thermal conductivity	λ $[W/m\cdot K]$	0.43 (0.03)	0.063 (0.005)	0.92 (0.06)	0.82 (0.04)	0.78 (0.05)	0.76 (0.03)
Open porosity	θ_{por} $[m^3/m^3]$	0.49 (0.02)	0.92 (0.01)	0.45 (0.02)	0.31 (0.02)	0.31 (0.02)	0.32 (0.02)
Effective saturation moisture content	θ_{eff} $[m^3/m^3]$	0.46 (0.02)	0.91 (0.01)	0.27 (0.02)	0.28 (0.02)	0.28 (0.02)	0.30 (0.02)
Capillary saturation moisture content	θ_{cap} $[m^3/m^3]$	0.32 (0.02)	0.81 (0.02)	0.03 (0.003)	0.25 (0.02)	0.21 (0.02)	0.12 (0.01)
Water absorption coefficient	A_w $[kg/m^2s^{0.5}]$	0.08 (0.005)	0.95 (0.05)	0.01 (0.002)	0.13 (0.02)	0.26 (0.02)	0.015 (0.003)
Water vapor diffusion resistance factor	μ_{dry} [-]	11.0 (1.5)	5.5 (0.5)	38.0 (3.0)	12.0 (1.5)	9.8 (1.5)	13.0 (1.5)
Liquid water conductivity at saturation moisture content	K_{eff} [s]	5.0E-11 (1.5E-11)	9.0E-09 (2.0E-09)	3.0E-11 (1.0E-11)	3.0E-09 (1.0E-09)	3.0E-9 (1.0E-9)	5.0E-09 (1.5E-09)

7.3.1.2 Boundary conditions

The outdoor condition adopted the weather data of test reference year of Potsdam, Germany, the same as the base case. The design indoor temperature and relative humidity, according to DIN EN 15026 (2007), were the functions of the daily average outdoor temperature.

To account for the uncertainties in the indoor environment, the indoor temperature and relative humidity function profiles were set as uncertain variables. The relative humidity function profile (Figure 7-6 top) were parallel to vary between the profiles of the normal (A) and the high (B) indoor moisture loads, following a uniform distribution. The temperature function profile (Figure 7-6 bottom) varied parallel to the design temperature function profile, following a normal distribution with a standard deviation of 0.5°C.

The boundary coefficients were assumed to follow the normal distributions. The design values and the corresponding standard deviations, referring to the summarized empirical values in Table 5-5, are listed in Table 7-2.
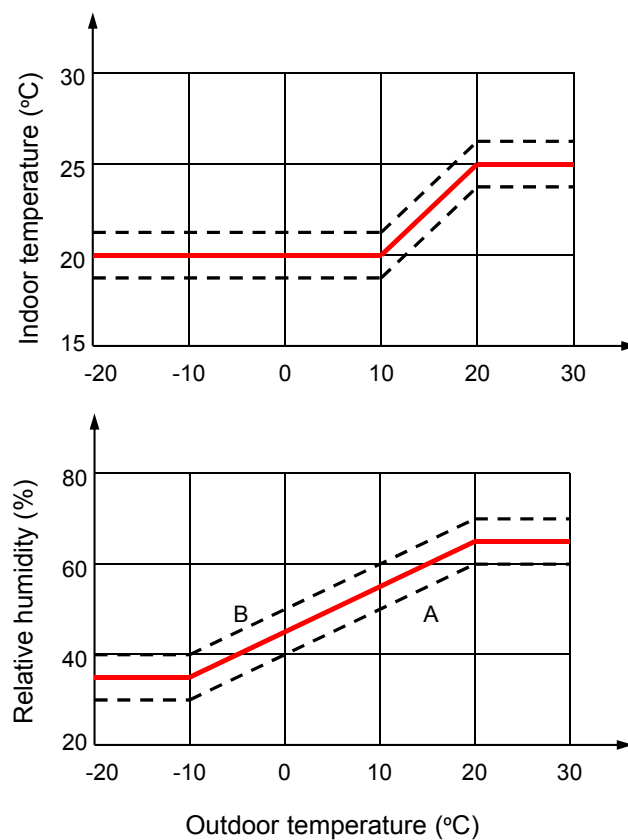
Figure 7-6 Indoor relative humidity (top) and temperature (bottom) function profiles. The dash lines outline the relevant variation range

Table 7-2 Boundary coefficients and the standard variations (in the parenthesis)

Boundary coefficient	Symbol	Unit	Value
Heat transfer coefficient _ interior	α_i	W/m^2K	8.0 (1.0)
Vapor transfer coefficient _ interior	β_{pi}	s/m	3e-08 (5e-09)
Heat transfer coefficient _ exterior	α_e	W/m^2K	25.0 (3.0)
Vapor transfer coefficient _ exterior	β_{pe}	s/m	2e-07 (5e-08)
Short wave radiation absorptivity	α_{sw}	-	0.6 (0.1)
Ground reflectivity	$\rho_{s,g}$	-	0.2 (0.04)
Long wave emissivity of building surface	ε	-	0.9 (0.06)
Rain exposure coefficient	α_R	-	0.60 (0.12)

7.3.1.3 Orientation

In the early design stage, the orientation of a wall assembly may be unknown. Thus, it

was considered as an uncertain variable. Customarily, the value of 0 is used to

represent a North oriented wall and the value of 90 is used to denote an East oriented

wall, etc. In this study, the orientation of the wall assembly was uniformly selected

from the values of 0, 45, 90, 135, 180, 225, 270, and 315. For a wall corner section,

the incident short wave radiation, long wave radiation, and rain impinging on the

two-component walls are different. Therefore, it needs to specify their respective

orientations in the simulation.

7.3.1.4 Dimension of material layer

The dimension of the material layer may also impact the hygrothermal response of the

wall assembly. So the dimension of the material layer prone to be influenced by the

craftsmanship was considered as an uncertain variable following a uniform

distribution. Those materials include the historical lime plaster, calcium silicate glue

mortar, and lime plaster. The design value and the variation range (in the parenthesis) of each material layer are listed in Table 7-3.

Table 7-3 Dimensions of material layers and their variation ranges (in the parenthesis)

Material	d [mm]
Lime plaster	5 (3-8)
Calcium silicate glue mortar	5 (3-8)
Historical lime plaster	15 (10-20)

7.3.1.5 Probability distributions of the input variables

The probability distributions of the input variables are summarized in Table 7-4. The variables are randomly selected from their respective distributions by the Latin hypercube sampling.

Table 7-4 Probability density functions of the input variables

Input variable	Distribution
Material property (basic parameter and material function)	Normal
Boundary coefficient	Normal
Orientation	Uniform
Dimension of material layer	Uniform
Indoor temperature	Normal
Indoor relative humidity	Uniform

7.3.1.6 Sample size

According to Lomas and Eppel (1992), the accuracy of the total uncertainty in the prediction can be denoted by the accuracy of the standard deviation of the prediction. The normalized 95% confidence interval of standard deviation of the prediction against the number of the Monte Carlo simulation is shown in Figure 7-7. After 200

simulations, the accuracy is only marginally improved with the total simulation

number. So 400 simulation project files with the randomly generated input variables

were built, according to the procedure described in Section 6.2.2. 400 simulations are

also sufficiently greater than the minimum sampling size $4k/3$ (k is the number of the

input variables; k=56 in this study) recommended by Iman and Helton (1985). Each

simulation project is referenced as one sample for uncertainty and sensitivity analysis.
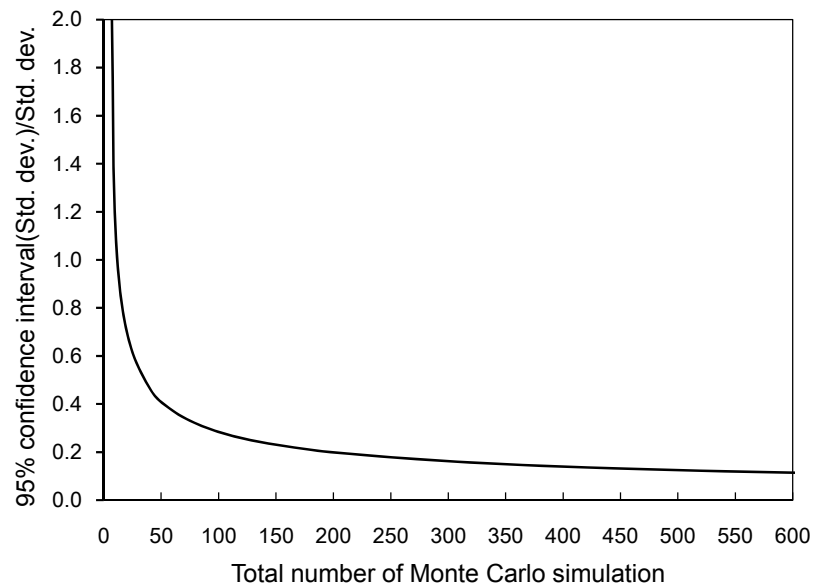
Figure 7-7   Accuracy of the standard deviation against the number of the Monte Carlo
simulation

7.3.2 Randomly Generated Material Parameters

7.3.2.1 Rank correlation matrix of material parameters

Rank correlation matrixes of the generated basic parameters of the materials are listed

from Table 7-5 to Table 7-10. The correlations between the randomly generated

parameters mostly achieves good agreement to the desired correlations described in

Section 3.6.

Table 7-5 Rank correlation matrix of the generated basic parameters of lime cement plaster

Ranked Correlation	ρ	c_0	λ	μ_{dry}	θ_{por}
ρ	1				
c_0	-0.40	1			
λ	0.97	-0.36	1		
μ_{dry}	0.60	0	0.65	1	
θ_{por}	-0.98	0.43	-0.96	-0.59	1

Table 7-6 Rank correlation matrix of the generated basic parameters of brick

Ranked Correlation	ρ	c_0	λ	μ_{dry}	θ_{por}
ρ	1				
c_0	-0.81	1			
λ	0.76	-0.55	1		
μ_{dry}	0.48	-0.32	0.51	1	
θ_{por}	-0.92	0.81	-0.67	-0.59	1

Table 7-7 Rank correlation matrix of the generated basic parameters of historical lime plaster

Ranked Correlation	ρ	c_0	λ	μ_{dry}	θ_{por}
ρ	1				
c_0	-0.41	1			
λ	0.97	-0.37	1		
μ_{dry}	0.60	0	0.65	1	
θ_{por}	-0.98	0.43	-0.97	-0.59	1

Table 7-8 Rank correlation matrix of the generated basic parameters of calcium silicate glue mortar

Ranked Correlation	ρ	c_0	λ	μ_{dry}	θ_{por}
ρ	1				
c_0	-0.41	1			
λ	0.97	-0.37	1		
μ_{dry}	0.60	0	0.65	1	
θ_{por}	-0.99	0.43	-0.96	-0.59	1

Table 7-9 Rank correlation matrix of the generated basic parameters of calcium silicate

Ranked Correlation	ρ	c_0	λ	μ_{dry}	θ_{por}
ρ	1				
c_0	-0.55	1			
λ	0.94	-0.40	1		
μ_{dry}	0.72	-0.40	0.66	1	
θ_{por}	-0.87	0.46	-0.89	-0.60	1

Table 7-10 Rank correlation matrix of the generated basic parameters of lime plaster

Ranked Correlation	ρ	c_0	λ	μ_{dry}	θ_{por}
ρ	1				
c_0	-0.40	1			
λ	0.97	-0.36	1		
μ_{dry}	0.60	0	0.64	1	
θ_{por}	-0.98	0.43	-0.97	-0.58	1

7.3.2.2 Material functions of each material

The uncertainties in the material properties will lead to the variation of the related material functions. The generated material functions of each material are presented from Figure 7-8 to Figure 7-13. These functions include the moisture retention curve, thermal conductivity, water vapor permeability, and liquid water conductivity. In each graph, the red curve presents the design material function for the deterministic simulation. The grey shadow region is the possible variation range of the material functions obtained from 400 samples.
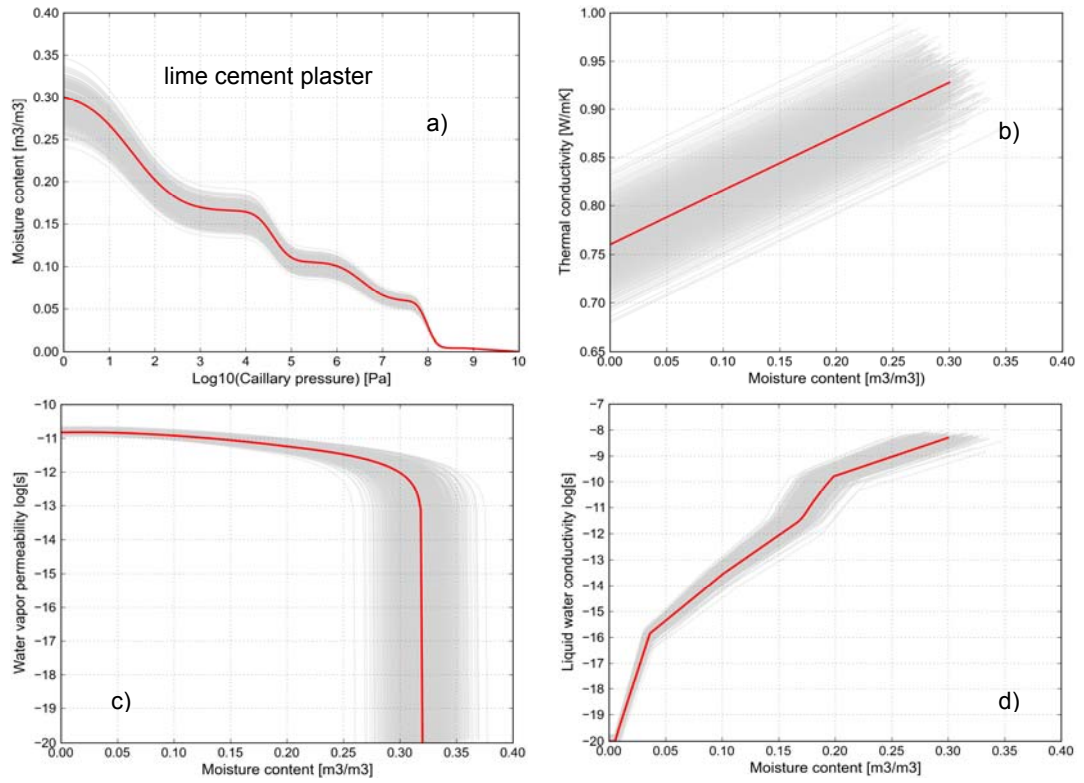
Figure 7-8 Material functions of lime cement plaster a) moisture retention curve b) thermal conductivity c) water vapor permeability d) liquid water conductivity
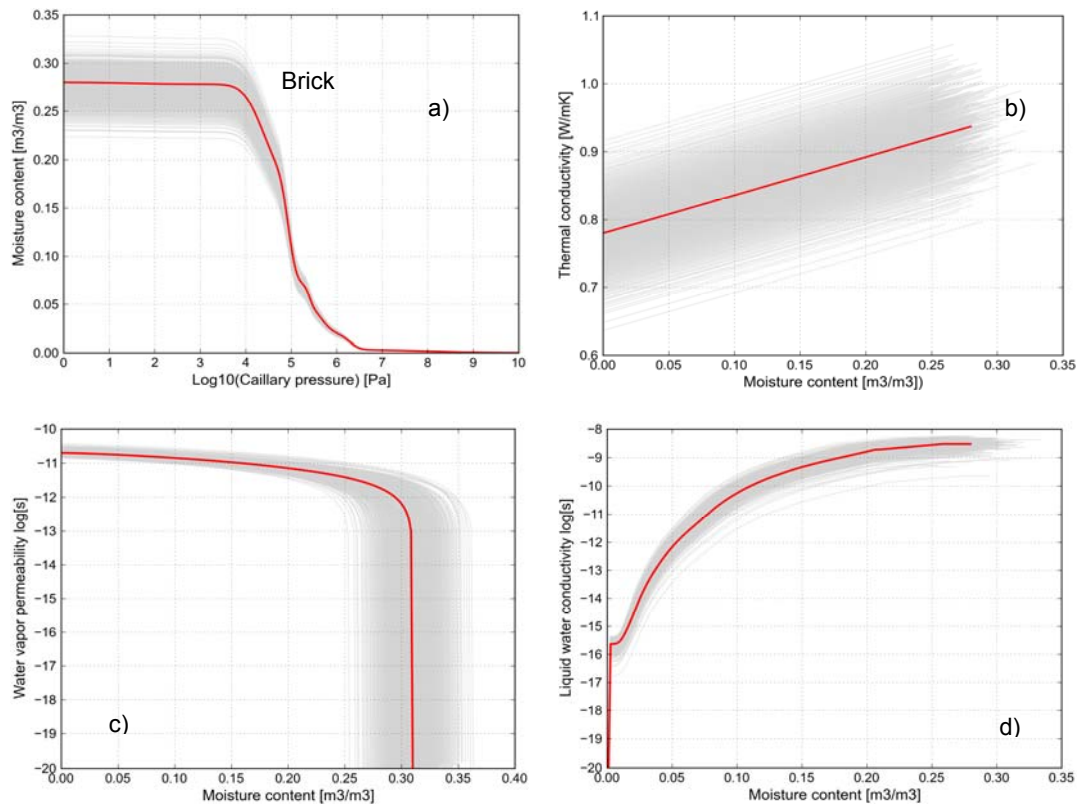
Figure 7-9 Material functions of brick a) moisture retention curve b) thermal conductivity c) water vapor permeability d) liquid water conductivity
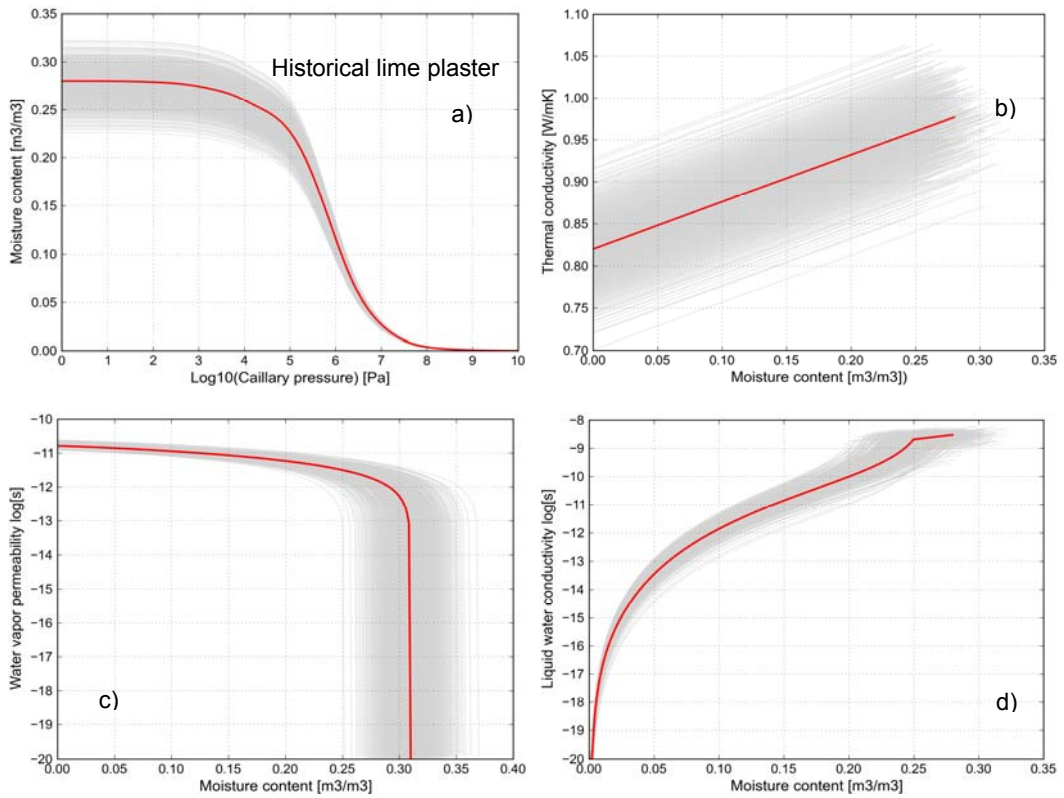
Figure 7-10 Material functions of historical lime plaster a) moisture retention curve b) thermal conductivity c) water vapor permeability d) liquid water conductivity
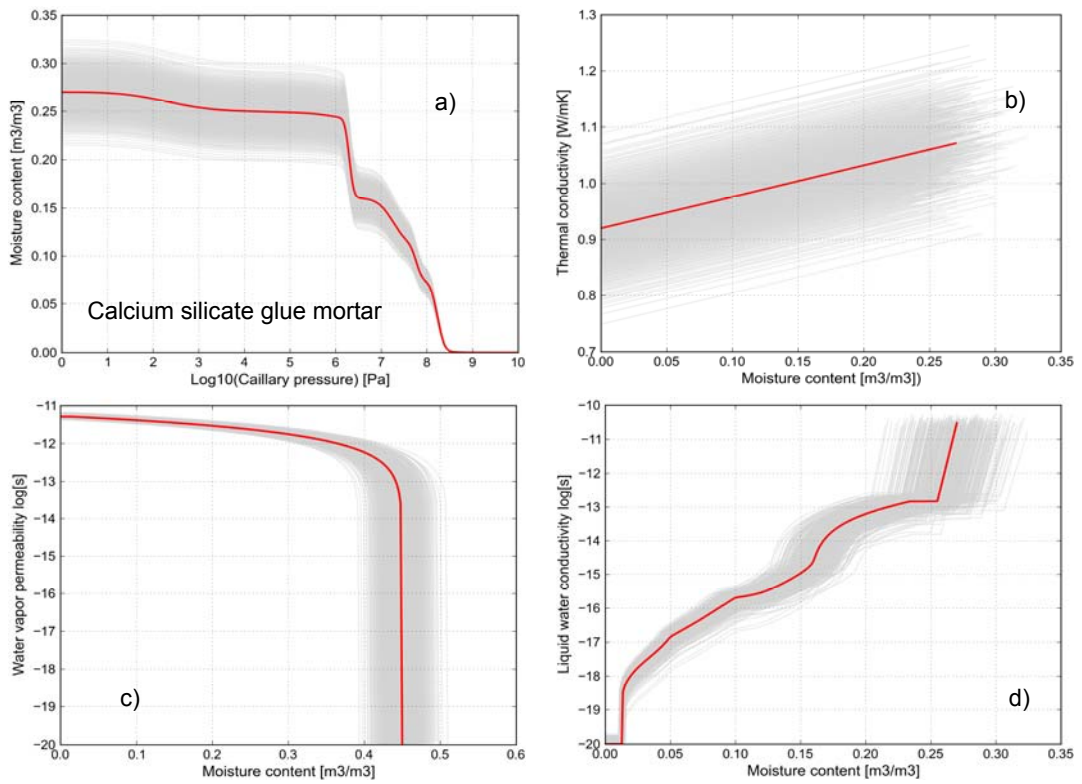
Figure 7-11 Material functions of calcium silicate glue mortar a) moisture retention curve b) thermal conductivity c) water vapor permeability d) liquid water conductivity
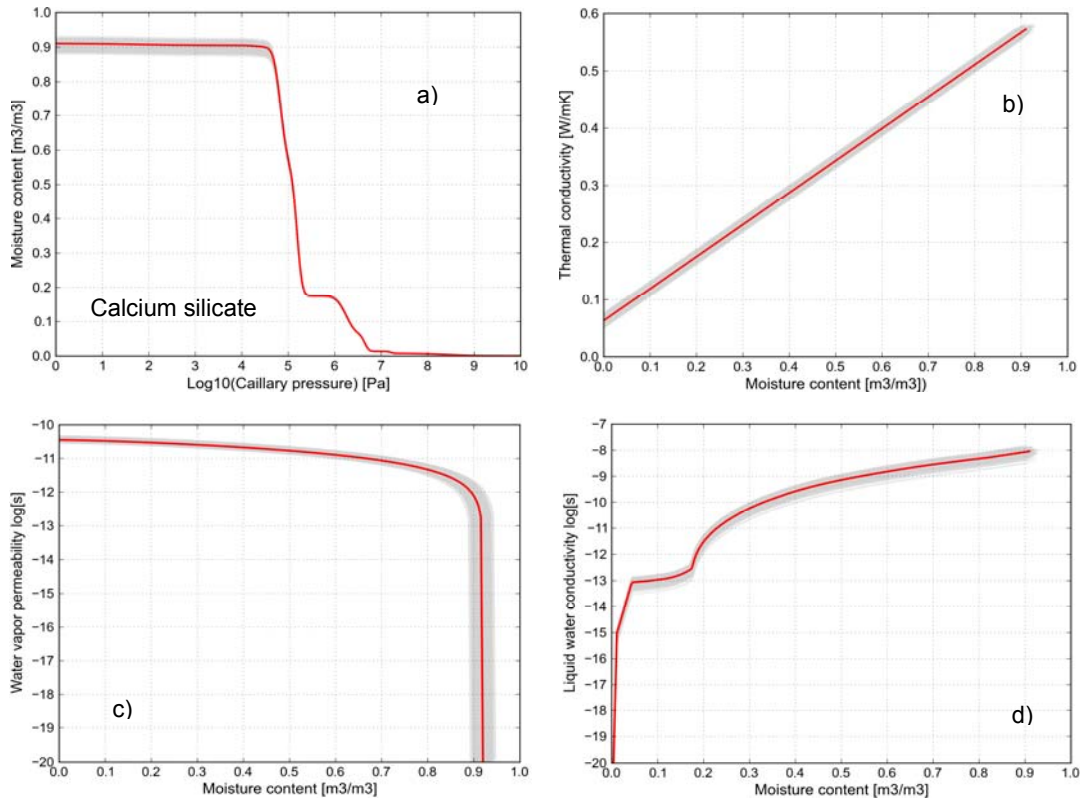
Figure 7-12 Material functions of calcium silicate a) moisture retention curve b) thermal conductivity c) water vapor permeability d) liquid water conductivity
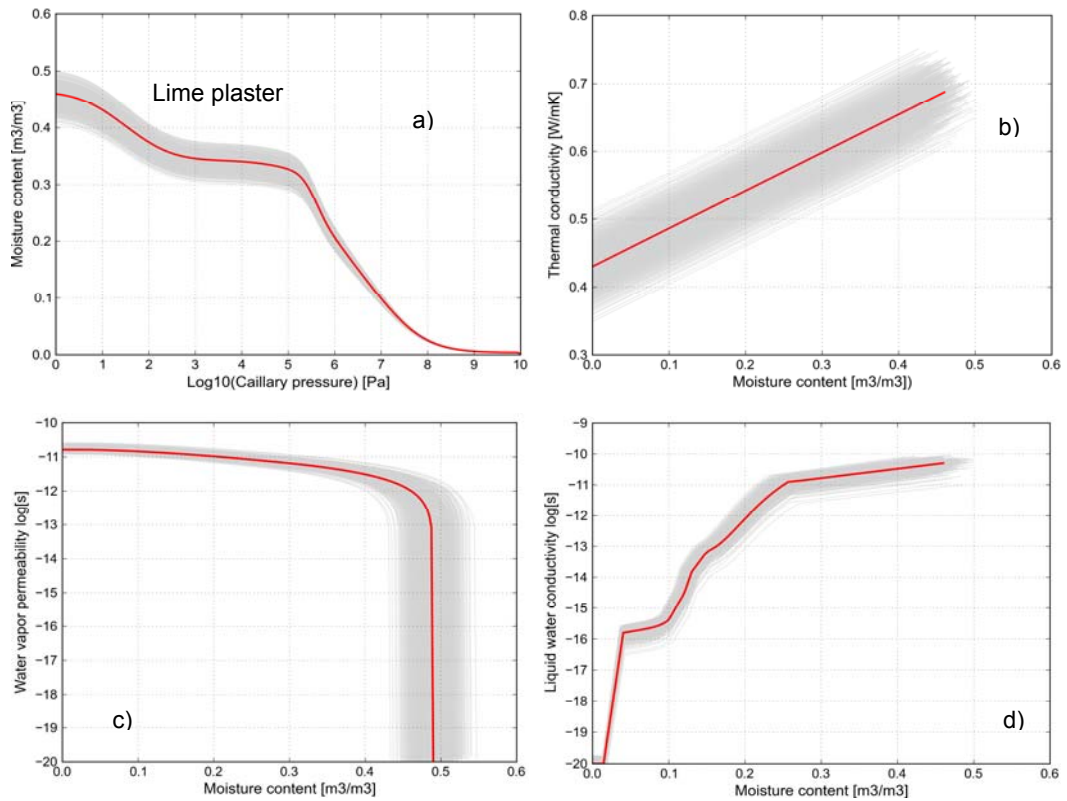
Figure 7-13 Material functions of lime plaster a) moisture retention curve b) thermal conductivity c) water vapor permeability d) liquid water conductivity

The materials with the high uncertainties in the properties have a wide distribution of the material function, e.g., calcium silicate glue mortar. Calcium silicate is a relatively homogenous material, so its material functions have smaller uncertainties compared to other materials.

7.3.3 Relative Humidity Distribution in the Wall Assembly

Figure 7-14 presents the relative humidity profiles of one-dimensional retrofitted wall on the 175th day, which has the highest relative humidity distribution in the wall assembly during the wintertime. The red line is the mean curve derived from the results of 400 samples. The mean curve is determined in the following way: a vertical line was drawn through all the curves at each time point. The mean value at one given time point was the averaged value of all the crossed values of this vertical line. Then, all the mean values were connected to form a continuous curve. The grey shadow region marks the possible variation range of the relative humidity profiles. The dimension of the material is outlined by the vertical blue line. The result demonstrates that relative humidity in the wall assembly is departed in two parts: from the exterior lime cement plaster to the calcium silicate glue mortar, relative humidity is in the level around 90%. In calcium silicate, relative humidity has a dramatic decrease, from 86% to 51%, due to its capillary-active character. Calcium silicate plays an important role in delivering the excessive moisture in the wall assembly to the indoor side during the wintertime. At the interior surface, relative humidity is less than 60%.
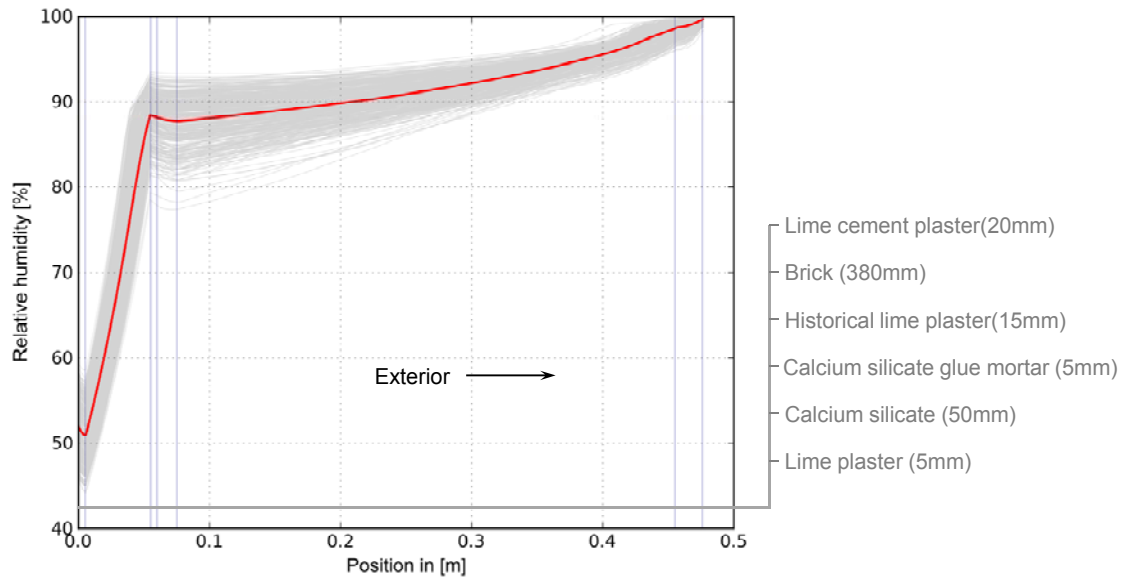
Figure 7-14 Relative humidity profiles in the retrofitted wall in the 175th day simulation

7.3.4 Condensation in the Wall Assembly

Condensation in the wall assembly can be partitioned into two aspects: internal condensation or internal overhygroscopic moisture due to the internal moisture load, and total overhygroscopic moisture across the whole wall assembly due to the moisture loads from both the internal and external environments. Internal condensation includes surface condensation and interstitial condensation resulted from the warm indoor humidity air contacting with the sufficiently cold surface, at or below its dew point. In this study, the external moisture load due to the water from the plumping leakage and foundation drainage are not taken into account.

To differentiate condensation due to different sources, the wall assembly was divided into two parts: one part was defined from the half thickness of the brick layer toward the interior surface of the wall, which has less impact from the rain. Another part was the rest part of the wall.
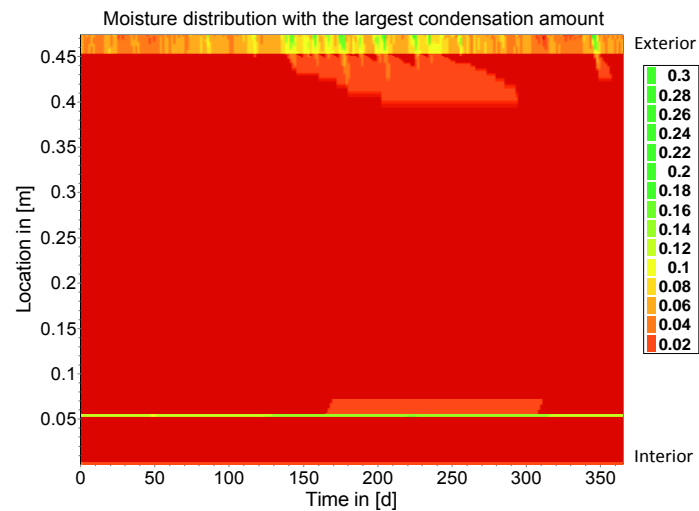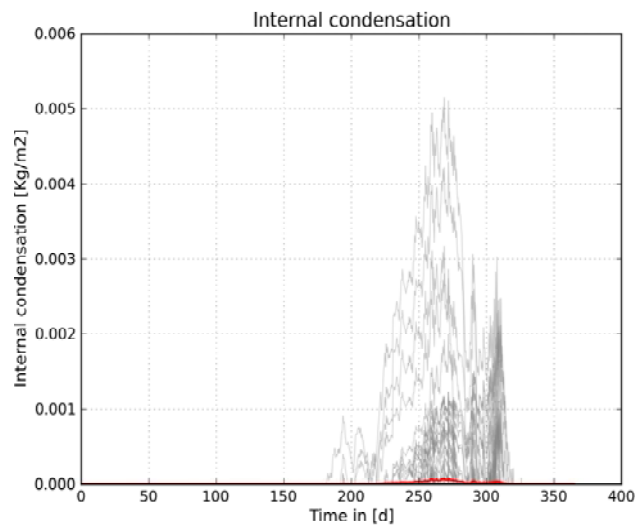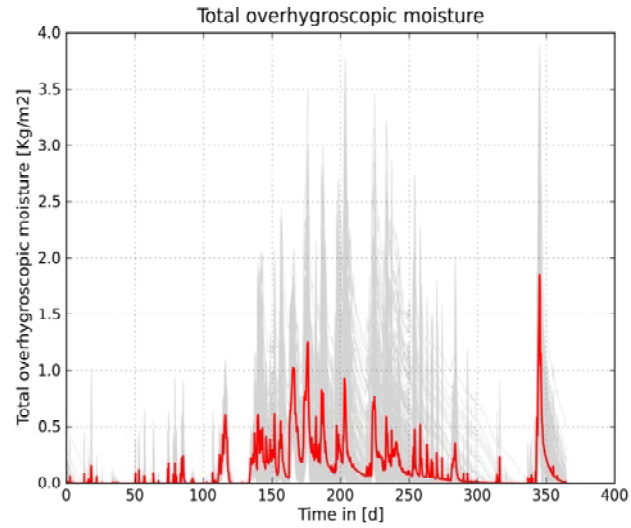
Figure 7-15 Total overhygroscopic moisture in the wall assembly (top), internal condensation (middle), and moisture distribution with the largest condensation across the wall assembly (bottom)

Figure 7-15 (top) shows the total overhygroscopic moisture in the wall assembly over time. The red curve represents the mean calculated from 400 samples. In most of the time, the mean curve has the value less than 1.0 kg/m^2 stipulated in DIN 4108-3 (2001). In addition, the condensation formed in the winter is substantially evaporated in the summer. The internal condensation has a very small value as shown in Figure 7-15 (middle), which implies that the total overhygroscopic moisture in the wall is mainly formed in the external part. The moisture distribution across the wall, from the sample that has the largest amount of condensation among 400 samples, is presented in Figure 7-15 (bottom). It is clear that the high moisture content mainly exists in the external lime cement plaster due to the rain penetration.

From above analysis, condensation is not an issue for this retrofitted wall assembly.

7.3.5 Probability of the Damages Induced by the Hygrothermal Loads

The damages induced by the hygrothermal loads on the outer surface region of the building enclosure assembly have been introduced in Section 6.3.3. They are mainly caused by the dramatic variations of temperature, relative humidity and moisture content over time, together with their differences at distinct positions of the material.

The probability of the damage can be measured either by the hygrothermal loads on the exterior surface of the wall assembly, which leads to the surface micro-cracks, or by the hygrothermal loads at the certain depth layer from the exterior surface, which

causes the cracks inside the material layer. The magnitude of the hygrothermal loads indicates the probability of the damages.

To evaluate the influence of installation of the interior insulation on the outer surface region of the wall, the ratios of the hygrothermal loads on one-dimensional retrofitted wall to those on one-dimensional base wall were calculated, given in equation 7.1 to 7.6.

$$HLSR_T = \frac{HLS_{T\_retrofit}}{HLS_{T\_base}}, \qquad (7.1)$$

$$HLSR_\varphi = \frac{HLS_{\varphi\_retrofit}}{HLS_{\varphi\_base}}, \qquad (7.2)$$

$$HLSR_\theta = \frac{HLS_{\theta\_retrofit}}{HLS_{\theta\_base}}, \qquad (7.3)$$

$$HLDR_T = \frac{HLD_{T\_retrofit}}{HLD_{T\_base}}, \qquad (7.4)$$

$$HLDR_\varphi = \frac{HLD_{\varphi\_retrofit}}{HLD_{\varphi\_base}}, \qquad (7.5)$$

$$HLDR_\theta = \frac{HLD_{\theta\_retrofit}}{HLD_{\theta\_base}}, \qquad (7.6)$$

where HLS_T, HLS_φ and HLS_θ denote the hygrothermal loads resulted from the variations of surface temperature, relative humidity and moisture content over time, respectively. HLD_T, HLD_φ, and HLD_θ denote the hygrothermal loads induced by the temperature difference, relative humidity difference and moisture content difference between the exterior surface and the certain depth layer over time, respectively.

A higher value of hygrothermal loads ratio indicates a greater potential of hygrothermal-related deterioration after the retrofit, i.e., a large ratio implies a relatively severe damage compared to a small one.

The base case has two scenarios: high indoor moisture load and normal indoor moisture load. So the ratios based on these two scenarios were compared.

The box plot was applied to represent hygrothemal load ratio. The box plot provides concise multiple distributions. The endpoints of the boxed are bounded by the lower and higher quartiles of data, namely $x_{25\%}$ and $x_{75\%}$. The horizontal line within the box represents the median, $x_{50\%}$. The star in the box represents the mean value. The bar on the top of the box extends to the minimum of $x_{75\%}+1.5 \cdot (x_{75\%}-x_{25\%})$ and the maximum value. In the same manner, the bar on the bottom of the box extends to the maximum of $x_{25\%}-1.5 \cdot (x_{75\%}-x_{25\%})$ and minimum value. The observations falling out side of these bars are shown with crosses.

Hygrothermal load ratios on the exterior surface

Figure 7-16 shows the hygrothermal load ratios on the exterior surface. The load ratios based on the high indoor moisture load and low indoor moisture load almost reach the same results, i.e., same mean, median, and standard deviation. So the indoor moisture load has no influence on the hygrothermal loads on the exterior surface.
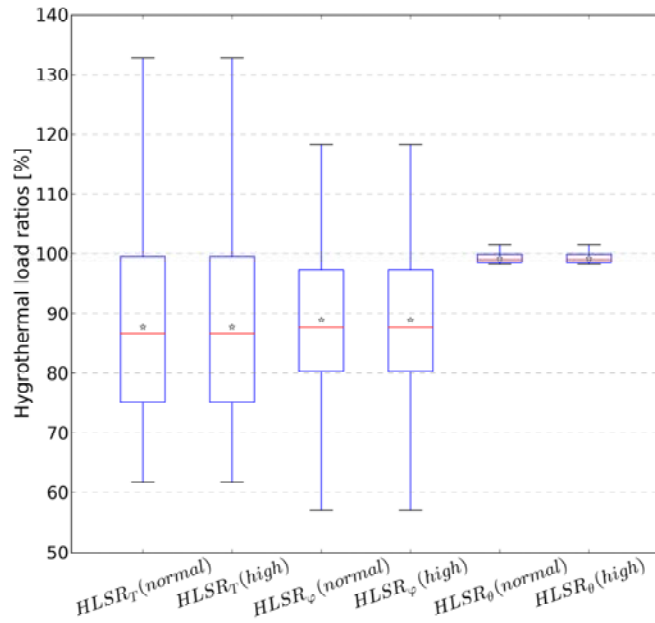
Figure 7-16 Hygrothermal load ratios on the exterior surface

As listed in Table 7-11, temperature and relative humidity load ratios vary in a wide range, from 61.75% to 132.88% and from 57.2% to 118.37%, respectively. But the mean and median of these two ratios are lower than 100%, indicating that the installation of the additional interior insulation will not increase the possibility of the damages induced by the temperature and relative humidity loads.

Moisture load ratio has relatively small variation. So the installation of the additional insulation has a minor influence on the moisture load on the exterior surface.

Table 7-11 Hygrothermal load ratios on the exterior surface

	$HLSR_T(\%)$ [normal]	$HLSR_T(\%)$ [high]	$HLSR_\varphi(\%)$ [normal]	$HLSR_\varphi(\%)$ [high]	$HLSR_\theta (\%)$ [normal]	$HLSR_\theta (\%)$ [high]
Minimum	61.746	61.749	57.2	57.203	98.356	98.355
Maximum	132.875	132.88	118.364	118.37	101.476	101.475
Median	86.529	86.532	87.676	87.68	99.049	99.049
Mean	87.761	87.764	88.903	88.908	99.266	99.266
Standard Dev	14.505	14.506	10.701	10.701	0.734	0.734

Hygrothermal load ratios at the certain depth layer from the exterior surface

Figure 7-17 presents hygrothermal load ratios at the 10mm depth layer from the exterior surface. The load ratios based on the high and normal indoor moisture loads are basically the same. So the indoor moisture load has no influence on this type of hygrothermal loads.
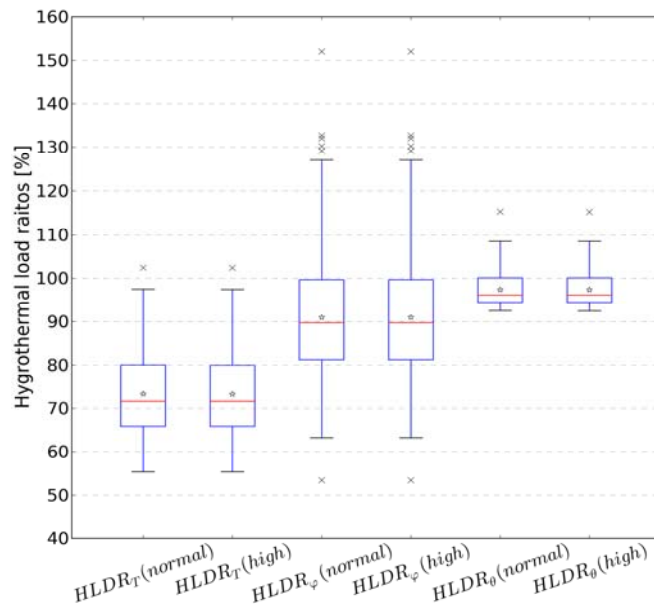
Figure 7-17 Hygrothermal load ratios at the 10mm depth layer from the exterior surface

As presented in Table 7-12, temperature load ratio varies in the range between 55% and 102%. The mean and median are around 72%, which is substantially lower than 100%, indicating that the installation of the additional insulation will not raise the temperature load inside the external material layer. Although relative humidity load ratio is across a wide range, from 53% to 152%, its mean and median are both under 100%. Moisture load ratio varies between 93% and 115%, so the installation of the additional insulation has a minor influence on the moisture load inside the external material layer.

Table 7-12 Hygrothermal load ratios at the 10mm depth layer from the exterior surface

	$HLDR_T$ (%) [normal]	$HLDR_T$ (%) [high]	$HLDR_\varphi$(%) [normal]	$HLDR_\varphi$(%) [high]	$HLDR_\theta$ (%) [normal]	$HLDR_\theta$ (%) [high]
Minimum	55.411	55.388	53.439	53.442	92.526	92.52
Maximum	102.441	102.397	152.04	152.05	115.272	115.264
Median	71.649	71.618	89.696	89.701	96.107	96.1
Mean	73.303	73.271	91.005	91.01	97.365	97.359
Standard Dev	9.269	9.265	13.02	13.021	3.766	3.766

The analyses on the hygrothermal load ratios on the exterior surface and at the 10mm depth layer from the exterior surface indicate that the installation of the additional interior insulation leads to a relatively low possibility of the damages on the outer surface region of the retrofitted wall assembly.

7.3.6 Daily Average Heat Flux and Transient Thermal Resistance

Daily average heat flux through interior surface of one-dimensional retrofitted wall is shown in Figure 7-18.
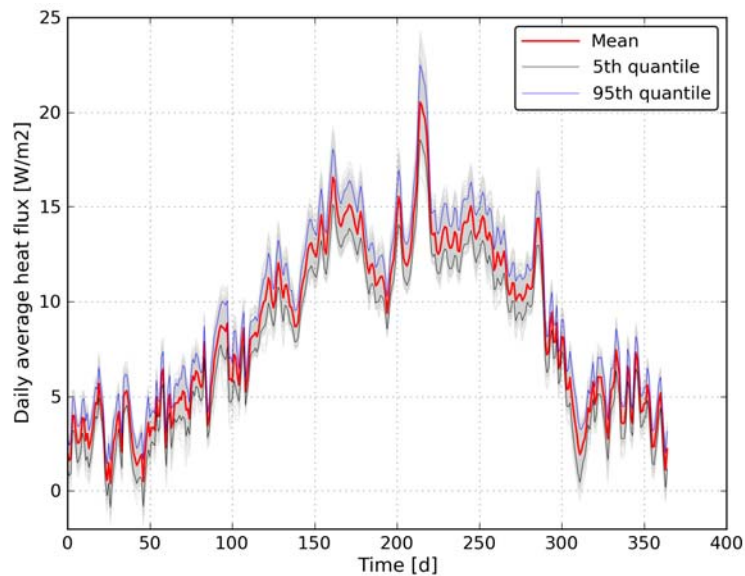
Figure 7-18 Daily average heat flux through the interior surface

The grey shadow region assembles the results from 400 randomly generated samples. The mean curve, 5% and 95% quartile curves are statistically determined and outlined in the graph. Those derived curves provide a more quantitative summary of the distribution of the generated curves. The average daily heat flux reaches the maximum value in the end of January and early February. The heat flux varies in the range of mean ± 3 W/m^2.

As introduced in Section 6.3.4, the derivation of transient thermal resistance requires the knowledge of the heating period. First, the daily average outdoor temperature of Potsdam, Germany was approximated by a Cosines' function to determine a continuous heating time, as shown in Figure 7-19. The heating period was considered to start when the daily average outdoor temperature was below 10 °C (EnEV 2007). For the weather of test reference year of the Potsdam, this period had 197 days starting from October 12 to April 27.
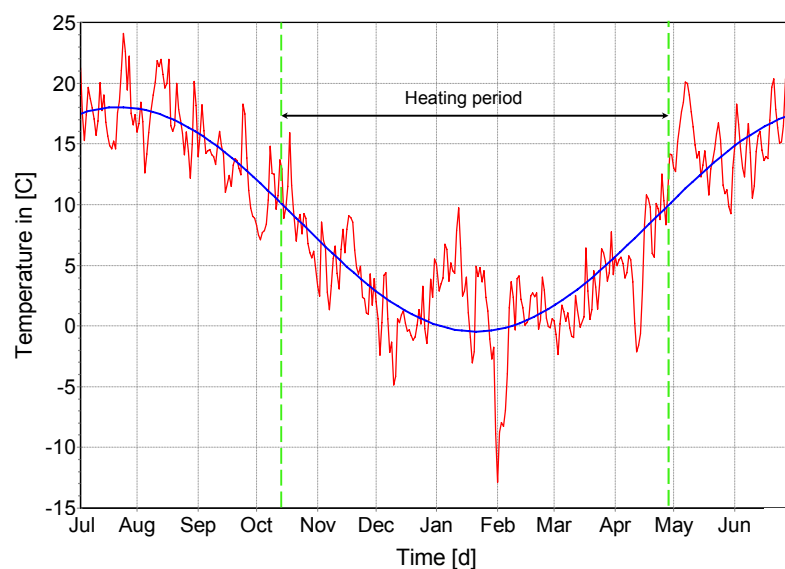
Figure 7-19 Heating period derived from the approximation of the daily average outdoor temperature by Cosines' function

The average heat flux through the interior surface and the transient thermal resistance

of the retrofitted wall during the heating period are listed in Table 7-13. Static thermal

resistance was also calculated with the consideration of uncertainties. The cumulative

density functions in Figure 7-20 show that there are 0.75% of static thermal resistance

and 7.25% of transient thermal resistance lower than 1.2 m^2k/W (DIN 4108-2 2003).

Thus, there is a low possibility of thermal resistances less than this threshold.

Transient thermal resistance with the mean of 1.28 m^2k/W faces a more critical

judgment than static thermal resistance with the mean of 1.35 m^2k/W. One possible

reason is that transient thermal resistance considers the transient environmental

impacts and thermal inertia of the wall assembly in additional to the characteristics of

the wall itself.

Table 7-13 Average heat flux and transient thermal resistance during the heating period

	Unit	Symbol	Mean	Stdev	Max	Min
Average heat flux	W/m^2	q_{HP}	12.165	0.675	14.173	10.426
Transient thermal resistance	m^2k/W	R_{HP}	1.282	0.06	1.450	1.137
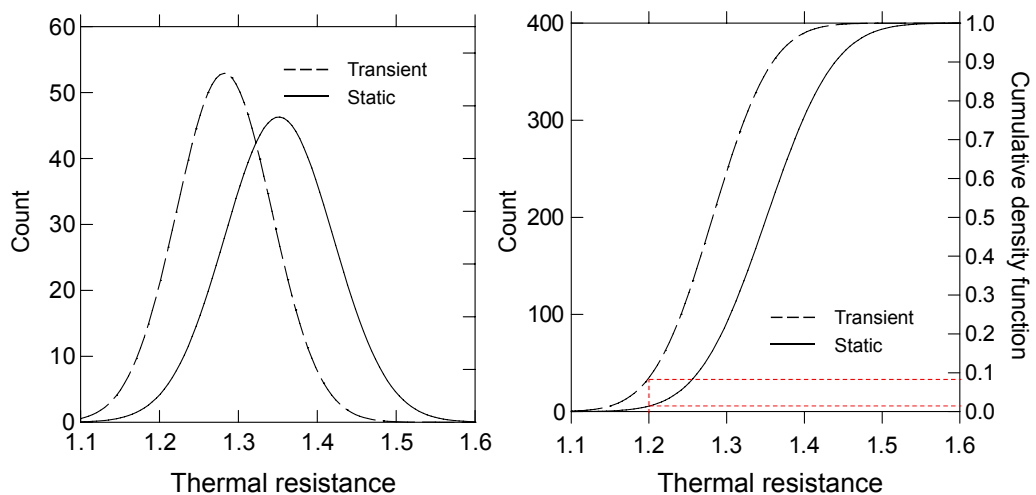
Figure 7-20 Probability density functions and cumulative density functions of transient and static thermal resistances

7.3.7 Mold Growth Risk

The retrofitted wall corner has the thermal bridge effect. Therefore, the mold growth risk at this local was assessed. To gain the sufficient and accurate information of temperature and relative humidity at this location, the discretization of the wall corner in the simulation requires a large amount of elements, around 5,000. This will increase the simulation cost, i.e., each sample approximately takes 9 hours. So, in this analysis, a total of 200 samples were generated. This sample size still meets the requirement discussed in Section 7.3.1.6.

The isopleth system for assessing the mold growth risk at the interior surface of the retrofitted wall corner, derived from 200 samples, is presented in Figure 7-21. The result was determined by the daily average relative humidity and temperature.

Relative humidity at the specified temperature was compared with the lines of Lowest Isopleth for Mold (LIM), spore germination after 16 days, and spore germination after 8 days. The result shows that a small amount of points are higher than the line of LIM, 0.25% from the total samples, which means that the probability of the fungi germination is relatively low. Only a few of them are higher than the line of spore germination after 16 days, 0.001% from 200 samples, indicating that there is a very low possibility that after 16 days some spores will start to appear under the specified temperature and relative humidity.
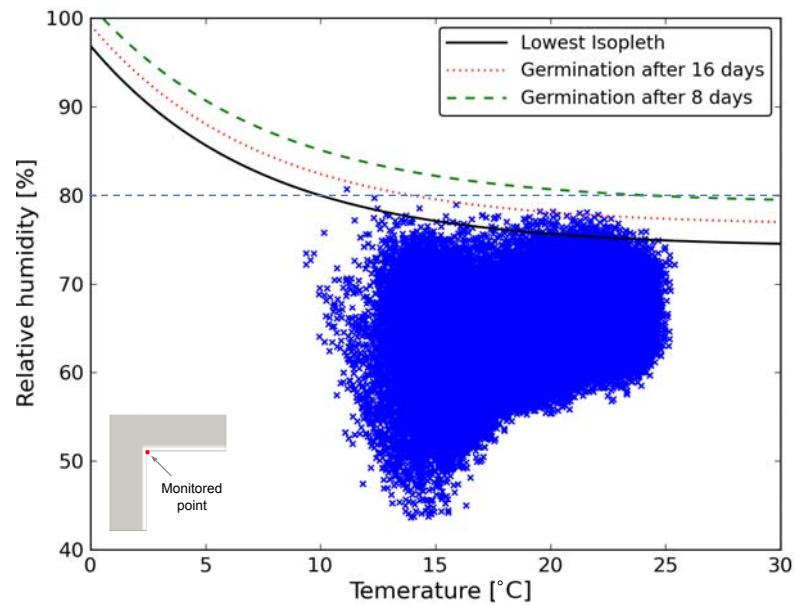
Figure 7-21 Isopleth system for assessing the mold growth risk at the interior surface of retrofitted wall corner

The 80% RH was also applied as a criterion to assess the mold growth risk. It was marked as a horizontal blue dot line in the graph. Only one value from the total 200 samples is higher than 80% RH line. So there is almost no possibility of mold growth.

The mold growth risk at this location of concern was also assessed by the mold index model. The result shows that all the index curves have the value near zero, indicating there is no possibility of mold growth.

Based on the above analyses, there is no mold growth risk at the interior surface of the retrofitted wall assembly.

7.3.8 Stability of the Results

To examine the stability of the results, the Monte Carlo simulation was replicated three times. The daily average heat flux through the interior surface and the transient

thermal resistance of the one-dimensional retrofitted wall assembly were compared among those three replicates.

The daily average heat flux curves of the three replicates, illustrated in Figure 7-22, overlap each other, indicating the stability from replicate to replicate.
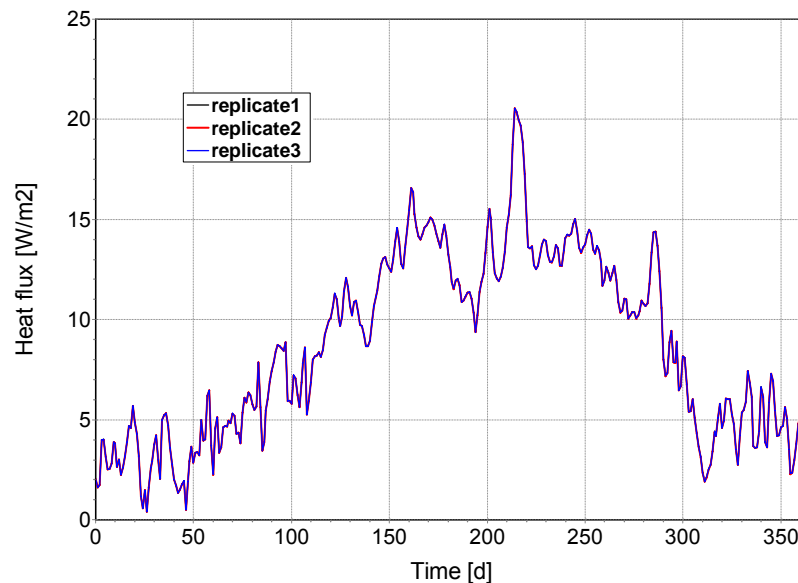
Figure 7-22 Daily average heat flux curves of the three replicates

Figure 7-23 shows the transient thermal resistance of the three replicates represented by the box plot and the plot of cumulative density functions. The mean, standard deviation, and maximum and minimum values from the three replicates are nearly the same. The 95% confidence intervals of the means of the three replicates are all in the range between 1.276 and 1.288. The density profiles closely follow each other. Therefore, the results are quite stable.
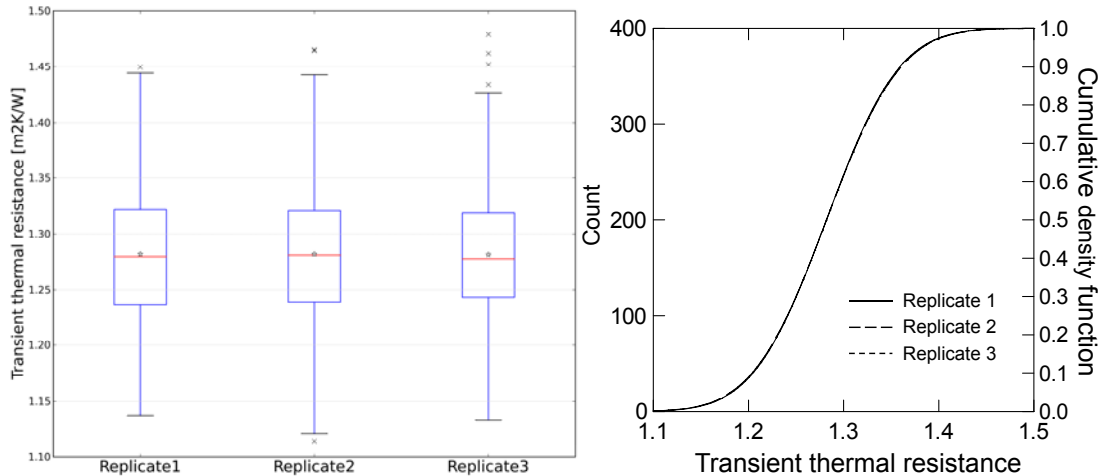
Figure 7-23 Box plot of transient thermal resistances of the three replicates (left) and the plot of their cumulative density functions (right)

7.4 Sensitivity Analysis in the Performance Evaluation

Sensitivity analysis usually follows uncertainty analysis. The purpose of sensitivity analysis is to identify the influenced input variables against the output variable of interest , so less effort can be made for the unimportant input variables and more attention are taken on the influential ones. The different sensitivity analysis techniques have been introduced in Section 5.3.

There are a total of 56 input variables, randomly generated, to account for the uncertainties from different sources. Capillary saturation moisture content (θ_{cap}) and water absorption coefficient (A_w) are not directly involved in the hygrothermal simulation, so they are omitted in sensitivity analysis. When correlated variables are involved in sensitivity analysis, the results derived from the regression-based techniques may provide unreliable indications of variable importance (Helton and

223

Davis 2008). Therefore, highly correlated input variables were excluded in the analysis to avoid the improper explanation of the results.

The correlation between open porosity and density is -0.94 in the building brick category, -0.99 in the plaster/mortar category, and -0.91 in the insulation category. The correlation between thermal conductivity and open porosity is -0.97 in the plaster/mortar category and -0.92 in the insulation category. For those highly correlated input variables, only one in each pair was kept for sensitivity analysis. So density of each material, open porosity of four plasters, and open porosity of calcium silicate were excluded. With those considerations, 45 input variables were used in sensitivity analysis. They are listed in Table 7-14.

Since the variation of basic parameters will also influence the material functions, it was assumed that the variation of the effective saturation moisture content (θ_{eff}) can be regarded as the change of the moisture retention curve. The shift of the water vapor diffusion resistance factor (μ_{dry}), the liquid conductivity at saturation moisture content (K_{eff}), and the effective saturation moisture content (θ_{eff}) could be regarded as the variations of the moisture transport characteristics. So if those parameters are addressed as the influential variables, the corresponding material functions are also important to the output variable of interest.

Table 7-14 Variables involved in sensitivity analysis

		Lime plaster	Calcium silicate	Calcium silicate glue mortar	Historical lime plaster	Brick	Lime cement plaster
	Orientation						
Indoor condition	Indoor temperature						
	Indoor relative humidity						
Boundary coefficients	Heat transfer coefficient _ interior						
	Vapor transfer coefficient _ interior						
	Heat transfer coefficient _ exterior						
	Vapor transfer coefficient _ exterior						
	Short wave radiation absorptivity						
	Ground reflectivity						
	Long wave emissivity of building surface						
	Rain exposure coefficient						
Dimension of material layers	Thickness of lime plaster						
	Thickness of calcium silicate glue mortar						
	Thickness of historical lime plaster						
Material properties	Density						
	Specific heat capacity	×	×	×	×	×	×
	Thermal conductivity	×	×	×	×	×	×
	Open porosity					×	
	Effective saturation moisture content	×	×	×	×	×	×
	Water vapor diffusion resistance factor	×	×	×	×	×	×
	Liquid water conductivity at saturation moisture content	×	×	×	×	×	×

The output of interest in sensitivity analysis can be a single value that represents one specific performance of the building enclosure assembly (e.g., transient thermal resistance) or a variable as a function of time (e.g., interior surface temperature). Sensitivity analyses on transient thermal resistance of the retrofitted wall were first exemplified, from Section 7.4.1 to Section 7.4.4, to address the most influential

variables by different techniques. Sensitivity analysis on the output variables as a function of time was presented in Section 7.4.5.

7.4.1 Scatter Plot

Scatter plot is a direct method to reveal the relationship between the input and output variables. The scatter plots of transient thermal resistance of the retrofitted wall ($R_{transient}$) against thermal conductivity of calcium silicate ($\lambda_{calcium\ silicate}$), thermal conductivity of brick (λ_{brick}), the indoor relative humidity (RH_{in}), and the thickness of lime plaster ($d_{lime\ plaster}$) are shown in Figure 7-24. The histogram density presented beside the frame of each plot can be used to check if the input variables are generated in consistency with the desired distribution. The plots in Figure 7-24 illustrate that $\lambda_{calcium\ silicate}$, λ_{brick}, RH_{in} and $d_{lime\ plaster}$ are very well generated from their respective distributions. This also confirms that the Latin hypercube sampling technique and selected sample size are reliable for this study.

The linear relationship between $R_{transient}$ and $\lambda_{calcium\ silicate}$ is apparent. The increase of $\lambda_{calcium\ silicate}$ leads to an associated decrease of $R_{transient}$, so they have a negative effect on each other. The similar relationship can be detected between $R_{transient}$ and λ_{brick}. The relationship between $R_{transient}$ and RH_{in} and relationship between $R_{transient}$ and $d_{lime\ plaster}$ are not so obvious to observe from the scatter plots.
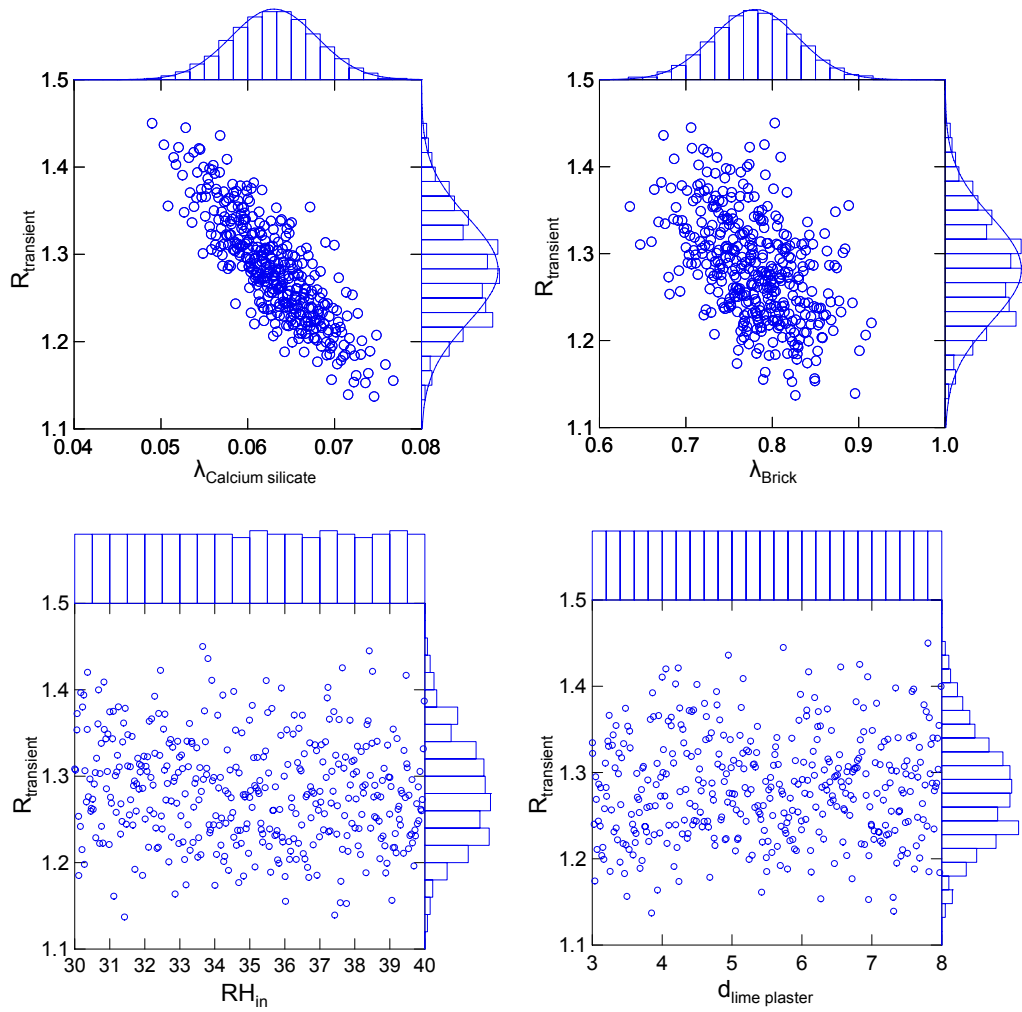
Figure 7-24 Scatter plots of transient thermal resistance against different input variables

7.4.2 Regression-Based Sensitivity Analysis and Partial Correlation

Regression-based sensitivity analysis and partial correlation were also applied to identify the key variables, which greatly influence the transient thermal resistance of the retrofitted wall. In Table 7-15, the six most influential variables and their corresponding SRCs (Section 5.3.1) and PCCs (Section 5.3.3) are listed in descending order. Other variables having a minor influence on the transient thermal resistance are not presented. The stability of sensitivity analysis was also examined by replicating

three Monte Carlo simulations. The three replicates achieve the same rank of variable importance. So the results are quite stable.

The good linear relationship between input variables and output variable is the assumption to achieve the reliable result of the regression-based sensitivity analysis. This assumption can be examined by the coefficient of determination R^2: High R^2 indicates the linearity is satisfied. So R^2 is provided for each sampling. The R^2 in the three replicated samplings are around 0.99, indicating that the rankings based on the magnitude of the SRCs are quite reliable.

PCCs usually have the values larger than SRCs, since partial correlation measures the importance of the input variable after excluding the effect of other variables.

$\lambda_{\text{calcium silicate}}$ is addressed as the most important variable. The second important variable is λ_{brick}. Both of them have the PCC and SRC quite larger than others. RH_{in} is the third important variable, but its SRC is dramatically reduced to less than 0.1. Other variables, e.g., thickness of material layer, have even smaller values, indicating that their influences on the transient thermal resistance are very weak.

A positive sign of PCC and SRC indicates the input and output variables tend to increase or decrease together, and a negative sign indicates that they tend to vary in the opposite direction. So the increase of $\lambda_{\text{calcium silicate}}$ and λ_{brick} will decrease $R_{\text{transient}}$.

Table 7-15 SRCs and PCCs of the six most influential variables against $R_{transient}$ in the three replicated samplings

| Variable name | Replicate1 (R^2=0.991) | | | | Replicate2 (R^2=0.990) | | | | Replicate3 (R^2=0.992) | | | |
| | SRC | | PCC | | SRC | | PCC | | SRC | | PCC | |
	Rank	Value	Rank	Value	Rank	Value	Rank	Value	Rank	Value	Rank	Value
$\lambda_{calcium\ silicate}$	1	-0.886	1	-0.989	1	-0.861	1	-0.988	1	-0.859	1	-0.988
λ_{brick}	2	-0.534	2	-0.969	2	-0.526	2	-0.969	2	-0.531	2	-0.968
RH_{in}	3	-0.084	3	-0.659	3	-0.070	3	-0.584	3	-0.091	3	-0.666
$d_{Historical\ lime\ plaster}$	4	0.066	4	0.576	4	0.061	4	0.528	4	0.065	4	0.554
$d_{lime\ plaster}$	5	0.047	5	0.447	5	0.046	5	0.434	5	0.044	5	0.402
$d_{calcium\ silicate\ glue\ mortar}$	6	0.037	6	0.359	6	0.035	6	0.338	6	0.034	6	0.329

7.4.3 Stepwise Regression Analysis

Stepwise regression analysis can help to identify the influential variables by constructing a sequence of regression models. The order of the input variable entering in the model gives the indication of the variable importance (Section 5.3.2). It is necessary to set a criterion to stop an unimportant variable entering the model, and a criterion to exclude an existing variable in the model if it is no longer needed. In this analysis, the α-value of 0.01 was adopted as a threshold to add a variable into a regression model and α-value of 0.05 was used as a threshold to drop a prior selected variable from the model.

Table 7-16 summarizes the results of stepwise regression analysis from the three replicated samplings. The listed SRC of each variable is the value in the final regression model. The listed R^2 is the cumulative value with the entry of a new variable into the model in each step. The R^2 at each step provides a measure of how much uncertainty of output that can be accounted for by the selected inputs in the model. $\lambda_{calcium\ silicate}$ and λ_{brick} account for 97% uncertainty of $R_{transient}$, so they are the two most important variables. The R^2 only has slight improvement after adding other variables.

Table 7-16 Stepwise regression coefficients in the three replicated samplings

Step	Replicate 1			Replicate 2			Replicate 3		
	Variable	SRC	R^2	Variable	SRC	R^2	Variable	SRC	R^2
1	$\lambda_{calcium\ silicate}$	-0.866	0.69	$\lambda_{calcium\ silicate}$	-0.858	0.705	$\lambda_{calcium\ silicate}$	-0.854	0.702
2	λ_{brick}	-0.536	0.974	λ_{brick}	-0.526	0.977	λ_{brick}	-0.521	0.974
3	RH_{in}	-0.085	0.981	RH_{in}	-0.068	0.982	RH_{in}	-0.091	0.982
4	$d_{Historical\ limeplaster}$	0.067	0.985	$d_{Historical\ limeplaster}$	0.063	0.986	$d_{Historical\ lime\ plaster}$	0.062	0.985
5	$d_{lime\ plaster}$	0.048	0.988	$d_{lime\ plaster}$	0.047	0.988	$d_{lime\ plaster}$	0.042	0.987
6	$d_{glue\ mortar}$	0.037	0.989	$d_{glue\ mortar}$	0.035	0.989	$d_{glue\ mortar}$	0.031	0.988

The stability of the result was also examined. In the three replicates, R^2 in the final model has the value above 0.98, implying that underlying assumption of linear relationship between the transient thermal resistance and selected input variables are strongly reliable.

7.4.4 Statistical F Test

The magnitude of the F value provides a direct measure of the importance of both quantitative and qualitative variables. If the model with the quantitative variables performs poorly in sensitivity analysis, i.e., low coefficient of determination R^2, some input variables could be alternatively treated as the qualitative variables. In this study, orientation can be treated as a qualitative input by employing the indicator variables to represent different orientated directions in regression analysis (Section 4.3.1.4). The indicator variable is also called dummy variable which can be set in the statistical software SYSTAT (SYSTAT11 2002). The input variables were firstly standardized before the analysis.

In Table 7-17, $\lambda_{\text{calcium silicate}}$ has the largest F value, indicating $R_{\text{transient}}$ is most sensitive to it. So it is ranked as the most important input variable. λ_{brick} has an F value one magnitude larger than other remains, so it is ranked second. RH_{in}, $d_{\text{historical lime plaster}}$, $d_{\text{lime plaster}}$, $d_{\text{glue mortar}}$, and T_{in} are ranked third to seventh, respectively. Orientation has an F value less than 1 and p-value larger than 0.05. So Orientation does not impact the transient thermal resistance of the wall assembly.

The rankings from the three replicated samplings obtain quite good agreement, indicating the stability of the analysis. The coefficients of determination R^2 in the three replicated samplings have the value larger than 0.99, implying that the linear assumption for the functional relation between the output and input variables is valid.

Table 7-17 F and p-values of the most influential variables against $R_{transient}$ in the three replicated samplings

Variable name	Replicate 1 (R^2=0.992)			Replicate 2 (R^2=0.991)			Replicate 3 (R^2=0.992)		
	F value	p-value	Rank	F value	p-value	Rank	F value	p-value	Rank
$\lambda_{calcium\ silicate}$	15714.8	<0.001	1	13672.5	<0.001	1	14186.5	<0.001	1
λ_{brick}	5284.7	<0.001	2	5088.8	<0.001	2	5299.6	<0.001	2
RH_{in}	265.6	<0.001	3	274	<0.001	3	181.2	<0.001	3
$d_{Historical\ lime\ plaster}$	175.7	<0.001	4	155.2	<0.001	4	132.5	<0.001	4
$d_{lime\ plaster}$	87.7	<0.001	5	63.3	<0.001	5	81	<0.001	5
$d_{glue\ mortar}$	51.2	<0.001	6	39.9	<0.001	6	45.2	<0.001	6
T_{in}	15.6	<0.001	8	21.5	<0.001	7	9. 1	0.003	7
Orientation	0.58	0.77	31	0.93	0.48	29	0.31	0.95	36

7.4.5 Sensitivity Analysis of Time-Dependent Output variables

It is common that the output variable of a hygrothermal simulation is time-dependent. Thus, its influential input variables and their influences may vary over time. Sensitivity analyses of three time-dependent output variables are conducted in this section.

As introduced in Section 6.3.2, mold growth requires the suitable temperature and relative humidity. Therefore, the identification of the input variables that greatly impact temperature and relative humidity on the interior surface of the retrofitted wall assembly is the interest of this study. In addition, daily average heat flux gives insight into how much energy flows through the wall assembly, so its influential variables were also addressed.

The plots of PCC and SRC provide insight into the relationship between input and output variables over time. The PCCs and SRCs of the eight most influential variables against interior surface temperature, interior surface relative humidity, and daily

average heat flux through interior surface of the retrofitted wall assembly are demonstrated in Figure 7-25, 7-26, and 7-27, respectively. PCC always has a larger value than SRC, since it provides a measure of the strength of the linear relationship after excluding the impact of other variables.

7.4.5.1 PCCs and SRCs of the eight influential variables against interior surface temperature

Figure 7-25 displays the PCCs and SRCs of the eight influential variables against interior surface temperature T_{si} over time. A substantially high PCCs and SRCs of indoor temperature T_{in} imply that it is the most influential variable to impact T_{si}. It is straightforward that the increase of T_{in} will cause the rise of T_{si}. The increment of the interior heat transfer coefficient α_i will also enlarge the heat transfer between the indoor climate and interior surface of the wall assembly. This impact is more obvious in winter. The rise of $\lambda_{calcium\ silicate}$ and λ_{brick} will reduce the thermal resistance, raise the heat flux through the wall assembly, and further decrease T_{si}. So they have a constantly negative effect on T_{si}.

The exterior boundary coefficients also have the influence on T_{si}: the rise of short wave radiation absorptivity α_{sw} will enhance the surface absorbability of the short wave radiation, thus further increase the exterior surface temperature and reduce the heat loss. This mechanism indirectly raises T_{si}. PCCs and SRCs of α_{sw} reach the highest value in summertime, due to the fact that short wave radiation is more intense in summertime than in other seasons. On the other hand, the rise of long wave emissivity ε and exterior heat transfer coefficient α_e will increase the heat loss from the wall assembly. So they have a negative effect on T_{si}. In some wintertime, the exterior surface temperature is lower than the outdoor air temperature, so the heat flux

is in the direction from the outdoor air to the wall. The rise of the α_e actually enhances the heat gain from the environment. This is why some PCCs of α_e in the wintertime are positive. Orientation also has the influence on the interior surface temperature T_{si}, and its effect is more obvious in the summertime.
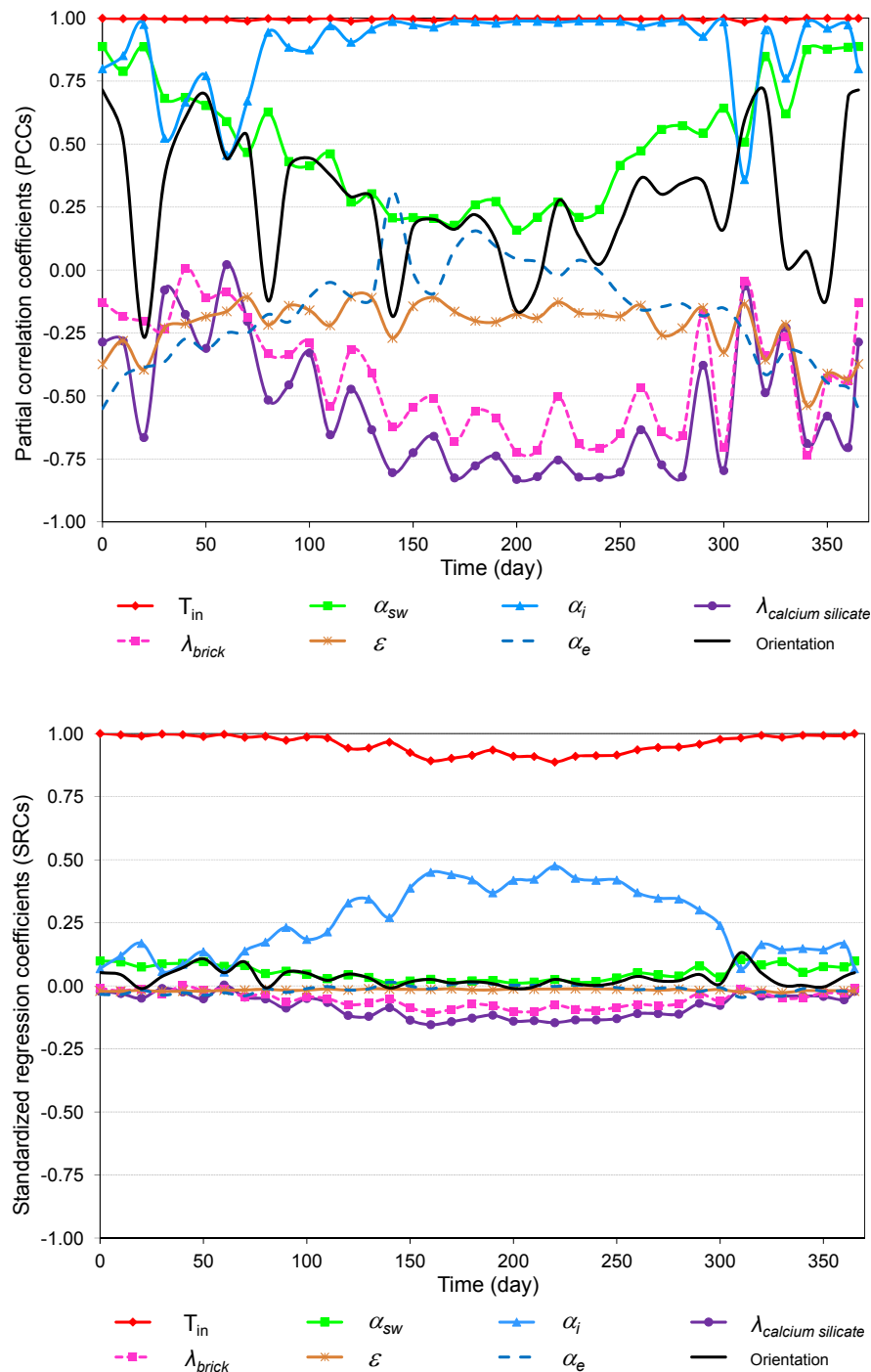
Figure 7-25 PCCs (top) and SRCs (bottom) of the eight influential variables against interior surface temperature

Figure 7-26 exhibits PCCs and SRCs of the eight influential variables against interior surface relative humidity RH_{si} over time. The indoor moisture load has a greater influence on RH_{si}. Excluding other factors, the rise of indoor relative humidity RH_{in} will cause a high vapor pressure potential, which will further give rise to the increase of RH_{si}. The increment of T_{in} will also increase the RH_{si}: for the same RH_{in}, the increase of T_{in} will enlarge indoor partial vapor pressure, and result in the increase of interior surface partial vapor pressure. In the meanwhile, the interior surface temperature T_{si} will also increase, as stated in Section 7.4.5.1. However, the increment of interior surface saturation vapor pressure due to the rise of T_{si} is lower than the increment of interior surface partial vapor pressure due to the rise of T_{in}. Thus, RH_{si} as the ratio of interior surface partial vapor pressure to interior surface saturation vapor pressure will increase.

The increase of α_i and α_{sw} will raise T_{si} as mentioned in Section 7.4.5.1. The rise of T_{si} increases interior surface saturation vapor pressure, thus decreases RH_{si}. On the other hand, the increase of $\lambda_{calcium\ silicate}$ and λ_{brick} will decrease T_{si}, and lower the surface saturation vapor pressure, thus increase the RH_{si}.

The interior vapor transfer coefficient β_{pi} enlarges the vapor transfer between indoor climate and interior surface of the wall assembly. Its influence on RH_{si} varies greatly over time.
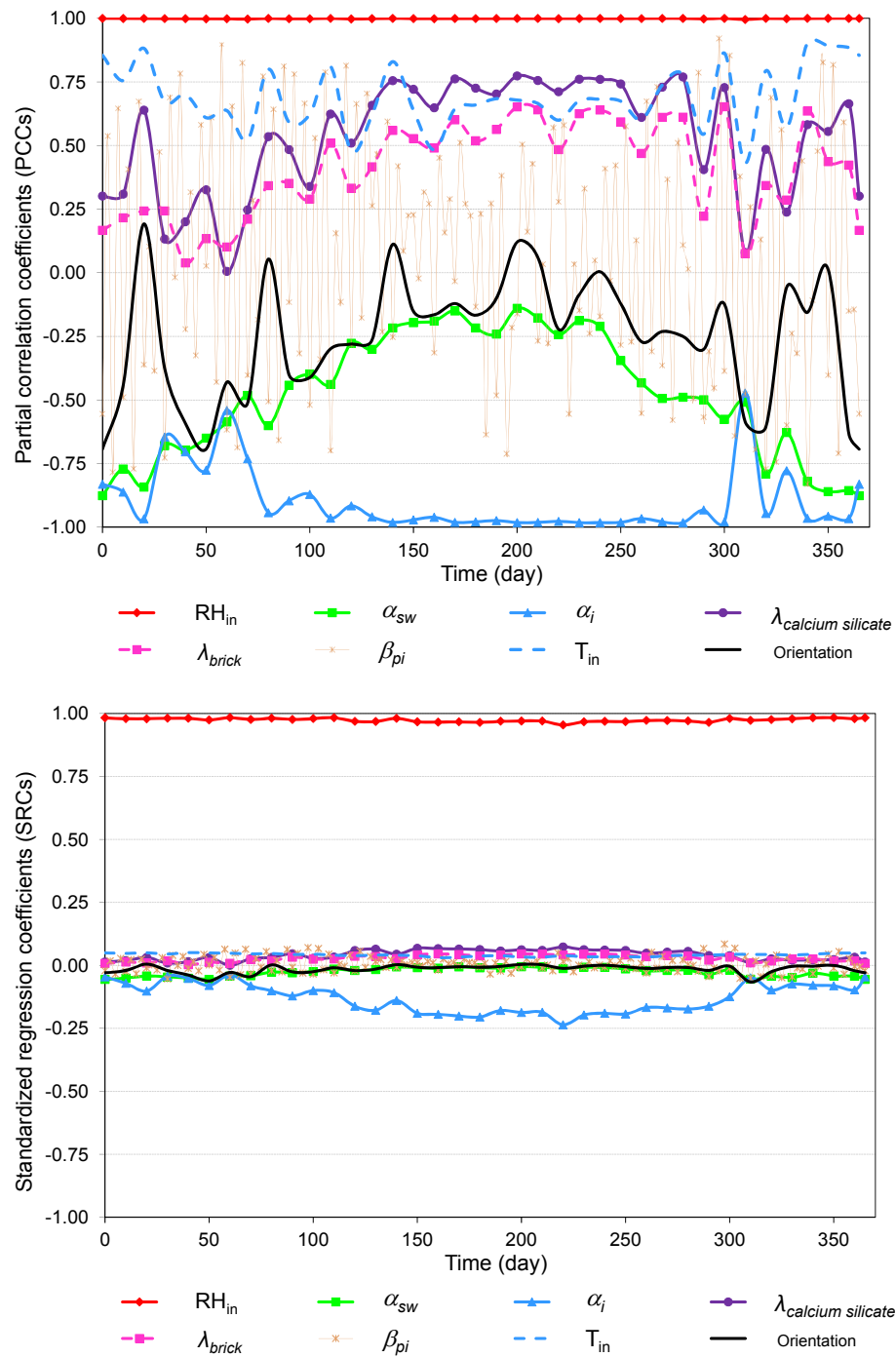
Figure 7-26 PCCs (top) and SRCs (bottom) of the eight influential variables against interior surface relative humidity

7.4.5.3 PCCs and SRCs of the eight influential variables against daily average heat flux through the interior surface

As shown in Figure 7-27, daily average heat flux q_d is positively correlated to the indoor temperature T_{in} and interior heat transfer coefficient α_i. The reason is explicit: A high T_{in} forms a high driving potential of heat flux. Large α_i enhances the heat transfer between interior surface and indoor climate. So increments of those two variables increase the heat flux through the wall assembly. The increase of $\lambda_{calcium\ silicate}$ and λ_{brick} will decrease the thermal resistance of the wall assembly, which will further increase q_d. Thus, these two variables positively correlated with q_d over time. α_{sw} has a negative influence on q_d because it increases the solar gain of exterior surface, thus reduces the heat loss. Its impact is more apparent in the summertime than in wintertime. The rise of long wave emissivity ε will increase the heat loss from the wall assembly. So it has a positive effect on q_d.
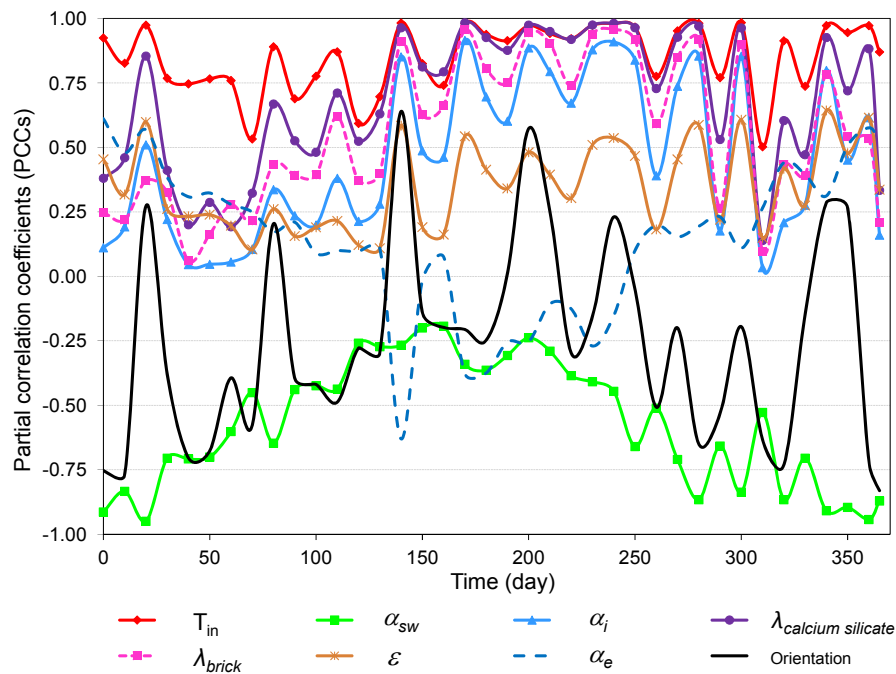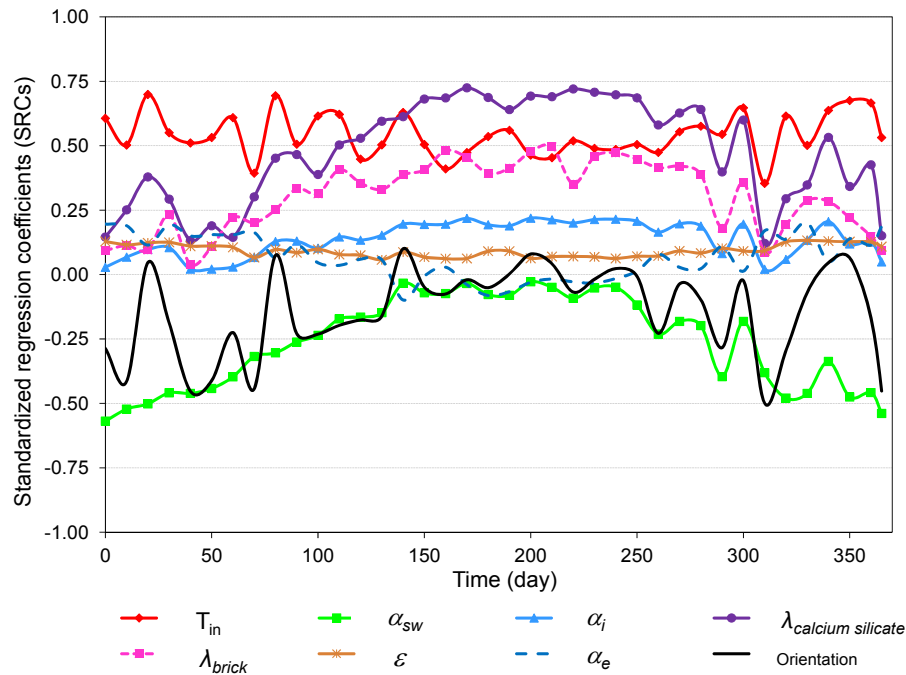
Figure 7-27 PCCs (top) and SRCs (bottom) of the eight influential variables against daily average heat flux through interior surface

7.5 Summary

In consideration of the uncertainties in the input variables, the simulation result is not a deterministic value, but rather a range of possibilities. The developed probabilistic approach was exemplified to assess the hygrothermal performance of a retrofitted wall. For each specific performance, one or more criteria were applied to obtain the reliable results.

1. Material functions are closely related to basic material parameters. When the related material parameter is randomly generated, the material function also varies in a certain range. Material function is subject to a large variation if the uncertainty in the related basic parameter is high, e.g., liquid conductivity of calcium silicate glue mortar has a large variation range due to the wide spread of effective saturation moisture content.

2. The sampled variables should follow the physical rules. The rank correlation matrix of sampled material parameters by the Latin hypercube sampling could achieve good agreement with the desired correlation matrix.

3. The calcium silicate could deliver most excessive moisture in the retrofitted wall to the interior surface due to its capillary-active characteristics. Thus, it reduces the possibility of condensation within the wall. Condensation formed during the wintertime can evaporate during the summertime. Therefore, there is no condensation risk in this retrofitted wall assembly.

4. To examine if the installation of the additional interior insulation will aggravate the surface crack or spalling, the ratios of the hygrothermal loads on the outer region of the wall assembly before and after retrofit were calculated. In addition, the impact of indoor moisture load on the hygrothermal loads was also evaluated. The result indicates that the installation of the additional insulation would not lead to extra deterioration and the indoor moisture load has no influence on the hygrothermal loads.

5. Mold growth risk at the interior surface of the retrofitted wall corner was assessed by 80% RH, mold index and isopleth model. The results show that there is no mold growth risk at this location of concern.

6. Compared to static thermal resistance, transient thermal resistance accounts for not only the thermal characteristics of the wall assembly itself, but also the influence from the surrounding environments.

7. The Latin hypercube sampling was replicated three times to check the stability of the results with respect to transient thermal resistance of the wall assembly

and daily average heat flux through the wall assembly. The results are quite stable.

A simulation model is composed of many components. Each component has its own role to play. However, it is hard to judge which component or which variable is dominant among others. So sensitivity analysis is applied to help the analyzers to obtain this information.

1. Five sensitivity analysis techniques, including scatter plot, regression-based sensitivity analysis, stepwise regression analysis, partial correlation, and statistical F test, were employed to identify the most influential variables against transient thermal resistance of the retrofitted wall. All these methods identify that thermal conductivity of the calcium silicate and thermal conductivity of brick were two most important variables among 45 input variables. So in order to improve the thermal performance of the wall assembly, selecting an appropriate calcium silicate insulation with low thermal conductivity is crucial.

2. Three replicated samplings were generated to check the stability of sensitivity analysis. The three replicates provide the some rank of the most influential input variables against transient thermal resistance of the retrofitted wall assembly.

3. The identified influential variables and their impacts are dependent on the output variables of interest. For the studied case, interior vapor transfer coefficient β_{pi} has a great influence on interior surface relative humidity, but it only slightly impacts the interior surface temperature. The rise of interior heat

transfer coefficient increases interior surface temperature, but decreases interior surface relative humidity.

4. If the output variable is time-dependent, its influential input variables and their influences may vary over time. For the studied case, short wave radiation absorptivity has a larger contribution to the heat flux through the wall assembly in summertime, but less in wintertime.

5. Indoor humidity is identified as the most important variable against interior surface relative humidity. Indoor temperature substantially influences interior surface temperature and the heat flux though the wall assembly. So choosing an appropriate indoor condition is crucial to predict the hygrothermal response of the wall assembly.

6. The variations of the boundary coefficients enhance or reduce the heat and moisture transfer between the wall assembly and its surrounding environments. Their contributions are also significant in the hygrothermal simulation and should not be ignored.

7. The influential variables are case-dependent. The conclusion drawn from this study should be revalidated, if the scenario is different.

Chapter 8 Summary, Conclusions and Recommendations

The research in this dissertation focuses on three aspects: 1) establishment of a high quality and comprehensive material database for the simulation tools. 2) application of statistical methods for hygrothermal material characterization. 3) development of a probabilistic approach to assess hygrothermal performance of building enclosure assemblies.

8.1 Establishment of a High quality and Comprehensive Material Database

A systematic approach was introduced to organize, classify, and characterize the materials. Total 13 material categories were defined according to the natural characteristics and the usages of the materials. The experimental methods to measure the complete material properties and the material modeling approach were introduced in detail for material characterization. By applying this approach, a significant amount of representative materials were evaluated, covering 173 materials in 8 material categories. For anisotropic materials, e.g., wood and sand stone, they were characterized in different spatial directions. Thus, a comprehensive material database was established for the simulation tools.

8.2 Application of Statistical Methods for Hygrothermal Material Characterization

1. By applying statistical methods, the measurement procedure to obtain the knowledge of moisture storage characteristics was greatly simplified.

- With the application of cluster analysis, the natural groups among moisture contents at specific capillary pressure were detected. The most similar moisture contents were aggregated into one cluster. Regression analysis was conducted to derive the relationships between moisture contents in the identified cluster. Thus, by only measuring one moisture content, the others in the same cluster are predictable by applying the regression models. For the building bricks and plaster/mortars, three characteristic moisture contents $w0$ (for building bricks)/$w3.78$ (for plaster/mortars), $w4.78$, and $w5.60$ in the overhygroscopic range and one moisture content $w7.59$ (75.4%) in the hygroscopic range were identified and verified to be sufficient to get a good knowledge of moisture storage characteristics. The moisture storage measurement is reduced to four steps.

- Moisture contents of building bricks in the overhygroscopic range are related to three material parameters: capillary saturation moisture content, water absorption coefficient, and open porosity. The relationships between moisture contents and basic parameters provide a possibility to quickly estimate the moisture storage data without any moisture measurement.

2. By applying statistical methods, a novel approach and procedure was developed to use the existing measured high-quality data to extend the use of the incomplete material data for hygrothermal simulation.

- For this purpose, an approach to identify material clusters from a group of specific materials was developed by the application of cluster analysis. The similar specific materials were aggregated into one material cluster by comparing their properties, including both the basic material parameters and identified characteristic moisture contents in the simplification of the moisture storage measurement. This approach was applied in the building brick category. The specific bricks in each identified brick cluster exhibit quite similar characteristics.

- A method to derive the generic material from the identified material cluster was developed. The generic material represents one type of specific materials with similar characteristics. One generic brick was exemplarily derived from one of the brick clusters.

- The application of generic material has a practical benefit for qualifying the incomplete material data and improving accuracy of the analysis in the building design stage. By comparing the available properties of the incomplete material with that of the generic materials in the same physical material group, a most similar generic material is selected. The missing properties of the incomplete material could be supplemented by adopting the properties of the most similar generic material. In the early design stage, the detailed material information is not necessary. The generic material, representing one type of specific materials, can be used in the analysis to reduce the risk of improper selection of specific material.

8.3 Development of a Probabilistic Approach to Assess Hygrothermal Performance of Building Enclosure Assemblies

A probabilistic approach based on the Monte Carlo method was developed and incorporated into a current simulation tool, to assess the hygrothermal performance of building enclosure assemblies against different performance criteria.

- The relations between material parameters and between material parameters and material functions were discussed. The rank correlations of material parameters in different material categories were derived. Those relations were incorporated in the Latin hypercube sampling.

- Probability density function of effective saturation moisture content was explored based on measurements of a number of building materials, and it is proposed as a normal distribution.

- The uncertainties in material properties, boundary coefficients, indoor condition, dimensions of material layers, and orientation of the construction were considered in the performance assessment.

- The performance evaluation was accomplished by analyzing the results from the hygrothermal simulations. The evaluation criteria covered three aspects in this study: durability, thermal efficiency and mold growth risk. The durability of the construction was evaluated by condensation accumulated in the assembly and the probability of damages induced by the hygrothermal loads on the outer surface region of the assembly. The thermal performance was examined by the static thermal resistance and transient thermal resistance of

the wall assembly. Mold risk was assessed by the isopleths model, model index and 80% relative humidity.

- By the application of the probabilistic approach, the risk assessment will not just provide a result of "failure" or "no failure", but will give a probability of "failure".

- Sensitivity analysis can effectively address the most influential input variables against the output of interest. Five sensitivity analysis techniques has been applied in this study, including scatter plot, regression-based sensitivity analysis, stepwise regression analysis, partial correlation, and statistical F test. These techniques identified the same influential input variables against the transient thermal resistance of the wall assembly.

- The influence of the input variable on the output variable may vary over time if the output variable is time-dependent.

- It needs to be noted that sensitivity analysis is case dependent. For the constructions with different design scenarios, the influential variables may be different.

8.4 Recommendations for Future Work

A method to derive the generic material from a group of the specific materials has been developed in this research work. One generic brick was exemplarily derived from one of the brick material clusters. This method should be extended to other physical material groups/categories. Furthermore, the relationships between material parameters in different material groups/categories need to be investigated by regression analysis, in order to build a statistical basis for the qualification of literature data as the input for the hygrothermal simulation.

Several uncertainties from different sources were considered in this research. However, there are still some limitations in processing the uncertainties in the input variables. The workmanship only took into account the influence of the dimension of the material layer, while other factors, e.g., the infiltration/ exfiltration through the enclosure assembly, may lead to a large impact on the results. The outdoor climatic condition adopts the weather data of test reference year, which is a deterministic data. Those uncertain variables should be accounted for in the future work.

Sensitivity analysis techniques applied in this study are limited by the linear assumption. In case the linear assumption is not satisfied, the results cannot provide reliable results. The model-independent sensitivity analysis approaches, e.g., Sobol's or FAST, are then preferred.

The influence of the input variables on the single output variable, e.g., transient thermal resistance and interior surface temperature of the retrofitted wall assembly, was assessed. Further work is needed to evaluate an entire set of physical quantities against all relevant criteria.

A simulation package, which can integrate current hygrothermal simulation tools with the probabilistic approach developed in this study, is needed. Once the package is developed, the designer can easily apply it to determine whether the proposed construction meets all the performance criteria and address the most influential parameters.

Nomenclature

List of Arabic symbols

Symbol	Unit	Definition
A_w	$kg/(m^2 \cdot s^{0.5})$	Water absorption coefficient
$c_g^{m_v}$	kg/kg	Water vapor mass concentration in gas phase
d	m	Thickness
D_l	m^2/s	Liquid water diffusivity
$D_{v,air}$	m^2/s	Water vapor diffusivity in free air
$D_{v,mat}$	m^2/s	Water vapor diffusivity in porous material
e	-	Residual
f_{Rsi}	-	Temperature factor
g_k	m/s^2	Gravitational constant
h_a	J/kg	Specific enthalpy of dry air
h_l	J/kg	Specific internal energy of liquid water
h_g	J/kg	Specific internal energy of gas phase (including dry air and water vapor)
h_v	J/kg	Specific enthalpy of water vapor
H_0		Null hypothesis
$j_{k,conv}^{m_a}$	kg/m^2s	Convective dry air mass flux
$j_{k,conv}^{m_g}$	kg/m^2s	Convective flux of gas phase
$j_{k,conv}^{m_l}$	kg/m^2s	Convective liquid water flux
$j_{k,conv}^{m_v}$	kg/m^2s	Convective water vapor flux
$j_{k,diff}^{m_v}$	kg/m^2s	Diffusion water vapor flux
$j_{k,diff}^{Q}$	W/m^2s	Conduction energy flux
k_{wind}	-	Wind coefficient
K	m^2	Permeability of the porous medium
K_{cap}	s	Liquid water conductivity at capillary moisture content
K_{eff}	s	Liquid water conductivity at effective saturation
K_g	s	Gas permeability

Symbol	Unit	Definition
K_l	s	Liquid water conductivity
K_{rel}	-	Normalized / relative liquid water conductivity
K_v	s	Water vapor permeability
K_{l+v}	s	Moisture conductivity
$\dot{m}$	kg/s	Design moisture generation rate
p_a	Pa	dry air pressure
p_l	Pa	Liquid water pressure
p_v	Pa	Water vapor pressure
p_g	Pa	Gas pressure
p_0	Pa	Standard air pressure
p_c	Pa	Capillary pressure
pC	log(Pa)	Logarithmic capillary pressure $pC = log(-p_c)$
q_d	W/ m^2	Daily average heat flux
$q_{H,dir}$	W/ m^2	Direct radiation gained on a horizontal surface
$q_{H,diff}$	W/ m^2	Diffuse radiation gained on a horizontal surface
q_{sky}	W/ m^2	Sky radiation
r	m	Capillary radius
R	$m^2 \cdot K/W$	Thermal resistance
R_a	J/kg·K	Gas constant of air
R_h	Kg/m^2s	Rain flux on a horizontal surface
R_v	J/kg·K	Gas constant of water vapor
R_{wdr}	Kg/ m^2s	Wind-driven rain flux
R^2	-	Coefficient of determination
R_{adj}^2	-	Adjusted Coefficient of determination
t	s	Time
T	K	Thermodynamic (absolute) temperature

List of Greek symbols

Greek	Unit	Definition
α	-	Significant level
α	degree	Contact angle between liquid and solid phases
α	$W/m^2 \cdot K$	Heat transfer coefficient
α_R	-	Rain exposure coefficient
α_{SW}	-	Short wave radiation absorptivity
β	-	Regression coefficient
β	degree	Inclination of the construction
β	s/m	Vapor transfer coefficient
β_s	-	Orientation of the construction
δ	degree	Sun decline angle
δ_a	$kg/m \cdot s \cdot Pa$	Water vapor permeability in still air
ε	-	Long wave emissivity of building surface
ε_g	-	Long wave emissivity of surrounding ground
η_l	$N \cdot s/m^2$	Dynamic viscosity of the liquid phase
θ_{cap}	m^3/m^3	Capillary saturation moisture content
θ_{eff}	m^3/m^3	Effective saturation moisture content
θ_l	m^3/m^3	Volumetric moisture content
θ_{por}	m^3/m^3	Open porosity
θ_s	degree	Solar elevation angle
λ	$W/m \cdot k$	Thermal conductivity
λ	$m/s^{0.5}$	Boltzmann variable $\lambda = x/\sqrt{t}$
μ	-	Water vapor diffusion resistance factor
ρ	Kg/m^3	Bulk density
$\rho_{s,g}$	-	Ground reflectivity
$\rho_g^{m_a}$	kg/ kg	dry air concentration in the gas phase
$\rho_g^{m_v}$	kg/ kg	Water vapor mass concentration in the gas phase
$\rho_{REV}^{m_{l+v}}$	kg/m^3_{REV}	Moisture density in REV
ρ_{REV}^{u}	W/m^3_{REV}	Internal energy density in REV

Greek	Unit	Definition
σ	W/m^2K^4	Stefan-Boltzmann constant $\sigma = 5.67 \times 10^{-8}$ W/m^2K^4
σ_l	N/m	Liquid water surface tension
σ_{REV}^u	W/m^3	Energy source/sink in REV
$\sigma_{REV}^{m_{l+v}}$	kg/m^2s	Moisture generation source/sink in REV
$\sigma_{REV}^{m_a}$	kg/m^2s	Air mass generation source/sink in REV
φ	-	Relative humidity
ϕ_s	degree	Solar azimuth angle
Φ	degree	Local latitude

List of abbreviations

Abbreviations	Description
ASTM	American Society for Testing and Materials
ASHRAE	American Society of Heating, Refrigerating, and Air-Conditioning Engineers
DIN	German Institute for Standardization
HAM	Heat, air and moisture
HLS	Hygrothermal loads on the exterior surface
HLD	Hygrothermal loads at the certain depth layer from the exterior surface
HP	Heating period
IBK	Institute of Building Climatology
LHS	Latin Hypercube Sampling
M	Mold index
MS	Mean square
RH	Relative humidity
PCC	Partial correlation coefficient
SS	Sum of square
SRC	Standardized regression coefficient
TRY	Test reference year

List of indices

Subscript	description
cap	*Capillary*
e	*Exterior*
g	*Ground*
i	*Interior*
l	*Liquid water*
R	*Rain*
R	*Regression*
Res	*Residual*
s	*Building surface*
sat	*Saturation*
T	*Total*
v	*Vapor*

Appendix A

The equilibrium condition at the surface of the liquid water in a capillary is expressed as:

$$F_g = F_l + F_c \cos(\alpha) \tag{A. 1}$$

$$\pi r^2 p_g = \pi r^2 p_l + 2\pi r \cdot \sigma_l \cos(\alpha) \tag{A. 2}$$

After reorganization,

$$p_g - p_l = -p_c = \frac{2\sigma_l \cos(\alpha)}{r} \tag{A. 3}$$
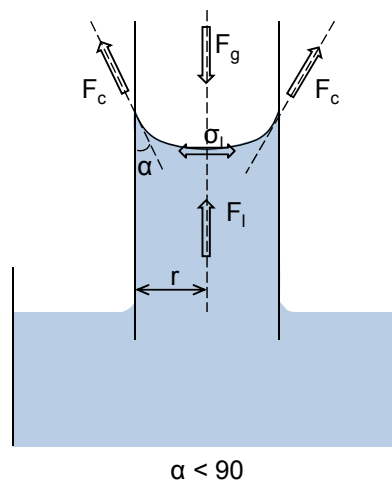
Figure A-1 Equilibrium condition at the surface of liquid water in a capillary

Appendix B

In the free water surface, when the water vapor and liquid water are in equilibrium (water molecular condensation and evaporation has the same rate), the specific free enthalpy of water vapor is equal to that of the liquid water.

$$g_{v,0} = g_{l,0} \tag{B. 1}$$
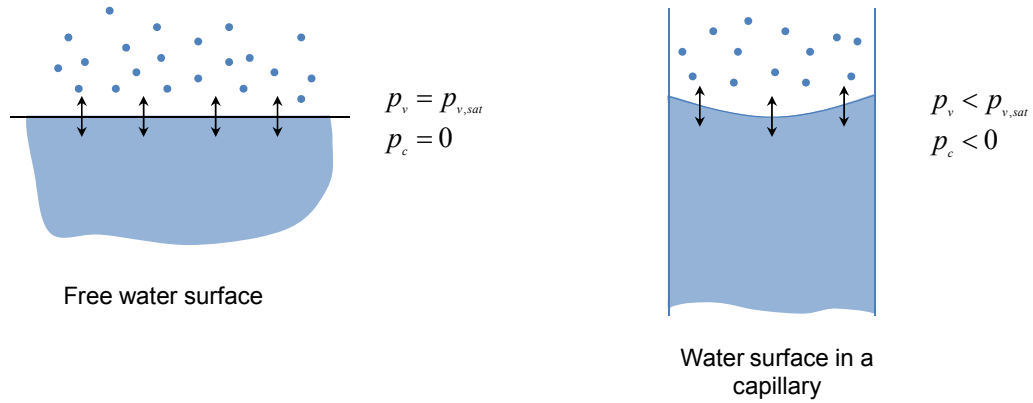
Figure B-1 Equilibrium pressure condition at the free water surface and water surface in a capillary

At the water surface in the capillary, specific free enthalpy get the new equilibrium as:

$$g_{v,0} + \Delta g_v = g_{l,0} - \Delta g_l \quad \text{with} \quad \Delta g = \int \left(\frac{1}{\rho}\right) dp \tag{B. 2}$$

$$g_{v,0} + \int_{p_{v,sat}}^{p_v} \left(\frac{1}{\rho_v}\right) dp_v = g_{l,0} - \int_0^{p_c} \left(\frac{1}{\rho_l}\right) dp_l \tag{B. 3}$$

Substituting ideal gas equation $\dfrac{1}{\rho_v} = \dfrac{R_v T}{p_v}$ into equation B.3,

$$R_v T \ln\left(\frac{p_v}{p_{v,sat}}\right) = -\frac{p_c}{\rho_l} \tag{B. 4}$$

After reorganization,

$$p_c = -\rho_l R_v T \ln(\varphi) \tag{B. 5}$$

254

Appendix C

Material properties of 23 specific bricks are presented in the following column graphs

with error bars.

ZBD

ZGZ

ZHS

ZJN

ZWB
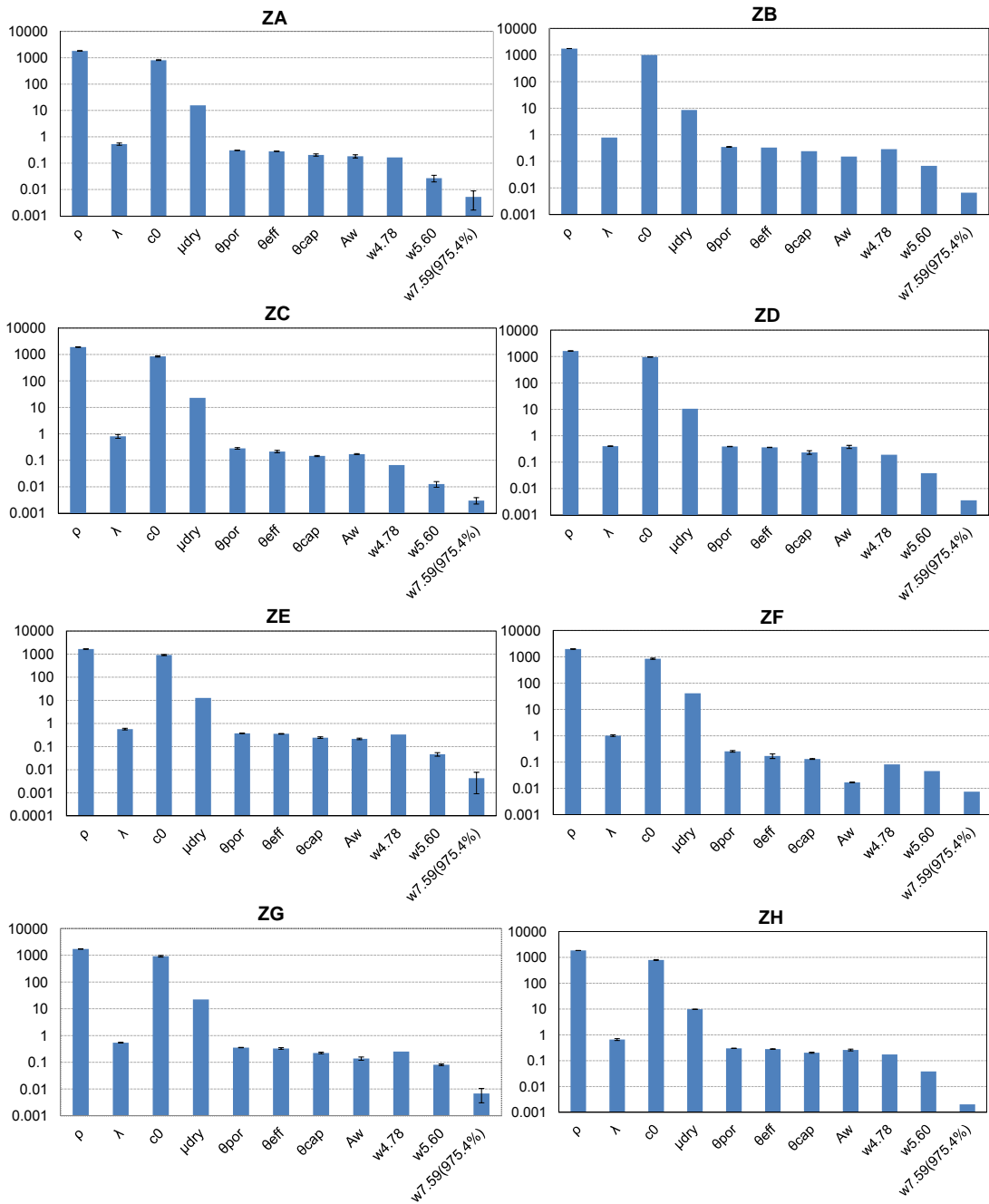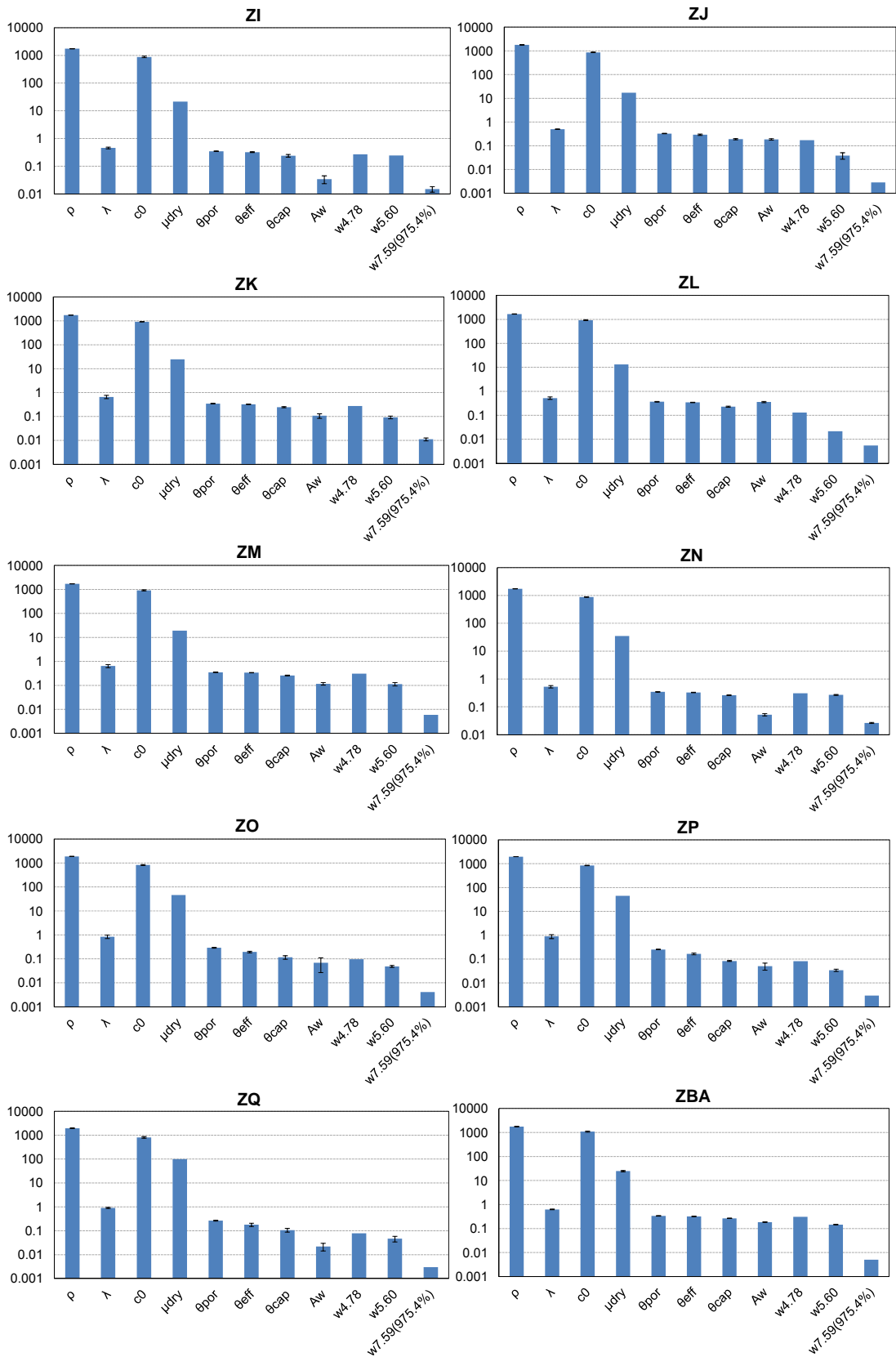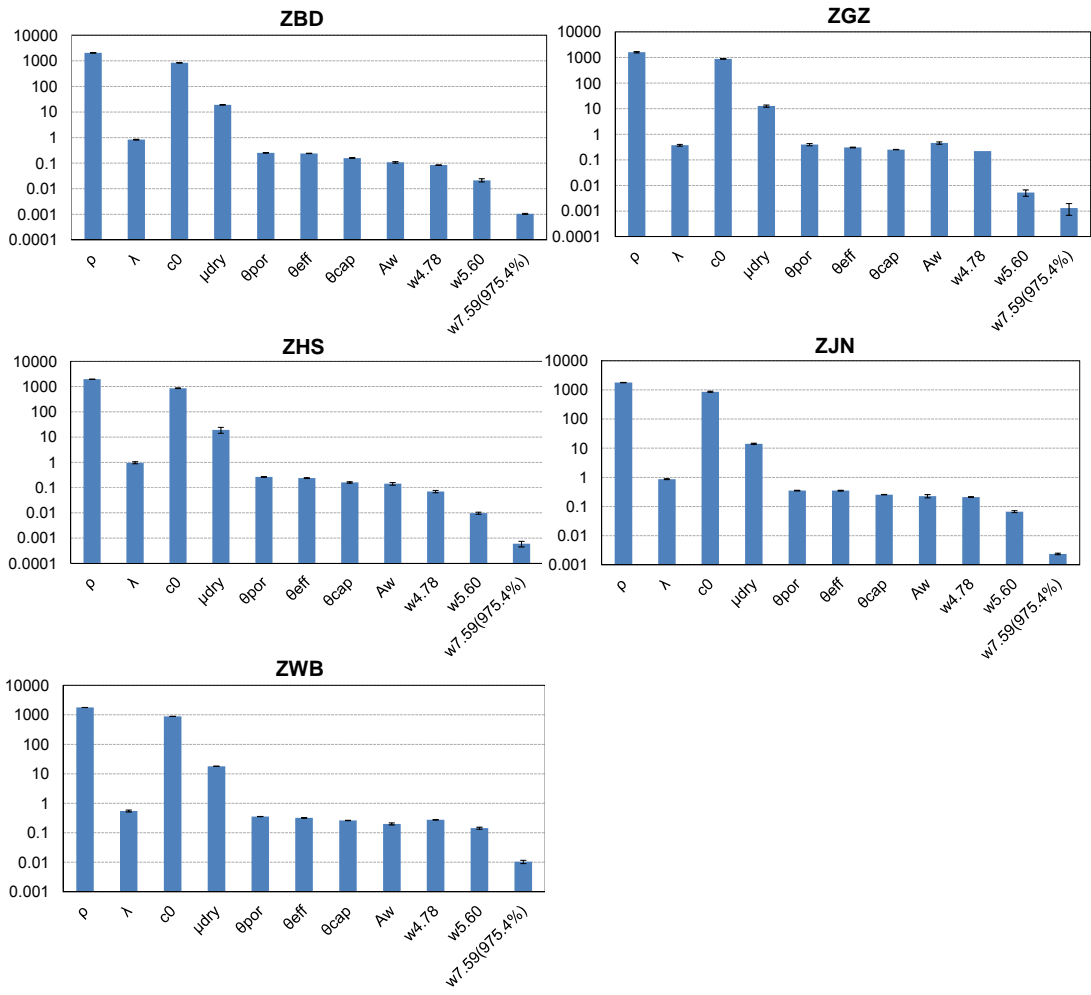
Appendix D

Table D-1 Joining distance of moisture contents in the building brick category by using Ward's method

Cluster containing	and	Cluster containing	Were joined at distance in	No.of members new cluster
w8.18(32.9%)		w8.06(43.2%)	0.001	2
w7.36(84.7%)		w7.16(90.0%)	0.001	2
w8.18(32.9%)		w7.87(58.2%)	0.002	3
w7.36(84.7%)		w7.59(75.4%)	0.003	3
w6.75(96.0%)		w6.56(97.4%)	0.011	2
w6.15		w5.90	0.012	2
w7.36(84.7%)		w8.18(32.9%)	0.013	6
w3.78		w3.48	0.013	2
w3.78		w0	0.021	3
w6.15		w5.60	0.025	3
w4.95		w4.78	0.029	2
w4.95		w4.48	0.046	3
w3.78		w4.18	0.051	4
w6.15		w5.30	0.076	4
w6.75(96.0%)		w7.36(84.7%)	0.096	8
w3.78		w4.95	0.253	7
w6.15		w6.75(96.0%)	0.336	12
w3.78		w6.15	1.409	19

Table D-2 Joining distance of moisture contents in the plaster/mortar category by using Ward's method

Cluster containing	and	Cluster containing	Were joined at distance in	No.of members new cluster
w8.18(32.9%)		w8.06(43.2%)	0.008	2
w5.90		w5.60	0.010	2
w4.18		w3.78	0.013	2
w4.95		w4.78	0.015	2
w7.36(84.7%)		w7.16(90.0%)	0.015	2
w6.75(96.0%)		w6.56(97.4%)	0.016	2
w5.90		w6.15	0.025	3
w7.36(84.7%)		w7.59(75.4%)	0.026	3
w8.18(32.9%)		w7.87(58.2%)	0.029	3
w4.18		w3.48	0.03	3
w5.90		w5.30	0.049	4
w6.75(96.0%)		w7.36(84.7%)	0.070	5

Cluster containing	and	Cluster containing	Were joined at distance in	No.of members new cluster
w4.18		w4.95	0.134	6
w6.75(96.0%)		w8.18(32.9%)	0.151	8
w4.18		w5.90	0.377	10
w4.18		w6.75(96.0%)	1.139	18

Table D-3 Joining distance of specific bricks by using Ward's method

Cluster containing	and	Cluster containing	Were joined at distance in	No.of members new cluster
ZBD		ZC	0.339	2
ZJ		ZA	0.354	2
ZK		ZG	0.356	2
ZL		ZD	0.390	2
ZBD		ZHS	0.397	3
ZP		ZO	0.412	2
ZF		ZP	0.478	3
ZWB		ZK	0.485	3
ZM		ZE	0.492	2
ZJ		ZH	0.502	3
ZGZ		ZL	0.602	3
ZWB		ZM	0.695	5
ZBA		ZB	0.712	2
ZN		ZI	0.729	2
ZJN		ZWB	0.943	6
ZF		ZQ	1.199	4
ZBA		ZJN	1.320	8
ZBD		ZF	1.656	7
ZJ		ZGZ	2.145	6
ZBA		ZN	2.659	10
ZJ		ZBA	3.233	16
ZBD		ZJ	8.693	23

Table D-4 Joining distance of specific bricks by using complete linkage method

Cluster containing	and	Cluster containing	Were joined at distance in	No.of members new cluster
ZBD		ZC	0.339	2
ZJ		ZA	0.354	2
ZK		ZG	0.356	2
ZL		ZD	0.390	2
ZBD		ZHS	0.398	3
ZP		ZO	0.412	2
ZWB		ZK	0.462	3
ZF		ZP	0.485	3
ZM		ZE	0.492	2
ZJ		ZH	0.543	3
ZGZ		ZL	0.614	3
ZM		ZB	0.654	3
ZN		ZI	0.729	2
ZM		ZJN	0.750	4
ZF		ZBD	0.768	6
ZWB		ZM	0.864	7
ZJ		ZGZ	1.211	6
ZBA		ZWB	1.301	8
ZQ		ZF	1.403	7
ZBA		ZJ	1.667	14
ZBA		ZN	2.249	16
ZBA		ZQ	2.540	23

Appendix E

The histogram plot and approximated probability density function of the measured

effective saturation moisture content of different building materials.

Building brick 1

Estimated: mean = 0.24, SD = 0.006
Kolmogorov-Smirnov test statistic = 0.13
Shapiro-Wilk test statistic for normality = 0.96
P-value = 0.245

Building brick 2

Estimated: mean = 0.352, SD = 0.011
Kolmogorov-Smirnov test statistic = 0.13
Shapiro-Wilk test statistic for normality = 0.95
P-value = 0.08

Building brick 3

Estimated: mean = 0.319, SD = 0.0097
Kolmogorov-Smirnov test statistic = 0.12
Shapiro-Wilk test statistic for normality = 0.949
P-value = 0.11

Building brick 4

Estimated: mean = 0.238, SD = 0.008
Kolmogorov-Smirnov test statistic = 0.083
Shapiro-Wilk test statistic for normality = 0.954
P-value = 0.11

Lime sands brick

Estimated: mean = 0.33, SD = 0.008
Kolmogorov-Smirnov test statistic =0.11
Shapiro-Wilk test statistic for normality = 0.969
P-value = 0.36

Calcium silicate

Estimated: mean = 0.903, SD = 0.007
Kolmogorov-Smirnov test statistic =0.129
Shapiro-Wilk test statistic for normality = 0.95
P-value = 0.12

Estimated: mean = 0.32 , SD = 0.008
Kolmogorov-Smirnov test statistic =0.083
Shapiro-Wilk test statistic for normality = 0.97
P-value = 0.38
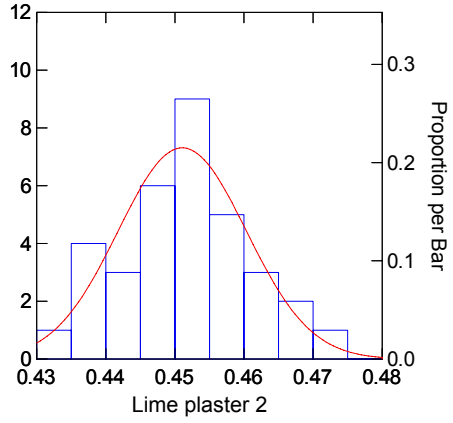
Estimated: mean = 0.451 , SD = 0.009
Kolmogorov-Smirnov test statistic = 0.075
Shapiro-Wilk test statistic for normality = 0.99
P-value = 0.98

Estimated: mean = 0.3, SD = 0.026
Kolmogorov-Smirnov test statistic =0.07
Shapiro-Wilk test statistic for normality = 0.98
P-value = 0.88

Estimated: mean = 0.33, SD = 0.013
Kolmogorov-Smirnov test statistic = 0.10
Shapiro-Wilk test statistic for normality = 0.96
P-value = 0.33

Estimated: mean = 0.4, SD = 0.011
Kolmogorov-Smirnov test statistic = 0.11
Shapiro-Wilk test statistic for normality = 0.98
P-value = 0.88

Estimated: mean = 0.26, SD = 0.005
Kolmogorov-Smirnov test statistic = 0.13
Shapiro-Wilk test statistic for normality = 0.95
P-value = 0.15

Sandstone Arholzen

Estimated: mean = 0.114, SD = 0.003
Kolmogorov-Smirnov test statistic = 0.128
Shapiro-Wilk test statistic for normality = 0.97
P-value = 0.34

Sandstone Obernkirchen

Estimated: mean = 0.132, SD = 0.007
Kolmogorov-Smirnov test statistic = 0.124
Shapiro-Wilk test statistic for normality = 0.96
P-value = 0.43

Sandstone Sander

Estimated: mean = 0.195, SD = 0.004
Kolmogorov-Smirnov test statistic = 0.12
Shapiro-Wilk test statistic for normality = 0.96
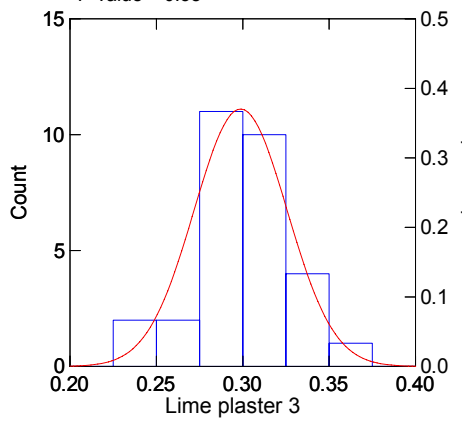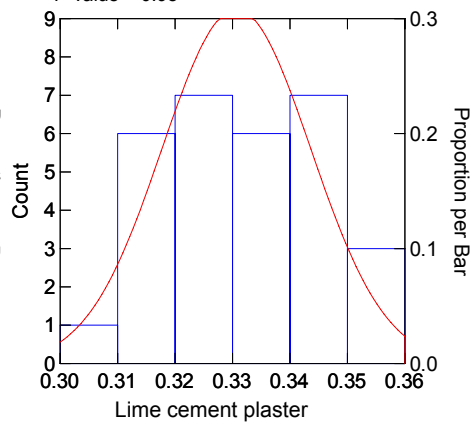P-value = 0.26

Aerated concrete

Estimated: mean = 0.18, SD = 0.009
Kolmogorov-Smirnov test statistic = 0.11
Shapiro-Wilk test statistic for normality = 0.96
P-value = 0.34

Cork

Estimated: mean = 0.144, SD = 0.028
Kolmogorov-Smirnov test statistic = 0.20
Shapiro-Wilk test statistic for normality = 0.94
P-value = 0.18

Gypsum board

Estimated: mean = 0.526, SD = 0.008
Kolmogorov-Smirnov test statistic = 0.135
Shapiro-Wilk test statistic for normality = 0.95
P-value = 0.185

263

Estimated: mean = 0.69, SD = 0.007
Kolmogorov-Smirnov test statistic = 0.13
Shapiro-Wilk test statistic for normality = 0.97
P-value = 0.6

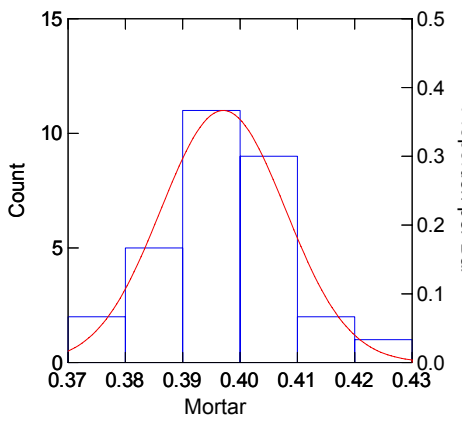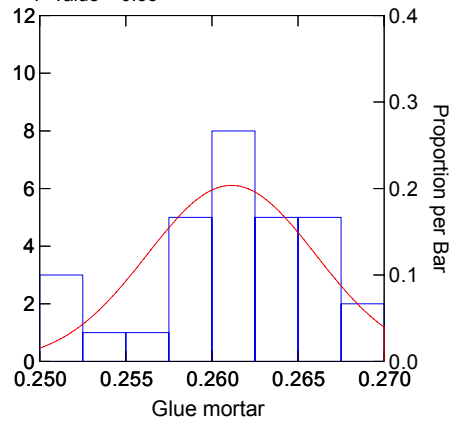Estimated: mean = 0.561, SD = 0.006
Kolmogorov-Smirnov test statistic = 0.13
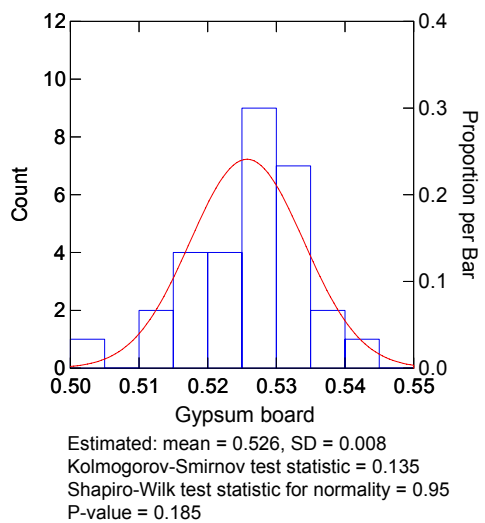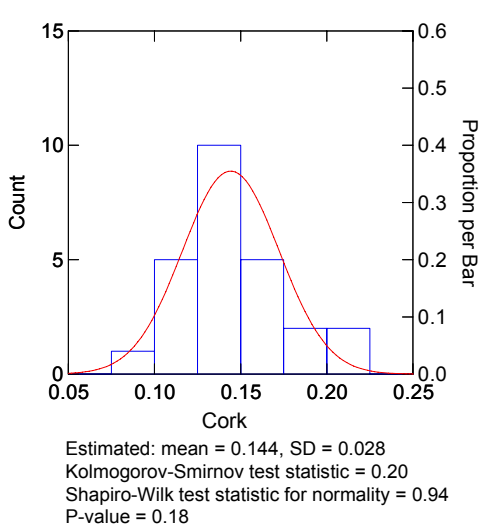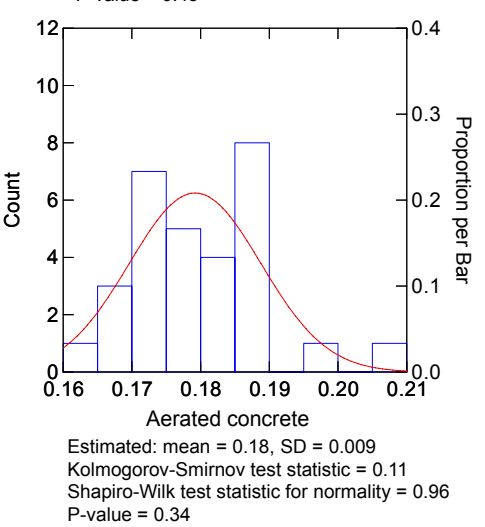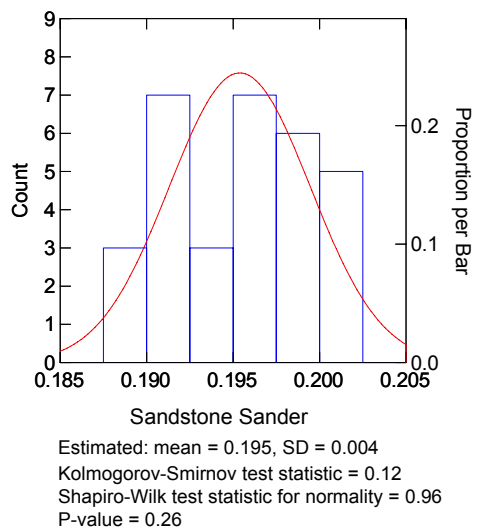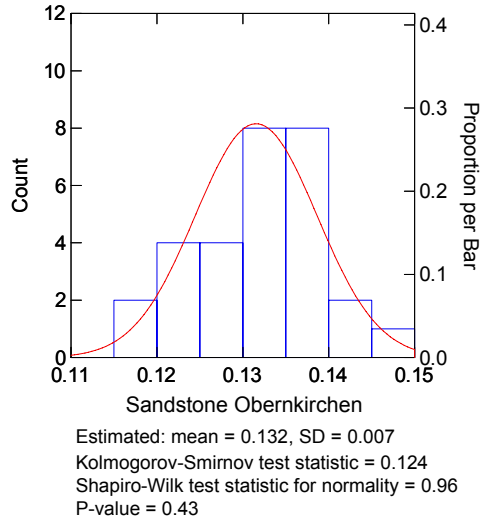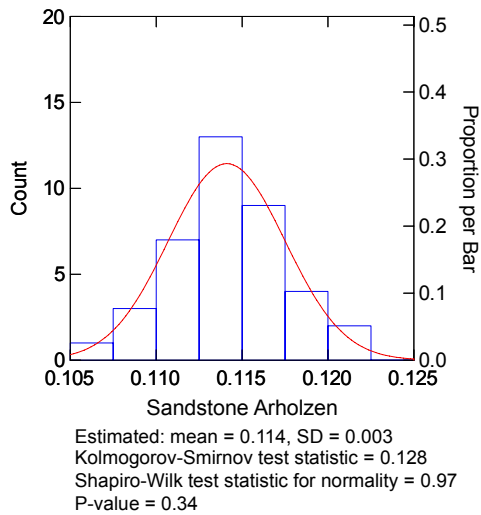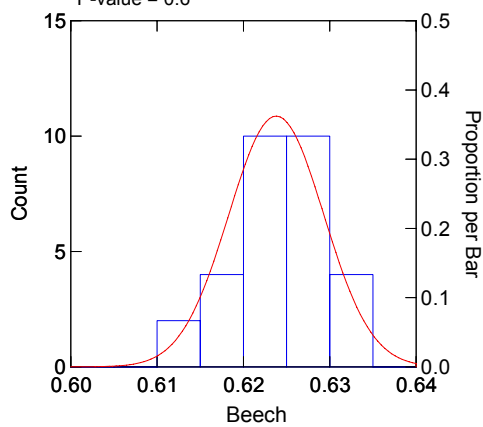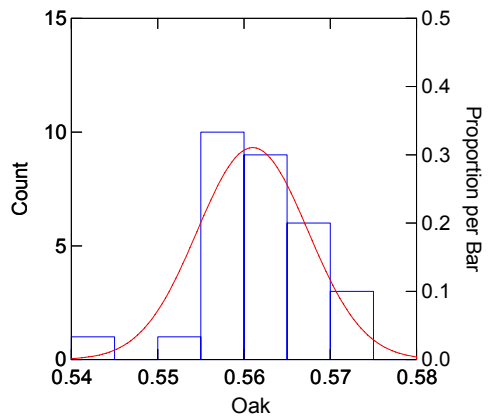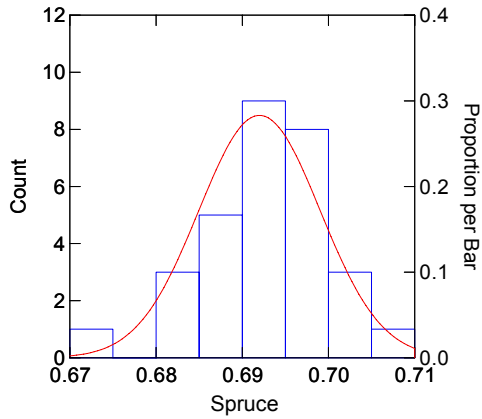Shapiro-Wilk test statistic for normality = 0.96
P-value = 0.37

Estimated: mean = 0.624, SD = 0.0054
Kolmogorov-Smirnov test statistic = 0.115
Shapiro-Wilk test statistic for normality = 0.96
P-value = 0.37

Appendix F

First, the definitions of the Pearson correlation coefficient and Spearman correlation coefficient are given.

Pearson correlation coefficient provides a measure of the strength and direction of the linear relationship between two variables. For two variables x_j and x_k with a random sample of size n, Pearson correlation coefficient is defined by:

$$r_{x_j x_k} = \frac{\sum_{i=1}^{n}(x_{ij} - \bar{x}_j)(x_{ik} - \bar{x}_k)}{\left[\sum_{i=1}^{n}(x_{ij} - \bar{x}_j)^2\right]^{1/2}\left[\sum_{i=1}^{n}(x_{ik} - \bar{x}_k)^2\right]^{1/2}} , \qquad (\text{F. 1})$$

where

$$\bar{x}_j = \sum_{i=1}^{n} x_{ij} / n , \quad \bar{x}_k = \sum_{i=1}^{n} x_{ik} / n$$

Pearson correlation coefficient has the range between -1.0 and 1.0. The value of 0 means there is no linear relationship between two variables and the value of ± 1.0 indicates an exact relationship between two variables. The negative coefficient and positive coefficient implies the two variables tend to move in the opposite direction and in the same direction, respectively.

Spearman correlation coefficient measures the strength of the monotonic relationship between two variables. It also has the range between -1.0 and 1.0. But unlike Pearson correlation coefficient using the variables directly, Spearman correlation coefficient employs the ranked variables in the calculation.

$$\rho_{x_j x_k} = \frac{\sum_{i=1}^{n}\left[R(x_{ij}) - \bar{R}(x_j)\right]\left[R(x_{ik}) - \bar{R}(x_k)\right]}{\left\{\sum_{i=1}^{n}\left[R(x_{ij}) - \bar{R}(x_j)\right]^2\right\}^{1/2}\left\{\sum_{i=1}^{n}\left[R(x_{ik}) - \bar{R}(x_k)\right]^2\right\}^{1/2}} , \qquad (\text{F. 2})$$

where $R(x_{ij})$ and $R(x_{ik})$ are the rank-transformed values of x_{ij} and x_{ik}, respectively. The smallest value of the variable has the rank of 1 and the largest one has the rank of n. $\bar{R}(x_j) = \bar{R}(x_k) = (n+1)/2$.

The procedure to generate correlated samples is introduced as follows.

A randomly generated matrix of m input variables and n samples can be represented as:

$$X = \begin{bmatrix} x_{11} & x_{12} & \cdots & x_{1m} \\ x_{21} & x_{22} & \cdots & x_{2m} \\ \vdots & \vdots & \vdots & \vdots \\ x_{n1} & x_{n2} & \cdots & x_{nm} \end{bmatrix}, \tag{F. 3}$$

where x_{ij} is the value for variable j in sample element i. The generated variables are independent of each other.

The desired rank correlation structure is represented by $m \times m$ matrix

$$C = \begin{bmatrix} \rho_{11} & \rho_{12} & \cdots & \rho_{1m} \\ \rho_{21} & \rho_{22} & \cdots & \rho_{2m} \\ \vdots & \vdots & \vdots & \vdots \\ \rho_{m1} & \rho_{m2} & \cdots & \rho_{mm} \end{bmatrix}, \tag{F. 4}$$

where ρ_{kl} is the desired rank correlation between variables x_k and x_l.

The key concept to obtain the variables with desired correlation is that it only adjusts the rank order of the randomly generated values, but does not change the values themselves.

To implement this aim, an $n \times m$ matrix R is first established. Each column of R contains a random permutation of the n van der Waerden scores $\Phi^{-1}(i/(n+1))$, $i=1,2\dots,n$, where Φ^{-1} is the inverse function of the standard normal distribution.

The desired correlation matrix C is decomposed by Cholesky factorization:

$$C = PP^T,$$ (F. 5)

where P is the lower triangular matrix.

If the correlation matrix associated with R is the identity matrix, then

$$R^* = RP^T$$ (F. 6)

has the correlation matrix equal to C.

For convenience, the correlation matrix of R is represented by matrix T. The Cholesky factorization for T is presented by:

$$T = QQ^T,$$ (F. 7)

where Q is lower triangular matrix.

In case T is not an $m \times m$ identity matrix, the matrix R^* with a correlation matrix equal to C is defined by:

$$R^* = R(Q^{-1})^T P^T$$ (F. 8)

In equation F.8, multiplication of R by $(Q^{-1})^T$ transforms R into a matrix whose associated correlation matrix is $m \times m$ identity matrix. And further multiplication of the product by P^T produces a matrix whose associated correlation matrix is C.

The desired X^* is obtained by simple rearrangement of the column of X as the same rank order as the values in the individual columns of R^*. So the correlation matrix of X^* will be C. Since the approach only rearranges the rank order of input variables, not the numbers themselves, the original marginal distributions of the input variables are kept.

References

ASTM C177. 2010. Standard Test Method for Steady-State Heat Flux Measurements and Thermal Transmission Properties by Means of the Guarded-Hot-Plate Apparatus. ASTM International, West Conshohocken, PA., pp. 23.

ASTM C518. 2010. Standard Test Method for Steady-State Thermal Transmission Properties by Means of the Heat Flow Meter Apparatus. ASTM International, West Conshohocken, PA., pp. 15.

ASTM C1498. 2004. Standard Test Method for Hygroscopic Sorption Isotherms of Building Materials. ASTM International, West Conshohocken, PA., pp. 4.

ASTM C1699. 2009. Standard Test Method for Moisture Retention Curves of Porous Building Materials Using Pressure Plates. ASTM International, West Conshohocken, PA., pp. 4.

ASTM E96 / E96M. 2010. Standard Test Methods for Water Vapor Transmission of Materials. ASTM International, West Conshohocken, PA., pp. 12.

ASTM E104-02. 2007. Standard Practice for Maintaining Constant Relative Humidity by Means of Aqueous Solution. ASTM International, West Conshohocken, PA., pp. 5.

DIN 4108-2. 2003. Wärmeschutz und Energie-Einsparung in Gebäuden - Teil 2: Mindestanforderungen an den Wärmeschutz. Deutsches Institut für Normung e.V., Berlin, pp. 31.

DIN 4108-3. 2001. Wärmeschutz und Energie-Einsparung in Gebäuden - Teil 3: Klimabedingter Feuchteschutz, Anforderungen, Berechnungsverfahren und Hinweise für Planung und Ausführung. Deutsches Institut für Normung e.V., Berlin., pp. 40.

DIN 4108-6. 2003. Wärmeschutz und Energie-Einsparung in Gebäuden - Teil 6: Berechnung des Jahresheizwärme- und des Jahresheizenergiebedarfs. Deutsches

Institut für Normung e.V., Berlin, pp. 110.

DIN EN 12664. 2001. Wärmetechnisches Verhalten von Baustoffen und Bauprodukten- Bestimmung des Wärmedurchlasswiderstandes nach dem Verfahren mit dem Plattengerät und dem Wärmestrommessplatten-Gerät- Trockene und feuchte Produkte mit mittlerem und niedrigem Wärmedurchlasswiderstand. Deutsches Institut für Normung e.V., Berlin., pp. 64.

DIN EN 15026. 2007. Wärme- und feuchtetechnisches Verhalten von Bauteilen und Bauelementen - Bewertung der Feuchteübertragung durch numerische Simulation. Deutsches Institut für Normung e.V., Berlin., pp. 26.

DIN EN ISO 6946. 2008. Wärmedurchlasswiderstand und Wärmedurchgangskoeffizient – Berechnungsverfahren. Deutsches Institut für Normung e.V., Berlin, pp. 35.

DIN EN ISO 12571. 2000. Wärme- und feuchtetechnisches Verhalten von Baustoffen und Bauprodukten- Bestimmung der hygroskopischen Sorptionseigenschaften. Deutsches Institut für Normung e.V., Berlin., pp. 13.

DIN EN ISO 12572. 2001. Wärme- und feuchtetechnisches Verhalten von Baustoffen und Bauprodukten - Bestimmung der Wasserdampfdurchlässigkeit. Deutsches Institut für Normung e.V., Berlin., pp. 28.

DIN EN ISO 13788. 2001. Wärme- und feuchtetechnisches Verhalten von Bauteilen und Bauelementen - Raumseitige Oberflächentemperatur zur Vermeidung kritischer Oberflächenfeuchte und Tauwasserbildung im Bauteilinneren - Berechnungsverfahren. DIN Deutsches Institut für Normung e.V., Berlin, pp. 33.

DIN EN ISO 15148. 2003. Wärme- und feuchtetechnisches Verhalten von Baustoffen und Bauprodukten- Bestimmung des Wasseraufnahmekoeffizienten bei teilweisem Eintauchen. Deutsches Institut für Normung e.V., Berlin., pp. 18.

DIN ISO 11272. 2001. Bodenbeschaffenheit-Bestimmung der Trockenrohdichte. Deutsches Institut für Normung e.V., Berlin., pp. 10.

Adan, O.C.G. 1994. On the Fungal Defacement of Interior Finishes. Ph.D. Thesis. Eindhoven University of Technology. Eindhoven, The Netherlands. 233 pp.

Arnfield, A.J. 1975. Note on the diurnal,latitudinal and seasonal variation of the surface reflection coefficient. *Journal of Applied Meteorology*, 14: 1603–1608.

ASHRAE 2009. ASHRAE Handbook of Fundamentals. American Society of Heating, Refrigerating and Air-Conditioning Engineers Atlanta, GA.

Bankwall, C.G. 1986. Thermal performance of the building envelope as influenced by workmanship. In: F.J. Powell and S.L. Matthews (Editors), *Thermal insulation: Materials and systems, ASTM STP 922*. American Society for Testing and Materials, Philadelphia, pp. 679-684.

Baughman, A. and Arens, E. 1996. Indoor Humidity and Human Health - Part1: Literature Review of Health Effects of Humidity-Influenced Indoor Pollutants. *ASHRAE Transactions*, 102 (Part 1): 193-211.

Beausoleil-Morrison, I. 2002. The adaptive simulation of convective heat transfer at internal building surfaces. *Building and Environment*, 37(8-9): 791-806.

Blocken, B. and Carmeliet, J. 2004. A review of wind-driven rain research in building science. *Journal of Wind Engineering and Industrial Aerodynamics*, 92(13): 1079-1130.

Bomberg, M., Pazera, M. and Plagge, R. 2005. Analysis of Selected Water Absorption Coefficient Measurements. *Journal of Thermal Envelope and Building Science*, 28(3): 227-243.

Brocken, H. 1998. Moisture Transport in Brick Masonry: The Grey Area between Bricks. Ph.D. Thesis. Eindhoven University of Technology. Eindhoven, The Netherlands.

Burr, M.L., Mullins, J., Merrett, T.G. and Stott, N.C. 1988. Indoor moulds and asthma. *Journal of the Royal Society for the Promotion of Health*, 108(3): 99-101.

Carmeliet, J., Descamps, F. and Houvenaghel, G. 1999. A Multiscale Network Model

for Simulating Moisture Transfer Properties of Porous Media. *Transport in Porous Media*, 35(1): 67-88

Carmeliet, J., Hens, H., Roels, S., Adan, O., Brocken, H., Cerny, R., Pavlik, Z., Hall, C., Kumaran, K. and Pel, L. 2004. Determination of the Liquid Water Diffusivity from Transient Moisture Transfer Experiments. *Journal of Thermal Envelope and Building Science*, 27(4): 277-305.

Carmeliet, J. and Roels, S. 2002. Determination of the Moisture Capacity of Porous Building Materials. *Journal of Building Physics*, 25(3): 209-237.

Cornick, S., Dalgliesh, W.A. and Maref, W. 2009. Sensitivity of Hygrothermal Analysis to Uncertainty in Rain Data. *Journal of ASTM International*, 6(4): 1-17.

Corrado, V. and Mechri, H.E. 2009. Uncertainty and Sensitivity Analysis for Building Energy Rating. *Journal of Building Physics*, 33(2): 125-156.

Cullen, A.C. and Frey, H.C. 1999. Probabilistic Techniques in Exposure Assessment. Plenum Press. New York. 352 pp.

De Wit, M.S. 2001. Uncertainty in predictions of thermal comfort in buildings. Ph.D. Thesis. Technische Universiteit Delft. Delft, The Netherlands. 234 pp.

Descamps, F. 1997. Continuum and discrete modelling of isothermal water and air transfer in porous media. Ph.D. Thesis. Catholic University of Leuven. Leuven, Belgium. 161 pp.

Downing, D.J., Gardner, R.H. and Hoffman, F.O. 1985. An examination of response-surface methodologies for uncertainty analysis in assessment models. *Technometrics*, 27(2): 151-163.

Durner, W. 1994. Hydraulic conductivity estimation for soils with heterogeneous pore structure. *Water Resour. Res.*, 30(2): 211-223.

USAID ECO-III. 2010. Sustainable building design education course material on introduction to building physics. http://eco3.org/downloads/sustainable-building-design-course.pdf. New Delhi,

India. Assessed April 25, 2011

EnEV 2007. Verordnung über energiesparenden Wärmeschutz und energiesparende Anlagentechnik bei Gebäuden (Energieeinsparverordnung – EnEV) Bundesgesetzblatt   Teil I Nr. 34 vom 26.

Everitt, B.S., Landau, S., Leese, M. and Stahl, D. 2011. Cluster analysis (5th edition). John Wiley & Sons. Chichester, West Sussex.

Frey, H.C., Mokhtari, A. and Danish, T. 2003. Evaluation of Selected Sensitivity Analysis Methods Based Upon Applications to Two Food Safety Process Risk Models. Prepared by North Carolina State University for Office of Risk Assessment and Cost-Benefit Analysis. Washington, DC: U.S. Department of Agriculture. http://www.ce.ncsu.edu/risk/Phase2Final.pdf . Accessed May 15, 2010.

Frey, H.C. and Patil, S.R. 2002. Identification and Review of Sensitivity Analysis Methods. *Risk Analysis*, 22(3): 553-578.

Givoni, B. 1998. Climate Considerations in Building and Urban Design. Van Nostrand Reinhold. New York.

Grunewald, J. 1997. Diffusiver und konvektiver Stoff- und Energietransport in kapillarporösen Baustoffen. Ph.D. Thesis. Dresden Univeristy of Technology. Dresden, Germany. 214 pp.

Grunewald, J., Häupl, P. and Bomberg, M. 2003. Towards an Engineering Model of Material Characteristics for Input to Ham Transport Simulations - Part 1: An Approach. *Journal of Building Physics*, 26(4): 343-366.

Grunewald, J., Plagge, R. and Häupl, P. 2002. A 2-levelled hygrothermal material database for the numerical simulation program Delphin4, *6th International Symposium on Building Physics in Nordic Countries*, Trondheim, Norway, pp. 39-46.

Gueymard, C. 1987. An anisotropic solar irradiance model for tilted surfaces and its comparison   with selected engineering algorithms. *Solar Energy*, 38: 367–386.

Hagentoft, C.E. 1998. IEA Annex 24 Final Report on Task 5 – Performances and Practice: The Impact of Heat, Air, and Moisture Transport on Energy Demand and Durability. Energy Conservation in Buildings and Community Systems Programme, K.U. Leuven, Belgium.

Hagentoft, C.E. 2011. Probabilistic Analysis of Hygrothermal Conditions and Mould Growth Potential in Cold Attics. Impact of Weather, Building System and Construction Design Characteristics, *12th International Conference on Durability of Building Materials and Components*, Porto, Portugal.

Hamby, D.M. 1994. A review of techniques for parameter sensitivity analysis of environmental models. *Environmental Monitoring and Assessment*, 32(2): 135-154.

Hands, S. and Everitt, B.S. 1987. A Monte Carlo study of the recovery of cluster structure in binary data by hierarchical clustering techniques. *Multivariate Behavioral Research*, 22: 235–243.

Häupl, P. 2008. Bauphysik - Klima Wärme Feuchte Schall: Grundlagen, Anwendungen, Beispiele, Aktiv in Mathcad. Ernst & Sohn. Berlin, Germany. 564 pp.

Häupl, P. and Fechner, H. 2003. Hygric Material Properties of Porous Building Materials. *Journal of Thermal Envelope and Building Science*, 26(3): 259-284.

Helton, J.C. 1993. Uncertainty and sensitivity analysis techniques for use in performance assessment for radioactive waste disposal. *Reliability Engineering & System Safety*, 42(2-3): 327-367.

Helton, J.C. 1997. Uncertainty and sensitivity analysis in the presence of stochastic and subjective uncertainty. *Journal of Statistical Computation and Simulation*, 57(1-4): 3-76.

Helton, J.C. and Davis, F.J. 2003. Latin hypercube sampling and the propagation of uncertainty in analyses of complex systems. *Reliability Engineering and System Safety*, 81: 23-69.

Helton, J.C. and Davis, F.J. 2008. Sampling-Based Methods. In: A. Saltelli, K. Chan and E.M. Scott (Editors), *Sensitivity analysis*. John Wiley & Sons Ltd, West Sussex, England

Hens, H. 1999. Fungal Defacement in Buildings: A Performance Related Approach. *HVAC&R Research*, 5(3): 265-280.

Hens, H. 2007. Building Physics - Heat, Air and Moisture. Fundamentals and Engineering Methods with Examples and Exercises. Ernst & Sohn. Berlin, Germany. 284 pp.

Holm, A. and Künzel, H.M. 2002. The influence of measurement uncertainties on the calculated hygrothermal performance Fourth Symposium on Insulation Materials: Testing and Applications. West Conshohocken, Pa.: ASTM, (ASTM STP 1426), Charleston, South Carolina, pp. 335-350

Hopfe, C. 2009. Uncertainty and sensitivity analysis in building performance simulation for decision support and design optimization. Ph.D. Thesis. Eindhoven University of Technology. Eindhoven, The Netherlands. 229 pp.

Hukka, A. and Viitanen, H.A. 1999. A mathematical model of mould growth on wooden material. *Wood Science and Technology*, 3(6): 475 - 485.

Iman, R.L. and Conover, W.J. 1982. A distribution-free approach to inducing rank correlation among input variables. *Communications in Statistics - Simulation and Computation*, 11(3): 311-334.

Iman, R.L. and Helton, J.C. 1991. The repeatability of uncertainty and sensitivity analyses for complex probabilistic risk assessments. *Risk Analysis* 11(4): 591-606.

Iman, R.L. and Helton, J.C. 1985. A comparison of uncertainty and sensitivity techniques for computer models, Sandia National Laboratories, Albuquerque, New Mexico, USA.

Incropera, F.P., DeWitt, D.P., Bergman, T.L. and Lavine, A.S. 2005. Fundamentals of Heat and Mass Transfer John Wiley & Sons. Hoboken, NJ. 1024 pp.

274

Ineichen, P., Guisan, O. and Perez, R. 1990. Ground-reflected radiation and albedo. *Solar Energy*, 44: 207–214.

Janssen, H., Blocken, B., Roels, S. and Carmeliet, J. 2007. Wind-driven rain as a boundary condition for HAM simulations: Analysis of simplified modelling approaches. *Building and Environment*, 42(4): 1555-1567.

Krieger, T.J., Durston, C. and Albright, D.C. 1977. Statistical determination of effective variables in sensitivity analysis. *Trans. Am. Nuclear Science*, 28: 515-516.

Krus, M. 1996. Moisture transport and storage coefficients of porous mineral building materials: theoretical principles and new test methods. Fraunhofer IRB Verlag. Stuttgart.

Krus, M. and Holm, A. 1999. Simple methods to approximate the liquid transport coefficients describing the absorption and drying process. *Proceedings of the 5th Symposium on Building Physics in the Nordic Countries*: 241-248.

Krus, M. and Künzel, H.M. 1993. Determination of D_w from A-value. IEA Annex XXIV Report T3-D- 93/02.

Kumaran, M., Mukhopadhyaya, P. and Normandin, N. 2006. Determination of equilibrium moisture content of building materials: some practical difficulties. *Journal of ASTM International*, 3(10): 1-9.

Kumaran, M.K. 1996. Final   report, Vol 3, Task 3: Material properties. International Energy Agency Annex 24, Laboratorium Bouwfysica, Katholieke University–Leuven, Belgium.

Kumaran, M.K. 1999. Moisture Diffusivity of Building Materials from Water Absorption Measurements. *Journal of Building Physics*, 22(4): 349-355.

Künzel, H.M. 1995. Simultaneous heat and moisture transport in building components one- and two dimensional calculation using simple parameters. Fraunhofer IRB Verlag. Stuttgart.

Kutner, M.H., Nachtsheim, C.J., Neter, J. and Li, W. 2004. Applied Linear

Regression Models (Fifth Edition). McGraw-Hill/Irwin. New York. 1424 pp.

Lacasse, M.A. and Vanier, D.J. 1999. Durability of building materials and components 8: Service life and asset management, Volume Two : Durability of Building assemblies and methods of service life prediction. NRC Research Press, Ottawa, Canada, pp. 661.

lEA 1991. lEA Annex 14 (Condensation and Energy), Guidelines and practice: Energy conservation in building and community systems International Energy Agency. Paris.

Lewis, C.W., Smith, J.E., Anderson, J.G. and Murad, Y.M. 1994. The Presence of Mycotoxin-Associated Fungal Spores Isolated from the Indoor Air of the Damp Domestic Environment and Cytotoxic to Human Cell Lines. *Indoor and Built Environment*, 3(6): 323-330.

Liu, B.Y.H. and Jordan, R.C. 1963. The long term average performance of flat plate solar energy collectors. *Solar Energy*, 7: 53-74.

Lomas, K.J. and Bowman, N.T. 1987. An investigation into analytical and empirical validation techniques for dynamic thermal models of buildings. Building Research Establishment. Watford, UK.

Lomas, K.J. and Eppel, H. 1992. Sensitivity analysis techniques for building thermal simulation programs. *Energy and Buildings*, 19(1): 21-44.

Macdonald, I.A. 2002. Quantifying the Effects of Uncertainty in Building Simulation. Ph.D. Thesis. University of Strathclyde. Glasgow, UK. 267 pp.

Monika, W. and Carsten, R. 2008. Tools for performance simulation of heat, air and moisture conditions of whole buildings. *Journal of Building Simulation*, 1: 5–24.

Montgomery, D.C., Peck, E.A. and Vining, G.G. 2006. Introduction to Linear Regression Analysis (4th Edition). John Willey & Sons. New Jersey. 640 pp.

Moon, H.J. 2005. Assessing Mold Risks in Buildings under Uncertainty. Ph.D. Thesis. Georgia Institute of Technology. Atlanta, USA. 245 pp.

Morgan, M.G. and Henrion, M. 1990. Uncertainty: A Guide to Dealing With Uncertainty in Quantitative Risk and Policy Analysis. Cambridge University Press. New York. 332 pp.

Muneer, T. 2004. Solar radiation and daylight models. Elsevier Butterworth-Heinemann. Oxford, UK. 392 pp.

Nicolai, A. 2007. Modeling and numerical simulation of salt transport and phase transitions in unsaturated porous building materials. Ph.D. Thesis. Syracuse University. Syracuse, USA. 253 pp.

Nicolai, A. and Grunewald, J. 2011. The DELPHIN simulation model for hygrothermal transport processes in porous materials. Institute of Building Climatology, Dresden University of Technology, pp. 13.

Pel, L. 1995. Moisture Transport in Building Materials. Ph.D. Thesis. Technical University of Eindhoven. Eindhoven, The Netherlands.

Philip, J. and De Vries, D. 1957. Moisture movement in porous materials under temperature gradients. *Transactions American Geophysical Union*, 38(2): 222-232.

Plagge, R., Grunewald, J., Fechner, H. and Häupl, P. 2004. Development of Water retention transfer functions of ceramic bricks of Dresden building stock, *Buildings IX Proceedings*. ASHRAE, Clearwater Beach, Florida.

Plagge, R., Grunewald, J., Häupl, P. and Bomberg, M. 2004. Analysis of water uptake experiments for building materials: methods, functions and parameters, *CIB W40*, Glasgow, Uk.

Plagge, R., Scheffler, G., Meissner, F., Häupl, P., Fitz, C., Lengfeld, K., Krus, M., Künzel, H. and Klaus, S. 2007. MASEA - Material Property Database of Old and New Building Materials for Software Tools in Building Construction, *Proceedings of the 12th Symposium on Building Physics*, Dresden, pp. 363 - 368.

Plagge, R., Scheffler, G. and Nicolai, A. 2007. Experimental Methods to Derive Hygrothermal Material Functions for Numerical Simulation Tools, *Buildings X*

Proceedings, Clearwater Beach, Florida.

Psiloglou, B.E., Balaras, C.A., Santamouris, M. and Asimakopoulos, D.N. 1997. Calculation of ground albedo for the estimation of global radiation on tilted surfaces, for four european locations. *International Journal of Solar Energy*, 18(4): 231-258.

Ramos, N., Zhao, J., Simões, M.L., Delgado, J. and Freitas, V.P. 2012. Principles and Tools Applicable to a Stochastic Data Base of Material Properties, *5th International Building Physics Conference*, Kyoto, Japan, pp. 6.

Ramos, N.M.M., Delgado, J.M.P.Q., Barreira, E. and de Freitas, V.P. 2010. Hygrothermal Numerical Simulation: Application in Moisture Damage Prevention. In: L. Angermann (Editor), *Numerical Simulations - Examples and Applications in Computational Fluid Dynamics*. InTech, Janeza Trdine, Croatia.

Ritschkoff, A.C., Viitanen, H. and Koskela, K. 2000. The response of building materials to the mould exposure at different humidity and temperature conditions, *Proceedings of Healthy Buildings*. Seppänen, O. & Säteri, J. (Editors), Espoo, Finland., pp. 317 - 322.

Roels, S., Carmeliet, J., Hens, H., Adan, O., Brocken, H., Cerny, R., Pavlik, Z., Ellis, A.T., Hall, C., Kumaran, K., Pel, L. and Plagge, R. 2004. A Comparison of Different Techniques to Quantify Moisture Content Profiles in Porous Building Materials. *Journal of Thermal Envelope and Building Science*, 27(4): 261-276.

Roels, S., Carmeliet, J., Hens, H., Adan, O., Brocken, H., Cerny, R., Pavlik, Z., Hall, C., Kumaran, K., Pel, L. and Plagge, R. 2004. Interlaboratory Comparison of Hygric Properties of Porous Building Materials. *Journal of Thermal Envelope and Building Science*, 27(4): 307-325.

Ruisinger, U. and Grunewald, J. 2009. Feuchteatlas zur Vermeidung planungsbedingter Feuchteschäden. Neue Beurteilungskriterien zur Bewertung innen gedämmter Konstruktionen, Institut für Bauklimatik. Technische Universität Dresden, Germany.

Salonvaara, M., Karagiozis, A. and Holm, A.H. 2001. Stochastic building envelope modeling -- the influence of material properties, *Proceedings for Performance of Exterior Envelopes of Whole Buildings VIII: Integration of Building Envelopes*, Clearwater Beach, Florida.

Saltelli, A., Chan, K. and Scott, E.M. 2009. Sensitivity Analysis. John Wiley & Sons Ltd. West Sussex, England. 492 pp.

Saltelli, A., Tarantola, S., Campolongo, F. and Ratto, M. 2004. Sensitivity Analysis in Practice: A Guide to Assessing Scientific Models. John Wiley & Sons. Hoboken, NJ. 232 pp.

Scheffler, G. 2008. Validation of hygrothremal material modelling under consideration of the hysteresis of moisture storage. Ph.D. Thesis. Dresden University of Technology. Dresden, Germany. 240 pp.

Scheffler, G., Grunewald, J. and Plagge, R. 2007. Evaluation of Functional Approaches to Describe the Moisture Diffusivity of Building Materials. *Journal of ASTM International*, 4(2): 55-70.

Scheffler, G. and Plagge, R. 2010. A whole range hygric material model: Modelling liquid and vapour transport properties in porous media. *International Journal of Heat and Mass Transfer*, 53(1-3): 286-296.

Schirmer, R. 1938. Die Diffusionszahl von Wasserdampf-Luftgemischen und die Verdampfungsgeschwindigkeit. *2. VDI Beiheft Verfarenstechnik*: 170-177.

Sedlbauer, K. 2001. Prediction of Mould Fungus Formation on the Surface of and Inside Building Component. Ph.D. Thesis. Fraunhofer Institute for Building Physics. Germany. 247 pp.

Simlab 2011. Software package for uncertainty and sensitivity analysis. Joint Research Centre of the European Commission. Downloadable for free at: http://simlab.jrc.ec.europa.eu.

Steskens, P.W.M.H., Janssen, H. and Rode, C. 2009. Influence of the Convective

Surface Transfer Coefficients on the Heat, Air, and Moisture (HAM) Building Performance. *Indoor and Built Environment*, 18(3): 245-256.

Struck, C., Jan, H. and Kotek, P. 2009. On the Application of Uncertainty and Sensitivity Analysis with Abstract Building Performance Simulation Tools. *Journal of Building Physics*, 33(1): 5-27.

SYSTAT11 2002. Systat Software Inc., Chicago, IL

Temps, R.C. and Coulson, K.L. 1977. Solar radiation incident upon slopes of different orientations. *Solar Energy*, 19: 179-184.

Thevenard, D. and Haddad, K. 2006. Ground reflectivity in the context of building energy simulation. *Energy and Buildings*, 38(8): 972-980.

Trethowen, H.A. 1991. Sensitivity of Insulated Wall and Ceiling Cavities to Workmanship. *Journal of Building Physics*, 15(2): 172-179.

van Genuchten, M.T. 1980. A closed-form equation for predicting the hydraulic conductivity of unsaturated soils. *Soil Science Society of America Journal*, 44: 892–898.

Viitanen, H. and Ojanen, T. 2007. Improved Model to Predict Mould Growth in Building Materials, *Thermal Performance of the Exterior Envelopes of Whole Buildings X*. ASHRAE, DOE, ORNL, Clearwater Beach, USA.

Viitanen, H., Vinha, J., Salminen, K., Ojanen, T., Peuhkuri, R., Paajanen, L. and Lähdesmäki, K. 2010. Moisture and Bio-deterioration Risk of Building Materials and Structures. *Journal of Building Physics*, 33(3): 201-224.

Viitanen, H.A. 1997. Modelling the time factor in the development of mould fungi - Effect of critical humidity and temperature conditions in pine and spruce sapwood. *Holzforschung*, 51(1): 6-14.

Vinha, J. 2007. Hygrothermal Performance of Timber-framed External Walls in Finnish Climatic Conditions: A Method for determining the Sufficient Water Vapour Resistance of the Interior Lining of a Wall Assembly. Ph.D. Thesis.

Tampere University of Technology. Tampere, Finland. 380 pp.

Zhao, J., Plagge, R. and Grunewald, J. 2010. A stochastic and systematic approach for determination of material properties, *1st central European symposium on building physics*, Cracow, Poland.

Zhao, J., Plagge, R., Nicolai, A., Grunewald, J. and Zhang, J. 2011. Stochastic study of hygrothermal performance of a wall assembly -The influence of material properties and boundary coefficients. *HVAC&R Research*, 17(4): 591-601.

Vita

NAME OF AUTHOR: Jianhua Zhao

PLACE OF BIRTH: Yingkou, China

DATE OF BIRTH: February 9, 1979

GRADUATE AND UNDERGRADUATE SCHOOLS ATTENDED:

Dalian University of Technology, Dalian, China

Dalian University of Technology, Dalian, China

DEGREES AWARDED:

M.S. Engineering Thermophysics , Dalian University of Technology, 2004, China

B.S. Thermal Energy and Power Engineering, Dalian University of Technology, 2001, China

PROFESSIONAL EXPERIENCE:

Research fellow, Institute of Building Climatology, Dresden University of Technology, Germany，2008-2012

Research and teaching assistant, Department of Mechanical and Aerospace Engineering, Syracuse University, USA, 2006-2008

Auditor, Deloitte Touche Tohmatsh CPA Ltd. (China), 2004-2005

Research and teaching assistant, Department of Engineering Thermophysics, Dalian University of Technology, China, 2001-2004